

**Selectivity in Ruthenium Catalyzed Olefin Metathesis:
Applications and Origins**

Thesis by
Benjamin K. Keitz

In Partial Fulfillment of the Requirements for the degree of
Doctor of Philosophy

CALIFORNIA INSTITUTE OF TECHNOLOGY
Pasadena, California

2013
(Defended July 18, 2012)

© 2013

Benjamin K. Keitz

All Rights Reserved

For Dad

(June 4, 1960 – October 30, 2010)

Acknowledgements

It's almost unbelievable how much work goes into producing a Ph.D. I don't mean my work in this thesis, but the effort put in by friends, family, and members of the community who have helped me reach this point. Now, near the end of this journey, it's left to me to acknowledge their contributions, without which this work would have been totally impossible.

I'd first like to thank my advisor, Bob Grubbs, who has supported me from day one. I was educated as an engineer, but trained as a chemist, and as eager and foolish as an incoming graduate student has ever been. Bob allowed me to develop at my own pace, which means he let me make mistakes, and I know I didn't disappoint in this regard. But, like any good safety net or belayer, Bob was always there to catch me when I fell off the rock. Ultimately, the freedom to learn from my mistakes was indispensable to my development as an independent researcher, and I will be forever grateful for this experience. Fortunately, I know that Bob's support will not end after I receive my degree, and I look forward to seeking his advice and wisdom as I enter a new unknown.

I'd next like to thank the members of my thesis committee: John Bercaw, Brian Stoltz, and Jonas Peters. In my various conversations with them, not once did they make me feel unequal to themselves, even though I obviously am. I (think) have developed a reputation of fearlessness (a.k.a. foolishness) over the years and it almost certainly has come off as disrespectful on occasion. I hope they know how much I look up to them/value their advice and realize I'd be content to experience a tenth of their success.

Now I'd like to thank the entire Grubbs group! Linda Syme has helped everyone in the group keep tabs on Bob and has been an indispensable resource for all things grant and funding related. John Matson and Donde Anderson looked out for me when I first arrived. Matt Whited taught me glove box technique and made sure I wasn't a menace to the lab. He and John also taught me the importance of the Athenaeum. Chris Daeffler and Jean Li (and the rest of the class above me) adopted me as one of their own when I came to Caltech in the summer before most of the other members of my class had arrived. Matthew Van Wingerden is my classmate in the Grubbs group and has been a great friend and milkshake buddy over the years. We agreed that if I thanked him enough times in this section, that he would give me 5% of his annual consultant income. A.J. Boydston was a sensational post-doc in the group who essentially taught me how to write a paper and helped me get through my "sophomore slump". Ian Stewart, Kevin Kuhn, Koji Endo, Renee Thomas, Myles Herbert, Alexey Fedorov, Pinky Patel, Vanessa Marx, and Lauren Rosebrugh have worked very closely with me on several projects and basically did most of the work described in this thesis. Ray Weitekamp deserves special mention as our resident physics and dub-step expert. I've had the privilege of mentoring three undergraduates, Mimi Yang, Jordan Theriot, and Alexandra Sullivan, all of whom have performed extraordinarily and will each go on to do great things. I'd also like to thank all of the people in the group who I have overlapped with for their time, encouragement, and general awesomeness. Daryl Allen and Materia Inc. provided the group with an endless amount of ruthenium catalysts, which has made all of our lives that much easier. Finally, the Grubbs

group sports teams get a special shout-out. I think our softball team went, like, 30–3 over the past few years and we won the soccer championship one year! If you're reading this and considering joining the group, my best suggestion is to grab some cleats and start training, because we take this stuff very seriously.

Several members of the Caltech community have made the work in this thesis possible. Jay Labinger always seemed to have the right answers and whenever I was stuck, I could count on him to suggest a solution. Scott Virgil taught me how to use the SYMYX robot and knew the perfect experiment for every question. I couldn't have characterized half the compounds I made without the help of Dave VanderVelde and his limitless knowledge of NMR spectroscopy. Anna Wenzel helped me with the ruthenacycle project and has been a great resource for chemistry and academic life. Of course, no research could happen without the help of Joe Drew, Ron Cohen, Paul Carroad, Rick Gerhart, Dan Nieman, Mike Roy, Agnes Tong, Anne Penney, Steve Gould, Leah Mentch, Chris Smith, Tom Dunn, CeCe Manoochehri, and Laura Howe. Also thanks to Pat Anderson for organizing the IOS speaker series. Special thanks to Mona Shagohli and Naseem Torian for running the mass spectrometry facility so smoothly. All of the crystal structures in this thesis were obtained by Larry Henling and Mike Day, so a very special thanks to them. I had the pleasure of working with Guy Bertrand and several members of his group, most notably Jean Bouffard. I could always count on them for interesting new ligands and important insights and project ideas.

Finally, I'd like to thank my friends (especially Eric, Chethana, Ian, Rachel, Leslie, Ted, Andrew, Young In, Matt, Taylor, Justin, plus many others) and family for

their continuous support over the years. That includes my siblings Kristen, Kendal, Katie, and Keaten (yes, all with K's) and Mom and Dad. A special thank you for my step-dad Chip, and his family as well. Last, but not least, I'd like to thank Chithra Krishnamurthy for her love and support over the years. If it wasn't for her, I'd probably still be a country bumpkin (maybe I still am), and there's so much of the world I would have missed out on. Thanks for keeping me honest and making me a better person!

Abstract

Ruthenium-based catalysts for olefin metathesis display high activity in the presence of common functional groups and have been utilized in a variety of chemical disciplines. This thesis describes the development of new catalysts with superior properties and mechanistic studies directed at understanding the factors governing catalyst activity and selectivity.

Chapter 2 describes the preparation of acid-activated olefin metathesis catalysts containing acetylacetonate (acac)-type ligands. The effect of ligand structure and the exogenous acid on catalytic activity was examined. The acid-activated catalysts were also combined with a photoacid generator (PAG), which resulted in a highly active system for photo-activated olefin metathesis.

Chapter 3 details the incorporation of mesoionic carbenes (MICs) into ruthenium metathesis catalysts. The activity of these catalysts in several metathesis assays was measured and correlated to their initiation rates. The protonolysis of a Ru-MIC bond and the incorporation of this reaction into an acid-activated catalyst are also described.

Chapter 4 explores the relationship between catalyst structure and degenerate metathesis. A ring-closing metathesis assay was used to measure the preference of different catalysts for productive or degenerate metathesis. The relationship between degenerate metathesis and reactions such as ethenolysis is also discussed.

Chapter 5 describes the study of ruthenacyclobutanes formed from the degenerate metathesis selective catalysts presented in Chapter 4. The rates of various chemical exchange processes were measured and correlated to catalyst structure. Kinetic parameters for the rate-limiting step in ring-closing metathesis were also measured and used to rationalize the

differences in productive/degenerate selectivity for various catalysts.

Chapter 6 details the preparation and study of C-H-activated ruthenium catalysts for *Z*-selective olefin metathesis. Ligand effects on catalyst activity and selectivity are explored along with the application of these catalysts in *Z*-selective cross-metathesis and ring-opening metathesis polymerization.

Table of Contents

Acknowledgements		iv
Abstract		viii
Table of Contents		x
Chapter 1	Introduction	1
	Introduction	2
	Metathesis Reactions	2
	Mechanism and Mechanistic Intermediates	4
	Ligand Effects	6
	Future Outlook	7
Chapter 2	Acid- and Photo-Activated Ruthenium Metathesis Catalysts	12
	Abstract	13
	<i>Acetylacetonate (acac) Ruthenium Alkylidene Complexes</i>	
	Introduction	13
	Results and Discussion	14
	Conclusion and Future Outlook	22
	<i>Ruthenium Carbonyl Alkylidene Complexes</i>	
	Introduction	23
	Results and Discussion	24
	Conclusion and Future Outlook	28
	Experimental Section	28
	References	34
Chapter 3	Preparation and Reactivity of Mesoionic (MIC)–Containing Ruthenium Metathesis Catalysts and their Acid-Activated Behavior	38
	<i>MIC-Based Ruthenium Metathesis Catalysts</i>	
	Abstract	39
	Introduction	39
	Results and Discussion	41
	Conclusions and Future Outlook	49
	<i>Acid-Activated, MIC-Based Ruthenium Metathesis Catalysts</i>	
	Introduction	49
	Results and Discussion	50
	Conclusions and Future Outlook	62
	Experimental	63
	References	75

Chapter 4	Degenerate (Nonproductive) Reactions with Ruthenium Metathesis Catalysts	80
	Abstract	81
	Introduction	81
	Results and Discussion	83
	<i>Kinetic Modeling</i>	94
	<i>Degenerate Metathesis and Ethenolysis</i>	96
	Conclusions and Future Outlook	101
	Experimental	102
	References	113
Chapter 5	Kinetics of Ruthenacyclobutanes Related to Degenerate Metathesis	116
	Abstract	117
	Introduction	117
	Results and Discussion	119
	Conclusions and Future Outlook	134
	Experimental	136
	References	146
Chapter 6	Z-Selective Ruthenium Metathesis Catalysts	150
	Abstract	151
	Introduction	151
	Results and Discussion	154
	Conclusions and Future Outlook	188
	Experimental	189
	References	212
Appendix A	Ruthenium Olefin Metathesis Catalysts Bearing Carbohydrate-Based N-Heterocyclic Carbenes	220
	Introduction	221
	Results and Discussion	222
	Conclusions	231
	Experimental	232
	References	238
Appendix B	Miscellaneous C-H-Activated Catalysts	243
	Introduction	244
	Nitrite Catalyst	244
	Catalysts with Chiral Carboxylates	245
	Acetylacetonate Complexes	248
	Perchlorate and Perrhenate Ligands	249
	Tetrazole Complexes	250
	Sulfonate Complexes	250
	References	250

Chapter 1

Introduction

Introduction

Olefin (alkene) metathesis is a chemical reaction that involves the redistribution of carbon-carbon double bonds via their scission and reformation (Figure 1.1). Over the past 60 years, olefin metathesis has evolved from an unusual occurrence in petroleum distillation and cracking processes, to the standard method for the construction of new C-C double bonds. As such, olefin metathesis is now widely employed as a synthetic methodology in a variety of fields including synthetic organic chemistry, polymer and materials science, green chemistry, and biochemistry. The application of olefin metathesis to these fields has been facilitated by the development of a wide variety of increasingly advanced and well-defined catalysts tailored to suit these applications.

Early metathesis catalysts, first discovered in the 1950s, consisted of heterogeneous mixtures of tungsten (W) and molybdenum (Mo) oxides.¹ The subsequent discovery of stable metal carbenes² and their identification as metathesis active species³ enabled the preparation of well-defined titanium (Ti), W, Mo, ruthenium (Ru), and rhenium (Re) catalysts (Figure 1.2). A variety of other metals in the transition metal block have exhibited metathesis activity, but they have not been explored to the same extent.⁴ Our group focuses on the preparation, development, and study of Ru-based olefin metathesis catalysts.

Metathesis Reactions

The versatility of olefin metathesis is largely due to the diverse types of olefins that can be reacted in or formed by this reaction. These include terminal,

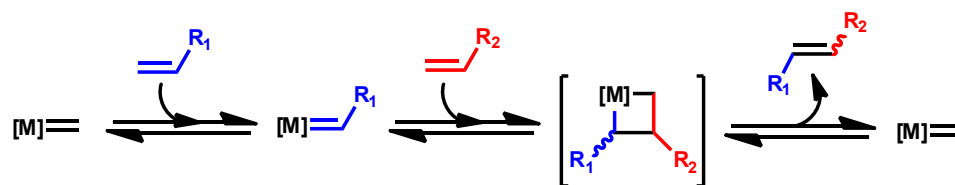


Figure 1.1. The olefin metathesis reaction

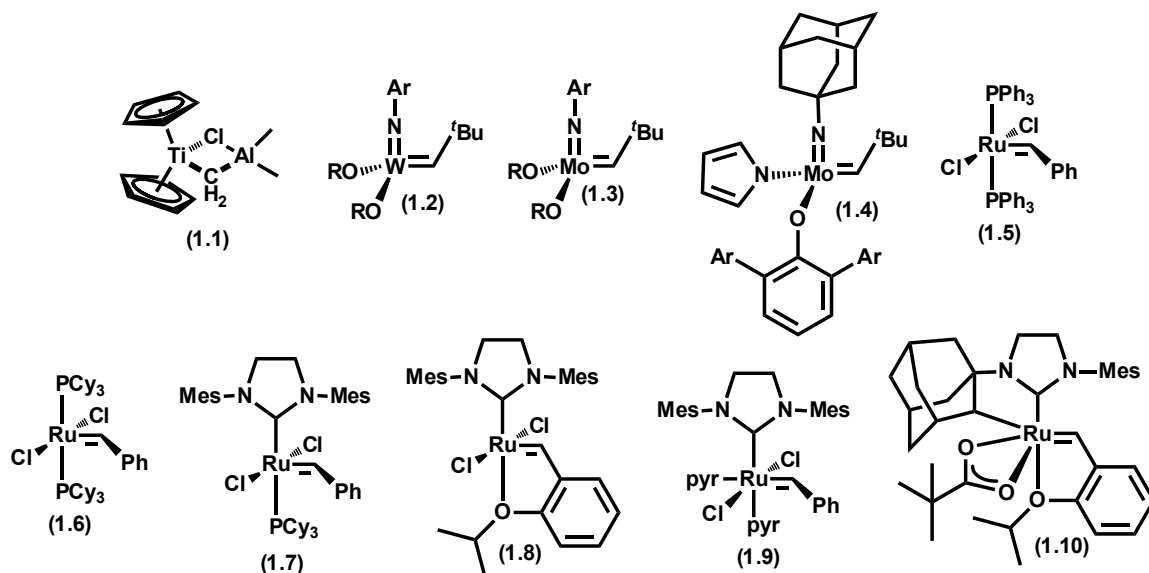


Figure 1.2. Common olefin metathesis catalysts. mes = 2,4,6-trimethylphenyl. ar = aryl. pyr = pyridine

internal, cyclic, macrocyclic, and polymeric olefins. In general, there are three major classes of metathesis reactions (Figure 1.3). For example, α,ω -dienes can undergo ring-closing metathesis (RCM) to form cyclic olefins. Strained cyclic or bicyclic olefins, such as norbornene, can undergo ring-opening metathesis polymerization (ROMP). Finally, cross-metathesis (CM), involves the intermolecular reaction of two terminal olefins to form a new internal olefin. These reactions are historically the most important and the most common, but several variations and combinations of ROMP, RCM, and CM are also known. For example, if the reaction concentration is high enough, α,ω -dienes will undergo *intermolecular* CM (instead of *intramolecular*

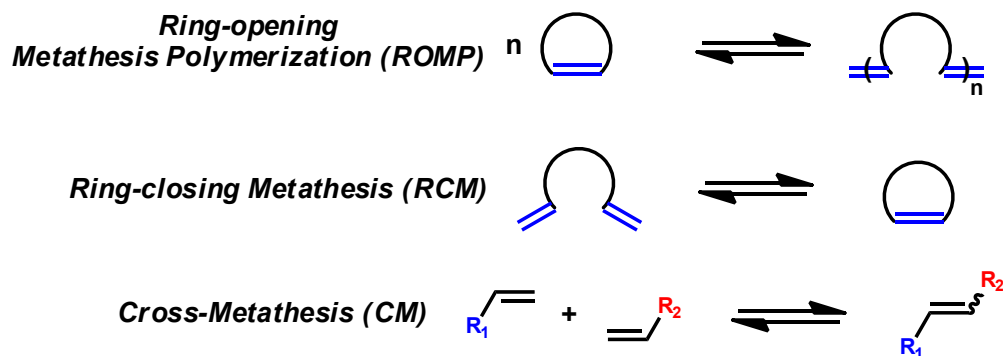


Figure 1.3. Common metathesis reactions

RCM) to form polymers in a process known as acyclic diene metathesis (ADMET). Similarly, when ROMP is performed in the presence of a large excess of terminal olefin, a ring-opening cross-metathesis reaction (ROCM) reaction may occur.

All metathesis reactions are thermodynamically controlled.⁵ Thus, they require a driving force to give a single product. In the case of ROMP, the driving force is the release of ring-strain in the monomer. For RCM and CM, the driving force for reaction is the release of a volatile product (e.g., ethylene) or the formation of a more stable olefin. However, the thermodynamic product of a metathesis reaction is not always desired because a synthetic chemist may wish to form the thermodynamically disfavored *cis*- or *Z*-olefin via metathesis. The formation of kinetic products, such as *Z*-olefins, has persisted as a significant challenge for olefin metathesis since its discovery.

Mechanism and Mechanistic Intermediates in Ru-Based Olefin Metathesis

The general mechanism of olefin metathesis, as proposed by Chauvin and Herrison, involves the formation of a metallocyclobutane from a metal alkylidene and subsequent cycloreversion to generate a different metal alkylidene

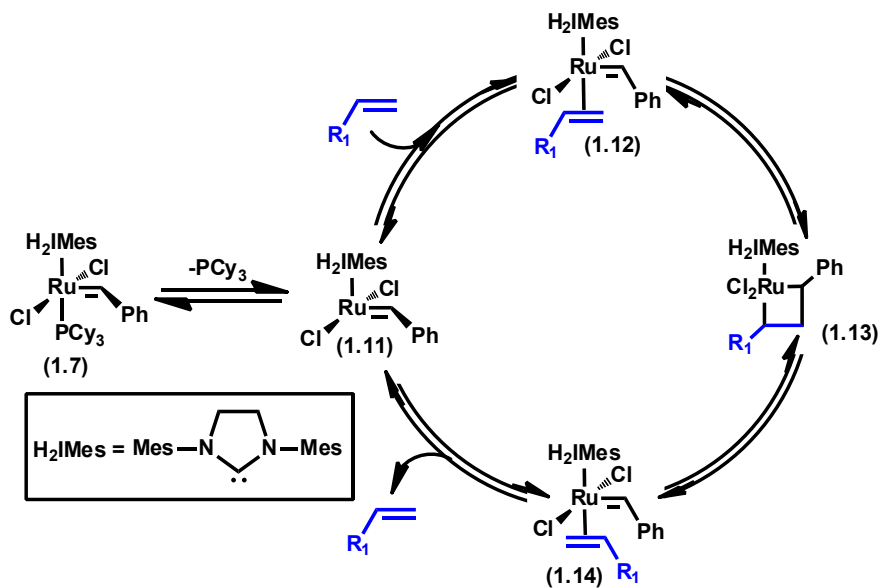


Figure 1.4. Catalytic cycle for Ru-based olefin metathesis including important intermediates

and an olefin product (Figure 1.4). All metathesis catalysts proceed through this mechanism, including Ru-based catalysts. However, there are a number of specific factors and reactions that change depending on the construction of the catalyst.

Prototypical Ru-based metathesis catalysts are 16 electron (e^-) Ru(II) species that require ligand dissociation in order to access the 14 e^- intermediate required for ruthenacyclobutane formation. Kinetic studies have established that phosphine dissociation in catalysts such as **1.7** is rate-determining.⁶ For catalysts with chelating alkylidenes, either oxygen dissociation or olefin binding is rate-determining depending on the nature of the catalyst and reacting olefin.⁷ Although catalyst initiation is well-understood, very little is known about the Ru-olefin (**1.12**) and ruthenacycle species (**1.14**) in the metathesis catalytic cycle.

Of particular interest is the geometry of the ruthenacyclobutane intermediate and whether it is primarily side-bound (*cis* to the NHC) or bottom-bound (*trans*

to the NHC). Studies on model complexes intended to mimic typical reaction intermediates have provided evidence for side-bound ruthenacycles.⁸ On the other hand, the majority of theoretical and experimental studies on actual metathesis-active species support a bottom-bound ruthenacycle.^{9,10} Based on this discrepancy, it is likely that the difference in energy between side-bound and bottom-bound structures is very small and dependent on the exact reaction conditions. The study of these structures remains important in order to resolve the exact nature of the intermediate. Moreover, greater understanding of this issue would facilitate improvements in selectivity during olefin metathesis.

Ligand Effects

Like many organometallic catalysts, the development of more efficient olefin metathesis catalysts has been facilitated by the preparation of new ligand frameworks. The majority of Ru-based catalysts have the general formula $X_2L_2Ru=CHR$ where X and L represent anionic and neutral donors, respectively. The first well-defined Ru-based catalysts was $Cl_2(PPh_3)_2Ru=CHPh$ (**1.5**), which showed good reactivity for the polymerization of norbornene and other strained monomers.¹¹ A significant improvement in catalyst activity was discovered when the PPh_3 in **1.5** was replaced with PCy_3 to generate **1.6**.¹² Both **1.5** and **1.6** were less reactive than their Mo counterparts (**1.3**), but demonstrated an impressive stability towards both dioxygen (O_2) and water that enabled their use on the benchtop without the need for an inert atmosphere.

The next major advance in catalytic activity occurred when one PCy_3 ligand in **1.6** was replaced with an N-heterocyclic carbene (NHC) ligand to yield

complex **1.7**.¹³ With the NHC ligand, catalyst **1.7** displayed activities comparable to Mo- and W-based catalysts. The subsequent exchange of the other phosphine in **1.7** with a chelating ether moiety resulted in catalyst **1.8**, which possessed enhanced stability.¹⁴ It is also worth noting that the PCy₃ in **1.7** has also been replaced with pyridine to prepare a fast initiating catalyst (**1.9**) that is exceptional at catalyzing ROMP.¹⁵ In addition to improving catalyst reactivity, the use of an NHC ligand has enabled the rigorous study of steric and electronic effects on Ru-based metathesis catalysts. Along these lines, a wide variety of catalysts containing both traditional (e.g., substituted, unsaturated) and relative exotic NHCs (e.g., abnormal, cyclic alkyl amino carbene) have been prepared and studied.¹⁶

Recently, a new class of Ru-based catalysts, formed via carboxylate-induced C-H activation of the NHC ligand, has emerged (**1.10**).¹⁷ These catalysts have displayed remarkable kinetic selectivity for the selective formation of Z-olefins and rival their Mo- and W-based counterparts in both activity and selectivity. The C-H activated catalysts also exhibit several interesting reactivity trends that will make them interesting to study for years to come.

Future Outlook

A convincing argument could be made that the continued development of Ru-based and other olefin metathesis catalysts is no longer necessary. Indeed, researchers have developed a number of ingenious methods for adapting the current ‘family’ of catalyst to their specific needs. However, while certain fields may no longer require catalysts that are more stable or more active, the development of such catalysts has facilitated the proliferation of the metathesis methodology into other

synthetic disciplines. In other words, there will always be a need for new catalysts in niche, but important applications, many of which are only starting to be explored.

One example of a new application is Z-selective olefin metathesis, and new, selective olefin metathesis catalysts based on Mo, W, and Ru have only recently been reported. The development of these catalysts has finally enabled the preparation of Z-olefins using metathesis. Despite this progress, significant improvements in both catalytic activity and selectivity are necessary for these catalysts to become industrially relevant. Moreover, mechanistic studies focused on catalyst stability and the origin of Z-selectivity will be essential to developing improved catalysts, just as they were in the development of previous generations of metathesis catalysts.

New catalysts for use in polymer synthesis and materials science will also be required. The importance of metathesis in these areas has been demonstrated by its inclusion as the basis for self-healing materials,¹⁸ as a method for the facile preparation of polymer photonic crystals¹⁹ and the development of advanced polymer composites.²⁰ Some of these applications require extremely fast initiating and active catalysts while others need slow, but stable catalysts. Clearly, one catalyst is not suitable for all materials science applications. The development of new metathesis catalysts has traditionally focused on the needs of synthetic organic chemists, but many of these catalysts are not suited to polymer applications. Therefore, the preparation of new catalysts with previously neglected attributes such as enhanced stability and slow initiation may prove beneficial to the materials science community.

A final area where the development of new catalysts can make an impact is in the industrial use of metathesis in processes such as ethenolysis. Compared

to other metathesis applications, ethenolysis is extremely difficult since it requires a catalyst that is both very stable and kinetically selective. Despite this challenge, the results in this thesis hint that an improved understanding of degenerate metathesis combined with the knowledge of the factors governing catalyst stability will facilitate the development of new catalysts for industrial-scale ethenolysis.

In conclusion, metathesis is among the most powerful methodologies for the preparation of new C-C bonds. Thus, the development of new catalysts with improved activity, selectivity, and stability will continue to expand the metathesis methodology into new areas of chemistry while rewarding the students and postdoctoral fellows who invest in this field.

References

- (1) (a) Ziegler, K.; Holzkamp, E.; Breil, H.; Martin, H. *Angew. Chem.* **1955**, 67, 426. (b) Truett, W. L.; Johnson, D. R.; Robinson, I. M.; Montague, B. A. *J. Am. Chem. Soc.* **1960**, 82, 2337. (c) Banks, R. L.; Bailey, G. C. *Indus. Eng. Chem. Prod. Res. Dev.* **1964**, 3, 170.
- (2) (a) Fischer, E. O.; Maasböl, A. *Angew. Chem. Int. Ed.* **1964**, 3, 580. (b) Schrock, R. R. *Chem. Rev* **2002**, 102, 145.
- (3) (a) Hérisson, J.-L.; Chauvin, Y. *Makromol. Chem.* **1970**, 141, 161. (b) Casey, C. P.; Burkhardt, T. J. *J. Am. Chem. Soc.* **1974**, 96, 7808. (c) Katz, T. J.; McGinnis, J. *J. Am. Chem. Soc.* **1975**, 97, 1592. (d) Grubbs, R. H.; Burk, P. L.; Carr, D. D. *J. Am. Chem. Soc.* **1975**, 97, 3265.
- (4) (a) Ivin, K. J. *Olefin Metathesis*, Chapter 2, Academic Press: New York, 1983. (b) Goodall, B. L.; McIntosh, L. H.; Rhodes, L. F. *Macromol. Symp.* **1995**, 89, 421.

- (5) Grubbs, R.H. *Handbook of Metathesis*, Wiley-VCH, Weinheim, **2003**.
- (6) Sanford, M. S.; Love, J. A.; Grubbs, R. H. *J. Am. Chem. Soc.* **2001**, *123*, 6543.
- (7) (a) Hejl, A. PhD. Dissertation, California Institute of Technology, **2007**. (b) Vorfalt, T.; Wannowius, K.-J.; Plenio, H. *Angew. Chem. Int. Ed.* **2010**, *1*, 5533.
- (c) Ashworth, I. W.; Hillier, I. H.; Nelson, D. J.; Percy, J. M.; Vincent, M. A. *Chem. Comm.* **2011**, *47*, 5428. (d) Thiel, V.; Hendann, M.; Wannowius, K.-J.; Plenio, H. *J. Am. Chem. Soc.* **2012**, *134*, 1104.
- (8) Tallarico, J. A.; Bonitatebus, P. J.; Snapper, M. L. *J. Am. Chem. Soc.* **1997**, *119*, 7157. (b) Trnka, T. M.; Day, M. W.; Grubbs, R. H. *Organometallics* **2001**, *20*, 3845.
- (c) Anderson, D. R.; Hickstein, D. D.; O'Leary, D. J.; Grubbs, R. H. *J. Am. Chem. Soc.* **2006**, *128*, 8386.
- (9) (a) Benitez, D.; Tkatchouk, E.; Goddard, W. a.; Iii, W. A. G. *Chem. Comm.* **2008**, 6194. (b) Rowley, C. N.; Eide, E. F. van der; Piers, W. E.; Woo, T. K.; Eide, E. F. V. D. *Organometallics* **2008**, *27*, 6043.
- (10) (a) Romero, P. E.; Piers, W. E.; McDonald, R. *Angew. Chem. Int. Ed.* **2004**, *43*, 6161. (b) Rowley, C. N.; Eide, E. F. van der; Piers, W. E.; Woo, T. K. *Organometallics* **2008**, *27*, 6043. (c) Eide, E. F. van der; Romero, P. E.; Piers, W. E. *J. Am. Chem. Soc.* **2008**, *130*, 4485. (d) Leitao, E. M.; Eide, E. F. van der; Romero, P. E.; Piers, W. E.; McDonald, R. *J. Am. Chem. Soc.* **2010**, *132*, 2784. (e) Eide, E. F. van der; Piers, W. E. *Nature Chemistry*. **2010**, *2*, 571.
- (11) (a) Nguyen, S. T.; Grubbs, R. H.; Ziller, J. W. *J. Am. Chem. Soc.* **1992**, *114*, 3974. (b) Nguyen, S. T.; Johnson, L. K.; Grubbs, R. H.; Ziller, J. W. *J. Am. Chem. Soc.* **1992**, *114*, 3974.

- (12) Schwab, P.; France, M. B.; Ziller, J. W.; Grubbs, R. H. *Angew. Chem. Int. Ed.* **1995**, *34*, 2039.
- (13) Scholl, M.; Ding, S.; Lee, C. W.; Grubbs, R. H. *Org. Lett.* **1999**, *1*, 953.
- (14) Kingsbury, J. S.; Harrity, J. P. A.; Bonitatebus, P. J.; Hoveyda, A. H. *J. Am. Chem. Soc.* **1999**, *121*, 791.
- (15) Love, J. A.; Sanford, M. S.; Day, M. W.; Grubbs, R. H. *J. Am. Chem. Soc.* **2003**, *125*, 10103.
- (16) (a) Samojłowicz, C.; Bieniek, M.; Grela, K. *Chem. Rev.* **2009**, *109*, 3708. (b) Vougioukalakis, G. C.; Grubbs, R. H. *Chem. Rev.* **2010**, *110*, 1746.
- (17) (a) Endo, K.; Grubbs, R. H. *J. Am. Chem. Soc.* **2011**, *133*, 8525. (b) Keitz, B. K.; Endo, K.; Patel, P. R.; Herbert, M. B.; Grubbs, R. H. *J. Am. Chem. Soc.* **2012**, *134*, 693.
- (18) (a) White, S. R.; Delafuente, D. A.; Ho, V.; Sottos, N. R.; Moore, J. S.; White, S. R. *Macromolecules* **2007**, *40*, 8830. (b) Mauldin, T. C.; Kessler, M. R. *Int. Mater. Rev.* **2010**, *55*, 317.
- (19) Xia, Y.; Olsen, B. D.; Kornfield, J. A.; Grubbs, R. H. *J. Am. Chem. Soc.* **2009**, *131*, 18525.
- (20) (a) Encyclopedia of Chemical Technology, 4th ed.; Howe Grant, M., Ed.; Wiley-Interscience: New York, 1996; Vol. 17, p. 829. (b) Jeong, W.; Kessler, M. R. *Chem. Mater.* **2008**, *20*, 7060.

Chapter 2

Acid- and Photo-Activated Ruthenium Metathesis Catalysts

The text in this chapter is reproduced in part with permission from:

Keitz, B. K.; Grubbs, R. H. *J. Am. Chem. Soc.*, **2009**, 131, 2038.

Copyright 2009 American Chemical Society

Abstract

The use of photoacid generators (PAG) in conjunction with acid-activated ruthenium olefin metathesis catalysts has been explored. The hydrochloric acid generated as a result of irradiation of samples with ultraviolet (UV) light was found to protonate a labile ligand on ruthenium. Displacement of this ligand with chloride anion resulted in the generation of a highly active metathesis catalyst that was effective in catalyzing a variety of reactions, including ring-closing metathesis (RCM) and ring-opening metathesis polymerization (ROMP). Investigations into the mechanism of the activation are also presented.

The preparation of ruthenium alkylidene carbonyl complexes is also described as are chemical and photochemical efforts to induce carbonyl dissociation in order to generate an active metathesis species.

Acetylacetonate (acac) Ruthenium Alkylidene Catalysts

Introduction

Latent olefin metathesis catalysts¹ require an external stimulus (e.g., heat,² light,^{3–6} acid (see Chapter 3),⁷ or mechanical stress) in order to activate.⁸ Consequently, they may be stored in the presence of reactive olefins until a metathesis reaction is desired. This attribute makes latent metathesis catalysts critical in a variety of applications including photolithography,⁹ roll-to-roll coating,¹⁰ polymer molding,¹¹ and self-healing materials.¹²

Compared to other methods for catalyst activation, photo-activation is relatively rare. However, photo-initiated ROMP has been reported for catalysts

based on ruthenium (Ru),³ tungsten (W),⁴ molybdenum (Mo),⁵ and rhenium (Re).⁶ The majority of these systems rely on the *in situ* generation of a reactive alkylidene following ligand dissociation, and thus their catalytic activity is relatively limited. We believed that catalyst activity, especially in more difficult reactions, such as RCM, could be improved via the inclusion of a reactive alkylidene in the pre-catalyst. Here, we validate this approach via the use of coordinatively saturated Ru-*acac* (*acac* = acetylacetonate) complexes that are activated by the addition of a variety of Brønsted acids, including photoacids. The reactivity of these complexes during RCM and ROMP is presented along with investigations into the mechanism of activation and the nature of the active metathesis species. Selected other approaches to photo-activated olefin metathesis are also presented.

Results and Discussion

Previous work from our group has shown that a metathesis inactive Ru-alkylidene complex ligated by *acac* may be converted into a metathesis active system by protonation and subsequent displacement of the labile *acac* ligands.^{7a} These complexes could be easily accessed via transmetalation of the chloride ligands in $(\text{PCy}_3)_2\text{Cl}_2\text{Ru}(=\text{CHPh})$ (**2.1**) with thallium (Tl) *acac* salts (Figure 2.1). Silver (Ag) *acac* salts could also be used in some circumstances, but their use generally resulted in incomplete transmetalation.

Using a similar strategy to that shown in Figure 2.1, several *acac*-containing complexes were prepared, starting from different Ru precursors (Figure 2.2). With these catalysts in hand, we initiated a study into their activity using the RCM of diethyldiallylmalonate (DEDAM, **2.8**) as a test reaction. When **2.8** was exposed to **2.2**-

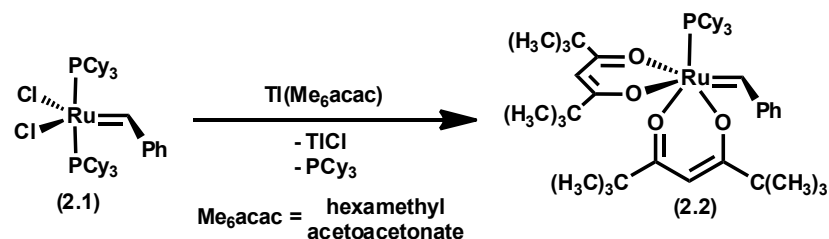


Figure 2.1. General method for preparation of Ru-acac complexes

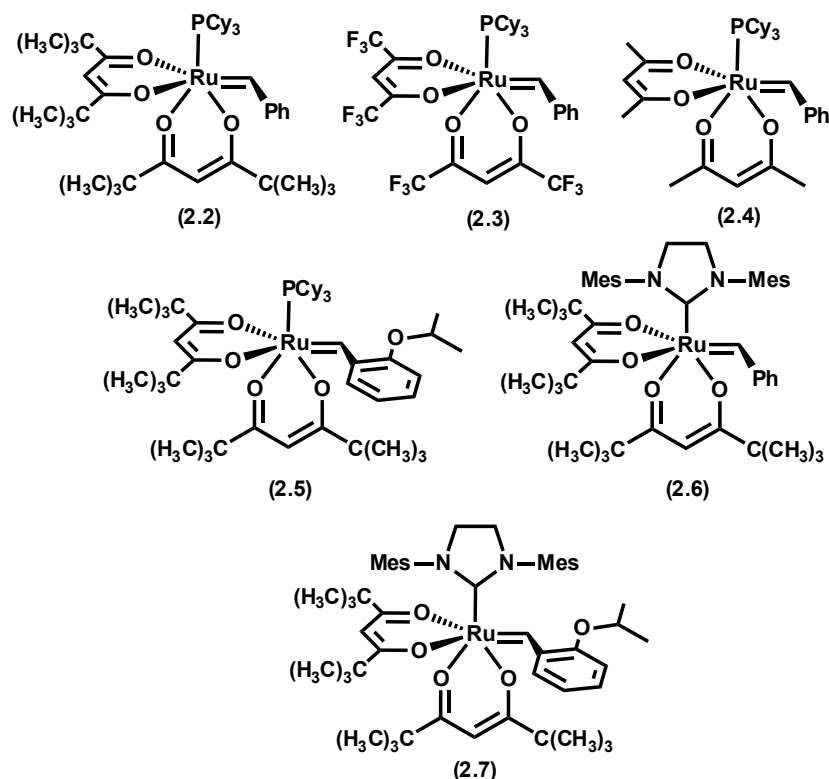


Figure 2.2. acac-containing latent metathesis catalysts. Mes = 2,4,6-trimethylbenzene

2.7 in the absence of acid, no conversion to the desired product (**2.9**) was observed. However, addition of 1 eq. of HCl (as a solution in diethyl ether) resulted in complete conversion to **2.9** within 30 min at room temperature (RT). A closer inspection of the RCM reaction revealed that the conversion profile of **2.8** to **2.9** is highly dependent on the amount of acid added and its relative strength (pK_a). For example, addition of 2 eq. of HCl led to faster formation of **2.9**, as did the use of stronger acids, such

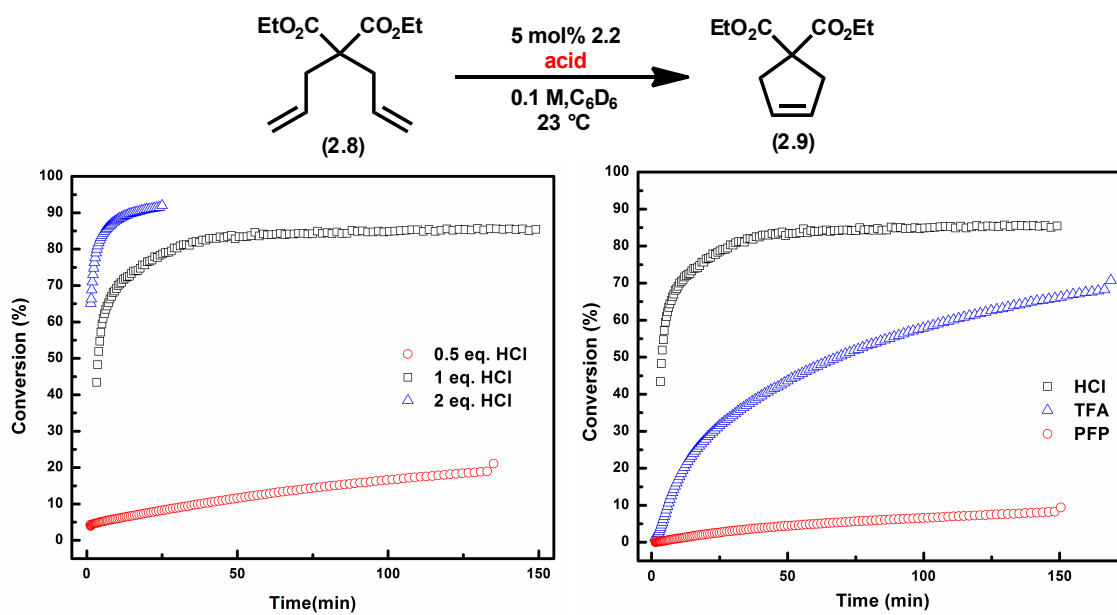


Figure 2.3. RCM of **2.8** to **2.9** with catalyst **2.2** with varying acid concentrations (left) and different acids (right). HCl = hydrochloric acid, TFA = trifluoroacetic acid, PFP = pentafluorophenol

as HCl versus TFA (Figure 2.3). Under our reaction conditions, the conversion of **2.8** was not amenable to simple kinetic analysis, which prevented a quantitative relationship between observed rates and concentration/ pK_a . Nevertheless, we were able to gain additional insight into the activation mechanism through the use of acids with noncoordinating conjugate bases. For example, tetrafluoroboric acid (HBF_4), despite its low pK_a , was unable to effectively activate **2.2**. This result suggests that nucleophilic attack by the conjugate base (e.g., Cl^-) is critical to catalyst activation (*vide infra*), an observation that is also consistent with the substitution of *acac* ligands on other metals.¹³ Overall, the above results suggest that acid plays a role in the rate-determining step of catalyst activation.

The RCM of **2.8** also allowed us to investigate the differences in reactivity between **2.2**–**2.7**. In general, when the *acac* ligand was kept constant (**2.2**, **2.5**, **2.6**,

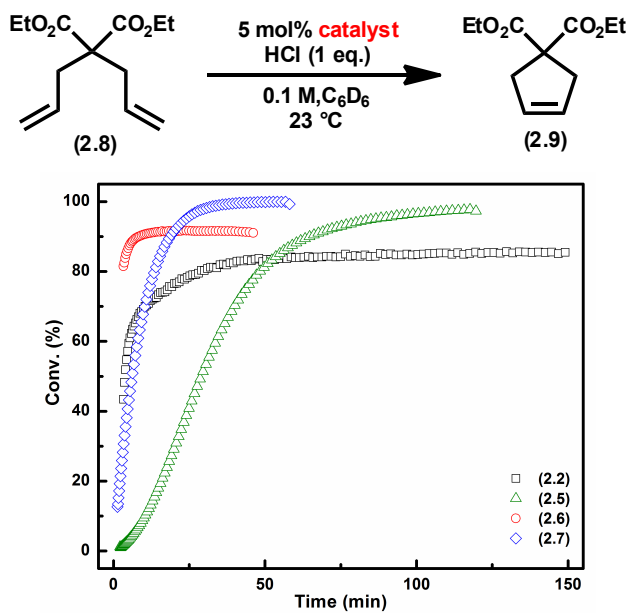


Figure 2.4. Comparison of catalysts **2.2**, **2.5**, **2.6**, and **2.7** in the RCM of **2.8** with 1 eq. HCl

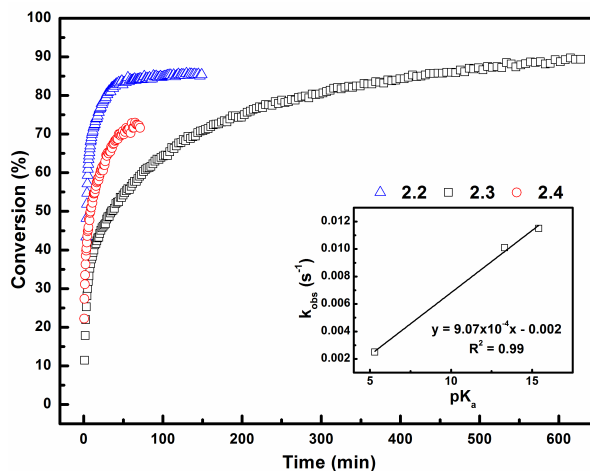


Figure 2.5. Comparison of catalysts **2.2**–**2.4** in the RCM of **2.8** with 1 eq. HCl. Linear plot of k_{obs} versus pK_a of *acac* ligand (inset)

and **2.7**), the trends in catalyst performance were reflective of the reactivity of the parent dichloride complexes (e.g., **2.1** for **2.2**) (Figure 2.4).¹⁴ However, an interesting trend appeared when the RCM of **2.8** was conducted with catalysts **2.2**–**2.4**. In these reactions, we were able to obtain first-order rate constants (k_{obs}) at early reaction times (initial rates). Plotting k_{obs} versus the pK_a of the conjugate acids of the *acac*

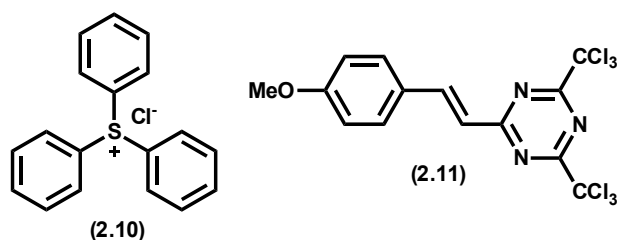
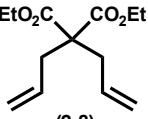
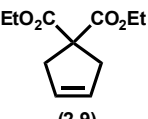
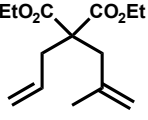
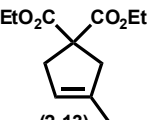
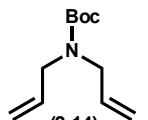
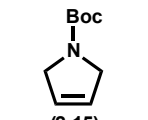
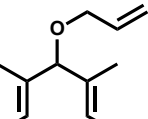
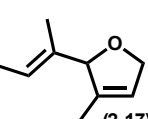


Figure 2.6. Photoacid generators (PAGs) **2.10** and **2.11**

Table 2.1. RCM with catalysts **2.2** and **2.6** with PAG **2.10**^a

Entry	Substrate	Product	Time, h	Catalyst	Conv., ^b %	Yield, ^c %
1	 <p>(2.8)</p>	 <p>(2.9)</p>	1	2.2	>95	77
			2	2.6	>95	83
2	 <p>(2.12)</p>	 <p>(2.13)</p>	1	2.2	55	42
			2	2.6	93	88
3	 <p>(2.14)</p>	 <p>(2.15)</p>	1	2.2	>95	70 ^d
			1	2.6	>95	93
4	 <p>(2.16)</p>	 <p>(2.17)</p>	3	2.2	47	23
			3	2.6	71	62

^a Reaction conditions were catalyst (**2.2** or **2.6**, 5 mol%) and **2.10** (10 mol%) in a quartz NMR tube with CD₂Cl₂ (0.1 M) and substrate. ^b Measured by ¹H NMR spectroscopy. ^c Isolated following column chromatography on silica gel. ^d Average yield over three runs

ligands in **2.2–2.4** revealed a linear trend consistent with acid involvement in the rate-determining step (Figure 2.5, inset). Qualitatively, hexafluoroacetylacetonate (**2.3**) is a weaker base (stronger conjugate acid) and thus, protonation of this ligand is more difficult compared to more electron-donating *acac*-type ligands (**2.2** and **2.4**). As a consequence of this effect, we are able to finely control the activity of the catalyst by adjusting either the pK_a of the exogenous acid or that of the *acac*-type ligand.

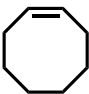
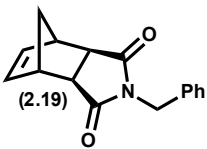
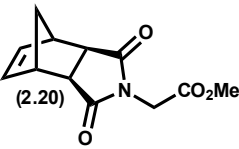
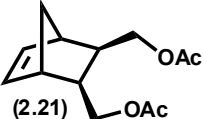
Having established the acid-activated nature of catalysts **2.2–2.7**, we

turned our attention to the use of photoacid generators (PAG) as sources of exogenous acid.¹⁵ The majority of PAGs used in applications such as photolithography generate acids with noncoordinating counter-ions;⁹ we desired a nucleophilic counterion having previously demonstrated that nucleophilic substitution is necessary to achieve catalyst activation. Therefore, PAGs **2.10** and **2.11** were selected for their ability to produce HCl upon irradiation with sub-300-nm light (Figure 2.6). Having selected appropriate PAGs, we examined the reactivity of our tandem activation system in RCM, since this reaction has been historically difficult for photo-activated metathesis catalysts.

The tandem system of PAG **2.10** and catalyst **2.2/2.6** was found to be very efficient in the RCM of **2.8**, reaching >95% conversion within 1 h of UV irradiation (Table 2.1, entry 1). Reactions run in the absence of UV light or PAG showed no metathesis activity, while irradiation of a solution containing only **2.10** and **2.2** or **2.6** resulted in eventual catalyst decomposition. For the RCM of **2.8**, the combination of catalyst **2.2** and PAG **2.11** was also effective, but required longer reaction times (ca. 2 h) to reach high conversions (80%), likely due to the lower quantum yield of **2.11** ($\Phi_f = 0.01^{16}$ compared to $\Phi_f = 0.6^{17}$ for **2.10**). More difficult RCM substrates, including tri-substituted olefins, cyclized in moderate conversion using PAG **2.10** (Table 1, entries 2 and 4). In these cases, catalyst **2.6** was found to be more active, which is consistent with the substitution of the phosphine in **2.2** with an N-heterocyclic carbene (NHC).¹⁸ Overall, the combination of PAG **2.10** and catalysts **2.2** and **2.6** was found to be very effective at the RCM of a variety of substrates.

Having established the effectiveness of PAG **2.10** at activating *acac*-

Table 2.2. ROMP of various monomers with catalysts **2.2** and **2.6** with PAG **2.10**^a

Entry	Monomer	Catalyst	Time, h	Conv., ^b %	Theo M _n , kDa	Exp M _n , ^c kDa	PDI ^c
1	 (2.18)	2.2	2	>95	2.2	13.9	1.38
		2.6	2	>95	2.2	8.5	1.56
2	 (2.19)	2.2	1	>95	5.2	57.5	1.33
		2.6	1	>95	5.8	127	1.25
3	 (2.20)	2.2	1	>95	4.7	59.9	1.44
		2.6	1	>95	4.9	157	1.29
4	 (2.21)	2.2/2.6	1	>95	4.6	- ^d	-

^a Reaction conditions were catalyst (5 mol%) and **2.10** (10 mol%) in a quartz NMR tube with CD₂Cl₂ (0.1 M) and substrate. ^b Determined by ¹H NMR spectroscopy. ^c Measured by multi-angle laser light scattering (MALLS) GPC. ^d Insolubility of polymer precluded GPC analysis

ligated catalysts for RCM, we turned our attention to ROMP. Many common ROMP monomers, such as norbornene derivatives and cyclooctene (**2.18**), underwent ROMP in excellent conversion using the combination of **2.2** and **2.10** (Table 2.2). Molecular weights (M_n), measured by GPC were consistently higher than predicted, which is indicative of incomplete catalyst initiation. Indeed, after irradiation for 2 h, a catalyst solution under ROMP reaction conditions displayed peaks in both ¹H and ³¹P NMR spectra characteristic of catalyst **2.2**. Integration relative to the free *acac* ligand in solution revealed that ca. 10% of the catalyst was activated during the reaction time, which is consistent with the higher M_n's obtained by GPC. It is worth noting that addition of excess HCl (as a solution in Et₂O) also resulted in incomplete catalyst activation. Thus, the

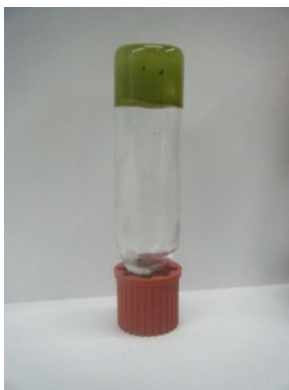


Figure 2.7. Quartz vial containing gel resulting from ROMP of **2.22** using catalyst **2.2** and PAG **2.10**

relatively small degree of catalyst activation is a result of limitations inherent to the *acac*-type ligand, and not a reflection of the efficiency of the PAG.

Despite the low degree of catalyst activation, we believed that the success of the tandem system in ROMP demonstrated its potential for industrial polymer molding applications. Therefore, with an eye toward potential industrial applications, we attempted to form a cross-linked solid from the ROMP of dicyclopentadiene (DCPD, **2.22**). Irradiation of a solution of **2.22**, **2.2**, and **2.10** in a minimal amount of CH_2Cl_2 (for solubility) resulted in complete gelation within 1 h (Figure 2.7). Attempted melting and solvation confirmed that the gel was not solidified monomer.

Having demonstrated the potential of the tandem system of acid-activated catalyst and PAG **2.10**, we focused on the nature of the active species. As was already discussed, the conjugate base of the activating acid was found to be critical in obtaining a highly active catalyst. This result implies that substitution of the *acac* ligands is an essential step in catalyst activation. To verify that the substitution process was occurring, we designed a trapping experiment for the active species, which consisted of irradiation of **2.2** in the presence of a reactive

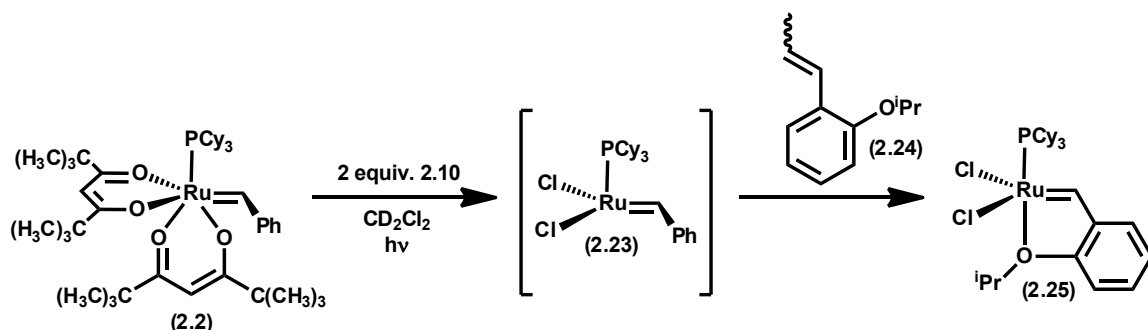


Figure 2.8. Trapping of reactive intermediate.

olefin (**2.24**) that would generate a stable catalyst upon cross-metathesis (**2.25**). Indeed, after a solution consisting of the preceding reagents was irradiated for 5 h, catalyst **2.25** was observed in both the ^1H and ^{31}P NMR spectra (Figure 2.8). This result indicates that at least one of the catalytically active species is the 14 electron complex **2.23**. Also recall the enhanced activity of catalyst **2.6** versus **2.2**; this result is also consistent with a 14 electron, dichloride active species. While the evidence for an active species such as **2.23** is strong, at this time we cannot rule out the presence of other active metathesis species which may be present in solution.¹⁹

Conclusion and Future Outlook

In summary, we have described a robust acid-activated catalytic system based on *acac*-ligated Ru-alkylidene complexes that are capable of both RCM and ROMP in good to excellent conversions. Mechanistic studies indicated that the identity of the exogenous acid and the electronics of the *acac* ligand play a critical role in catalyst activation. With this knowledge in hand, we were able to develop a photo-activated olefin metathesis system, via the use of a photoacid generator

(PAG) that was effective at RCM and ROMP. Notably, the combination of a PAG and acid-activated catalyst is not limited to *acac*-ligated complexes, but should be applicable to other acid-activated metathesis catalysts.⁷ For example, the acid activated catalyst can be modified to increase activity in addition to improving stability (especially towards O₂), latency, and ease of synthesis (see Chapter 3). Alternatively, the PAG may be modified to create a complex with improved solubility and a chromophore tuned to a specific wavelength of light. Exogenous sensitizers can also be added to further improve the sensitivity and quantum yield of the PAG.²⁰

Ruthenium Carbonyl Alkylidene Complexes

Introduction

The photo-induced dissociation of carbonyl (CO) ligands is a well-known reaction in coordination and organometallic chemistry.²¹ In general, a d-d transition populates a M-CO antibonding orbital (σ^*), which weakens the M-CO bond and results in favorable conditions for CO dissociation. We believed that this chemistry could be used to generate an open coordination site on a Ru metathesis catalyst and serve as the basis for a photo-activated catalyst system. However, a number of challenges are inherent to such an approach. First, Ru-CO complexes containing alkylidenes are relatively rare because CO coordination often induces C-H activation and subsequent insertion into the alkylidene.^{22,23} For example, Diver et al. has reported that exposure of Grubbs' 2nd generation catalyst (**2.26**) to an atmosphere of CO results in CO coordination followed by alkylidene insertion into

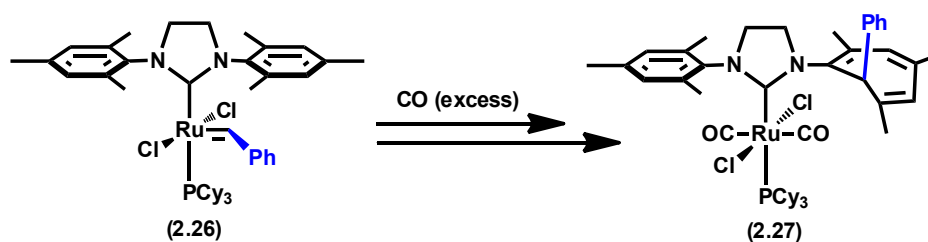


Figure 2.9. CO-induced insertion of alkylidene ligand into Mes substituent

the Mes substituent of the NHC (Figure 2.9).²⁴ A second problem arises from the fact that going from a 16 electron (e^-) complex, such as **2.26**, to an analogous CO-containing complex requires the generation of a cationic catalyst. This is the only viable approach since the alternative substitution of the phosphine ligand in **2.26** with CO was just shown to be infeasible. Fortunately, cationic Ru-based metathesis catalysts are known, although they are often less active than their neutral counterparts.²⁵ A final obstacle inherent to the use CO dissociation as a method for photo-activation is the fact that Ru^{2+} photochemistry is dominated by metal-to-ligand charge transfer (MLCT) transitions.²⁶ Despite this complication, and the others mentioned above, we believed that an investigation into the use of Ru-CO dissociation as the basis for a photo-activated metathesis system was a worthwhile endeavor.

Results and Discussion

The generation of alkylidene-containing cationic Ru^{2+} complexes via chloride abstraction in the presence of an L-type ligand (phosphine, pyridine, etc.) is well-known.²⁷ We believed that a similar approach could be used to generate a stable CO complex. Indeed, reaction of catalyst **2.26** with AgBF_4 at -78°C

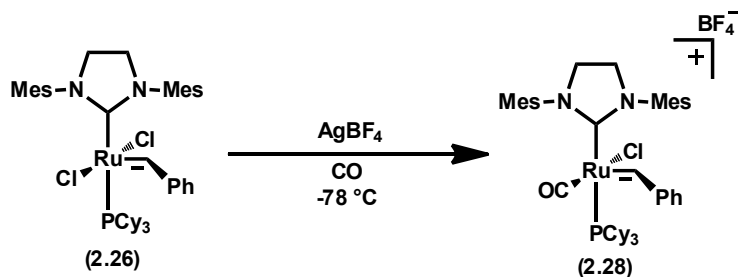


Figure 2.10. Preparation of CO complex **2.28**

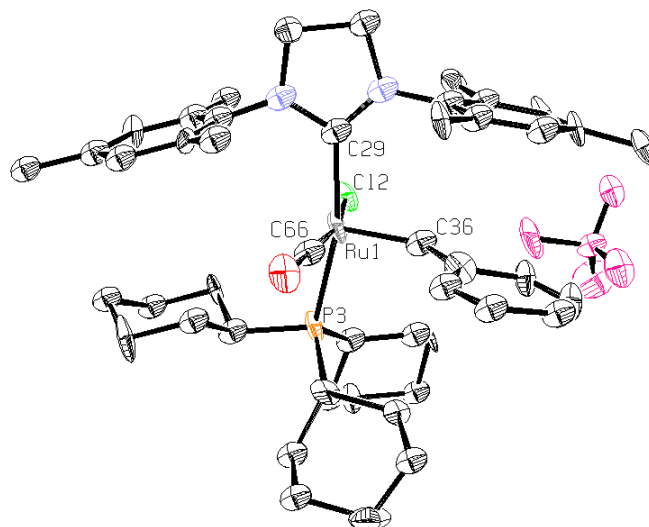


Figure 2.11. Solid-state structure of **2.28** with ellipsoids drawn at 50% probability. Selected bond lengths (Å) : Ru-C29 = 2.124, Ru-C36 = 1.881, Ru-C66 = 1.779, Ru-P3 = 2.427, Ru-C12 = 2.372

under an atmosphere of CO resulted in the isolation of a stable cationic Ru-CO complex (Scheme 4, **2.28**). Complex **2.28** possesses a single infrared (IR) CO stretch at 1961 cm^{-1} which shifts to 1915 cm^{-1} upon ^{13}CO isotopic substitution. This result is in good agreement with the shift to 1917 cm^{-1} predicted from a simple harmonic oscillator approximation. In C_6D_6 , the benzylidene resonance of **2.28** is observed at 15.75 ppm in the ^1H spectrum while a single resonance at 41 ppm is observed by ^{31}P NMR spectroscopy. Finally, the structure of **2.28** was confirmed by single-crystal x-ray diffraction (Figure 2.11). Curiously, the use of precursors

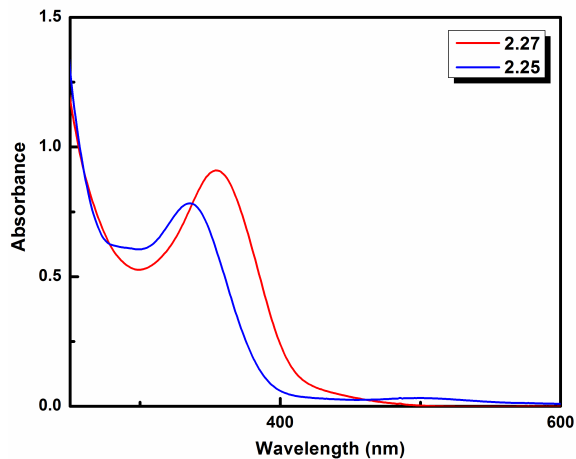


Figure 2.12. UV-vis spectrum of **2.26** and **2.28** in THF at RT

similar to **2.26** (e.g., **2.2**) did not result in the formation of stable CO complexes.

As expected, the UV-Vis spectra of **2.26** and **2.28** (in THF) are characterized by intense MLCT bands, which are assigned to a Ru→CHPh transition (Figure 2.12).¹⁸ The λ_{max} (354 nm) of **2.28** is slightly red-shifted with respect to the λ_{max} (336 nm) **2.26**, consistent with stabilization provided by the CO ligand. No ligand field transitions (d-d) in either **2.26** or **2.28** are obvious in Figure 2.12. Accordingly, UV irradiation of **2.28** produced no evidence of CO dissociation and the starting complex was recovered quantitatively. Irradiation in the presence of excess phosphine ligand (PCy₃) did not produce any bis-phosphine product. Our attempts to chemically induce CO dissociation using triethylamine oxide also failed, as did attempts to generate the neutral 18 e⁻ complex via reaction of **2.28** with a variety of halide salts. This latter result is particularly surprising, since the closely analogous (H₂IMes)(PCy₃)(CO)Cl₂Ru=CH(CHC(CH₃)₂) [H₂Imes = 1,3-dimesitylimidazolidine-2-ylidene] has been previously reported.²⁸ Interestingly, when **2.28** was reacted with MeLi followed by the alkylating agent Et₃O⁺BF₄⁻, complex **2.29** was recovered

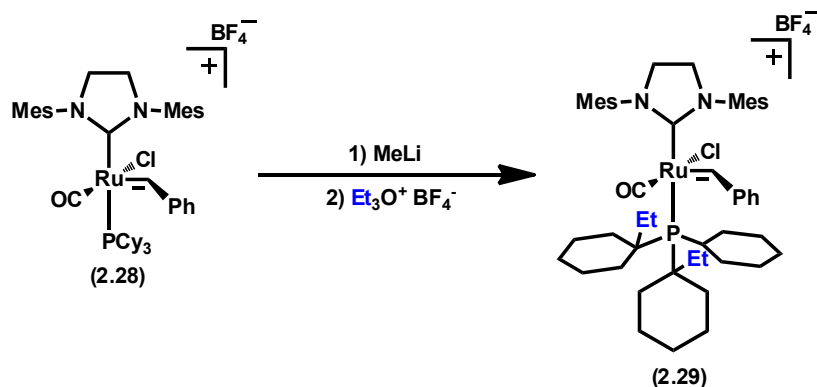


Figure 2.13. Reaction of **2.28** with MeLi followed by alkylating agent ($\text{Et}_3\text{O}^+\text{BF}_4^-$)

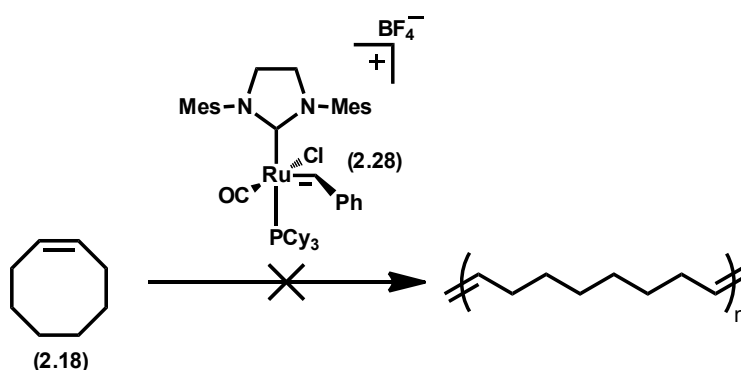


Figure 2.14. Failed ROMP reaction of **2.18** with **2.28**

(Figure 2.13). Complex **2.29** results from deprotonation at C1 of the cyclohexyl groups of PCy_3 and subsequent alkylation at this position. A similar transformation was observed by Piers et al. with a PMe_3 ligated tungsten carbyne complex.²⁹

Despite the lack of reactivity between **2.28** and various small molecules, we believed that it could potentially undergo traditional phosphine dissociation in order to enter the metathesis catalytic cycle. Unfortunately, under a variety of forcing conditions, no conversion to polymer was observed when a solution of ROMP monomer **2.18** was exposed to **2.28** (Figure 2.14).

Conclusion and Future Outlook

The preparation of a stable CO-containing Ru-alkylidene complex was described. This complex was prepared in an attempt to develop a photo-active metathesis catalyst based on photoinduced CO dissociation and represents a rare example of a stable Ru-CO carbene complex. Unfortunately, UV irradiation of the complex (**2.28**) did not result in CO dissociation or indeed, any change in the complex. Similarly, our efforts to use **2.28** as a catalyst for ROMP were also unsuccessful. Despite these setbacks, the preparation and stability of **2.28** demonstrates the feasibility of combining Ru-CO and Ru-carbene chemistry.

Experimental Section

General: All reactions unless otherwise specified were carried out in dry glassware under argon using standard Schlenk techniques or in a Vacuum Atmospheres Glovebox under a nitrogen atmosphere. Solvents were purified by passage through solvent purification columns and further degassed with bubbling argon. NMR solvents were dried over CaH_2 and vacuum transferred to a dry Schlenk flask and subsequently degassed with argon. Commercially available reagents were used as received with the following exceptions. Triphenylsulfonium chloride (**2.10**) was dissolved in CH_2Cl_2 , passed through a column of basic alumina and concentrated *in vacuo*. Diethyldiallylmalonate (**2.8**), cyclooctene (**2.18**), *t*-butyldiallyl carbamate (**2.14**), dicyclopentadiene (**2.21**), and diethyl 2-allyl-2-(2-methylallyl)malonate (**2.12**) were distilled prior to use. Norbornene monomers were prepared by modification of literature procedures. Triphenylsulfonium nonaflate was acquired from Midori

Kagaku Inc.¹H, ¹³C, and ³¹P spectra were recorded on a Varian Mercury 300 Spectrometer and the chemical shifts are reported in ppm relative to the appropriate solvent. High-resolution mass spectra were provided by the California Institute of Technology Mass Spectrometry Facility. Gel Permeation Chromatography was carried out in THF on two I-Series MBLMW ViscoGel columns (Viscotek) connected in series with a DAWN EOS multi-angle laser light scattering (MALLS) detector and an Optilab DSP differential refractometer. No standards were used, and dn/dc values were obtained for each injection by assuming 100% mass recovery from the columns. Photoreactions were performed in quartz glassware using a 450 W medium pressure mercury arc lamp (Hanovia PC4510-50) surrounded by a water cooled quartz jacket. The reaction vessel was positioned ca. 5 cm from the center of the irradiating lamp. In some cases, a handheld UV lamp typically used for TLC illumination was used as the light source. IR spectra were taken on a PerkinElmer Spectrum BX FT-IR (NaCl). X-ray quality crystals were grown as indicated. The crystals were mounted on a glass fiber with Paratone-N oil. X-ray diffraction studies were carried out in the Beckman Institute Crystallographic Facility on a Bruker Smart 1000 CCD diffractometer. Structures were determined using direct methods with standard Fourier techniques using the Bruker AXS software package.

Caution! Thallium complexes are extremely toxic and should be handled with extreme care.

Preparation of 2.2: In a glovebox, **2.1** (69 mg, 0.084 mmol) and 2,2,6,6-tetramethyl-3,5-heptanedionato thallium (65.6 mg, 0.168 mmol) were combined in a 20 mL scintillation vial and dissolved in 5 mL of benzene. The resulting green solution

was stirred at RT for 24 hours after which it was filtered through a plug of celite. CuCl (115 mg, 1.16 mmol) was added to the filtered solution and stirred for 2 h at room temperature. The solution was frozen at -30°C and the solvent sublimed off under vacuum after which the resulting green residue was dissolved in pentane, filtered through celite, and concentrated *in vacuo* to yield **2a** (54 mg, 77%) as a green powder. ^1H NMR (C_6D_6): δ 1.03 (s, 9H), 1.26 (br s, 20H), 1.38 (d, $J = 3.9$ Hz, 18H), 1.6–1.8 (m, 13H), 2.12 (br q, 9H), 5.32 (s, 1H), 5.99 (s, 1H), 7.24 (t, $J = 9$ Hz, 2H), 7.42 (t, $J = 9$ Hz, 1H), 8.46 (d, $J = 9$ Hz, 2H), 19.27 (d, $J = 12$ Hz, 1H). ^{13}C NMR (C_6D_6): δ 27.1, 29.0, 34.8, 41.5, 87.9, 90.8, 127.7, 128.7, 131.9, 154.1, 193.6, 195.2, 196.8, 199.0. ^{31}P NMR (C_6D_6): δ 39.12. HRMS (FAB+): calculated 838.4603, found 838.4617.

Preparation of 2.3: In a glovebox, **2.1** (50 mg, 0.061 mmol) and thallium (I) hexafluoroacetylacetonate (49 mg, 0.122 mmol) were dissolved in 3 ml of benzene and stirred at RT for 1 h. The reaction mixture was conc. and the resulting residue was dissolved in pentane and filtered after which CuCl (50 mg, 0.508 mmol) was added and the suspension stirred for 2 h. Finally, the solution was filtered and conc. to give **2.3** (40 mg, 74%) as a brown powder. ^1H NMR (C_6D_6): δ 0.94–2.02 (m, 33H), 5.95 (s, 1H), 6.57 (s, 1H), 7.19–7.28 (m, $J = 3$ Hz, 3H), 8.15 (d, $J = 9$ Hz, 2H), 18.91 (d, $J = 12$ Hz, 1H). ^{31}P NMR (C_6D_6): δ 42.3. HRMS (FAB+): Calculated 886.1594, found 886.1631.

Preparation of 2.4: In a glovebox, **2.1** (50 mg, 0.061 mmol) and thallium (I) acetylacetonate (36 mg, 0.120 mmol) were dissolved in 3 ml of benzene and stirred at RT for 2 h. The reaction was then worked up in a manner similar to catalyst **2.3**

above to yield **2.4** (29 mg, 81%) as a green powder. ^1H NMR (C_6D_6): δ 1.15–1.33 (m, 33H), 1.63 (s, 3H), 1.77 (s, 3H), 2.08 (s, 3H), 2.14 (s, 3H), 4.72 (s, 1H), 5.54 (s, 1H), 7.33 (t, J = 9 Hz, 2H), 7.44 (t, J = 9 Hz, 1H), 8.55 (d, J = 6 Hz, 2H), 19.32 (d, J = 12 Hz, 1H). ^{31}P NMR (C_6D_6): δ 38.92. HRMS (FAB+): Calculated 670.2725, found 670.2769.

Preparation of 2.5: In a glovebox, commercially available $(\text{PCy}_3)\text{Cl}_2\text{Ru}(\text{=CH-}o\text{-iPrPh})$ (50 mg, 0.083 mmol) and 2,2,6,6-tetramethyl-3,5-heptanedionato thallium (46 mg, 0.118 mmol) were combined in a 20 ml vial and dissolved in 2 ml of benzene. The vial was sealed and heated to 60°C for 10 h after which it was cooled to RT, filtered and conc. to a greenish-brown powder (49 mg, 67%). ^1H NMR (C_6D_6): δ 1.09 (d, J = 6 Hz, 3H), 1.27 (m, 12H), 1.70 (br s, 18H), 1.78 (br s, 18H), 2.06 (br d, J = 9 Hz, 3H), 2.13 (s, 3H), 2.18 (br s, 18H), 4.22 (q, J = 9 Hz, 1H), 4.75 (s, 1H), 5.59 (s, 1H), 6.62 (d, J = 9 Hz, 1H), 7.23 (t, J = 9 Hz, 1H), 7.54 (t, J = 9 Hz, 1H), 9.47 (d, J = 6 Hz, 1H), 19.95 (d, J = 15 Hz, 1H). ^{31}P NMR (C_6D_6): δ 40.53. HRMS (FAB+): Calculated 896.5022, found 896.5013.

Preparation of 2.6: In a glovebox, $(\text{H}_2\text{IMes})(\text{PCy}_3)\text{Cl}_2\text{Ru}(\text{=CHPh})$ (31 mg, 0.037 mmol) and 2,2,6,6-tetramethyl-3,5-heptanedionato thallium (27 mg, 0.069 mmol) were combined in a 20 mL scintillation vial and dissolved in 5 mL of benzene. The vial was sealed and heated to 60°C for ca. 1 h at which point the solution had turned green and a white precipitate had formed. After filtration through celite, CuCl (40 mg, 0.404 mmol) was added and the solution stirred for 2 h at RT. The solution was frozen at –30°C and the solvent sublimed off under vacuum after which the resulting green residue was dissolved in pentane, filtered through celite,

and concentrated *in vacuo* to yield **2.6** (24 mg, 80%) as a green crystalline solid. ^1H NMR (C_6D_6): δ 0.89 (s, 9H), 1.15 (s, 9H), 1.37 (s, 9H), 1.61 (br s, 9H), 1.86 (s, 3H), 1.99 (s, 3H), 2.06 (s, 3H), 2.59 (s, 3H), 2.62 (s, 3H), 2.66 (s, 3H), 3.45 (m, 4H), 6.03 (s, 1H), 6.37 (s, 1H), 6.781 (s, 2H), 6.86 (s, 2H), 7.04 (t, $J = 6$ Hz, 2H), 7.28 (t, $J = 6$ Hz, 1H), 8.14 (d, $J = 7.5$ Hz, 2H), 17.82 (s, 1H). ^{13}C NMR (C_6D_6): δ 18.7, 19.2, 20.2, 20.9, 21.4, 27.2, 28.5, 28.8, 29.6, 29.8, 31.0, 33.2, 41.2, 41.5, 41.9, 50.4, 51.9, 91.0, 129.0, 129.5, 130.0, 130.5, 131.0, 135.1, 137.1, 137.8, 138.2, 139.0, 140.6, 152.0, 197.2, 198.5, 222.4. HRMS (FAB+): calculated 864.4370, found 864.4397.

Preparation of 2.7: In a glovebox, $(\text{H}_2\text{IMes})\text{Cl}_2\text{Ru}(=\text{CH}-o\text{-iPrPh})$ (50 mg, 0.080 mmol) and 2,2,6,6-tetramethyl-3,5-heptanedionato thallium (62.4 mg, 0.159 mmol) were placed in a 20 ml vial and dissolved in 2 ml of benzene. The vial was sealed and heated to 60°C for 1.5 h. After cooling to room temperature, the reaction was worked up in a manner similar to that of **2.5** to give **2.7** (52 mg, 71%). ^1H NMR (C_6D_6): δ 0.68 (s, 18H), 1.21 (s, 18H), 1.34 (s, 18H), 1.94 (s, 3H), 2.63 (s, 3H), 3.30 (m, 4H), 3.94 (q, $J = 6$ Hz, 1H), 5.19 (s, 1H), 5.77 (s, 1H), 6.17 (d, $J = 6$ Hz, 1H), 6.52 (br s, 2H), 6.77 (br s, 3H), 7.20 (m, 1H), 9.72 (dd, $J = 3$ Hz, $J = 6$ Hz, 1H), 18.38 (s, 1H). HRMS (FAB+): Calculated 922.4798, found 922.4759.

General Kinetics Experiment: In a glovebox, an NMR tube was charged with substrate **2.8** (14 mg), and **2.2** (2 mg, 5 mol %). C_6D_6 (0.1 M) was added and the NMR tube was capped with a rubber septum and removed from the glovebox. Acid was then injected as a solution in organic solvent (1 M HCl in Et_2O) after which the tube was inverted once to insure proper mixing and immediately placed into a ready NMR spectrometer. The 'pad array' function was used to monitor the

progress of the reaction until no further conversion was observed.

Ring-Closing Metathesis Procedure: In a glovebox, a quartz NMR tube was charged with substrate **2.18** (14 mg), **2.2** (2 mg, 5 mol %), and **2.10** (1.6 mg, 10 mol %). CD_2Cl_2 (0.1 M) was added and the NMR tube was capped with a rubber septum and irradiated for 1 h at RT after which the conversion was determined via ^1H NMR spectroscopy. The contents of the tube were emptied and concentrated before purifying the product by column chromatography on silica gel.

Ring-Opening Metathesis Polymerization: In a glovebox, a quartz NMR tube was charged with **2.18** (13 mg), **2.2** (2 mg, 5 mol %), and **2.10** (1.6 mg, 10 mol %). CD_2Cl_2 (0.1 M, relative to substrate, 0.5–0.75 ml) was added and the NMR tube was capped with a rubber septum and irradiated for the duration indicated in Table 2 at RT during which time the solution changed color from green to orange/brown. The contents of the NMR tube were emptied into a vial and the solvent was removed under reduced pressure, after which the residue was dissolved in a minimal amount of THF and precipitated into cold MeOH (poly-(cylcooctene)) or cold 1:1 Et_2O /Hexanes (polynorbornenes). The precipitate was then collected by filtration and dried under vacuum for several hours.

Trapping Experiment Procedure: In a glovebox, a 20 ml scintillation vial was charged with **2.2** (12.7 mg, 0.015 mmol) and **2.10** (9 mg, 0.030 mmol). The contents of the vial were dissolved in 0.75 ml of CD_2Cl_2 and loaded into a quartz NMR tube which was then capped with a rubber septum. β -methyl-*o*-isopropoxystyrene, then **2.23** (53 mg, 0.3 mmol) was injected and the sample irradiated for 5 hours, after

which a ^1H NMR spectrum revealed the presence of catalyst **2.25**. The presence of **2.25** was also confirmed by ^{31}P NMR spectroscopy.

Preparation of 2.27: In a glovebox, a Schlenk was charged with AgBF_4 (12 mg, 0.030 mmol), a stirbar, and 4 ml of dry CH_2Cl_2 . The Schlenk flask was removed from the glovebox and cooled to -78°C . After reaching this temperature, carbon monoxide was bubbled through the solution using a needle and **2.27** (21 mg, 0.027 mmol) was added in one portion as a solution in 1 ml of dry CH_2Cl_2 . The solution immediately changed color from green to brown to yellow/orange within the span of about a minute. Once the solution had stopped changing color, the CO was turned off and the flask was opened to vacuum while warming to RT. Complex **2.27** was purified by column chromatography on TSI silica gel using 10% acetone in CH_2Cl_2 as the eluant. ^1H -NMR (CD_2Cl_2): δ 1.01 (br m, 18H), 1.62 (br m, 18H), 1.93 (s, 3H), 2.05 (s, 3H), 2.58 (s, 9H), 4.11 (m, 4H), 5.83 (s, 1H), 6.62 (s, 1H), 6.86 (s, 1H), 7.00 (s, 1H), 7.09 (s, 1H), 7.31 (s, 1H), 7.55 (s, 1H), 7.75 (t, $J = 6$ Hz, 1H), 8.35 (s, 1H), 15.75 (s, 1H). FT-IR: ν (cm^{-1}) = 2929.7, 2853.2, 2056.4, 1960.5, 1607.8, 1585.9, 1489.9, 1447.3, 1281.9, 1175.9, 1057.1. HRMS (FAB+): Calculated 841.3567, found 841.3566.

References

- (1) (a) Szadkowska, A.; Grela, K. *Current Organic Chemistry* **2008**, 12, 1631 (b) Monsaert, S.; Lozano Vila, A.; Drozdak, R.; Van Der Voort, P.; Verpoort, F. *Chem. Soc. Rev.* **2009**, 38, 3360.
- (2) (a) Slugovc, C.; Bartscher, D.; Stelzer, F.; Mereiter, K. *Organometallics* **2005**,

24, 2255. (b) Ung, T.; Hejl, A.; Grubbs, R. H.; Schrodi, Y. *Organometallics* **2004**, 23, 5399. (c) Hejl, A.; Day, M. W.; Grubbs, R. H. *Organometallics* **2006**, 25, 6149. (d) Thomas, R. M.; Fedorov, A.; Keitz, B. K.; Grubbs, R. H. *Organometallics* **2011**, 30, 6713.

(3) (a) Delaude, L.; Demonceau, A.; Noels, A. F. *Chem. Comm.* **2001**, 986. (b) Delaude, L.; Szypa, M.; Demonceau, A.; Noels, A. F. *Adv. Syn. Catal.* **2002**, 344, 749. (c) Zhang, Y.; Wang, D.; Lonnecke, P.; Scherzer, T.; Buchmeiser, M. R. *Macromolecular Symposia* **2006**, 236, 30. (d) Wang, D.; Wurst, K.; Knolle, W.; Decker, U.; Prager, L.; Naumov, S.; Buchmeiser, M. R. *Angew. Chem., Int. Ed.* **2008**, 47, 3267.

(4) (a) van der Schaaf, P. A.; Hafner, A.; Muehlebach, A. *Angew. Chem., Int. Ed.* **1996**, 35, 1845. (b) Tarasov, A. L.; Shelimov, B. N.; Kazansky, V. B. *Kinetics and Catalysis (Translation of Kinetika i Kataliz)* **1998**, 39, 86.

(5) Subbotina, I. R.; Shelimov, B. N.; Kazansky, V. B. *Kinetics and Catalysis (Translation of Kinetika i Kataliz)* **1997**, 38, 678.

(6) Tarasov, A. L.; Shelimov, B. N.; Kazansky, V. B.; Mol, J. C. *J. Mol. Cat. A : Chem.* **1997**, 115, 219.

(7) (a) Lynn, D. M.; Mohr, B.; Grubbs, R. H. *J. Am. Chem. Soc.* **1998**, 120, 1627. (b) Sanford, M. S.; Henling, L. M.; Grubbs, R. H. *Organometallics* **1998**, 17, 5384. (c) Sanford, M. S.; Henling, L. M.; Day, M. W.; Grubbs, R. H. *Angew. Chem. Int. Ed.* **2000**, 39, 3451. (d) Hahn, F. E.; Paas, M.; Fröhlich, R. *J. Organomet. Chem.* **2005**, 690, 5816. (e) Gulajski, L.; Michrowska, A.; Bujok, R.; Grela, K. *J. Mol. Cat. A—Chem.* **2006**, 254, 118. (f) Gawin, R.; Makal, A.; Wozniak, K.; Mauduit, M.; Grela,

- K. *Angew. Chem. Int. Ed.* **2007**, *46*, 7206. (g) P'Pool, S. J.; Schanz, H. J. *J. Am. Chem. Soc.* **2007**, *129*, 14200. (h) Balof, S. L.; Yu, B.; Lowe, A. B.; Ling, Y.; Zhang, Y.; Schanz, H.-J. *Eur. J. Inorg. Chem.* **2009**, *2009*, 1717. (i) Dunbar, M. A.; Balof, S. L.; Roberts, A. N.; Valente, E. J.; Schanz, H. J. *Organometallics* **2011**, *30*, 199.
- (8) Piermattei, A.; Karthikeyan, S.; Sijbesma, R. P. *Nat. Chem.* **2009**, *1*, 133.
- (9) Ito, H.; Willson, C. G. *ACS Symposium Series* **1984**, *242*, 11.
- (10) Zhang, Y.; Wang, D.; Lonnecke, P.; Scherzer, T.; Buchmeiser, M. R. *Macromolecular Symposia* **2006**, *236*, 30.
- (11) Yao, Z.; Zhou, L. W.; Dai, B. B.; Cao, K. *J. Appl. Poly. Sci.* **2012**, *125*, 2489.
- (12) Wilson, G. O.; Caruso, M. M.; Reimer, N. T.; White, S. R.; Sottos, S. R.; Moore, J. S. *Chem. Mater.* **2008**, *20*, 3288.
- (13) Vicente, J.; Chicote, M. T. *Coord. Chem. Rev.* **1999**, *193–5*, 1143.
- (14) Vougioukalakis, G. C.; Grubbs, R. H. *Chem. Rev.* **2010**, *110*, 1746.
- (15) Keitz, B. K.; Grubbs, R. H. *J. Am. Chem. Soc.*, **2009**, *131*, 2038.
- (16) (a) Pohlers, G.; Scaiano, J. C.; Sinta, R. *Chem. Mat.* **1997**, *9*, 3222. (b) Pohlers, G.; Scaiano, J. C.; Sinta, R.; Brainard, R.; Pai, D. *Chem. Mat.* **1997**, *9*, 1353.
- (17) Selvaraju, C.; Sivakumar, A.; Ramamurthy, P. *J. Photochem. Photobio. A—Chem.* **2001**, *138*, 213.
- (18) Sanford, M. S.; Love, J. A.; Grubbs, R. H. *J. Am. Chem. Soc.* **2001**, *123*, 6543.
- (19) Samec, J. S. M.; Grubbs, R. H. *Chem. Eur J.* **2008**, *14*, 2686.
- (20) (a) Crivello, J. V.; Lam, J. H. W. *J. Poly. Sci. A—Poly. Chem.* **1978**, *16*, 2441. (b) Dektar, J. L.; Hacker, N. P. *J. Am. Chem. Soc.* **1990**, *112*, 6004.
- (21) Miessler, G. L.; Tarr, D. A. *Inorganic Chemistry*, 3rd ed.; Pearson-Prentice

Hall: Upper Saddle River, New Jersey, 2004, p. 183.

(22) (a) Gallop, M. A.; Roper, W. R. *Adv. Organomet. Chem.* **1986**, 25, 121. (b) Boyd, L. M.; Clark, G. R.; Roper, W. R. *J. Organomet. Chem.* **1990**, 397, 209.

(23) (a) Hong, S. H.; Chlenov, A.; Day, M. W.; Grubbs, R. H. *Angew. Chem. Int. Ed.* **2007**, 46, 5148. (b) Hong, S. H.; Day, M. W.; Grubbs, R. H. *J. Am. Chem. Soc.* **2004**, 126, 7414. (c) Hong, S. H.; Wenzel, A. G.; Salguero, T. T.; Day, M. W.; Grubbs, R. H. *J. Am. Chem. Soc.* **2007**, 129, 7961.

(24) Galan, B. R.; Pitak, M.; Gembicky, M.; Keister, J. B.; Diver, S. T. *J. Am. Chem. Soc.* **2009**, 131, 6822.

(25) (a) Fürstner, A.; Liebl, M.; Lehmann, C. W.; Picquet, M.; Kunz, R.; Brunaeu, C.; Touchard, D.; Dixneuf, P. H. *Chem. Eur. J.* **2000**, 6, 1847. (b) Wang, D.; Wurst, K.; Knolle, W.; Decker, U.; Prager, L.; Naumov, S.; Buchmeiser, M. R. *Angew. Chem. Int. Ed.* **2008**, 47, 3267. (c) Zirngast, M.; Pump, E.; Leitgeb, A.; Albering, J. H.; Slugovc, C.; Albering, H. *Chem. Comm.* **2011**, 5.

(26) (a) Vlcek, A. *Coord. Chem. Rev.* **1998**, 177, 219. (b) Campagna, S.; Puntoriero, F.; Nastasi, F.; Bergamini, G.; Balzani, V. *Photochem. Photophys. Coord. Comp.* **2007**, 280, 117.

(27) Sanford, M. S.; Henling, L. M.; Grubbs, R. H. *Organometallics* **1998**, 17, 5384.

(28) Sanford, M. S. Ph.D. Thesis, Caltech, 2001.

(29) van der Eide, E. F.; Piers, W. E.; Parvez, M.; McDonald, R. *Inorg. Chem.* **2007**, 46, 14.

Chapter 3

Preparation and Reactivity of Mesoionic Carbene (MIC)–Containing Ruthenium Metathesis Catalysts and their Acid-Activated Behavior

The text in this chapter is reproduced in part with permission from:

Bouffard, J.; Keitz, B. K.; Tonner, R.; Guisado-Barrios, G.; Frenking, G.; Grubbs, R. H.; Bertrand, G. *Organometallics* **2011**, 30, 2617.

Keitz, B. K.; Bouffard, J.; Bertrand, G.; Grubbs, R. H. *J. Am. Chem. Soc.* **2011**, 133, 8498.

Copyright 2011 American Chemical Society

Abstract

The preparation of mesoionic carbenes (MICs) from the cycloaddition of 1,3-diaza-2-azoniaallenes and alkynes is described, as is their use as ligands in ruthenium olefin metathesis catalysts. These MIC-ligated catalysts displayed reactivities in ring-opening metathesis polymerization (ROMP) and ring-closing metathesis (RCM) comparable to that of their N-heterocyclic carbene (NHC)-based counterparts.

Specific MICs exhibited unique protonolysis behavior, which resulted in dissociation of the MIC from the ruthenium center. Taking advantage of this phenomenon, we describe the development of extremely stable and reactive acid-activated metathesis catalysts. Detailed mechanistic studies on the activation mechanism and reactivity comparisons to previously reported metathesis catalysts are also presented.

MIC-Based Ruthenium Olefin Metathesis Catalysts

Introduction

Like many organometallic complexes, the activity and stability of ruthenium metathesis catalysts depends on the nature of the ligands connected to the metal.¹ For instance, the identity of the dissociating ligand, whether a phosphine (**3.2**) or oxygen (**3.3**) has a significant effect on catalyst stability by enabling or disabling specific decomposition pathways.² Similarly, the ligand that remains attached to the metal throughout the catalytic cycle has a significant effect on catalyst initiation, propagation, and selectivity (Chapters 4 and 5).³ As a specific

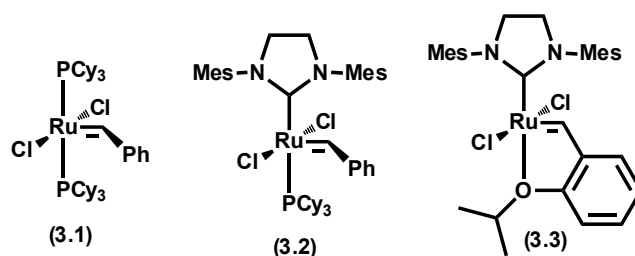


Figure 3.1. Common ruthenium olefin metathesis catalysts. Mes = 2,4,6-trimethylbenzene

example, consider the reactivity differences between catalysts **3.1** and **3.2**. The phosphine-containing catalyst **3.1** initiates much faster (large k of phosphine dissociation) than the NHC-based catalyst **3.2** (small k of phosphine dissociation), yet **3.2** is considerably more active. The explanation is that **3.2** has a much higher preference for olefin binding compared to **3.1**, and thus appears to react faster. From this result, as well as those presented in the following chapters of this thesis, it is clear that the L-type ligand has a significant effect on catalyst activity. Thus, despite the difficulties in quantitatively relating the properties of this ligand to catalyst properties,⁴ it has become a favored target for catalyst optimization.⁵

Among NHC-type ligands (Figure 3.2), many sub-types have been explored in the context of metathesis chemistry, including saturated/unsaturated (**3.4**),⁶ abnormal (aNHCs, **3.6**),⁷ and cyclic alkyl amino carbenes (CAACs, **3.5**).⁸ Abnormal NHCs, where the carbene center is not adjacent to a donor atom (e.g., nitrogen), are part of a larger subclass of NHCs termed mesoionic carbenes (MICs, **3.6** and **3.7**). Their name is derived from the fact that a canonical resonance form of the carbene cannot be drawn without the introduction of formal charges.⁹ While MICs based on imidazolium salts (two nitrogen atoms in the ring) and their metal complexes are well known,¹⁰ triazolium-derived MICs (containing three nitrogen

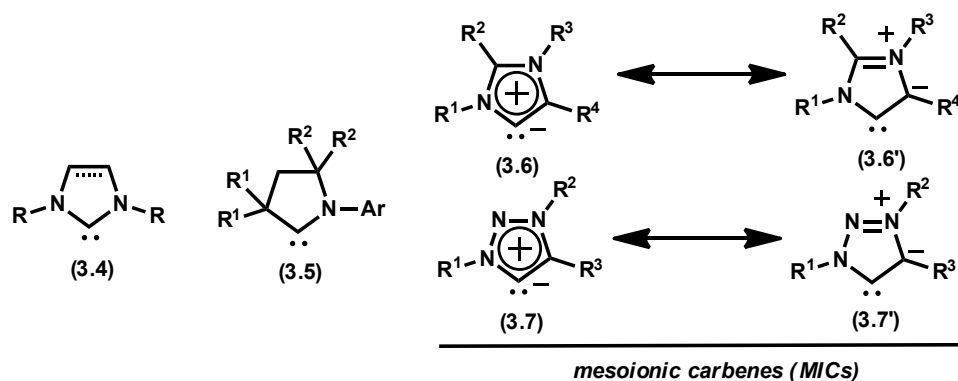


Figure 3.2. Various stable carbene species including traditional N-heterocyclic carbenes (NHCs, **3.4**), cyclic-alkyl amino carbenes (CAACs, **3.5**), and mesoionic carbenes (MICs, **3.6** and **3.7**)

atoms in the ring) are less common, despite their availability from Cu-catalyzed azide-alkyne cycloaddition ('click') chemistry. However, the Bertrand group has recently reported the facile preparation of stable, triazolium-derived MICs and their incorporation into simple metal complexes.¹¹ The distinct electronic properties of these carbenes, mainly their greater σ -donation and decreased π -accepting ability (compared to **3.6**), along with their reduced susceptibility to decomposition via dimer formation made them attractive targets for incorporation into metathesis catalysts.¹² Thus, in this chapter, we describe the preparation and activity of ruthenium metathesis catalysts containing stable MICs. We also demonstrate that certain MICs undergo facile protonolysis when attached to the ruthenium center, and that this ability can be used as the basis for an acid-activated metathesis catalyst.

Results and Discussion

As previously mentioned, triazolium salt precursors to carbenes like **3.7** can

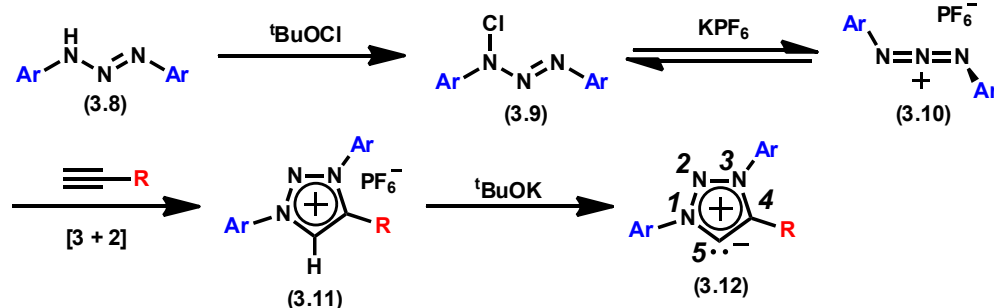


Figure 3.3. Preparation of 1,3-diaryl-1,2,3-triazolium salts (**3.11**) via the [3+2] cycloaddition of triazenes (**3.10**) with terminal alkynes and their deprotonation to give stable MICs (**3.12**)

be readily prepared by click chemistry followed by alkylation at the N3 position. Unfortunately, the 1,3-*dialkyl*-1,2,3-triazolium salts that are most amenable to this chemistry do not give stable MICs upon deprotonation. As a result, they are challenging to incorporate into organometallic complexes. In contrast, the Bertrand group has recently reported that *diaryl* triazolium salts yield stable and isolable MICs upon deprotonation at low temperature with potassium *tert*-butoxide (KO^tBu).¹¹ While these salts cannot be prepared through traditional Click chemistry, they are readily synthesized from the cycloaddition of chlorotriazenes and alkyne or alkyne equivalents (vinyl halides) (Figure 3.3). Using this methodology, a wide variety of differentially substituted MICs were prepared and fully characterized by ^1H and ^{13}C NMR spectroscopy. Their electronic structure was also studied using density functional theory (DFT).¹³ Thus, having established the synthesis and electronic structure of several MICs, we turned our attention to their application as ligands in ruthenium olefin metathesis catalysts.

Free MICs of the type **3.12** bearing flanking aryl groups of varying steric demand were selected for the synthesis of new metathesis catalysts via simple

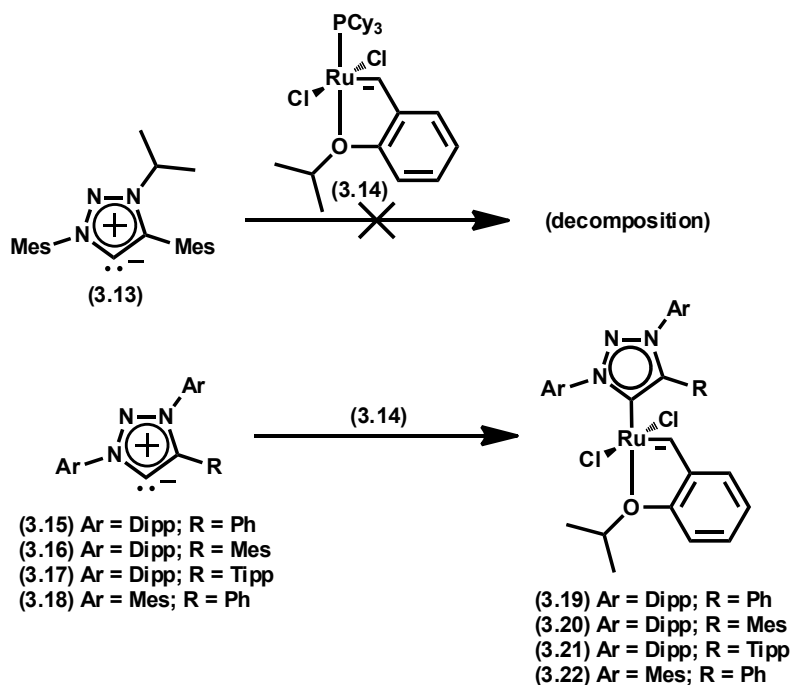


Figure 3.4. Synthesis of ruthenium complexes (**3.19-3.22**) via ligand substitution with MICs (**3.15-3.18**). Dipp = 2,6-diisopropylphenyl, Tipp = 2,4,6-triisopropylphenyl

ligand substitution of **3.14**. The new complexes represent MIC-based analogues of the standard NHC-based metathesis catalysts (e.g., **3.3**). Early attempts using the MIC **3.13** alkylated at N3 resulted in complete decomposition of **3.14** as evidenced by the disappearance of the benzyldiene ¹H resonance. Gratifyingly, the use of more robust MICs arylated at N3 (**3.15-3.18**) provided the desired catalysts (**3.19-3.22**). For example, combining a free MIC with complex **3.14** in benzene resulted in complete consumption of the starting ruthenium catalyst within a few hours. The resulting catalysts were isolated by recrystallization from CH₂Cl₂-pentane (**3.19**, **3.20**, **3.22**) or pentane (**3.21**) at -30 °C without the need for column chromatography. Complexes **3.19-3.22** were found to decompose relatively quickly in solution (within 6 h) upon exposure to oxygen, but were indefinitely

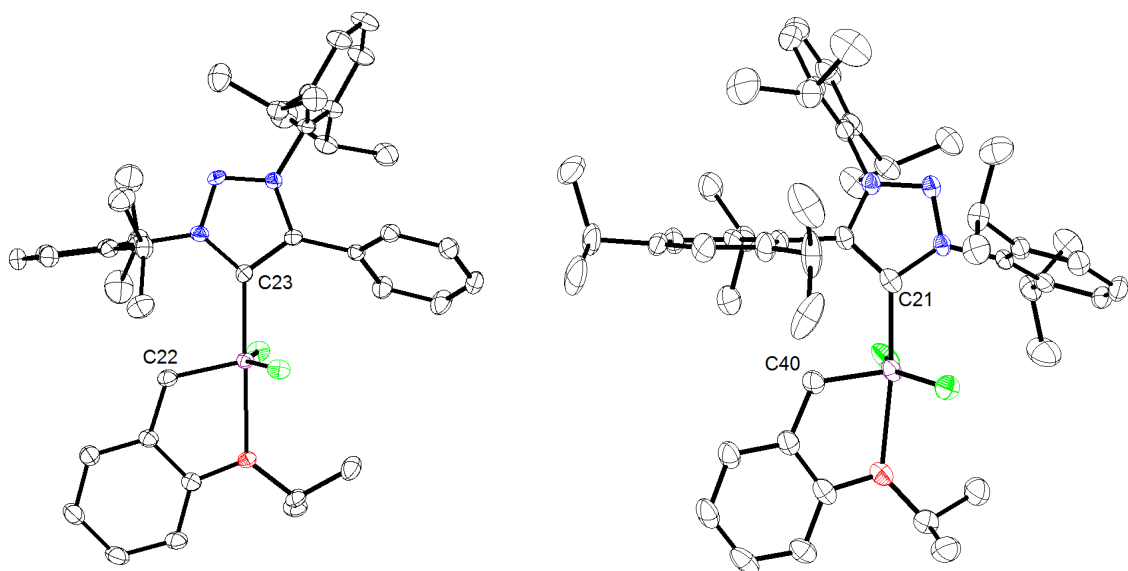


Figure 3.5. Solid-state structures of **3.19** (left) and **3.21** (right) with 50% thermal ellipsoids. Selected bond lengths (Å) for **3.19**: C23-Ru: 1.9913(1), C22-Ru: 1.8235(1), O-Ru: 2.2696(1). For **3.21**: C21-Ru: 1.9852(1), C40-Ru: 1.8157(1), O-Ru: 2.3176(1)

stable in the solid state under an inert atmosphere. NMR spectroscopy studies on the ligand displacement reaction with **3.14** indicated that a MIC-phosphine complex where the MIC initially displaces the chelating ether moiety in **3.14** was formed before subsequently yielding the desired complex.¹⁴ This intermediate usually persisted for several hours before forming the desired complex (*vide infra*).

Complexes **3.19** and **3.21** were characterized by single-crystal x-ray diffraction (Figure 3.5) after crystallizing from slow evaporation of a saturated CH_2Cl_2 solution. The bond lengths in **3.19** and **3.21** are very similar to those found in **3.3**. For example, the MIC carbon – Ru bond length (1.99 Å versus 1.98 Å in **3.3**), the benzylidene C – Ru bond length (1.82 Å versus 1.82 Å) and the O – Ru bond length (2.27 Å versus 2.26 Å) are largely conserved across the three species.¹⁵ Notably, the smaller aryl substituent (on C4 in **3.19** and N1 in **3.21**) is positioned above the

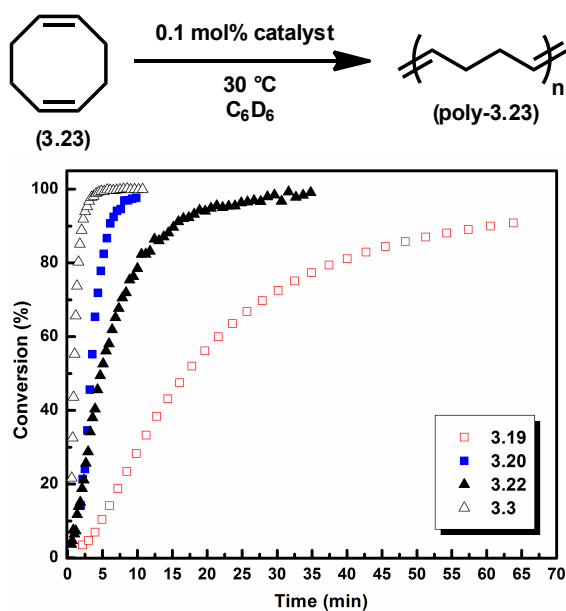


Figure 3.6. ROMP of cyclooctadiene (**3.23**) with MIC-catalysts **3.19**, **3.20**, and **3.22**

Table 3.1. Comparison of activation parameters for catalysts **3.19**–**3.22**^a

Catalyst	ΔG^\ddagger , kcal·mol ⁻¹	ΔH^\ddagger , kcal·mol ⁻¹	ΔS^\ddagger , eu
3.19	21.6 ± 0.8	12.1 ± 0.5	-31.9 ± 1.5
3.20	20.2 ± 0.2	13.5 ± 0.8	-22.5 ± 2.7
3.21	23.5 ± 0.1	13.6 ± 0.6	-33.0 ± 1.9
3.22	20.8 ± 0.3	14.6 ± 0.5	-21 ± 1.6

^a Conditions: catalyst (0.003 mmol), butyl vinyl ether (0.09 mmol, 0.15 M) in d₈-toluene at varying temperatures

Cl-Ru-Cl plane in order to minimize steric interactions with the chlorines, while the large substituent is positioned above the benzylidene.¹⁶ Thus, in the solid state, **3.19** and **3.21** exist as distinct rotamers. For the most part, the crystal structures of the MIC catalysts were unremarkable and did not provide any insight into their reactivity.

To evaluate the catalytic activity of the MIC-catalysts, they were subjected to several standard metathesis screens.¹⁷ Catalysts **3.19**, **3.20**, and **3.22** showed good ring-opening metathesis polymerization (ROMP) activity (Figure 3.6), while

catalyst **3.21** reached only low conversions, even after a period of several days. Comparing the ROMP conversion profiles of MIC-based catalysts to standard catalyst **3.3** revealed a few similarities and differences. For instance, **3.20** displayed a very similar conversion profile to **3.3**, while **3.22** is slightly slower, but still relatively fast, and **3.19** is much slower, although it does reach 100% conversion after ca. 1 h.

The most surprising result is the difference in reactivity between catalysts **3.19** and **3.20**, since the only distinction between the two is the substitution of a Mes group for a phenyl at C4. We hypothesized that the observed behavior might be largely due to a difference in initiation rates, and in order to probe this, we constructed several Eyring plots for the reaction of each catalyst with butyl vinyl ether.^{2,18} The results of the initiation parameters are given in Table 3.1. Catalysts **3.19–3.22** all exhibited a negative entropy of activation (ΔS^\ddagger), which is consistent with an associative or associative interchange mechanism previously reported for catalysts incorporating a Hoveyda-type chelate (e.g., **3.3**).¹⁹

Interestingly, while **3.19** and **3.21** were found to have very similar activation entropies, catalysts **3.20** and **3.22** different by ca. 10 entropy units (eu) from these. Furthermore, the activation enthalpy (ΔH^\ddagger) for **3.19** was found to be lower than that of **3.20**. Nevertheless, a 1.4 kcal·mol⁻¹ difference in the free energy of activation (ΔG^\ddagger) between **3.19** and **3.20** was observed when combining the ΔH^\ddagger and ΔS^\ddagger parameters at RT. This difference accounts nicely for the observed variations in initiation while also explaining the almost complete inactivity of catalyst **3.21** at RT. Unfortunately, while it is clear that sterics play a significant role in catalyst initiation and activity, so far a quantitative structural model that accounts for the observed

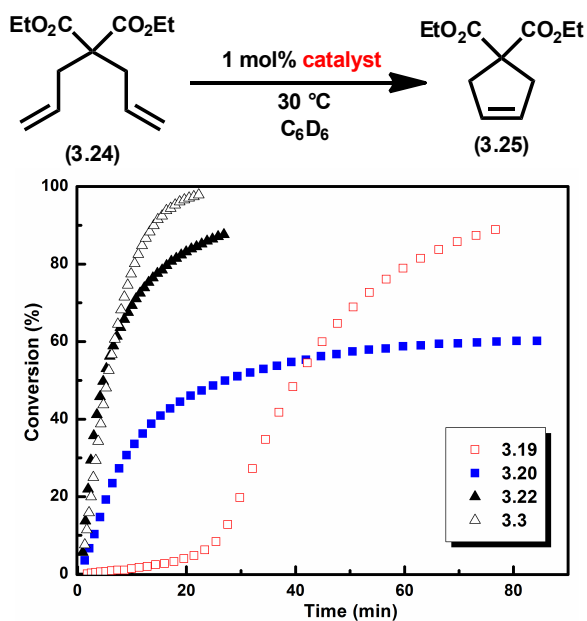


Figure 3.7. RCM performance of catalysts **3.19**, **3.20**, **3.22**, and **3.3**

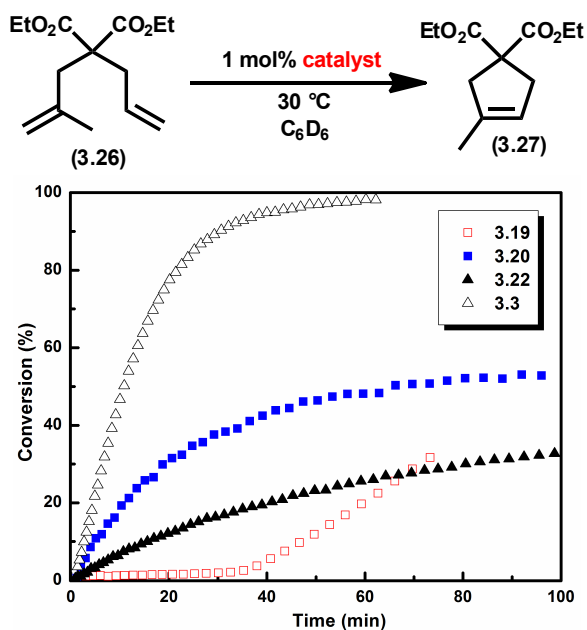


Figure 3.8. Trisubstituted RCM performance of catalysts **3.19**, **3.20**, **3.22**, and **3.3**

differences in initiation, particularly between **3.19** and **3.20**, has eluded us.¹³

Following our initiation rate studies, the performance of each catalyst in ring-closing metathesis (RCM) was assessed. Again, catalyst **3.21** was

found to be almost completely inactive at 30 °C. The other catalysts displayed conversion profiles consistent with their initiation activation energies. For instance, **3.20** shows a fast increase in conversion followed by a plateau that most likely results from catalyst decomposition. On the other hand, catalyst **3.19** exhibits an induction period characteristic of slow initiation followed by a gradual increase toward 100% conversion. Notably, even though **3.19** initiates at a slower rate than **3.20**, it is able to reach 100% conversion under the examined conditions while **3.20** is not. The best performing MIC-catalyst in the RCM assay was **3.22**, which displayed fast initiation and good stability throughout the reaction. In fact, **3.22** closely matched the performance of **3.3**.

To further examine the differences in reactivity between the catalysts, trisubstituted RCM was attempted (Figure 3.8). As expected, **3.19** and **3.20** exhibited the same relative behavior as stated above, with **3.19** displaying a lengthy induction period, while **3.20** began conversion to product almost immediately. Catalyst **3.20** reached a maximum conversion of ca. 50% while **3.19** was able to reach 100% conversion after a period of ca. 16 h. These results confirm that not only does the change from Ph (**3.19**) to Mes (**3.20**) have a profound effect on the initiation rate but it also impacts the relative stability of the catalysts. Catalyst **3.22** was relatively sluggish over the time period examined but was able to reach 100% after ca. 24 h at 30 °C. Overall, in the trisubstituted RCM assay, the MIC-based catalysts were clearly inferior to **3.3**, in contrast to the previous assays, where they displayed similar activity.

Conclusion and Future Outlook

The enhanced stability of N-arylated MICs allowed for the preparation of new ruthenium olefin metathesis catalysts via simple ligand substitution. These catalysts were proficient at the ROMP of cyclic olefins and at RCM reactions leading to both di- and trisubstituted cyclic olefins. In general, the catalytic properties of the MIC-Ru complexes, in particular with respect to their rates of initiation and resistance to deactivation, were found to be strongly influenced by the nature of the MIC substituents and in several cases rivaled the performance of well-established NHC-based ruthenium metathesis catalysts. In conclusion, the combination of their practical, versatile, and modular preparation, enhanced stability, and the demonstration of their effectiveness in a catalytic setting foreshadows the development of MIC transition metal complexes for numerous catalytic applications, including olefin metathesis.

Acid-Activated, MIC-Based Ruthenium Metathesis Catalysts

Introduction

The motivation behind the preparation of latent metathesis catalysts was discussed in Chapter 2. In that chapter, several examples of catalysts that relied on protonation and subsequent displacement of a labile ligand in order to generate an active species were presented. Unfortunately, these catalysts were oxygen-sensitive and could only be prepared with toxic metal salts. In order to address these deficiencies, we sought to prepare superior acid-activated catalysts based on a bis-NHC motif. Here, we report that ruthenium complexes incorporating a

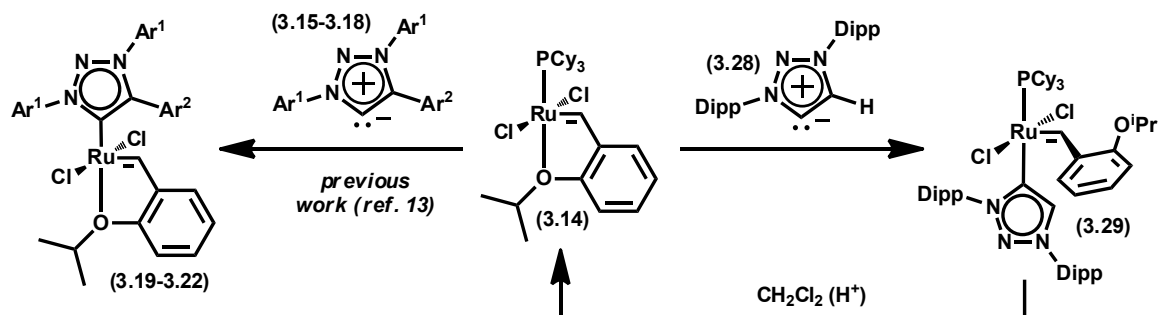


Figure 3.9. Initial discovery of acid-induced dissociation of MIC **3.28** from **3.29** (Dipp = 2,6-diisopropylphenyl)

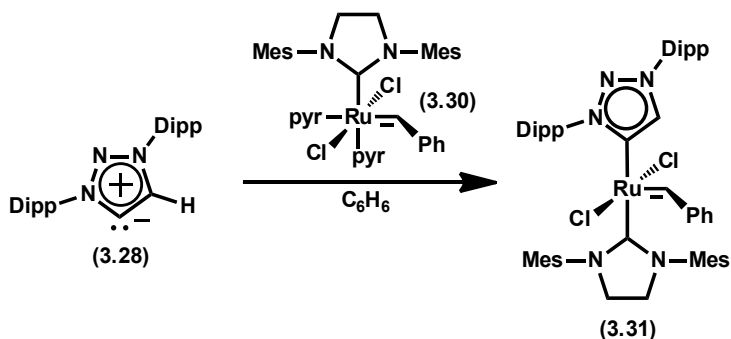


Figure 3.10. Preparation of **3.31** from MIC **3.28** and **3.30**. pyr = pyridine

traditional NHC and a MIC (see above) may be activated by the addition of a Brønsted acid. The resulting catalyst combines the stability and latency of bis-NHC complexes while maintaining low activation temperatures. Furthermore, we demonstrate that in some reactions, the performance of this catalyst surpasses that of the best commercially available catalysts (e.g., **3.3**).

Results and Discussion

Previously in this chapter, we reported the synthesis and activity of ruthenium olefin metathesis catalysts bearing MICs (**3.19–3.22**) in place of more traditional NHCs (Figure 3.4). In our attempts to prepare analogues bearing the unhindered H-substituted (at C4) MIC **3.28** from **3.14**, we observed the formation of compound

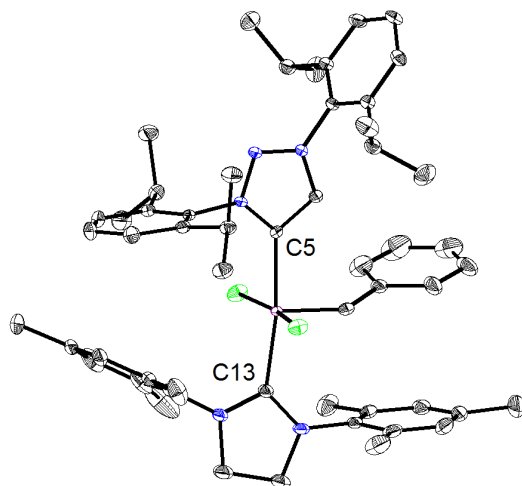


Figure 3.11. Solid-state structure of **3.31** with 50% probability ellipsoids. H atoms have been omitted for clarity. Selected bond lengths (Å) and angle (deg): C13 – Ru, 2.086, C5 – Ru, 2.097, C13 – Ru – C5, 169.34

3.29. In contrast to similar intermediates observed during the metalation of MICs **3.15–3.18**, compound **3.29** was indefinitely stable and phosphine dissociation never occurred to give the desired MIC catalyst. However, we noticed that in the presence of a solvent containing acidic impurities, the transformation of **3.29** to **3.14** occurred, a reaction that represents the formal protonolysis of a metal-NHC bond (Figure 3.9). Although relatively rare, protonolysis reactions of metal-NHC bonds have been observed for ruthenium and other late metals.^{20,21} Given these precedents, we concluded that MIC **3.28** was acid-labile and imagined that it could be incorporated into a metathesis catalyst as a dissociating ligand.

Combining free MIC **3.28** with **3.30** in C₆H₆ resulted in the new complex **3.31**, which was isolated in excellent yield after washing with cold pentane (Figure 3.10). Crystals of **3.31** suitable for x-ray diffraction were grown from slow diffusion of pentane onto a saturated toluene solution of **3.31**. The solid-state structure of **3.31** (Figure 3.11) was consistent with previously reported bis-NHC complexes

Table 3.2. RCM of **3.24** with **3.31** (1 mol%) and acid (ca. 20 mol%) in C₆D₆ (0.1 M)^a

entry	acid	time, h	conv., % ^a
1	None	18+	<5
2	HCl (1 M in Et ₂ O)	0.3	>95
3	Perchloric (70%)	4	73
4	Trifluoroacetic	0.3	>95
5	Acetic	18	20
6	Formic (88%)	18	91
7	Hydrobromic (48%)	4	>95
8	Hydroiodic (57%)	4	>95
9	HBF ₄ (Et ₂ O)	1	16
10	BH ₃ (THF)	18	19
11	B(C ₆ F ₅) ₃	17	33
12	ZnCl ₂	1	>95
13	SnCl ₄	18	<5

^a measured by ¹H NMR spectroscopyand MIC-Ru complexes (**3.19** and **3.21**).

Initial metathesis screens revealed that **3.31** is completely inactive at RT. For instance, 1 mol% of **3.31** in C₆H₆ was unable to polymerize 1,5-cyclooctadiene (**3.23**) to any detectable extent within a period of 12 h at RT.²² Some minimal conversion was observed after extended periods, presumably as a result of very slow catalyst initiation due to acidic glassware or acid impurities. Under similar reaction conditions, < 5% conversion of the RCM substrate **3.24** was observed over a period of several weeks at RT. In contrast, addition of HCl (1 M in Et₂O) resulted in complete and immediate conversion of **3.24** to the RCM product **3.25** within 20 min (Table 3.2, entry 2). Having established the feasibility of our initial hypothesis, we set about studying the protonolysis reaction in greater detail.

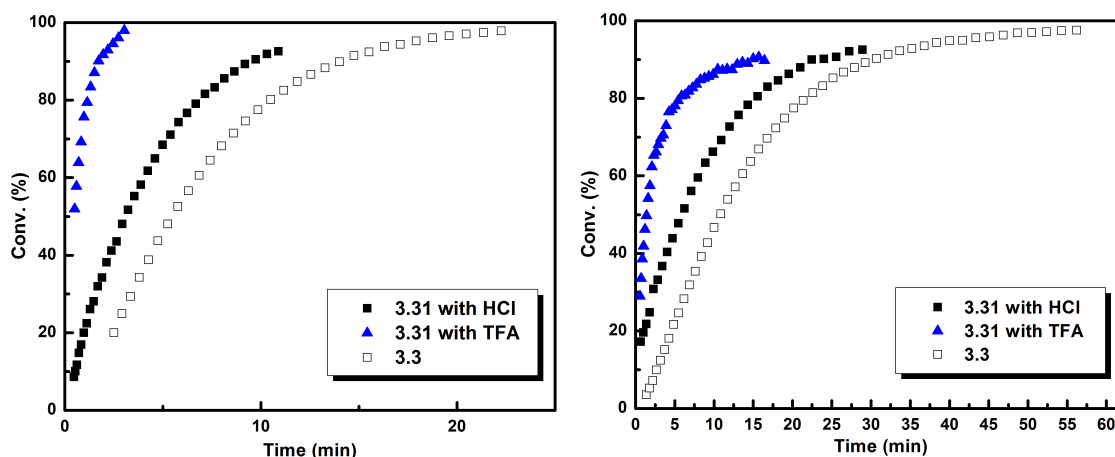


Figure 3.12. (left) RCM of **3.24** with **3.31** and TFA (blue triangles) or HCl (black squares) and RCM of **3.24** with **3.3** (white squares). Conditions: **3.24** (0.08 mmol), **3.31** or **3.3** (0.0008 mmol), and HCl (1 M in Et₂O, 31 equiv., 0.025 mmol) or TFA (160 equiv., 0.130 mmol) in C₆D₆ (0.8 mL) at 30 °C. (right) RCM of **3.26** with **3.31** and TFA (blue triangles) or HCl (black squares) and RCM of **3.26** with **3.3** (white squares). Conditions: **3.26** (0.08 mmol), **3.31** or **3.3** (0.0008 mmol), and HCl (1 M in Et₂O, 31 equiv., 0.025 mmol) or TFA (160 equiv., 0.130 mmol) in C₆D₆ (0.8 mL) at 30 °C. Conversion was measured by ¹H NMR spectroscopy

Table 3.3. Polymerization results with catalyst **3.31**^a

Solvent	Monomer	Acid	[Monomer], M	[3.31], M	[Acid], M ^a	M _n , g/mol ^b	PDI
PhH	3.32	TFA	0.26	0.003	0.04	12,000	1.42
PhH	3.32	MSA	0.26	0.003	0.04	19,000	1.53
PhH	3.32	HCl	0.5	0.0005	0.059	42,000	1.48
PhH	3.32	HCl	0.5	0.0005	0.08	29,500	1.65
PhH	3.23	HCl	0.5	0.001	0.059	50,000	1.48
PhCH ₃	3.23	HCl	0.5	0.001	0.059	31,000	1.47

^a HCl was added as a 1 M solution in Et₂O. MSA = methane sulfonic acid. ^b Molecular weights measured by multi-angle laser light scattering (MALS) GPC

Our initial efforts focused on the effects of different acids on the RCM of **3.24** (Table 3.2). Strong acids (entries 2–4, 7, and 8) were found to be the most effective and were capable of initiating the reaction even when added as aqueous solutions. However, the identity of the conjugate base was also important, as HBF₄

performed poorly (entry 9) in comparison to acids with similar pK_a 's. A similar result was observed for the *acac*-based, acid-activated complexes presented in Chapter 2. Weaker acids (entries 5 and 6) were less efficient and reached full conversion only after several hours or not at all. Interestingly, some Lewis acids were also capable of affecting the transformation. For instance, addition of $ZnCl_2$ resulted in complete conversion with 2 h at RT, while addition of $B(C_6F_5)_3$ resulted in only 33% conversion after several hours. Other Lewis acids such as $SnCl_4$ were found to be even less effective. In general, Brønsted acids significantly outperformed Lewis acids.

Because of their proficiency in activating **3.31**, HCl and trifluoroacetic acid (TFA) were chosen to investigate the RCM of **3.24** to **3.25** more closely. Under standard RCM screening conditions, a mixture of **3.31** and either HCl or TFA showed complete conversion of **3.24** to **3.25** within 10 min at 30 °C (Figure 3.12, left). The reaction with TFA was particularly fast, reaching 100% conversion within only a few minutes. Catalyst **3.31** also excelled at the RCM of trisubstituted substrate **3.26** (Figure 3.12, right). Notably, in the above RCM reactions, catalyst **3.31** was found to be superior to commercial catalysts such as $(H_2IMes)Cl_2Ru(=CHPhO^iPr)$ (**3.3**, H_2IMes = 1,3-dimesitylimidazolidin-2-ylidene).²³ As expected on the basis of these results, **3.31** also performed exceptionally well at the ring-opening metathesis polymerization (ROMP) of **3.23** and *cis*-cyclooctene (**3.32**) with both HCl and TFA as activators (Table 3.3). Molecular weights (M_n) were largely consistent with the predicted values and molecular weight distributions (PDI) were comparable to those obtained from the ROMP of **3.23** and **3.32** with

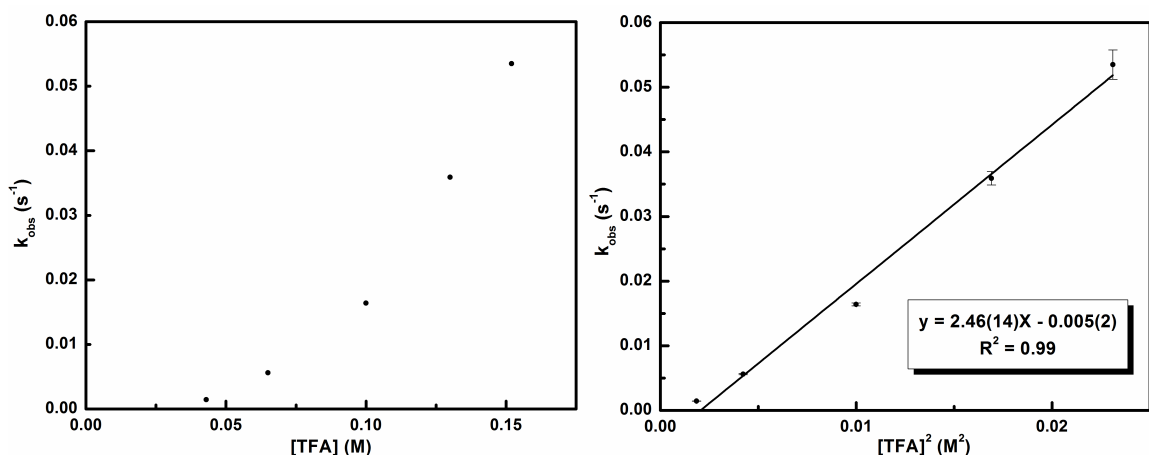


Figure 3.13. Observed rate constant versus [TFA] (left) and [TFA]² showing 2nd-order dependence on [TFA]

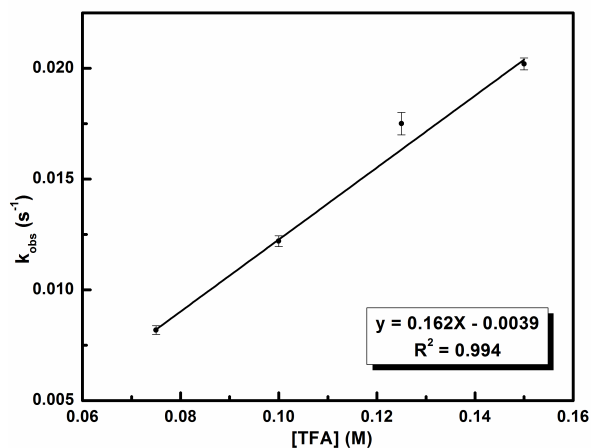


Figure 3.14. Observed rate constant versus [TFA] in CD₃CN at RT and constant pH. Conditions were **3.31** (0.003 mmol), KTFA (0.003–0.006 mmol), and TFA (0.045–0.09 mmol) in CD₃CN (0.6 mL)

catalysts **3.2** and **3.3**.²⁴

After the activation of **3.31** had been established, additional experiments were performed with the two best acid activators, TFA and HCl, to study the mechanism of activation in greater detail. The benzylidene proton resonance of **3.31** was monitored by ¹H NMR spectroscopy following the addition of varying amounts of TFA. A plot of the observed rate constant (k_{obs}) versus concentration of TFA in C₆D₆ displayed a second-order dependence on TFA concentration (Figure

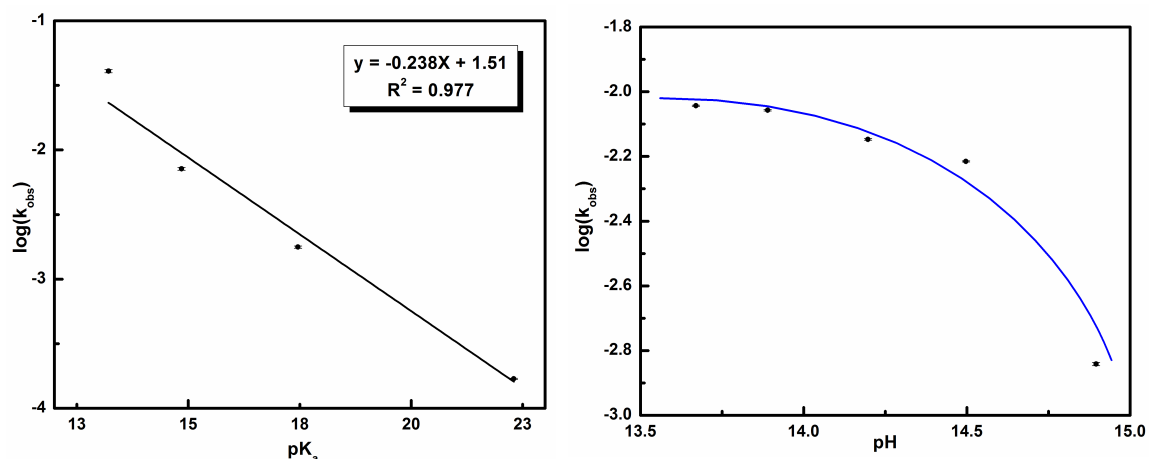


Figure 3.15. (left) Bronsted plot for initiation of **3.31** at RT in CD_3CN . Conditions: **3.31** (0.003 mmol) and acid (0.045 mmol) in CD_3CN (0.6 mL). Acids were acetic acid, $\text{Cl}_2\text{HCCO}_2\text{H}$, $\text{F}_3\text{CCO}_2\text{H}$ (TFA), and $\text{CH}_3\text{SO}_3\text{H}$ (MSA). (right) $\log(k_{\text{obs}})$ versus pH for reaction of **3.31** with TFA in CD_3CN . Blue line represents ideal curve based on pK_a of TFA in CD_3CN

3.13). This behavior is consistent with protonation of **3.31** by an acid dimer instead of an acid monomer. Indeed, carboxylic acids are known to form dimers via hydrogen bonding in hydrocarbon solvents such as PhH and PhCH_3 .²⁵ However, in order for the above situation to be plausible, protonation must be involved in the rate-determining step of the reaction. To probe this possibility and also to simplify the acid – base chemistry of the system, we decided to monitor the initiation of **3.31** in CD_3CN rather than in C_6D_6 .

If protonation is involved in the rate-determining step of the initiation reaction, a plot of k_{obs} versus acid concentration should be linear *at constant pH*.²⁶ This would parallel the behavior of general acid-catalyzed reactions, although in this case, kinetic runs were conducted under pseudo-first-order conditions. When an initiation study was performed with TFA in CD_3CN using potassium trifluoroacetate (KTFA) to maintain an approximately constant pH, a linear plot was obtained

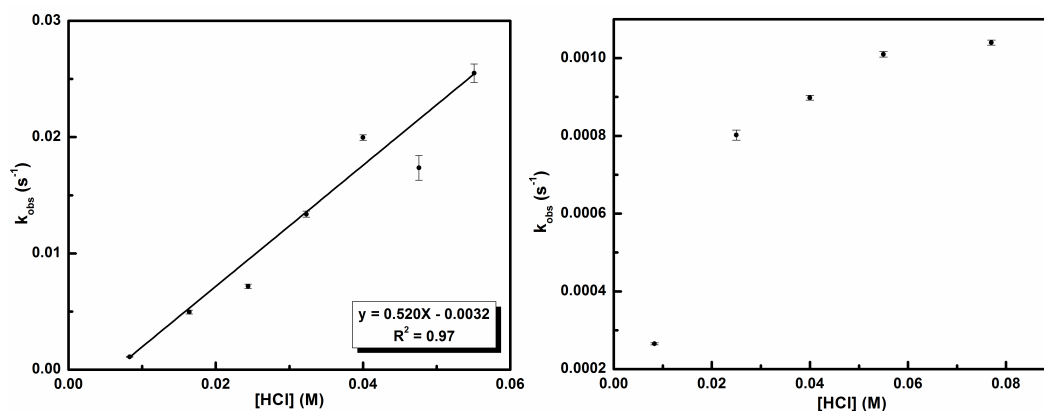


Figure 3.16. (left) Plot of k_{obs} versus [HCl] for reaction of **3.31** with HCl in CD₃CN. (right) Plot of k_{obs} versus [HCl] in C₆D₆. Conditions were **3.31** (0.003 mmol), and C₆D₆ (0.6 mL) with varying amounts of HCl (0.0083 M–0.077 M)

(Figure 3.14). Further evidence of the involvement of acid in the rate-determining step was provided by a Brønsted plot (Figure 3.15, left), which displays a linear relationship between the pK_a of the acid in CD₃CN and the logarithm of the initiation rate of **3.31**.²⁷ Finally, a plot of log(k_{obs}) versus the pH of the solution exhibited behavior characteristic of the involvement of acid in the rate-determining step (Figure 3.15, right). When HCl was used in place of TFA in CD₃CN, a first-order dependence on HCl concentration was observed (Figure 3.16, left). All of the above results are strong indications that a protonation event rather than dissociation is the rate-determining step in catalyst activation.

Compared to the initiation experiments conducted in CD₃CN, the initiation mechanism of **3.31** in the presence of inorganic acids in solvents of lower polarity (C₆D₆, toluene-d₈) is far more complex and likely involves poorly understood solvation and/or counterion effects, as suggested from the screening of acid initiators (Table 3.2). For instance, the reaction of **3.31** in C₆D₆ following the addition of excess HCl (> 15 equiv) resulted in a decrease in the benzyldiene proton signal

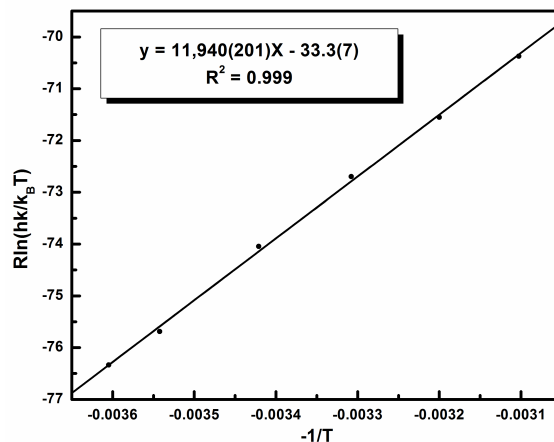


Figure 3.17. Eyring plot for activation of **3.31** at saturation conditions with HCl and toluene- d_8

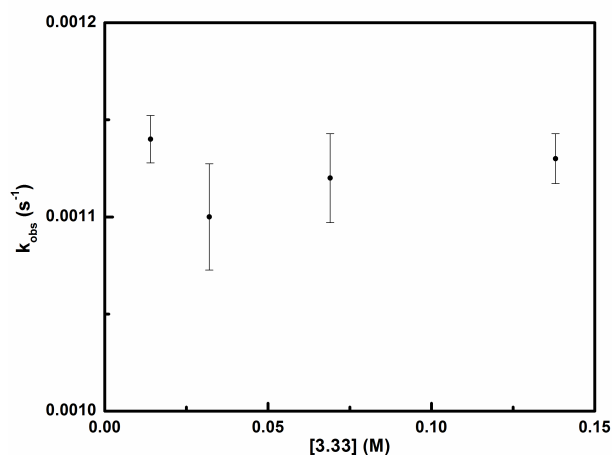


Figure 3.18. Plot of k_{obs} versus $[3.33]$ in C_6D_6 . Conditions were **3.31** (0.003 mmol) and HCl (1 M in Et_2O , 0.077 m) in C_6D_6 (0.6 mL) with varying amounts of **3.33** (0.014 M–0.14 M)

intensity that followed clean first-order kinetics. A plot of k_{obs} versus HCl concentration displayed saturation kinetics, which is inconsistent with a protonation event being rate-determining under these conditions and *may* be indicative of a pre-equilibrium step (Figure 3.16, right). However, a more likely explanation is that the saturation behavior is due to the limited solubility of HCl in the hydrocarbon solvents under study, since in CD_3CN a linear dependence of k_{obs} on $[HCl]$ was observed.²⁸ In

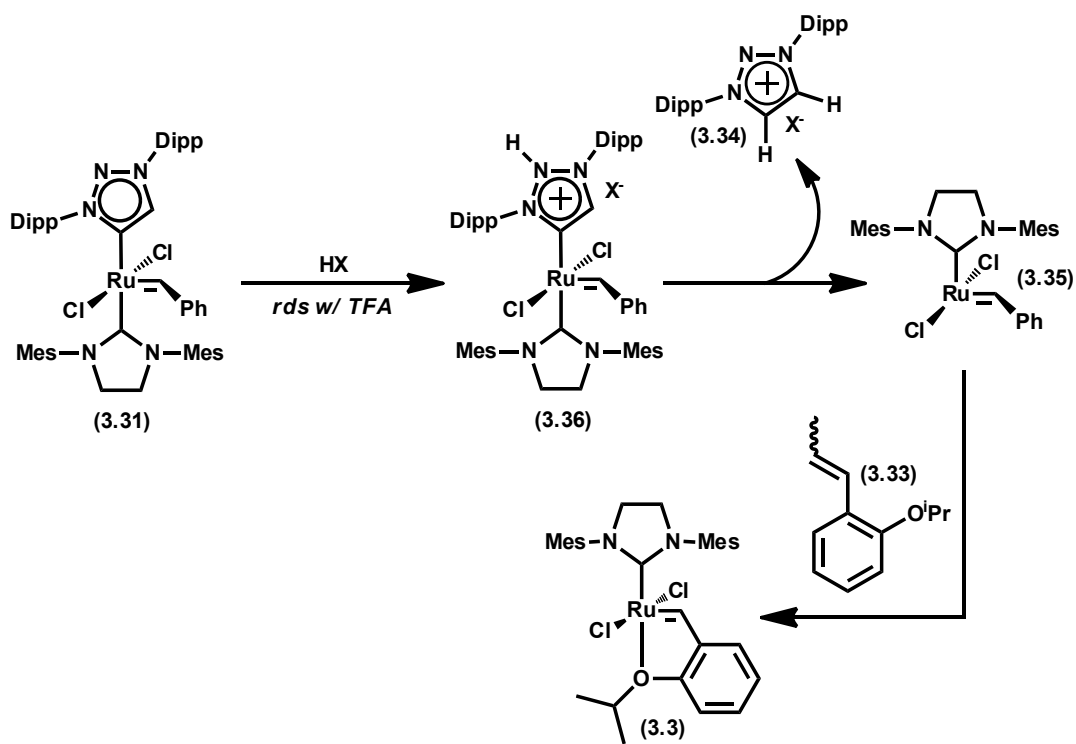


Figure 3.19. Proposed mechanism for initiation of **3.31**

support of this, we note that an Eyring plot of the activation reaction with HCl in toluene- d_8 under saturation conditions (Figure 3.17) yielded the values $\Delta H^\ddagger = 11.9 \pm 0.2$ kcal/mol and $\Delta S^\ddagger = -33.3 \pm 0.7$ eu, which are inconsistent with the description of the above saturation kinetics as a fast protonation equilibrium followed by a slow ligand dissociation. However, any conclusions based on ΔS^\ddagger alone are complicated by the likely formation of charged transition states in solvents that are largely incapable of supporting them (e.g., C_6D_6). A further complication arises from the fact that HCl was added as a solution in Et_2O , thus the polarity of the solvent ($C_6D_6:Et_2O$ mixture) is continuously changing. Regardless of the exact activation mechanism of **3.31** in C_6D_6 with HCl, the saturation behavior explains why a weaker acid (TFA) can, under some conditions, more efficiently activate **3.31** (e.g., Figure

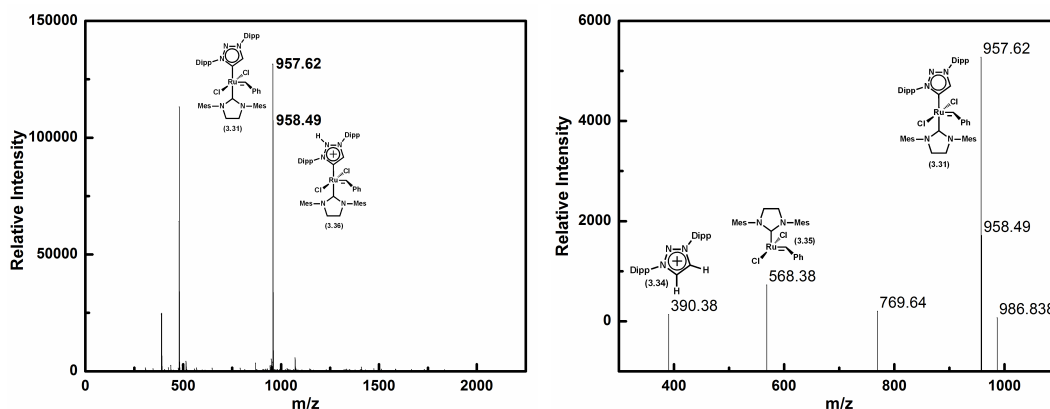


Figure 3.20. (left) Mass spec (ESI) of **3.31** immediately following addition of TFA. (right) Collision-induced dissociation (CID) of mass current 957.6 showing daughter peaks

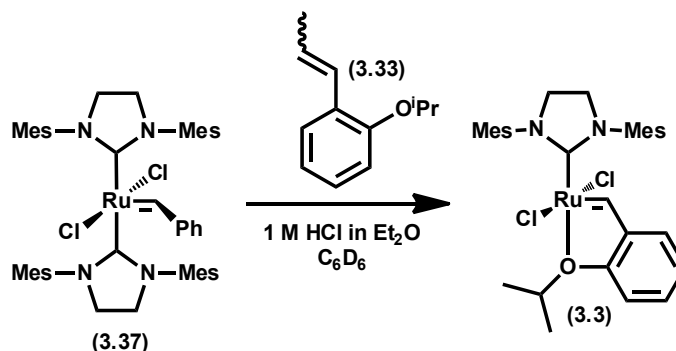


Figure 3.21. Initiation study of **3.37**. Conditions were **3.37** (0.0032 mmol), **3.33** (0.032 mmol), and HCl (0.05 mmol) in C_6D_6

3.12). Similarly, the observed initiation rate of **3.31** in C_6D_6 under saturation conditions at RT (0.0011 s^{-1}) is slightly higher than that of catalyst **3.2** (0.00046 s^{-1} at $35\text{ }^\circ\text{C}$),³ which explains the superior performance of **3.31** in RCM compared to more conventional catalysts.

Continuing our mechanistic studies, the growth of product **3.3** was monitored after treatment of **3.31** with acid in the presence of varying amounts of olefin **3.33** as a trapping agent. A plot of k_{obs} for this reaction versus the concentration of **3.33** showed no dependence on **3.33** concentration, indicating that any reaction with olefin must take place after the rate-determining step has occurred (Figure 3.18).

The above experiment also allowed us to identify **3.34**, which precipitated from solution. Taken together, the formation of **3.3** and **3.34** suggests that protonation of **3.31** generates catalytic intermediate **3.35**, which is the same active species that is postulated to follow thermally induced ligand dissociation in common ruthenium metathesis catalysts.³

Unlike the initiation of traditional metathesis catalysts, which only slightly depends on solvent,³ the various transformations depicted in Figure 3.19 are extremely sensitive to the identity of the solvent. For example, efficient initiation occurs in both C_6H_6 and CH_2Cl_2 , as does metathesis activity. Similarly, efficient initiation also occurs (**3.31** to **3.35**) in CH_3CN ; however, no catalytic activity is observed (**3.31** to **3.3**), presumably because **3.35** is immediately sequestered by solvent. In contrast to both of the above cases, the protonation event (**3.31** to **3.36**) does not occur (e.g., there is no disappearance of the benzyldiene resonance) to any extent in THF. At this point, it is unclear why no reaction occurs in THF, but both the initiation mechanism and resulting catalytic activity are clearly highly dependent on the identity of the solvent.

A complete proposed initiation mechanism for **3.31** is shown in Figure 3.19. Although our mechanistic studies could not definitively establish the nature of the protonation event the fact that some Lewis acids also activated the catalyst strongly suggests that the unsubstituted nitrogen (N2) on the MIC ligand plays an important role. Previously reported density functional theory calculations on free MICs (e.g., **3.28**) indicate that N2 has the second-highest proton affinity after the carbene itself, meaning that protonation at this position is plausible.¹³ Thus, it is likely that

initiation entails protonation at the MIC N2 in **3.31** to give **3.36**, followed by dissociation with a concomitant 1,3-proton shift to give **3.33** and **3.34**, both of which were observable by mass spectrometry (Figure 3.20). This mechanism is consistent with our experimental results to date, but at this time we cannot definitively rule out other possibilities, such as direct protonolysis of the Ru-MIC bond.

A final question we wished to answer was whether the behavior of **3.31** was due to the unique nature of the MIC ligand or if other conventional NHC (e.g., in **3.3**) would act in a similar manner. In order to determine this, $(\text{H}_2\text{IMes})_2\text{Cl}_2\text{Ru}(=\text{CHPh})$ (**3.37**) was added to **3.24**, and no RCM activity was observed at RT.²⁹ Upon addition of HCl (10 equiv.), no immediate activity was detected either. However, after a period of ca. 12 h at RT, ca. 70% conversion to **3.25** was observed by NMR spectroscopy. When HCl was added to a mixture of **3.37** and **3.33** in order to approximate the extent of catalyst initiation, only 12% conversion to catalyst **3.3** was achieved after a period of 24 h at RT (Figure 3.21). This result is in contrast to that observed for **3.31**, which was able to achieve complete conversion to **3.3** within a matter of minutes. Thus, although **3.37** is capable of being activated by acid, this occurs much less efficiently than for **3.31**. A similar conclusion was reached for complexes containing MICs **3.15–3.18**, which were efficiently activated with acid, but to a lesser extent than **3.31**.

Conclusions and Future Outlook

In summary, we have demonstrated that in the presence of acid, a MIC ligand may act as a leaving group, allowing an otherwise inactive metathesis complex (**3.31**) to enter the metathesis catalytic cycle. Furthermore, under

standard metathesis reactivity screening conditions, **3.31** was superior to the latest commercial catalysts and can complete RCM reactions with a matter of minutes at RT. A mechanistic study of the initiation mechanism concluded that protonation is the rate-determining step with the most efficient initiator, TFA, but that the activation step and resulting catalytic activity is strongly influenced by the identity of the acid and solvent. With strong-acid initiators, **3.31** was able to quickly and effectively access the same reactive intermediate as other catalysts (e.g., **3.3**) and thus combines latency with exceptional reactivity at RT. Finally, we established that the observed protonolysis behavior of **3.31** can also occur, but only to a limited extent in other bis-NHC complexes, enabling the incorporation of these activation mechanisms in future generations of metathesis catalysts.

Experimental

General Information: All reactions were carried out in dry glassware under an argon atmosphere using standard Schlenk line techniques or in a Vacuum Atmospheres Glovebox under a nitrogen atmosphere unless otherwise specified. Solvents were purified by passage through solvent purification columns and further degassed with argon.³⁰ NMR solvents were dried over CaH₂ and vacuum transferred to a dry Schlenk flask and subsequently degassed with argon. Commercially available reagents were used as received unless otherwise noted.

1D-NMR experiments were conducted on a Varian 600 MHz spectrometer equipped with a Triax (¹H, ¹³C, ¹⁵N) probe or a Varian Inova 400 Mhz spectrometer, while VT and kinetic experiments were conducted on a Varian 500 MHz spectrometer equipped with an AutoX probe. Accurate temperature measurements of the NMR

probe were obtained using a thermocouple connected to a multimeter with the probe immersed in an NMR tube containing a minimal amount of toluene. Experiments and pulse sequences from Varian's Chempack 4 software were used without modification except for changes in the number of FIDs and scans per FID. Reaction conversions were obtained by comparing the integral values of starting material and product, no internal standard was used. Chemical shifts are reported in ppm downfield from Me₄Si by using the residual solvent peak as an internal standard. Spectra were analyzed and processed using MestReNova Ver. 6.2.0 – 7163.³¹

High-resolution mass spectrometry (HRMS) data was obtained on a JEOL MSRoute mass spectrometer using FAB+ ionization. ESI-MS analyses were performed on a Finnigan LCQ classic mass spectrometer using the following conditions: spray voltage, 41 kV; sheath-gas flow rate, 20; cap. voltage, 5 V; cap. temp., 190 °C; tube lens voltage, 8 V; spectrum averaging, 10. In the daughter mode, a collision energy of 30 V was employed using He as the collision gas.

Ruthenium Complex 3.19: In a glovebox, a 20 mL scintillation vial was charged with carbene **3.15** (29 mg, 0.062 mmol),¹³ catalyst **3.14** (29 mg, 0.048 mmol), and C₆H₆ (5 mL). The solution was stirred at RT for 10 h after which it was concentrated to a brown residue. The residue was dissolved in a minimal amount of CH₂Cl₂ and pentane was carefully layered on top. The vial was cooled to –30 °C for ca. 12 h at which point small brown crystals had crashed out. The solvent was decanted away and the crystals were washed with cold pentane (3X) and dried to give **3.19** (24 mg, 49%). ¹H NMR (400 MHz, C₆D₆) δ 16.83 (s, 1H), 8.47 (d, *J* = 7.5 Hz, 2H), 7.43 (t, *J* = 8 Hz, 1H), 7.30–7.17 (m, 6H), 7.16–7.01 (m, 4H), 7.01–6.92 (m, 1H),

6.82 (d, $J = 7.8$ Hz, 2H), 6.72 (td, $J = 7.4, 0.7$ Hz, 1H), 6.41 (d, $J = 8.4$ Hz, 1H), 4.53 (sept, $J = 6.2$ Hz, 1H), 3.11 (sept, $J = 6.8$ Hz, 2H), 2.81 (sept, $J = 6.8$ Hz, 2H), 1.56 (d, $J = 6.1$ Hz, 6H), 1.18 (d, $J = 6.9$ Hz, 6H), 1.15 (d, $J = 6.7$ Hz, 6H), 1.05 (d, $J = 6.8$ Hz, 6H), 0.93 (d, $J = 6.8$ Hz, 6H). ^{13}C NMR (101 MHz, C_6D_6) δ 165.31, 151.45, 145.96, 144.01, 142.92, 135.81, 134.23, 129.81, 129.70, 129.45, 127.50, 122.63, 122.43, 120.53, 119.35, 111.30, 72.93, 27.23, 27.03, 24.08, 23.84, 21.56, 20.57, 20.09. HRMS (FAB+): Calculated—785.2453, Found—785.2482.

Ruthenium Complex 3.20: **3.20** was prepared in a manner analogous to **3.19**. Carbene **3.16** (27 mg, 0.053 mmol), **3.14** (25 mg, 0.041 mmol), and PhH (2 mL). **3.20** (9 mg, 27%). ^1H NMR (400 MHz, CD_2Cl_2) δ 17.19 (s, 1H), 7.67 (t, $J = 7.7$ Hz, 1H), 7.55 (t, $J = 7.8$ Hz, 1H), 7.45 (m, 3H), 7.23 (d, $J = 7.7$ Hz, 2H), 7.09 (d, $J = 7.5$ Hz, 1H), 6.96 (s, 2H), 6.90 (m, 2H), 4.96 (sept, $J = 6$ Hz, 1H), 2.95 (sept, $J = 6.8$ Hz, 2H), 2.66 (sept, $J = 6.8$ Hz, 2H), 2.34 (s, 3H), 2.26 (s, 6H), 1.45 (d, $J = 6.0$ Hz, 6H), 1.33 (d, $J = 6.5$ Hz, 6H), 1.17 (d, $J = 6.8$ Hz, 6H), 1.13 (d, $J = 6.5$ Hz, 6H), 1.10 (d, $J = 6.8$ Hz, 6H). ^{13}C NMR (101 MHz, CD_2Cl_2) δ 287.37, 165.07, 152.74, 148.83, 148.39, 146.77, 145.53, 141.20, 140.48, 136.79, 131.85, 131.75, 130.35, 129.23, 128.80, 125.77, 125.17, 124.86, 124.35, 123.08, 121.74, 113.63, 75.41, 54.53, 54.26, 53.99, 53.72, 53.45, 30.11, 29.88, 29.63, 28.19, 27.53, 23.03, 22.67, 22.19, 22.10, 21.43. HRMS (FAB+): Calculated—827.2923, Found—827.2905.

Ruthenium Complex 3.21: **3.21** was prepared in a manner analogous to **3.19**. Carbene **3.17** (63 mg, 0.106 mmol), **3.14** (38 mg, 0.063 mmol), and PhH (3 mL). **3.21** (28.5 mg, 50%). ^1H NMR (500 MHz, CD_2Cl_2) δ 17.32 (s, 1H), 7.67 (t, $J = 7.8$

Hz, 1H), 7.54 (m, 2H), 7.49 (d, $J = 7.8$ Hz, 2H), 7.28 (d, $J = 7.8$ Hz, 2H), 7.24 (s, 2H), 6.99–6.82 (m, 2H), 5.10 (sept, $J = 6$ Hz, 1H), 3.17–2.96 (m, 4H), 2.80 (sept, $J = 6.5$ Hz, 2H), 2.49 (sept, $J = 6.5$ Hz, 2H), 1.57 (d, $J = 6.6$ Hz, 6H), 1.53 (d, $J = 6.2$ Hz, 6H), 1.38 (d, $J = 6.9$ Hz, 6H), 1.20 (d, $J = 6.8$ Hz, 6H), 1.16 (d, $J = 6.7$ Hz, 6H), 0.87 (d, $J = 6.6$ Hz, 6H), 0.82–0.72 (m, 12H). ^{13}C NMR (126 MHz, CD_2Cl_2) δ 168.04, 152.68, 151.66, 150.40, 149.99, 148.20, 145.93, 135.35, 131.84, 131.09, 130.89, 128.26, 128.07, 125.03, 124.20, 123.78, 122.80, 122.43, 121.00, 113.09, 34.50, 30.97, 29.50, 29.29, 27.93, 27.31, 25.61, 23.83, 23.02, 22.89, 21.87, 21.62. HRMS (FAB+): Calculated—911.3862, Found—911.3891.

Ruthenium Complex 3.22: **3.22** was prepared in a manner analogous to **3.19**. Carbene **3.18** (69 mg, 0.181 mmol), **3.14** (84 mg, 0.139 mmol), and PhH (2 mL). **3.22** (12.4 mg, 12.7%). ^1H NMR (400 MHz, CD_2Cl_2) δ 16.89 (s, 1H), 8.13–8.05 (m, 2H), 7.66–7.52 (m, 2H), 7.49–7.42 (m, 2H), 7.22 (s, 2H), 7.17 (d, $J = 7.1$ Hz, 1H), 7.11 (dd, $J = 7.6, 1.4$ Hz, 1H), 7.04–6.93 (m, 3H), 5.09 (sept, $J = 6.0$ Hz, 1H), 2.55 (s, 3H), 2.34 (s, 3H), 2.18 (s, 6H), 2.11 (s, 6H), 1.62 (d, $J = 6.1$ Hz, 6H). ^{13}C NMR (101 MHz, CD_2Cl_2) δ 167.18, 163.85, 152.99, 145.21, 141.81, 141.59, 137.86, 137.27, 135.23, 135.01, 134.66, 132.82, 132.13, 130.95, 130.60, 130.54, 130.30, 129.98, 129.85, 129.74, 129.28, 129.12, 128.84, 128.69, 123.19, 121.95, 113.60, 75.42, 22.28, 21.69, 21.51, 18.17, 17.99. HRMS (FAB+): Calculated—701.1514, Found—701.1512

Representative Procedure for ROMP of 3.23: In a glovebox, a stock solution of **3.19** (3.6 mg, 0.0043 mmol) in C_6D_6 (1 mL) was prepared, and 93 μL (4×10^{-4} mmol catalyst) of this solution was added to an NMR tube followed by 700 μL of C_6D_6 .

The NMR tube was capped with a rubber septum, removed from the glovebox, and placed in the spectrometer where it was allowed to equilibrate at 30 °C. **3.23** (49 μL , 0.4 mmol) was injected through the septa ($t = 0$) and the tube was quickly inverted once and placed back into the spectrometer. Spectra were recorded by arraying the 'pad' function in vNMRj (starting time = 0 s, increment = 5 s). Percent conversion was determined by integration of the product peaks versus starting material peaks.

Representative Procedure for RCM of 3.24: 186 μL (8×10^{-4} mmol) of the above stock solution was added to an NMR tube followed by 615 μL of C_6D_6 . The NMR tube was capped with a rubber septum and placed in the spectrometer as before. **3.24** (19.3 μL , 0.08 mmol) was injected and spectra were recorded as described above.

Representative Procedure for RCM of 3.26: Kinetics for the RCM of **3.26** were performed in a manner analogous to **3.24**. **3.26** (20 μL , 0.08 mmol).

Initiation Rate Measurement and Eyring Plot. In a glovebox, a 2 mL volumetric flask was charged with **3.19** (19 mg, 0.024 mmol) and d_8 -toluene (0.012 M). 0.25 mL (0.003 mmol catalyst) of the stock solution was added to an NMR tube followed by 0.35 mL of d_8 -toluene. The tube was capped with a rubber septum, removed from the glovebox, and placed in the spectrometer where it was allowed to equilibrate at the desired temperature for ca. 10 min. The exact temperature was determined as described in the General Information. Butyl vinyl ether (12 μL , 0.09 mmol) was then injected through the septum and the NMR tube quickly

placed back into the spectrometer. The disappearance of the benzyldiene proton resonance was monitored over time for at least three half-lives by arraying the 'pad' function in vNMRj. All reactions showed clean first-order kinetics and k_{obs} was determined from a plot of $\ln(C/C_0)$ versus time.

According to the Activated Complex Theory of Henry Eyring,

$$k = \left(\frac{k_B T}{h} e^{\Delta S^\ddagger / R} \right) e^{-\Delta H^\ddagger / RT} \quad (1)$$

where k is the rate in s^{-1} , k_B is Boltzmann's constant, h is Planck's constant, R is the gas constant, and T is the temperature in Kelvin. Eq. 1 can be reworked to yield a linear equation which gives ΔH^\ddagger as the slope and ΔS^\ddagger as the intercept (Eq. 2).

$$R \ln \frac{hk}{k_B T} = \Delta S^\ddagger + \left(\frac{-1}{T} \right) \Delta H^\ddagger \quad (2)$$

The uncertainty in the slope and intercept was determined directly from the output provided by the linear regression function of OriginPro 8.1.³² The uncertainty in ΔG^\ddagger was calculated using the error in the slope, intercept, and the off-diagonal component of the variance-covariance matrix (because ΔH^\ddagger and ΔS^\ddagger are correlated) created by OriginPro.³³

1,3-Bis(2,6-diisopropylphenyl)-1*H*-1,2,3-triazol-5-ylidene (3.28): Anhydrous THF (10 mL) is added to a stirred mixture of triazolium salt **3.28·HPF₆** (268 mg, 0.5 mmol) and potassium *tert*-butoxide (112 mg, 1.0 mmol) at 0 °C. The reaction mixture was stirred for 30 min at 0 °C, then warmed to room temperature while stirring for an additional 30 min. Volatiles were evaporated under reduced pressure, and dry benzene (20 mL) was added. The mixture was triturated for 15–30 min, and filtered

through a filter cannula. Evaporation of the solvents under reduced pressure afforded **3.28** (156 mg, 80%) as a pale yellow solid. M.p.: 141–143°C (dec). *Note:* The NMR spectra of **3.28** presents some concentration-dependent broadening/coalescence, attributed to the exchange of protons at the C4/C5 position. At low concentration in the presence of ~ 1 eq. residual PhMe, the spectra of **2** is clearly asymmetric, but shows some peak broadening, indicative of slow proton exchange at C4/C5 with respect to the NMR timescale. At higher concentrations, the exchange accelerates and the spectra of **3.28** becomes symmetric, and displays resonances at the expected midpoint chemical shifts of the low [**3.28**] resonances. *Low [**3.28**]:* ¹H NMR (C₆D₃, 300 MHz): δ = 7.53 (br s, 1H), 7.32 (br m, 1H), 7.20 (br m, 1H), 7.14–7.10 (m, 2H), 7.07–7.00 (m, 2H), 2.94 (br m, 2H), 2.47 (br m, 2H), 1.28 (br m, 6H), 1.23 (br m, 6H), 1.05 (br m, 12H). ¹³C NMR (C₆D₆, 75 MHz): δ = 201.9 (C), 146.0 (C), 145.9 (C), 139.9 (C), 138.4 (CH), 133.9 (C), 131.4 (CH), 130.2 (CH), 124.4 (CH), 124.1 (CH), 29.2 (2 CH), 25.0 (CH₃), 24.8 (CH₃), 24.4 (CH₃), 24.2 (CH₃)

*High [**3.28**]:* ¹H NMR (C₆D₆, 300 MHz): δ = 7.56 (br s, 1H), 7.27 (t, *J* = 7.6 Hz, 2H), 7.10 (d, *J* = 7.7 Hz, 4H), 2.70 (br sept, *J* = 6.8 Hz, 4H), 2.47 (br m, 2H), 1.15 (d, *J* = 6.8 Hz, 12H), 1.11 (d, *J* = 6.8 Hz, 12H). ¹³C NMR (C₆D₆, 75 MHz): δ = ~ 170 (br, C/CH), 145.9 (C), 136.8 (C), 130.8 (CH), 124.3 (CH), 29.2 (CH), 24.9 (CH), 24.2 (CH).

Ruthenium Complex 3.31: In a glovebox, a 20 mL scintillation vial was charged with MIC **3.28**¹³ (208 mg, 0.535 mmol), **3.30**³⁴ (300 mg, 0.412 mmol), and C₆H₆ (7 mL). The brown solution was stirred for one hour and concentrated *in vacuo*

to a brown residue which was washed with cold pentane until the washes were colorless. The remaining brown solid was dried to give **3.31** (375 mg, 95%) which was subsequently lyophilized from C₆H₆. ¹H NMR (400 MHz, CD₂Cl₂) δ 18.52 (s, 1H), 7.53 (m, 3H), 7.33 (s, 1H), 7.31 (s, 1H), 7.20 (tt, J = 7.6, 0.8 Hz, 1H), 6.97–6.81 (m, 5H), 6.76 (d, J = 7.8 Hz, 2H), 6.59 (s, 1H), 6.28 (br s, 1H), 4.03–3.86 (m, 4H), 2.57 (s, 6H), 2.47 (sept, J = 6.8 Hz, 2H), 2.23 (sept, J = 6.8 Hz, 2H), 2.14 (br s, 6H), 2.00 (s, 3H), 1.93 (s, 3H), 1.17 (d, J = 6.8 Hz, 6H), 1.09 (d, J = 6.9 Hz, 6H), 1.05 (d, J = 6.6 Hz, 6H), 0.77 (d, J = 6.9 Hz, 6H). ¹³C NMR (101 MHz, CD₂Cl₂) δ 225.91, 183.63, 150.56, 146.18, 145.84, 140.71, 137.07, 136.19, 134.23, 132.51, 131.98, 130.65, 130.44, 129.69, 129.31, 128.85, 127.53, 126.99, 125.39, 124.57, 123.32, 52.03, 51.79, 28.78, 28.60, 26.65, 25.38, 24.06, 22.22, 20.83, 18.62. HRMS (FAB+): Calculated—958.3896, Found—958.3917.

Representative Procedure for RCM of 3.24 with 3.31 and HCl: In a glovebox, a 1 mL volumetric flask was charged with **3.31** (5.6 mg, 0.0058 mmol) and filled to the 1 mL line with C₆D₆. A portion of the stock solution (140 μL, 0.0008 mmol **3.31**) was added to an NMR tube and diluted with C₆D₆ (660 μL). Compound **3.24** (19.3 μL, 0.08 mmol) was added and the NMR tube was capped with a rubber septum, removed from the glovebox, and placed inside the spectrometer. The tube was ejected and HCl (1M in Et₂O) (25 μL, 31 eq.) was injected after which the tube was quickly inverted once and placed back inside the spectrometer. An array of ¹H spectra were collected using the ‘pad’ function in vNMRj and processed according to the General Information.

Representative Procedure and Kinetic Plots for Reaction of 3.31 with HCl in

C₆D₆: In a glovebox, a 1 mL volumetric flask was charged with **3.31** (11.5 mg, 0.012 mmol) and filled to the 1 mL line with C₆D₆ to form a stock solution of catalyst. A portion (0.25 mL) of the stock solution above was transferred to an NMR tube and diluted with C₆D₆ (0.35 mL) such that the final concentration of **3.31** was ca. 0.005 M. The NMR tube was capped with a rubber septum, removed from the glovebox, and placed inside the spectrometer. After equilibration at the desired temperature for 10 min, HCl in Et₂O (between 5 and 50 μL) was injected through the rubber septum and the tube was quickly inverted once and placed back inside the spectrometer. An array of 1D ¹H spectra were collected using the 'pad' function in vNMRj.

Representative Procedure and Kinetic Plots for Reaction of 3.31 with HCl in C₆H₆ with Olefin 3.33: Inside a glovebox, an NMR tube with stock catalyst solution (0.25 mL) and C₆D₆ (0.35 mL) was prepared as above. Olefin **3.33** (1.6 μL, 0.009 mmol) was added along with anthracene (35 μL of a 0.086 M solution) as an internal standard and the tube was capped with a rubber septum and removed from the box. After equilibrating in the spectrometer, HCl (50 μL, 1 M in Et₂O) was added through the rubber septum and data was collected as above. Completion of the reaction was characterized by a change in color from yellow/brown to green and the formation of a white precipitate. The precipitate was collected by filtration and identified as **3.34** by ¹H NMR spectroscopy and HRMS (FAB+ : C – 390.2909, F – 390.2898). The green filtrate was concentrated and identified as **3.3** by HRMS (FAB+ : C – 626.1405, F – 626.1397) and ¹H NMR spectroscopy by comparison with authentic samples.

Eyring Plot Procedure (with Acid): In a glovebox, a 2 mL volumetric flask was charged with **3.31** (23 mg, 0.024 mmol) and filled to the line with d_8 -toluene. A portion (0.25 mL) of the catalyst stock solution was added to an NMR tube and diluted with d_8 -toluene (0.35 mL). The NMR tube was capped with a rubber septum, removed from the glovebox, and placed in the spectrometer at the desired temperature and allowed to equilibrate for ca. 10 min. The exact temperature of the NMR probe was determined as described in the General Information. After equilibrating, the tube was ejected and HCl (50 μ L, 1 M in Et_2O) was added, after which the tube was inverted once and quickly placed back inside the spectrometer. Data was collected with the vNMRj array function as above. All reactions showed clean first-order kinetics over period of at least three half-lives and k_{obs} was determined from a plot of $\ln(C/C_0)$ versus time.

Mass Spectrometry Study of Reaction Mechanism: A 1 mM solution of **3.31** in C_6H_6 was prepared and TFA (5 μ L) was added. The solution was loaded into a syringe and placed on a syringe pump connected to a mass spectrometer running on continuous electrospray ionization. Masses corresponding to SM and protonated SM were obtained (Figure 3.20). Parent and CID daughter peaks were collected according to the General Information.

Representative Procedure and Kinetic Plots for Reaction of 3.31 with TFA in C_6D_6 : In a glovebox, a 1 mL volumetric flask was charged with **3.31** (13 mg, 0.0134 mmol) and filled to 1 mL with C_6D_6 to form a stock solution of catalyst. A portion of the stock solution (0.225 mL, 0.003 mmol **3.31**) was added to an NMR tube and diluted with C_6D_6 (0.375 mL). The NMR tube was capped with a rubber septum,

removed from the glovebox, and placed inside the spectrometer. TFA (0.026 mmol –0.091 mmol) was injected, the tube was inverted once, and placed back inside the spectrometer. Data was collected as above.

Representative Procedure and Kinetic Plots for Reaction of 3.31 with TFA in CD₃CN at Constant pH: In a glovebox, a 1 mL volumetric flask was charged with potassium trifluoroacetate (KTFA) (15 mg, 0.0986 mmol) which had been dried under vacuum at 70 °C for 12 h, and the flask was filled to the line with CD₃CN. A portion of the stock solution (30.4 µL, 0.003 mmol KTFA) was added to a vial containing **3.31** (2.9 mg, 0.003 mmol) and CD₃CN (0.570 mL). The resulting fine suspension was shaken and quickly transferred to an NMR tube which was capped with a rubber septum. (Note : Over prolonged periods of time (hours), **3.31** would decompose in the presence of CD₃CN, therefore, all samples for kinetic runs were prepared immediately prior to use.) The NMR tube was removed from the glovebox and placed inside the spectrometer. TFA (3.4 µL, 0.045 mmol) was injected through the rubber septum and the tube was quickly inverted before being placed back inside the spectrometer. NMR spectra were recorded as described previously.

Representative Procedure for Brønsted Plot: In a glovebox, a 1 mL volumetric flask was charged with **3.31** (9.7 mg, 0.01 mmol) and filled to the line with CD₃CN to make a 0.01 M stock solution. An aliquot of the stock solution (300 µL) was added to an NMR tube and diluted with CD₃CN (300 µL). The NMR tube was capped with a rubber septum, removed from the glovebox, and placed inside the spectrometer. TFA (3.5 µL, 0.045 mmol, 15 eq.) was injected after which the

tube was inverted once and placed back inside the spectrometer. Spectra were recorded periodically as described above. The same procedure was repeated for the following acids: Methane-sulfonic acid (3 μ L, 0.045 mmol), Dichloroacetic acid (3.7 μ L, 0.045 mmol), and Acetic acid (2.6 μ L, 0.045 mmol). Acid dissociation constants in acetonitrile were estimated from Eq. 3³⁵ using pK_a values in DMSO.³⁶

$$pK_a(AN) = b + \alpha pK_a(DMSO) \quad (3)$$

$$b = 11.80 \quad \alpha = 0.884$$

Representative Procedure and Kinetic Plots for Reaction of 3.31 with TFA in CD₃CN Containing Varying Amounts of KTFA (Variable pH): A 1 mL volumetric flask was charged with KTFA (13.6 mg, 0.0907 mmol) and filled to the line with CD₃CN. A portion of the KTFA stock solution (55 μ L, 0.005 mmol) was transferred to a vial containing **3.31** (2.9 mg, 0.003 mmol) and CD₃CN (550 μ L). The resulting suspension was quickly shaken and transferred to an NMR tube and capped with a rubber septa. TFA (3.4 μ L, 0.045 mmol) was injected and the tube was quickly inverted and placed inside the spectrometer. Spectra were recorded as above.

Representative Procedure and Kinetic Plots for Reaction of 3.31 with HCl (1 M in Et₂O) in CD₃CN: In a glovebox, a 4 mL vial was charged with **3.31** (2.9 mg, 0.003 mmol) and CD₃CN (0.6 mL). The fine suspension was transferred to an NMR tube which was capped with a rubber septum and removed from the box. The NMR tube was placed inside the spectrometer and equilibrated at 25 °C after which it was ejected and HCl (1 M in Et₂O, 5 μ L) was added via syringe. After inverting once, the tube was placed back inside the spectrometer and data was

collected as above. Note that in the case of a small amount of HCl (5 μ L), pseudo-first-order conditions are not applicable. Therefore, only the first few minutes of the reaction were used to obtain k_{obs} . All other amounts of HCl displayed good first-order behavior until completion of the reaction.

References

- (1) (a) Fürstner, A. *Angew. Chem. Int. Ed.* **2000**, 39, 3012. (b) Trnka, T. M.; Grubbs, R. H. *Acc. Chem. Res.* **2001**, 34, 18. (c) Astruc, D. *New J. Chem.* **2005**, 29, 42.
- (2) (a) Kingsbury, J. S.; Harrity, J. P.; Bonitatebus, P. J.; Hoveyda, A. H. *J. Am. Chem. Soc.* **1999**, 121, 791. (b) Garber, S. B.; Kingsbury, J. S.; Gray, B. L.; Hoveyda, A. H. *J. Am. Chem. Soc.* **2000**, 122, 8168. (c) Hong, S. H.; Day, M. W.; Grubbs, R. H. *J. Am. Chem. Soc.* **2004**, 126, 7414. (d) Hong, S. H.; Wenzel, A. G.; Salguero, T. T.; Day, M. W.; Grubbs, R. H. *J. Am. Chem. Soc.* **2007**, 129, 7961. (e) Hong, S. H.; Chlenov, A.; Day, M. W.; Grubbs, R. H. *Angew. Chem. Int. Ed.* **2007**, 46, 5148. (f) Vehlouw, K.; Gessler, S.; Blechert, S. *Angew. Chem. Int. Ed.* **2007**, 46, 8082. (g) Leitao, E. M.; Dubberley, S. R.; Piers, W. E.; Wu, Q.; McDonald, R. *Chem. Eur. J.* **2008**, 14, 11565. (h) Mathew, J.; Koga, N.; Suresh, C. H. *Organometallics* **2008**, 27, 4666.
- (3) Sanford, M. S.; Love, J. A.; Grubbs, R. H. *J. Am. Chem. Soc.* **2001**, 123, 6543.
- (4) Getty, K.; Delgado-Jaime, M. U.; Kennepohl, P. *J. Am. Chem. Soc.* **2007**, 129, 15774.
- (5) (a) Samojłowicz, C.; Bieniek, M.; Grela, K. *Chem. Rev.* **2009**, 109, 3708. (b) Vougioukalakis, G. C.; Grubbs, R. H. *Chem. Rev.* **2010**, 110, 1746.
- (6) Bourgeois, D.; Pancrazi, A.; Nolan, S. P.; Prunet, J. *J. Organomet. Chem.* **2002**,

643–644, 247.

(7) (a) Arnold, P. L.; Pearson, S. *Coord. Chem. Rev.* **2007**, *251*, 596 (b) Albrecht, M. *Chem. Commun.* **2008**, 3601 (c) Schuster, O.; Yang, L.; Raubenheimer, H. G.; Albrecht, M. *Chem. Rev.* **2009**, *109*, 3445 (d) Albrecht, M. *Chimia* **2009**, *63*, 105.

For comparisons of the properties of normal, abnormal, and remote carbenes, see for examples: (e) Heydenrych, G.; von Hopffgarten, M.; Stander, E.; Schuster, O.; Raubenheimer, H. G.; Frenking, G. *Eur. J. Inorg. Chem.* **2009**, 1892 (f) Stander-Grobler, E.; Schuster, O.; Heydenrych, G.; Cronje, S.; Tosh, E.; Albrecht, M.; Frenking, G.; Raubenheimer, H. G. *Organometallics* **2010**, *29*, 5821.

(8) (a) Lavallo, V.; Canac, Y.; Präsang, C.; Donnadiou, B.; Bertrand, G. *Angew. Chem. Int. Ed.* **2005**, *117*, 5851. (b) Lavallo, V.; Canac, Y.; DeHope, A.; Donnadiou, B.; Bertrand, G. *Angew. Chem. Int. Ed.* **2005**, *117*, 7402. (c) Anderson, D. R.; Lavallo, V.; O’Leary, D. J.; Bertrand, G.; Grubbs, R. H. *Angew. Chem. Int. Ed.* **2007**, *46*, 7262. (d) Anderson, D. R.; Ung, T. A.; Mkrtumyan, G.; Bertrand, G.; Grubbs, R. H.; Schrodi, Y. *Organometallics* **2008**, *27*, 563.

(9) IUPAC. Compendium of Chemical Terminology, 2nd ed. (the “Gold Book”). Compiled by A. D. McNaught and A. Wilkinson. Blackwell Scientific Publications, Oxford (1997). XML on-line corrected version: <http://goldbook.iupac.org> (2006) created by M. Nic, J. Jirat, B. Kosata; updates compiled by A. Jenkins. ISBN 0-9678550-9-8. [doi:10.1351/goldbook](https://doi.org/10.1351/goldbook)

(10) a) Grundemann, S.; Kovacevic, A.; Albrecht, M.; Faller, J. W.; Crabtree, R. H. *Chem. Commun.* **2001**, 2274 (b) Grundemann, S.; Kovacevic, A.; Albrecht, M.; Faller, J. W.; Crabtree, R. H. *J. Am. Chem. Soc.* **2002**, *124*, 10473.

- (11) Guisado-Barrios, G.; Bouffard, J.; Donnadieu, B.; Bertrand, G. *Angew. Chem. Int. Ed.* **2010**, *49*, 4759.
- (12) Alder, R. W.; Blake, M. E.; Chaker, L.; Harvey, J. N.; Paolini, F.; Schütz, J. *Angew. Chem. Int. Ed.* **2004**, *43*, 5896.
- (13) Bouffard, J.; Keitz, B. K.; Tonner, R.; Guisado-Barrios, G.; Frenking, G.; Grubbs, R. H.; Bertrand, G. *Organometallics* **2011**, *30*, 2617.
- (14) Gessler, S.; Randl, S.; Blechert, S. *Tetrahedron Lett.* **2000**, *41*, 9973.
- (15) Van Veldhuizen, J. J.; Garber, S. B.; Kingsbury, J. S.; Hoveyda, A. H. *J. Am. Chem. Soc.* **2002**, *124*, 4954.
- (16) Ragone, F.; Poater, A.; Cavallo, L. *J. Am. Chem. Soc.* **2010**, *132*, 4249.
- (17) Ritter, T.; Hejl, A.; Wenzel, A. G.; Funk, T. W.; Grubbs, R. H. *Organometallics* **2006**, *25*, 5740.
- (18) Hejl, A. S. Thesis, California Institute of Technology, 2007.
- (19) (a) Vorfalt, T.; Wannowius, K.-J.; Plenio, H. *Angew. Chem. Int. Ed.* **2010**, *49*, 5533. (b) Ashworth, I. W.; Hillier, I. H.; Nelson, D. J.; Percy, J. M.; Vincent, M. *A. Chem. Commun.* **2011**, *47*, 5428. (c) Thiel, V.; Hendann, M.; Wannowius, K.-J.; Plenio, H. *J. Am. Chem. Soc.* **2012**, *134*, 1104.
- (20) (a) da Costa, R. C.; Hampel, F.; Gladysz, J. *Polyhedron* **2007**, *26*, 581. (b) Leitao, E. M.; van der Eide, E. F.; Romero, P. E.; Piers, W. E.; McDonald, R. *J. Am. Chem. Soc.* **2010**, *132*, 2784.
- (21) (a) Simonovic, S.; Whitwood, A. C.; Clegg, W.; Harrington, R. W.; Hursthouse, M. B.; Male, L.; Douthwaite, R. E. *Eur. J. Inorg. Chem.* **2009**, *2009*, 1786. (b) McGuinness, D. S.; Yates, B. F.; Cavell, K. J. *Chem. Commun.* **2001**, 355. (c)

Wang, C.-Y.; Liu, Y.-H.; Peng, S.-M.; Chen, J.-T.; Liu, S.-T. *J. Organomet. Chem.* **2007**, *692*, 3976. (d) Blue, E.; Gunnoe, T.; Petersen, J.; Boyle, P. *J. Organomet. Chem.* **2006**, *691*, 5988. (e) Fu, C.-F.; Lee, C.-C.; Liu, Y.-H.; Peng, S.-M.; Warsink, S.; Elsevier, C. J.; Chen, J.-T.; Liu, S.-T. *Inorg. Chem.* **2010**, *49*, 3011. (f) Díez-González, S.; Nolan, S. P. *Angew. Chem. Int. Ed.* **2008**, *47*, 8881.

(22) When no acid was added, **3.31** began to show evidence of polymerization at temperatures of ca. 60 °C, indicating that thermal initiation is also viable.

(23) Ritter, T.; Hejl, A.; Wenzel, A. G.; Funk, T. W.; Grubbs, R. H. *Organometallics* **2006**, *25*, 5740.

(24) Bielawski, C. W.; Grubbs, R. H. *Prog. Poly. Sci.* **2007**, *32*, 1.

(25) (a) Fujii, Y.; Kawachi, Y.; Tanaka, M. *J. Chem. Soc., Faraday Trans.* **1981**, 63.

(b) Zaugg, N. S.; Kelley, A. J.; Woolley, E. M. *J. Chem. Eng. Data.* **1979**, *24*, 218.

(c) Nagai, Y.; Simamura, O. *Bull. Chem. Soc. Japan* **1962**, *2*, 132.

(26) Jencks, W. *Acc. Chem. Res.* **1980**, *13*, 161.

(27) Lewis, E. W. *J. Phys. Org. Chem.* **1990**, *3*, 1.

(28) For likely structures of HCl in PhH see : Buch, V.; Mohamed, F.; Krack, M.; Sadlej, J.; Devlin, J. P.; Parrinello, M. *J. Chem. Phys.* **2004**, *121*, 12135.

(29) Trnka, T. M.; Morgan, J. P.; Sanford, M. S.; Wilhelm, T. E.; Scholl, M.; Choi, T.-L.; Ding, S.; Day, M. W.; Grubbs, R. H. *J. Am. Chem. Soc.* **2003**, *125*, 2546.

(30) Love, J. A.; Morgan, J. P.; Trnka, T. M.; Grubbs, R. H. *Angew. Chem. Int. Ed.* **2002**, *41*, 4035.

(31) www.mestrelab.com

(32) <http://www.originlab.com/index.aspx?go=Products/OriginPro>

- (33) For a more detailed explanation on the method used to calculate the uncertainty in ΔG^\ddagger see: Anderson, D. R.; Hickstein, D. D.; O'Leary, D. J.; Grubbs, R. H. *J. Am. Chem. Soc.* **2006**, *128*, 8386.
- (34) Love, J. A.; Sanford, M. S.; Day, M. W.; Grubbs, R. H. *J. Am. Chem. Soc.* **2003**, *125*, 10103.
- (35) Kütt, A.; Leito, I.; Kaljurand, I.; Sooväli, L.; Vlasov, V. M.; Yagupolskii, L. M.; Koppel, I. A. *J. Org. Chem.* **2006**, *71*, 2829.
- (36) Ding, F.; Smith, J. M.; Wang, H. *J. Org. Chem.* **2009**, *74*, 2679 and references therein.

Chapter 4

Degenerate (Nonproductive) Reactions with Ruthenium Metathesis Catalysts

The text in this chapter is reproduced in part with permission from:

Stewart, I. C.; Keitz, B. K.; Kuhn, K. M.; Thomas, R. M.; Grubbs, R. H. *J. Am. Chem. Soc.* **2010**, 132, 8534.

Thomas, R. M.; Keitz, B. K.; Champagne, T.; Grubbs, R. H. *J. Am. Chem. Soc.* **2011**, 133, 7490.

Copyright 2010 and 2011 American Chemical Society

Abstract

The study of degenerate (nonproductive) metathesis events during ring-closing metathesis (RCM) is discussed. Catalyst structure, specifically with regard to the N-heterocyclic carbene (NHC) ligand, was found to have a significant effect on degenerate versus productive selectivity. For example, catalysts with N-aryl/N-aryl NHC ligands displayed high selectivity for productive metathesis while those with N-aryl/N-alkyl NHC ligands exhibited selectivity for degenerate metathesis. Finally, the relationship between degenerate metathesis and selectivity for kinetic metathesis products is also discussed, along with the application of degenerate-selective catalysts towards the ethenolysis of methyl oleate.

Introduction

Degenerate or nonproductive events are common during both cross metathesis (CM) and ring-closing metathesis (RCM). These events are defined as catalytic turnovers that produce an equivalent of the starting material, but are distinct from simply undergoing the reverse process in an equilibrium reaction. As such, degenerate reactions can only be visualized through isotopic labeling (cross-over) experiments (Figure 4.1). Indeed, with the aid of multiple isotopologues of propylene (e.g., $Z-d_1, d_2$ -propene and d_3 -propene), the effect of degenerate metathesis during cross-metathesis has been studied extensively for early hetero- and homogeneous molybdenum (Mo) and tungsten (W) catalysts.¹ In these studies, the rate of degenerate metathesis was found to exceed that of productive metathesis by approximately an order of magnitude. Furthermore, evidence was provided for the

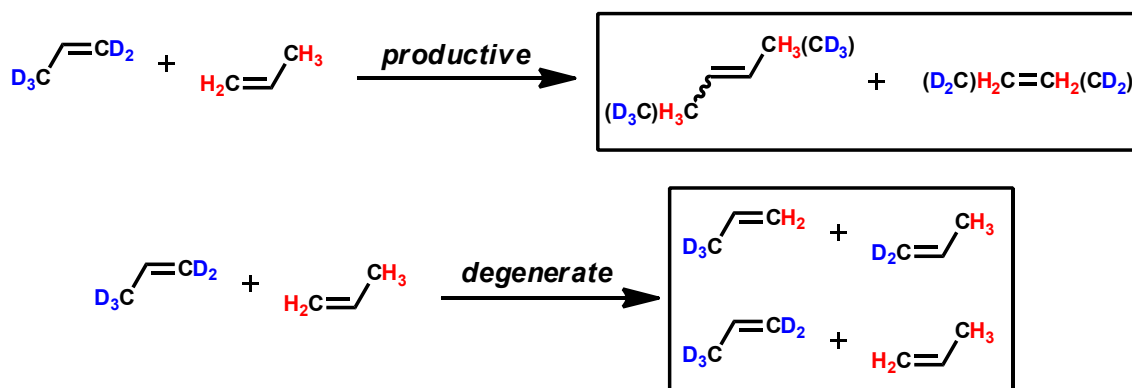


Figure 4.1. (top) Productive metathesis and (bottom) degenerate/nonproductive metathesis (bottom) of propylene

presence of a chain-carrying metal alkylidene intermediate ($\text{M}=\text{CHR}$) as opposed to a metal methyldene ($\text{M}=\text{CH}_2$). While these reports were the first to explore the role of degenerate metathesis, similar studies using modern ruthenium-based olefin metathesis catalysts and synthetically relevant reactions have not been undertaken.

Understanding such degenerate reactivity can provide insight into a number of important catalyst attributes relevant to metathesis reactions. First, catalytic activity, specifically turnover frequency (TOF), is significantly affected by degenerate versus productive selectivity. For instance, a degenerate-selective catalyst (**A**) may perform 10 degenerate turnovers (D-TON) per second and 1 productive turnover (P-TON) per second giving the catalyst a TOF of 1 $[\text{product}] \cdot [\text{catalyst}]^{-1} \cdot \text{s}^{-1}$. In contrast, a productive-selective catalyst (**B**) may have a P-TON of 10 and a D-TON of 1 per second, giving it a TOF of 10 $[\text{product}] \cdot [\text{catalyst}]^{-1} \cdot \text{s}^{-1}$. Clearly, all else being equal, catalyst **B** would be considered superior. A second rationale for studying degenerate metathesis concerns catalyst stability, which can be quantified by the total number of turnovers (TON). Under ideal conditions, degenerate reactions do not cause a net change in the concentration of catalyst. However, under realistic conditions,

they provide additional opportunities for catalyst decomposition. For example, catalyst decomposition can occur directly from ruthenacycle intermediates,² so the more time a catalyst exists as this intermediate, the more likely it is to decompose. Furthermore, the species responsible for degenerate metathesis (e.g., $M=CH_2$) are often more prone to decomposition. These examples clearly demonstrate that degenerate metathesis has a significant effect on both catalyst activity and stability. In addition, the Hoveyda and Schrock groups have reported that degenerate processes are essential to achieving high enantioselectivity in asymmetric ring-closing reactions for Mo/W systems.³ Although less relevant to Ru catalysts, their work further illustrates the importance of studying degenerate metathesis.

Here, we present the first studies of degenerate metathesis in ruthenium-based olefin metathesis catalysts and demonstrate that a catalyst's structure determines its selectivity for either productive or degenerate metathesis. We also show that for some reactions, such as ethenolysis, selectivity for degenerate metathesis is actually advantageous, and that this observation can be used as a foundation from which to develop new industrially relevant catalysts.

Results and Discussion

We chose to initiate our studies on degenerate metathesis by examining the RCM of a deuterium labeled variant of diethyl diallylmalonate (**4.5-d₂**), one of the benchmark substrates for evaluating olefin metathesis catalysts.⁴ Compound **4.5-d₂** was prepared by straightforward organic synthesis (Figure 4.2) starting from propargyl alcohol (**4.1**) and deuterium oxide (D₂O). The RCM of **4.5-d₂** entails one productive metathesis pathway and two potential degenerate pathways (Figure

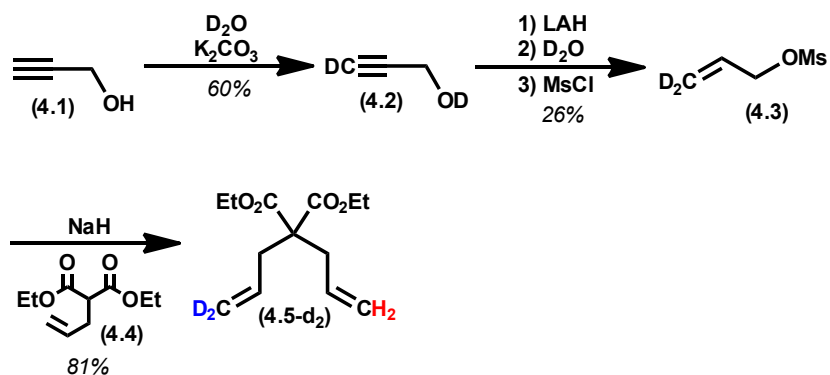


Figure 4.2. Preparation of labeled RCM substrate **4.5-d₂**. Ms = methane sulfonyl, LAH = lithium aluminum hydride

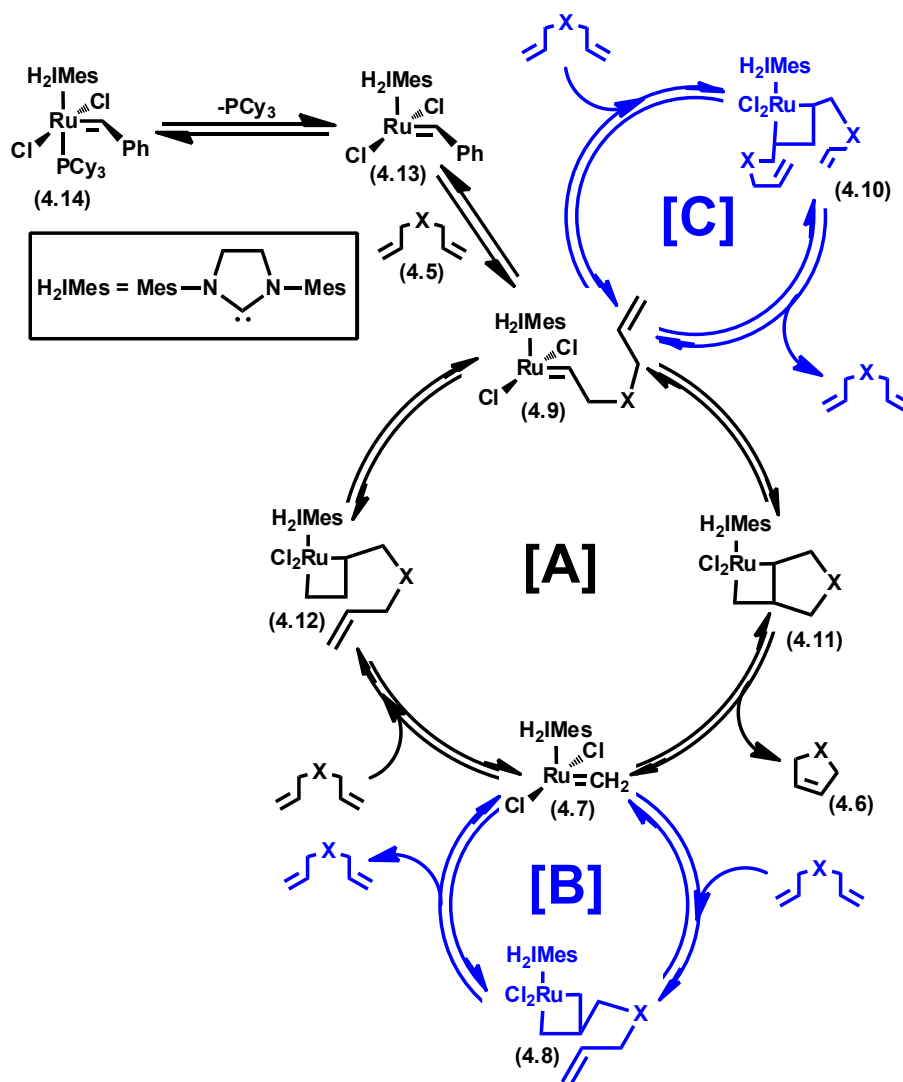


Figure 4.3. (A) Productive catalytic cycle for RCM of **4.5** to **4.6** and degenerate cycles starting from (B) methyldiene ($\text{Ru}=\text{CH}_2$) and (C) alkylidene ($\text{R}=\text{CHR}$). Mes = 2,4,6-trimethylphenyl

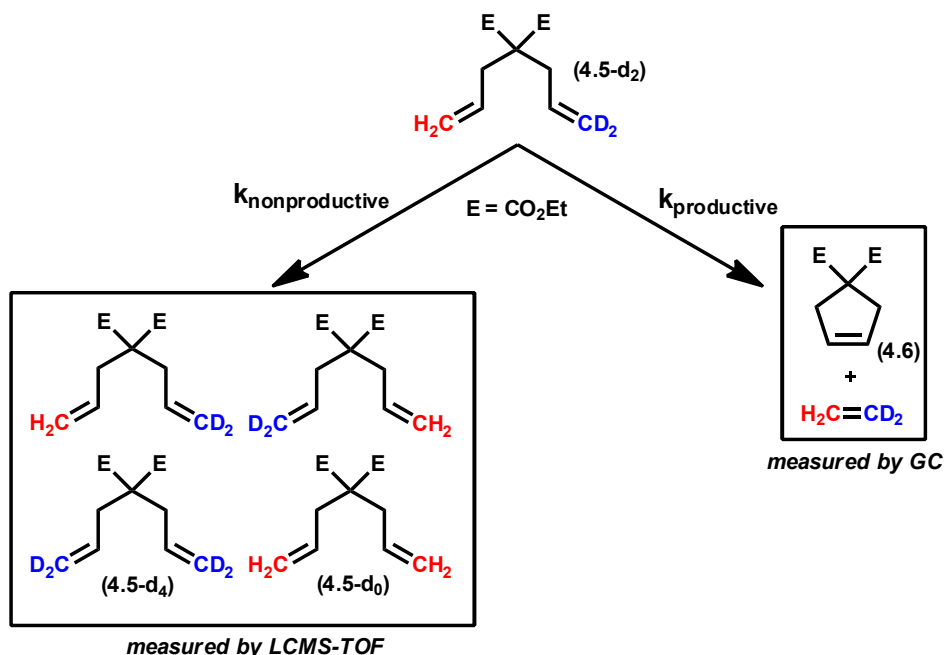


Figure 4.4. Products generated from the degenerate and productive metathesis of 4.5- d_2

4.3). The first degenerative pathway begins with a Ru methylenide (**4.7**) that reacts with an olefin to form a β -substituted ruthenacycle (**4.8**). Subsequent breakdown of this ruthenacycle regenerates the starting material but exchanges the methylene termini. An alternative degenerate pathway begins with a Ru alkylidene (**4.9**) and ends with the retrocycloaddition of an α,α -disubstituted ruthenacycles (**4.10**). Overall, through the combination of productive and degenerative metathesis, a mixture of compounds **4.6**, **4.5- d_4** , and **4.5- d_0** is generated from the RCM of 4.5- d_2 (Figure 4.4).⁵

In order to investigate the dependence of the relative amounts of **4.5- d_4** , **4.5- d_0** (from degenerate metathesis), and **4.6** (from productive metathesis) on catalyst structure, 4.5- d_2 was subjected to catalysts **4.14–4.21**. The conversion to cyclopentene **4.6** was monitored by gas chromatography (GC) while the relative

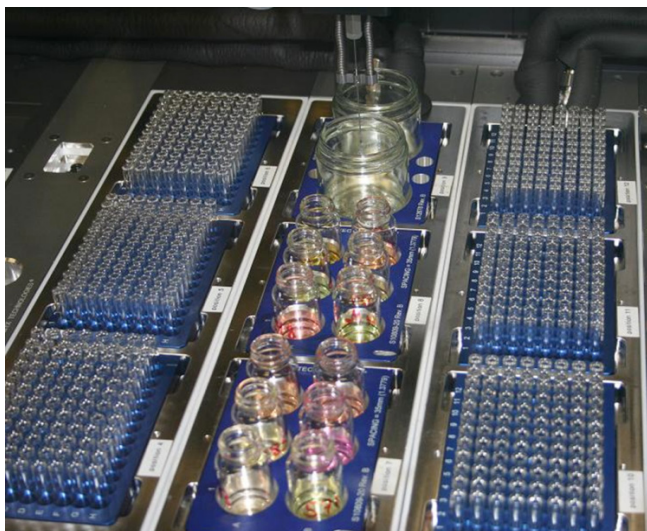


Figure 4.5. Example SYMYX set up of RCM of **4.5-d₂** using different catalysts. Reaction solutions are in the middle, flanked by chilled aliquot vials filled with ethyl vinyl ether solutions (in toluene) to quench the catalysts.

amounts of **4.5-d₄** and **4.5-d₀** were determined by time-of-flight mass spectrometry (TOF-MS). We were aided in the execution of our experiments by the use of a SYMYX robotics core module,⁶ which automated the collection of reaction aliquots for multiple catalysts simultaneously and in triplicate (Figure 4.5). Reactions run by hand faithfully reproduced the results from the robot, but were discouraged in lieu of the high degree of reproducibility provided by the robot. The relative amounts of **4.5-d₄**, **4.5-d₀**, and **4.6** were used to calculate degenerate and productive TON, respectively, and these values were plotted versus one another for each catalyst (Figure 4.6).⁷

As shown in Figure 4.6, the ratio of degenerate to productive TON varied widely as a function of catalyst structure. For example, ‘good’ catalysts (e.g., **4.14**–**4.17**) displayed remarkable selectivity for productive metathesis over degenerate

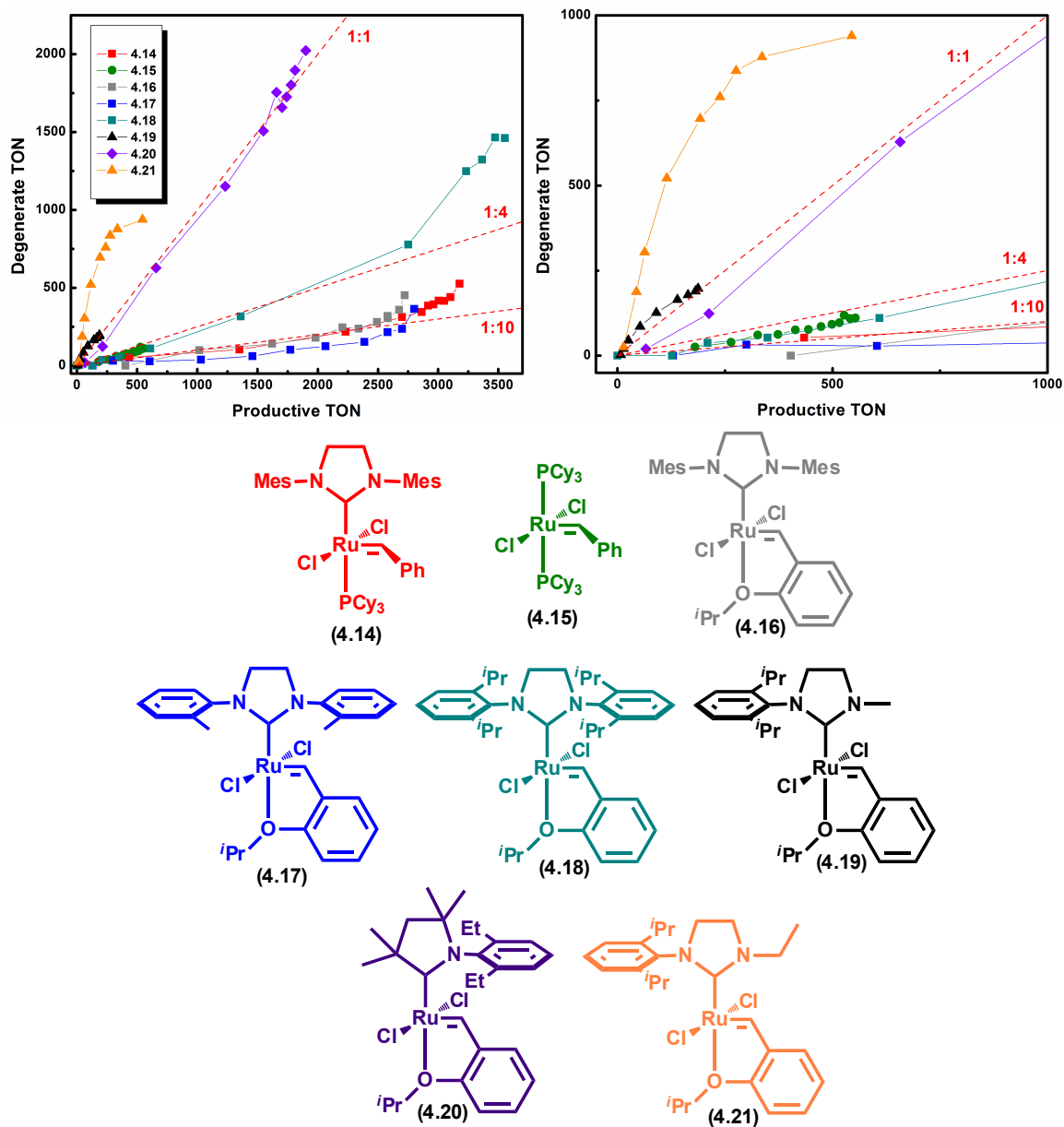


Figure 4.6. (top left) Degenerate TON versus productive TON for the RCM of **4.5-d₂** with catalysts **4.14–4.21**. (top right) blow up of low TON region. Reaction conditions were 50 °C in toluene (1 mL) with **4.5-d₂** (0.1 mmol) and catalyst (**4.15**—1000 ppm, **4.14**, **4.16**, **4.17**, **4.18**—250 ppm, **4.19**—5000 ppm, **4.20**—500 ppm, **4.21**—1000 ppm).

metathesis. This result is consistent with the general evolution of these catalysts, since they would not have been developed and optimized if they were unable to

efficiently perform the RCM of **4.5**. However, small differences were observed among the productive metathesis selective catalysts. Specifically, phosphine containing catalyst **4.15** performed slightly more degenerate TON (falling close to the 1:4 line, Figure 4.6) compared to the NHC-containing catalysts (**4.14**, **4.16**, and **4.17**), which favored productive metathesis (falling on the 1:10 line). However, due to catalyst decomposition, **4.15** did not reach nearly as many total TON, which complicates direct comparisons between the two catalyst types. Nevertheless, the slight preference of catalysts **4.14**, **4.16**, and **4.17** for productive metathesis, along with their higher stability and preference for olefin binding,⁸ explains their general superiority in metathesis reactions when compared to **4.15**.

More significant differences were observed between catalysts containing different types and structures of NHCs (**4.16–4.21**). For example, switching the aryl group of the NHC from Mes (**4.14**, **4.16**) or ortho-tolyl (**4.17**) to the larger 2,6-diisopropylphenyl (DIPP, **4.18**) resulted in a large increase in selectivity for degenerate metathesis (teal line in Figure 4.6). A more striking change occurred when the NHC was replaced with a cyclic alkyl amino carbene (CAAC, **4.20**). In this case, a 1:1 ratio of degenerative to productive metathesis was achieved. Similar selectivity for degenerate metathesis was measured when catalysts with N-aryl/N-alkyl NHCs (**4.19**, **4.21**) were tested. In addition to being remarkably selective for degenerative metathesis, catalyst **4.21** (orange line) also showed an interesting saturation effect, which we attribute to the achievement of thermodynamic equilibrium between the isotopologues of **4.5**.

Initially, we believed that the increase in degenerate selectivity observed in

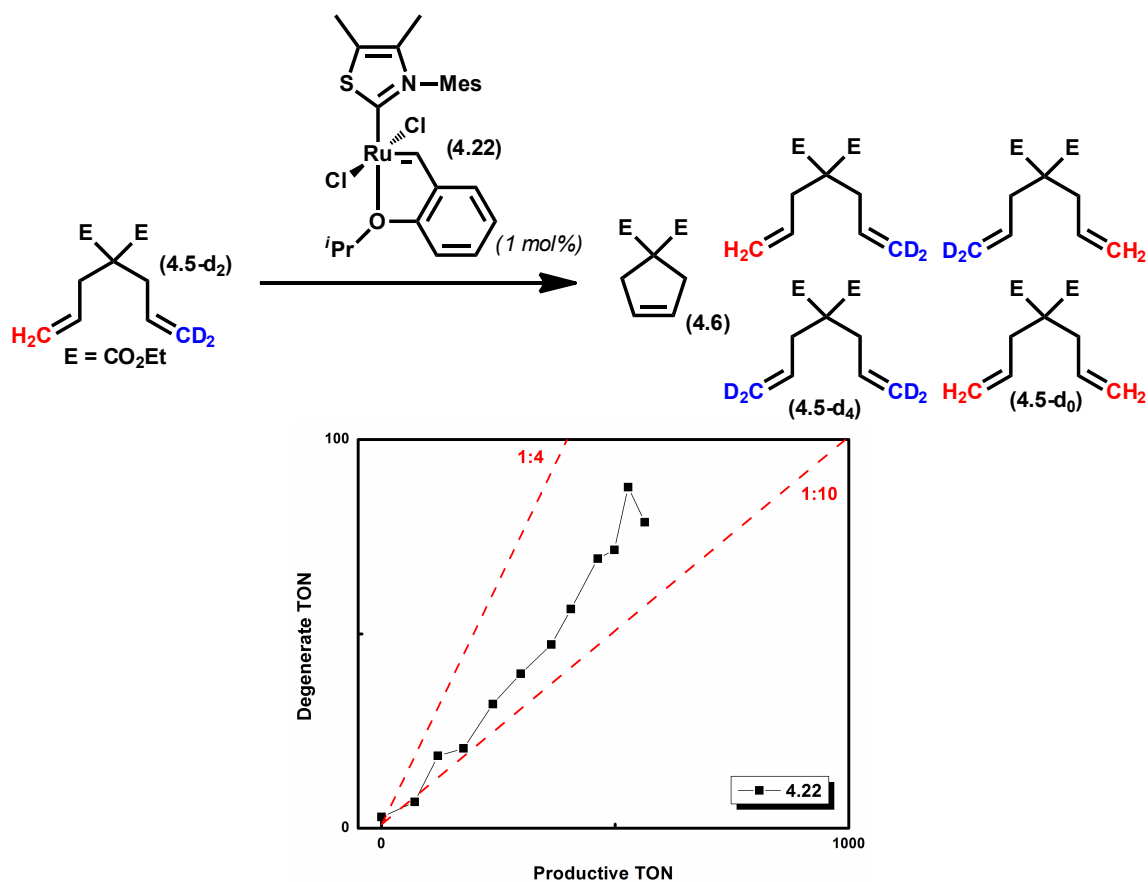


Figure 4.7. RCM of **4.5-d₂** with catalyst **4.22** and plot of degenerate versus productive TON

catalysts **4.19–4.21** arose from a decrease in the steric environment around the metal center. For instance, catalysts **4.19–4.21** contain asymmetric NHCs (or a CAAC) with at least one small N-substituent (methyl in **4.19**, dimethyl in **4.20**, ethyl in **4.21**). In order to examine whether or not this small substituent was responsible for the increase in degenerate selectivity, the thiazolium carbene-based catalyst **4.22** was prepared and subjected to our ring-closing conditions.⁹ Unfortunately, catalyst **4.22** was fairly unstable and did not give high total TON (Figure 4.7). However, it was very selective for *productive* metathesis, suggesting that a less congested steric environment does not necessarily result in selectivity for

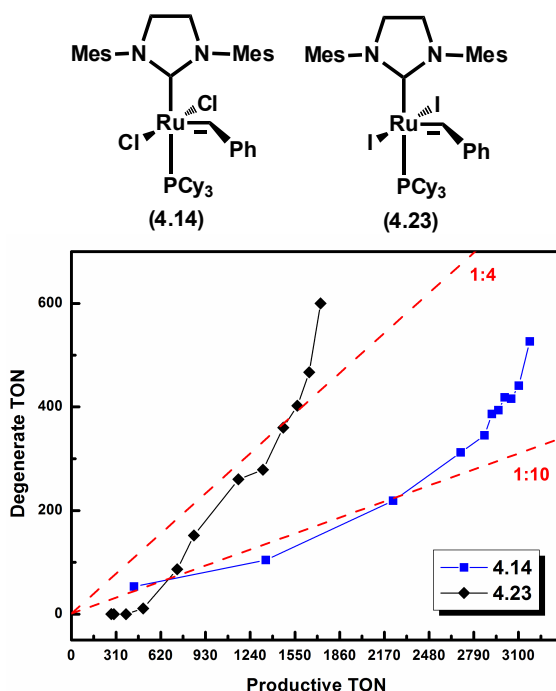


Figure 4.8. RCM of **4.5-d₂** and plot of degenerate versus productive TON for catalysts **4.14** and **4.23**

degenerate metathesis. This analysis is obviously complicated by the ability of the NHC to rotate about the C–Ru bond;⁷ nevertheless, there is no obvious relationship between the sterics of the NHC and selectivity for degenerate metathesis. Clearly the relationship between catalyst structure and selectivity for degenerate or productive metathesis is more complex, and as such, a more thorough treatment will be presented in Chapter 5. For now we will continue to focus on more empirical results.

Continuing with our goal of evaluating the effect of structural changes on degenerate selectivity, we next focused on the effect of the halide ligands. Iodo-catalyst **4.23** was prepared from **4.14** using sodium iodide (NaI) and subjected to the standard reaction conditions described in Figure 4.6. Figure 4.8 clearly shows that the diiodo catalyst **4.23** is much less selective for productive metathesis.

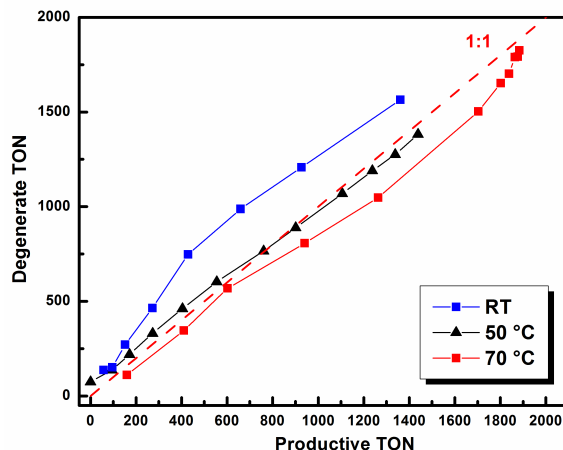


Figure 4.9. RCM of **4.5-d₂** with catalyst **4.20** at room temperature (RT), 50 °C, and 70 °C

Catalyst **4.23** is known to initiate faster than **4.14** (k_{obs} of phosphine dissociation) but is less selective for olefin binding over phosphine reassociation.⁷ As such, dichloro catalyst **4.14** is generally considered superior to **4.23**. However, catalyst **4.23**'s selectivity for degenerate over productive metathesis may also contribute to its inferiority when compared to **4.14**. Although we do not currently have a mechanistic rationale for the increase in degenerate selectivity, future investigators may wish to study the dynamics of ruthenacycles with halide ligands other than chloride (see Chapter 5).

We next turned to examining the effect of temperature on selectivity for degenerate over productive metathesis. The RCM of **4.5** to **4.6** is both kinetically and thermodynamically favored whereas the degenerate metathesis of **4.5-d₂** to **4.5-d₀** and **4.5-d₄** is essentially thermo-neutral excluding kinetic and thermodynamic isotope effects.¹⁰ Moreover, RCM to **4.6** is functionally irreversible, whereas the isotopologues of **4.5** are in equilibrium. For these reasons and because we cannot observe every degenerate event (e.g., **4.5-d₂** to **4.5-d₂**), we anticipated that an

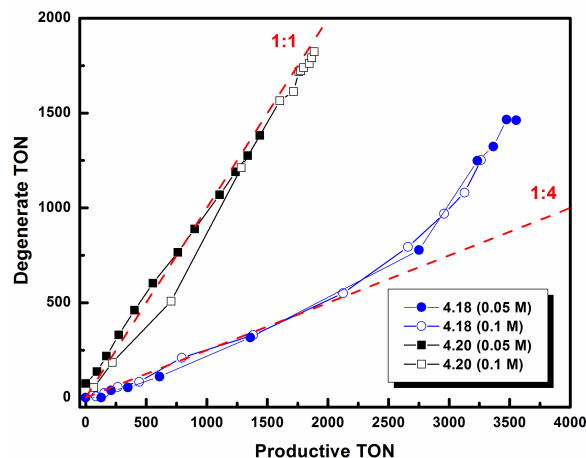


Figure 4.10. RCM of **4.5-d₂** with catalysts **4.18** and **4.20** at different substrate concentrations

increase in temperature would result in a small increase in productive metathesis selectivity. To probe this, we performed the RCM of **4.5-d₂** with catalyst **4.20**, since this catalyst is relatively selective for degenerate metathesis but is also able to reach very high TON. Indeed, under our standard conditions, catalyst **4.20** displayed a slight increase in productive selectivity as a function of temperature (Figure 4.9). The effect is not dramatic, but does demonstrate that small changes in degenerate selectivity can be affected by changes in temperature.

Following our temperature studies, we next examined the effect of concentration on degenerate metathesis selectivity. As shown in Figure 4.10, no significant change was observed with varying substrate concentration for either catalyst **4.18** or **4.20** in the RCM of **4.5-d₂**. This result implies that degenerate metathesis is proceeding through a Ru–methylidene propagating species (e.g., Figure 4.3, B), since an alkylidene propagating species (Figure 4.3, C) would be expected to exhibit some concentration dependence. Both **4.18** and **4.20** are stable as methylidenes, which have also been identified as the propagating species in

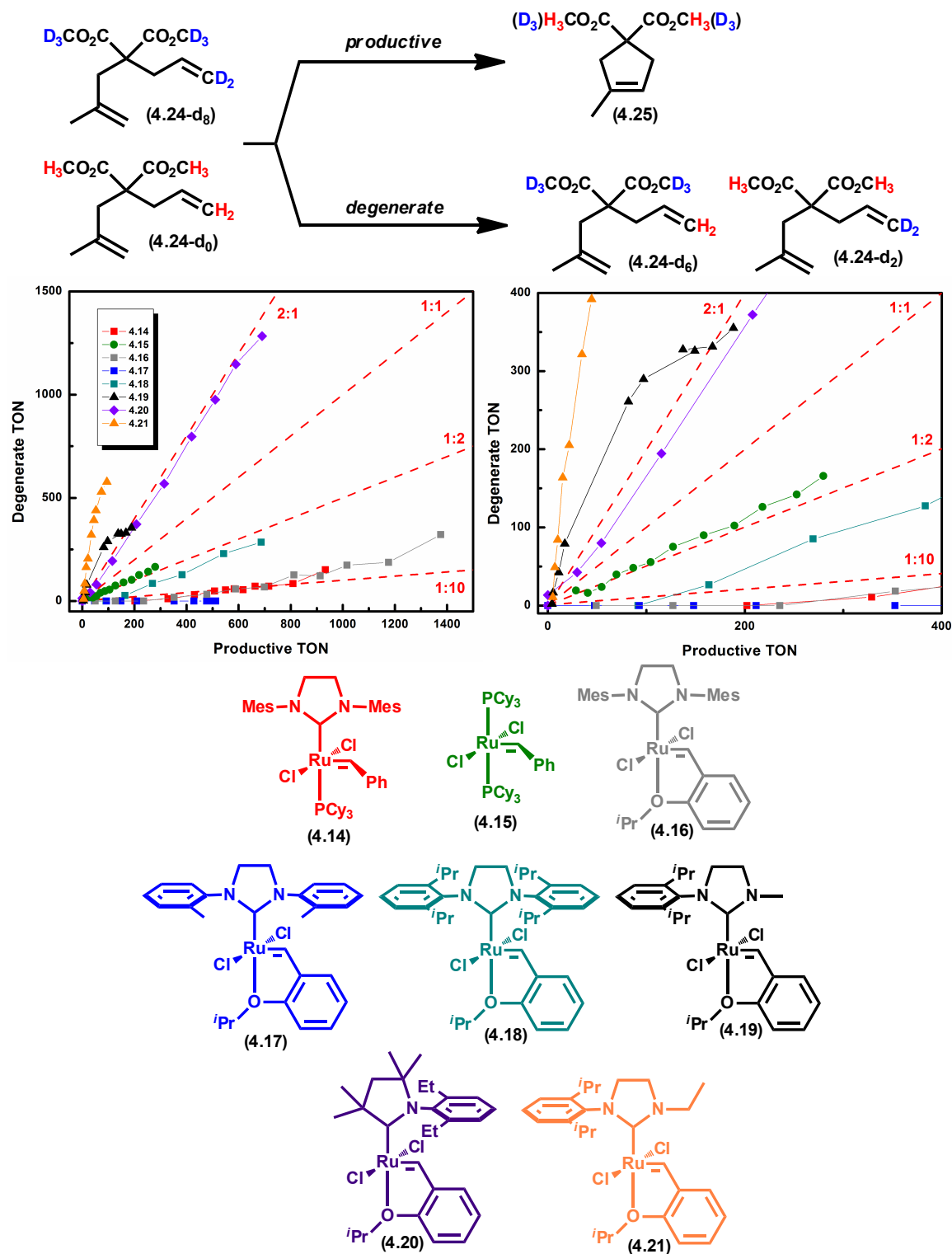


Figure 4.11. (top) RCM of **4.24** to form **4.25**. (bottom) Plot of degenerate TON versus productive TON for the RCM of **4.24-d₈** and **4.24-d₀**. Reaction conditions were 50 ° in PhCH₃ (1 mL) with substrate (0.1 mmol total, **4.24-d₈**:**4.24-d₀**, 1:1) and catalyst (**4.15**—000 ppm, **4.14**, **4.16**, **4.17**, **4.18**—250 ppm, **4.19**—5000 ppm, **4.20**—500 ppm, **4.21**—1000 ppm)

certain reactions, such as ethenolysis.¹¹ However, recall that an alkylidene complex was proposed as the active degenerate species in heterogeneous metathesis catalysts. Therefore, despite the above results favoring a methylidene, new assays will need to be developed that are more sensitive over a larger concentration regime in order to precisely determine the species responsible for degenerate metathesis.

In order to evaluate the effect of degenerate metathesis in a more challenging reaction, the RCM of **4.24** was attempted. For this reaction, a mixture of **4.24-d₈** and **4.24-d₀**, which were prepared in an analogous manner to **4.5**, were subjected to catalysts **4.14–4.21**. As before, productive metathesis was measured by GC while degenerate metathesis (to **4.24-d₆** and **4.24-d₂**) was monitored by LCMS-TOF (Figure 4.11). In line with previous results for substrate **4.5-d₂**, NHC catalysts **4.14**, **4.16**, and **4.17** performed the fewest degenerate events. In the case of catalyst **4.17**, almost no degenerate reactions were detected. Bulky NHC-bearing catalyst **4.18** and bisphosphine catalyst **4.15** performed around one degenerate reaction for every two productive turnovers. Catalysts **4.19–4.21**, on the other hand, perform two or more degenerate reactions for every productive RCM event. Overall, the relative differences in selectivity between catalysts were the same as in the RCM of **4.5**. However, the ratio of degenerate to productive TON was typically larger in the case of **4.24**, which reflects the increased difficulty of this RCM reaction. In other words, there are more opportunities for degenerate metathesis because the RCM of **4.24** is comparatively slow.

Kinetic Modeling

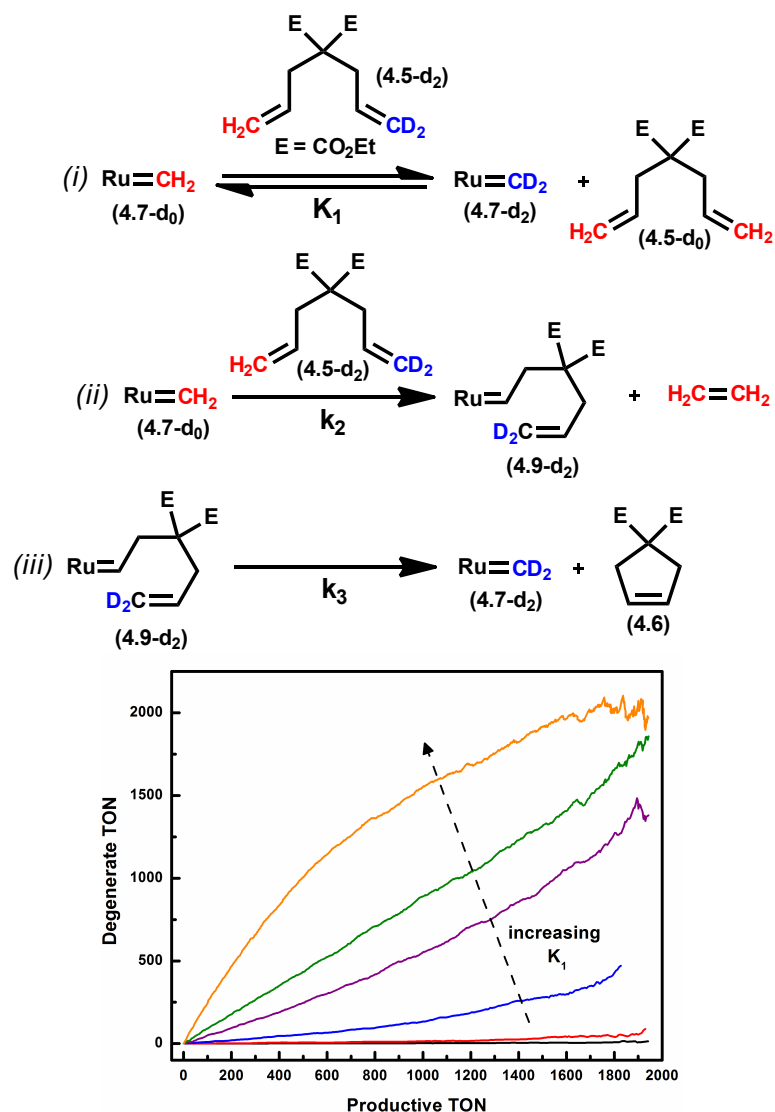


Figure 4.12. Simplified kinetic model for RCM of **4.5-d₂**. See experimental section for complete model. (i) Methyldene equilibrium (K_1 , forward and reverse rate constants) = varied (0.001 – 3), (ii) methyldene to alkylidene ($k_2 = 1$), (iii) alkylidene to product ($k_3 = 10$)

The catalytic cycle for the RCM of both **4.5** and **4.24** is fairly complex (as shown in Figure 4.3) and involves multiple reversible and irreversible steps that are difficult to observe experimentally. Only recently has it become possible to experimentally elucidate the potential energy surface (i.e., the relative energy of intermediates and transition states) for the productive component of RCM.⁹

Due to the limitations described above, we turned to kinetic modeling in order to reproduce the selectivity curves in Figure 4.6 and Figure 4.11 and to further our understanding of the reactions giving rise to degenerate metathesis. A simple kinetic model that accounts for catalyst initiation, initial formation of either an alkylidene or methylidene, degenerate exchange, and productive metathesis was developed using IBM's Chemical Kinetics Simulator.¹² Since we could not determine rate constants experimentally, arbitrary rate constants were chosen and varied relative to one another. We chose a Ru methylidene as the active species for degenerate metathesis since we assumed intramolecular cyclization (k_3) from alkylidene **4.9** would be much faster than intermolecular reactions (e.g., degenerate metathesis). As shown in Figure 4.12, by progressively increasing the forward and reverse rate constants corresponding to degenerate exchange, we were able to reproduce the experimentally observed selectivity curves. Obviously, this assumes that all other rate constants remain constant across the entire catalyst series, which we later determined not to be true (Chapter 5). Nevertheless, this simple model effectively captures the experimentally observed behavior of catalysts **4.14–4.21**. Moreover, it also provides a framework that can be used when rate constants for productive and degenerate metathesis become available from theoretical and experimental studies.

Degenerate Metathesis and Ethenolysis

Ethenolysis is the reaction of an internal olefin with ethylene to generate thermodynamically disfavored terminal olefins (Figure 4.13). There is a significant interest in this reaction as a method for converting fatty acids derived

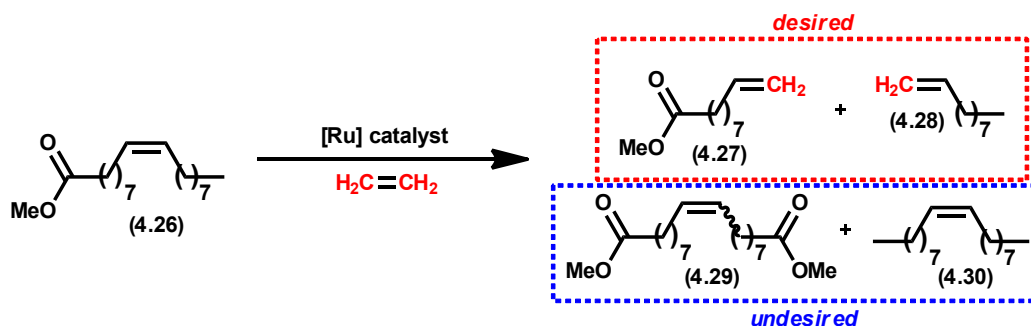


Figure 4.13. Ethenolysis of methyl oleate (4.26)

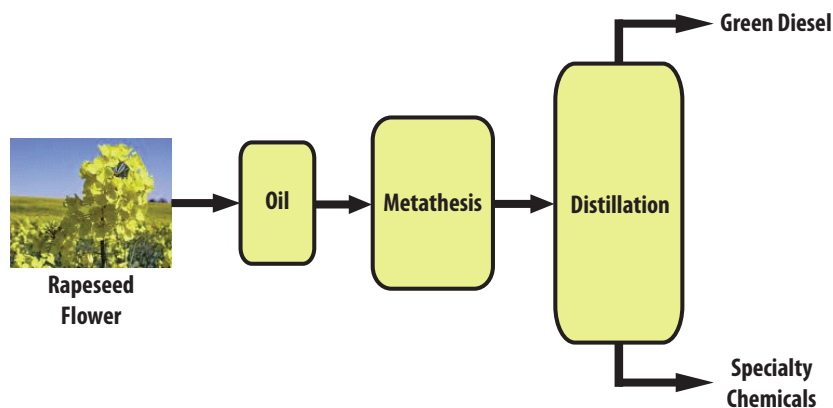


Figure 4.14. Incorporation of ethenolysis of seed oils into an industrial process for fuel and specialty chemical production

from renewable biomass into valuable commercial products (Figure 4.14).¹³ Therefore, the development of a suitable catalyst to effect such a process would facilitate the green synthesis of commodity chemicals from renewable source materials instead of from petroleum. Unfortunately, because ethenolysis is thermodynamically disfavored relative to cross-metathesis (CM), selectivity, or the ratio of terminal olefins (desired) to internal olefins, is often low. In order to develop a commercially viable process, the selectivity and activity (TON) of current catalysts, based on both Ru and Mo, must be improved significantly.

During the course of our investigations into degenerate metathesis, we noted that catalysts with a higher selectivity for degenerate metathesis

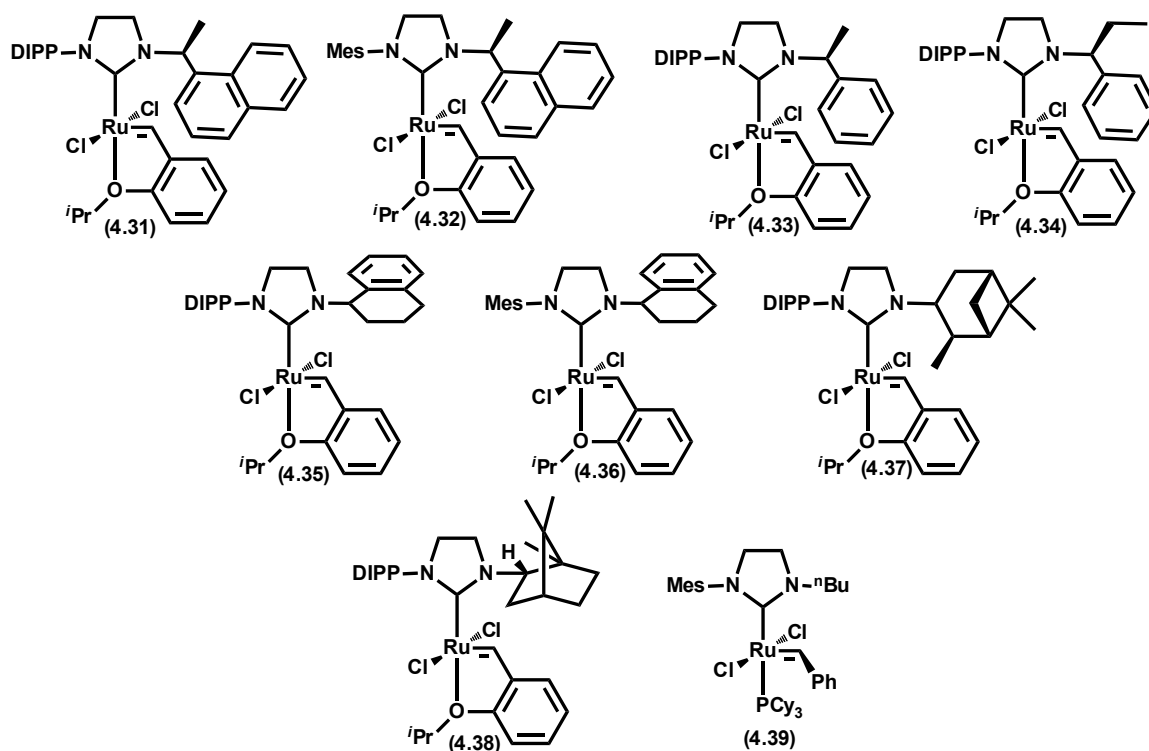


Figure 4.15. Catalysts examined for the ethenolysis of **4.26**

Tabel 4.1. Catalyst comparison for the ethenolysis of **4.26**

entry	catalyst	Conv., % ^b	Selectivity, % ^c	Yield, % ^d	TON ^e
1	4.31	54	86	46	4620
2	4.32	11	77	9	845
3	4.33	52	86	45	4450
4	4.34	42	86	36	3600
5	4.35	59	87	51	5070
6	4.36	17	69	11	1120
7	4.37	52	89	46	4604
8	4.38	15	95	15	1460
9	4.39	40	79	31	3080

^a Reaction conditions were 100 ppm of catalyst in neat **4.26** with 150 psi ethylene for 6 h at 40 °C. ^b Conv. = 100 - [(final moles **4.26**) x 100/(initial moles **4.26**)]. ^c Selectivity = (moles **4.27** + **4.28**) x 100/(moles total product). ^d Yield = (moles **4.27** + **4.28**) x 100/(initial moles **4.26**). ^e TON = yield x [(moles of **4.26**)/moles of catalyst]. Determined by gas chromatography (GC)

were also more effective ethenolysis catalysts. For example, CAAC-based catalyst **4.20** underwent ca. one degenerate TON for every productive one and has been reported to be one of the most selective Ru-based ethenolysis catalysts.¹⁰ Based on this result, we hypothesized that N-aryl/N-alkyl NHC-based catalysts such as **4.19** and **4.21** would also show good selectivity in ethenolysis reactions, without the need for a relatively exotic CAAC.

Unfortunately, when the ethenolysis of **4.26** was attempted with catalysts **4.19** and **4.21**, only catalyst decomposition was observed under our experimental conditions. This is not a surprising result considering neither catalyst reached very high TON in the RCM of **4.5** or **4.24**. Fortunately, several complexes with similar motifs, which were originally designed for asymmetric olefin metathesis, were found to catalyze the ethenolysis of **4.26**. As shown in Table 4.1, catalysts **4.31–4.39** exhibited selectivities for the desired products **4.27** and **4.28** of around 80% or above and demonstrated good TON. For comparison, under the same reaction conditions, catalyst **4.14** yielded a relatively low selectivity of 44% at a TON of 2800. On the other hand, a selectivity of 92% was measured for the ethenolysis of **4.26** catalyzed by **4.20**, which is comparable to the selectivities measured for catalysts **4.31–4.39**. Recall that **4.20**, as well as catalysts similar in structure to **4.31–4.39** displayed increased selectivity for degenerate metathesis. With this in mind, the above results clearly demonstrate that there is a correlation between degenerate selectivity and selectivity for terminal olefins (**4.27** and **4.28**) in ethenolysis. An understanding of this relationship is critical for the development of new ethenolysis catalysts for industrial applications.

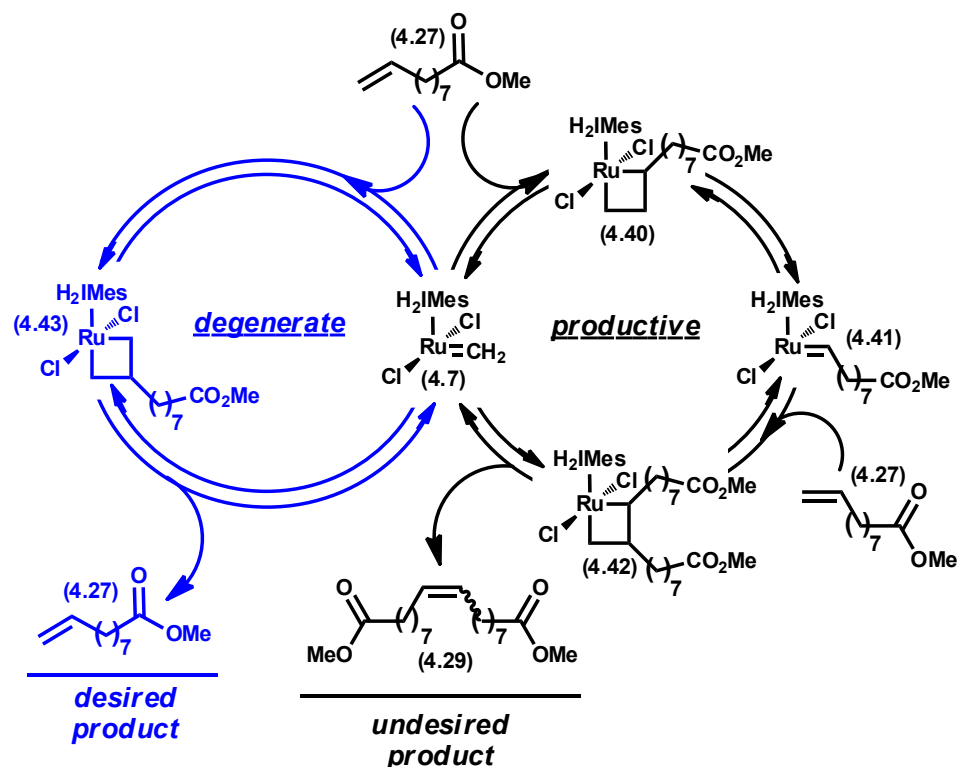


Figure 4.16. Degenerate (blue, left) and productive (black, right) metathesis pathways in the ethenolysis of **4.26**

Due to the high ethylene pressures used in ethenolysis, a propagating methylidene (**4.7**) is the most likely active species.¹⁰ Starting from this intermediate, the catalyst has two choices which affect the selectivity observed in the ethenolysis reaction (Figure 4.16). If an α -substituted ruthenacycle (**4.40**) is formed, a productive metathesis cycle is initiated and undesired product is formed (**4.29**). In contrast, formation of a β -ruthenacycle (**4.43**) from **4.7** yields no change in the concentration of desired product **4.27**. [Note that degenerate metathesis may also proceed through an α,α' -ruthenacycle (e.g. **4.10**) such that formation of **4.40** does not necessarily lead to generation of **4.29** (not shown)]. Regardless of the identity of the degenerate propagating species, we have already established that certain catalysts are more susceptible to degenerate metathesis. As such, these same

catalysts prefer the degenerate pathway (blue) in Figure 4.16; thereby reducing the consumption of the desired products (**4.27** and **4.28**) after their formation. In other words, in the ethenolysis of **4.26**, selectivity for degenerate metathesis is actually beneficial!

Conclusions and Future Outlook

Using a SYMYX core robotic module, we were able to rapidly screen a wide variety of metathesis catalysts in an isotopic cross-over assay that effectively measured the amount of degenerate (nonproductive) to productive olefin metathesis. The structure of the catalyst, in particular the nature of the NHC, was found to have a substantial effect on a catalysts' selectivity for degenerate over productive metathesis. Specifically, N-aryl/N-aryl NHC-based catalysts displayed a preference for productive metathesis while N-aryl/N-*alkyl* catalysts demonstrated much lower preferences for productive metathesis. We also investigated the effects of temperature and substrate concentration on degenerate selectivity, but found these effects to be less significant compared to changes caused by catalyst structure.

We also investigated the consequences of degenerate metathesis selectivity in the ethenolysis of methyl oleate (**4.26**), a reaction with potential industrial applications. For this reaction, catalysts with structures known to increase susceptibility to degenerate metathesis were the most selective for the desired terminal olefin products of ethenolysis. In contrast, productive metathesis-selective catalysts exhibited poor selectivity for the desired ethenolysis products. These results demonstrate that in some circumstances, selectivity for degenerate metathesis can actually be beneficial. With this result in mind, future work should

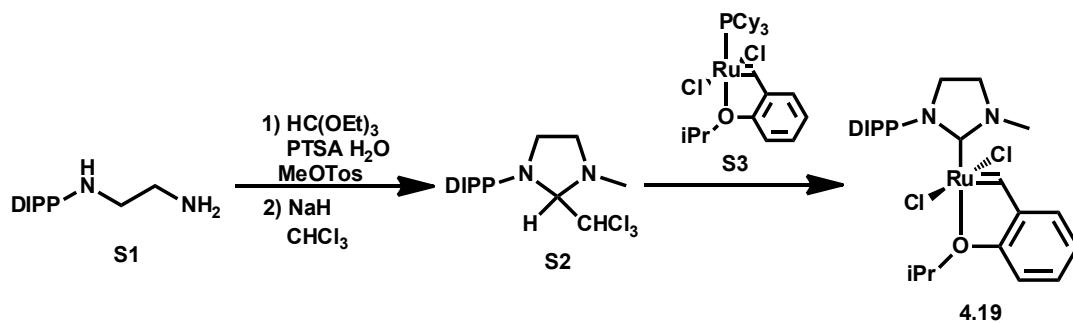
focus on developing degenerate-selective catalysts that are capable of extremely high TON in ethenolysis reactions. Clearly, CAAC-based catalysts, such as **4.20**, appear to be promising in this regard.

Experimental

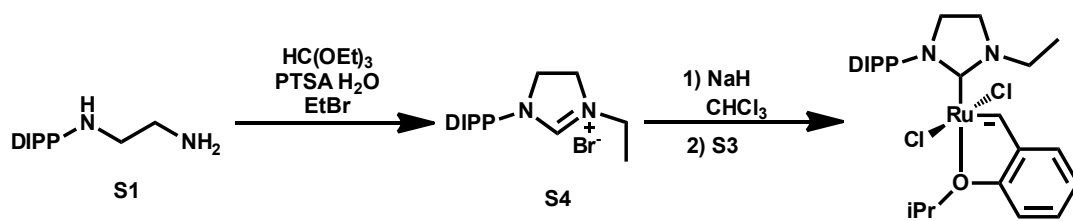
General Information: All reactions were carried out in dry glassware under an argon atmosphere using standard Schlenk techniques or in a Vacuum Atmospheres Glovebox under a nitrogen atmosphere unless otherwise specified. All solvents were purified by passage through solvent purification columns and further degassed with argon.¹⁵ NMR solvents were dried over CaH_2 and vacuum transferred to a dry Schlenk flask and subsequently degassed with argon. Commercially available reagents were used as received unless otherwise noted. Silica gel used for the purification of organometallic compounds was obtained from TSI Scientific, Cambridge, MA (60 Å, pH 6.5-7.0).

Catalysts **4.14**, **4.15**, **4.16**, and **4.17** are commercially available and were used as received. **4.18**¹⁶ and **4.20**¹⁰ and **4.31–4.39**¹⁷ were prepared according to the literature procedure. Productive TONs were measured using an Agilent 6850 Network GC equipped with a HP-1 column (L = 30 m, I.D. = 0.32 mm, Film = 0.25 μm). Response factors were calculated for all compounds prior to determining conversion. Degenerate TONs were measured with an Agilent 6200 Series TOF LC/MS equipped with an Agilent 1200 series HLPC stack using a 100% MeCN Direct Inject method.

Preparation of 4.19: **S1**¹⁸ (91 mg, 0.41 mmol), methyl tosylate (92 mg, 0.49



mmol), PTSA·H₂O (4 mg, 0.02 mmol), CH(OEt)₃ (0.9 mL), and toluene (0.9 mL) were placed in a 20 mL scintillation vial and sealed under air using a teflon cap. The sealed vial was heated to 110 °C for 14 h and then allowed to cool to RT. Et₂O was added to precipitate the product and the solution was stirred for 2 h after which the solvent was decanted off and the remaining solid dried under vacuum. The crude product (280 mg, 0.67 mmol) was dissolved in dry CHCl₃ (10 mL) in a Schlenk flask and 95% NaH (97 mg, 4.0 mmol) was added in portions. The flask was sealed and heated to 55 °C for 14 h. After cooling, the solution was diluted with Et₂O and passed through a pad of silica gel. The filtrate was concentrated without heating and used without further purification. A 50 mL round-bottom flask was dried and charged with **S2** (112 mg, 0.34 mmol), **S3** (103 mg, 0.17 mmol), and THF (20 mL). The flask was heated to 70 °C under argon for 10 h and then concentrated. The residue was dissolved in a minimal amount of C₆H₆ and purified by flash chromatography on silica gel eluting with 10% Et₂O/Pentane to collect a brown band (**S3**), and then 30% Et₂O/Pentane to collect a green/tan band (**7**, 7 mg, 7%). ¹H NMR (500 MHz, C₆D₆): δ 1.04 (m, 6H), 1.11 (m, 6H), 1.72 (m, 6H), 2.92 (m, 2H), 3.34 (m, 4H), 3.82 (s, 3H), 4.63 (sept, *J* = 3.5 Hz, 1H), 6.42 (dd, *J* = 8.5 Hz, *J* = 3.5 Hz, 1H), 6.67 (dt, *J* = 7.5 Hz, 4 Hz, 1H), 7.08 (m, 2H), 7.19 (dd, *J* = 7.5 Hz, *J* = 4 Hz, 2H), 7.36 (dt, *J* = 8 Hz, 4 Hz, 1H), 16.33 (s, 1H). ¹³C NMR (126 MHz, C₆D₆) δ



270.08, 211.51, 153.58, 149.32, 148.20, 144.18, 138.64, 130.10, 129.19, 128.66, 125.44, 122.81, 122.37, 113.49, 107.56, 75.51, 55.44, 51.29, 38.79, 30.54, 28.49, 26.03, 24.57, 22.52. HRMS (FAB⁺): Calculated: 564.1249, Found: 562.1240.

Preparation of 4.21: **S1** (202 mg, 0.917 mmol), EtBr (82 μL , 1.1 mmol), PTSA $\cdot\text{H}_2\text{O}$ (9 mg, 0.05 mmol), CH(OEt)₃ (2.25 mL), and toluene (2.25 mL) were placed in a 20 mL scintillation vial and sealed under air using a Teflon cap. The vial was heated to 110 °C for 16 h, after which it was cooled to RT and the toluene was removed in vacuo. Et₂O (ca. 8 mL) was added to the resulting solution and it was stirred vigorously for 1 h. The Et₂O was decanted off and the remaining precipitate was washed with copious amounts of Et₂O and dried under vacuum. Flash chromatography on silica gel using 7% MeOH:CH₂Cl₂ gave **S4** (92 mg, 30%) as an off white solid. ¹H NMR (300 MHz, CDCl₃): δ 9.50 (s, 1H), 7.34–7.27 (m, 1H), 7.11 (d, J = 7.8 Hz, 2H), 4.33–4.24 (m, 2H), 4.17–4.07 (m, 2H), 3.94 (q, J = 7.2 Hz, 2H), 2.78 (dt, J = 13.6, 6.8 Hz, 2H), 1.32–1.24 (m, 4H), 1.15 (dd, J = 6.8, 3.8 Hz, 12H).

S4 (64 mg, 0.189 mmol) was placed in a 20 mL vial followed by dry CHCl₃ (2 mL). 95% NaH (23 mg, 0.945 mmol) was added in small portions after which the vial was sealed under nitrogen and heated to 55 °C for 10 h. After cooling to RT, the solution was diluted with Et₂O, filtered through a small pad of silica washing with Et₂O, and conc. without heating to give the chloroform adduct (48 mg, 67%) which

was used without further purification. A 100 mL RB flask was dried and charged with the chloroform adduct (306 mg, 0.81 mmol), **S3** (361 mg, 0.60 mmol), and THF (50 mL). The RB was heated to 70 °C for 24 h after which it was cooled to RT and conc. in vacuo. The resulting residue was dissolved in a minimal amount of PhH and flashed on silica gel using 30% Et₂O/Pentane to collect the left over **S3** followed by 60% Et₂O/Pentane to collect **4.21** (40 mg, 9%). ¹H NMR (500 Mhz, C₆D₆): δ 1.01 (d, 6H, *J* = 6.6 Hz), 1.09 (d, 6H, *J* = 6.6 Hz), 1.28 (t, 3H, *J* = 6.6 Hz), 3.05 (m, 2H), 3.30 (sept, 2H, 6.6 Hz), 3.42 (m, 2H), 4.50 (d, 2H, *J* = 6.6 Hz), 4.59 (sept, 1H, *J* = 6 Hz), 6.38 (d, 1H, *J* = 8.4 Hz), 6.65 (dt, 1H, *J* = 7.2 Hz, *J* = 1.2 Hz), 7.04-7.08 (m, 2H), 7.11 (br s, 3H), 7.16 (s, 1H), 7.17 (s, 1H), 7.33 (t, 1H, *J* = 7.8 Hz), 16.32 (s, 1H). ¹³C NMR (151 MHz, C₆D₆) δ 285.32, 210.77, 153.55, 150.67, 149.36, 144.29, 138.68, 130.08, 129.21, 128.90, 128.66, 125.44, 122.82, 122.46, 113.51, 75.41, 55.37, 47.67, 47.25, 28.53, 26.04, 24.59, 22.52, 14.19. HRMS (FAB+): Calculated: 578.1405, Found: 578.1433.

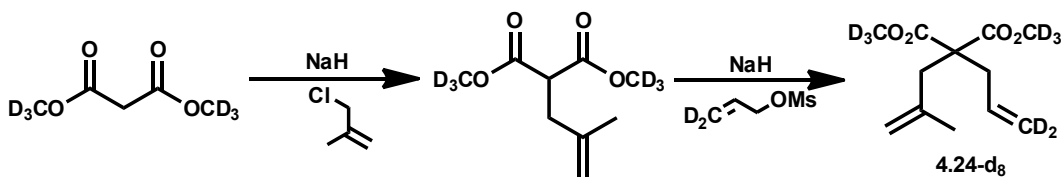
Preparation of 4.5-d₂: Propargyl alcohol (**4.1**, 4 mL, 67.7 mmol), K₂CO₃ (2.8 g, 20.3 mmol), and D₂O (12 mL, Aldrich 99.9%) were combined in a Biotage 20 mL microwave vial with a stir bar. Two other vials with the same reagents were prepared and all three were microwaved at 100 °C for 10 min using a Biotage Initiator microwave. The three vials were combined in a separatory funnel and NaCl was added. The aqueous layer was extracted with Et₂O (3X) and the organic layers were combined, dried with Na₂SO₄, and carefully conc. to yield deuterated propargyl alcohol showing ca. 90% D incorporation. The same procedure was repeated to obtain deuterated propargyl alcohol (**4.2**, 7.06 g, 60%) with >96%

incorporation after distillation under Ar. ^1H NMR (CDCl_3 , 300 MHz): δ 4.23 (s, 2H).

A 250 mL round-bottomed flask was dried and charged with LiAlH_4 (4.94 g, 130 mmol), and Et_2O (150 mL) in a glovebox. The flask was capped with an addition funnel, removed from the box and cooled to 0 °C under Ar. Propargyl alcohol- d_2 (**4.2**, 7.06 mL, 121.6 mmol) was dissolved in Et_2O (28 mL) and added to the addition funnel. The alcohol solution was added drop-wise to the LAH suspension at 0 °C over a period of 1 h after which the solution was allowed to warm to RT and stirred for 6 h. D_2O (5 mL) was added slowly at 0 °C followed by a 15 wt% NaOH in D_2O solution (5 mL). Finally, D_2O (15 mL) was added quickly and the suspension was allowed to stir at RT overnight. MgSO_4 and celite were added and the suspension was filtered through celite, washing with Et_2O , and the filtrate was conc. Allyl alcohol- d_3 (4 g, 55%) was recovered via fractional distillation under Ar. ^1H NMR (CDCl_3 , 300 MHz): δ 5.98 (m, 1H), 4.14 (t, J = 6 Hz, 2H). A 250 mL RB flask was dried and charged with dry triethylamine (6.4 mL, 44.9 mmol), allyl alcohol- d_3 (2.5 g, 40.8 mmol), and Et_2O (120 mL) and cooled to 0 °C. MsCl (3.5 mL, 44.9 mmol) was added drop-wise and the reaction was stirred at 0 °C for 1 h after which it was warmed to RT and stirred for 12 h. The reaction was quenched with H_2O , and the aqueous layer was extracted with Et_2O (3X). The organic layers were combined and stirred with sat. NaHCO_3 for 30 minutes after which the org. layer was separated, washed with brine, and dried with MgSO_4 , and conc. to yield mesylate- d_2 (**4.3**, 1.5 g, 26%) which was used immediately without further purification.

A 100 mL round-bottomed flask was dried and charged with 60% NaH (0.48 g, 20.1 mmol) and THF (20 mL). Diethyl allyl malonate (**4.4**, 3.2 mL, 15.9 mmol)

was added drop-wise and the solution was heated to 60 °C for 30 min. After cooling to RT, mesylate- d_2 (**4.3**, 0.96 g, 6.9 mmol) was added slowly as solution in THF and the reaction was heated to 60 °C for 12 h. After cooling to RT, the reaction was quenched with sat. NH_4Cl and the aq. layer was extracted with Et_2O (2X). The organic layers were combined, dried over Na_2SO_4 and conc. to give the crude product which was purified via flash chromatography on silica gel (5% $\text{EtOAc}/$



Hexanes) to give **4.5- d_2** (1.87 g, 81%). ^1H NMR (300 MHz, CDCl_3) δ 5.65 (dddd, J = 14.8, 10.7, 9.3, 7.4 Hz, 1H), 5.14–5.07 (m, 1H), 4.22–4.13 (m, 2H), 2.63 (dd, J = 7.4, 1.3 Hz, 2H), 1.27–1.22 (m, 3H). ^{13}C NMR (151 MHz, CDCl_3) δ 170.65, 132.27, 132.04, 119.02, 61.12, 57.17, 36.67, 36.57, 14.04.

HRMS (FAB+): Calculated: 243.1570, Found: 243.1560.

Preparation of 24- d_8 : A 100 mL round-bottomed flask was dried and charged with 60% NaH (0.92 g, 38 mmol) and THF (30 mL). Dimethyl malonate- d_6 ¹⁹ (2.5 mL, 20.9 mmol) was added drop-wise and the reaction was heated to 60 °C for 30 min. After cooling to RT, 1-chloro-2-methyl propene (2.27 mL, 23 mmol) was added drop-wise and the reaction was again heated to 60 °C for 12 h. After cooling to RT, the reaction was quenched with sat. NH_4Cl and extracted with Et_2O (3X). The organic layers were combined, dried over Na_2SO_4 and conc. to give the crude product which was purified via flash chromatography (7% $\text{EtOAc}/$

Hexanes) on silica gel (2.23 g, 77%). ^1H NMR (300 MHz, CDCl_3) δ 4.78 (s, 3H), 4.71 (s, 4H), 3.61 (td, $J = 7.8, 1.9$ Hz, 2H), 2.61 (d, $J = 7.1$ Hz, 7H), 1.73 (s, 10H).

The same alkylation procedure as above with the previous product (1.9 g, 9.8 mmol), mesylate- d_2 (**4.3**, 1.5 g, 10.8 mmol), and 60% NaH (0.43 g, 17.9 mmol) yielded **4.24- d_8** (1.62 g, 73%). ^1H NMR (300 MHz, CDCl_3) δ 5.66 (s, 1H), 4.86 (s, 1H), 4.72 (s, 1H), 2.70 (s, 1H), 2.66 (d, $J = 7.4$ Hz, 1H), 1.52 (s, 1H). ^{13}C NMR (151 MHz, CDCl_3) δ 171.43, 140.33, 132.35, 117.47, 115.67, 57.23, 40.23, 36.80, 23.02. HRMS (FAB+): Calculated: 235.1780, Found: 235.1796.

Typical Reaction Procedure: The RCM of **4.5- d_2** and **4.24- d_8** /**4.24- d_0** using the catalysts described were conducted using a SymyxTM Technologies Core Module (Santa Clara, CA) housed in an mBraun nitrogen-filled glovebox and equipped with Julabo LH45 and LH85 temperature-control units for separate positions of the robot tabletop.

For experiments where aliquots were taken during the course of the reaction, the entire operation could be performed on 12 reactions simultaneously in 1 or 2 mL vials by an Epoch software-based protocol as follows. To prepare catalyst stock solutions (1 mM), 20 mL glass scintillation vials were charged with catalyst (5 μmol) and diluted to 5 mL total volume in toluene. Catalyst solutions, 6 to 800 μL depending on desired final catalyst loading, were transferred to reaction vials and solvent was removed via centrifugal evaporation. The catalysts were preheated to 50 $^\circ\text{C}$ using the LH45 unit, and stirring was started. Substrates (0.1 mmol), containing dodecane (0.025 mmol) as an internal standard, were dispensed simultaneously to 4 reactions at a time using one arm of the robot

equipped with a 4-needle assembly. Immediately following substrate addition, toluene was added to reach the desired reaction molarity. The reaction vials were left open to the glovebox atmosphere during the course of the reaction.

After the 2 minutes required for completion of the transfer, 50 μL aliquots of each reaction were withdrawn using the other robot arm and dispensed to 1.2 mL septa-covered vials containing 5% v/v ethyl vinyl ether in toluene cooled to $-20\text{ }^{\circ}\text{C}$ in two 96-well plates. The needle was flushed and washed between dispenses to prevent transfer of the quenching solution into the reaction vials. 16 time points were sampled at preprogrammed intervals and the exact times were recorded by the Epoch protocol. All reactions were conducted in either duplicate or triplicate in order to ensure reproducibility.

Alternatively, reactions could also be performed on the bench as follows. In a glove box, 126 μL of a stock solution prepared from **4.5-d₂** (244 μL , 1 mmol), dodecane (23 μL , 0.1 mmol), and toluene (1 mL) was added to 2 (duplicate) or 3 (triplicate) 4 mL scintillation vials equipped with stir bars. Toluene (0.9 mL) was added and the vials were sealed with septa caps, removed from the box, and heated to $50\text{ }^{\circ}\text{C}$ under a continuous flow of Ar. The desired amount of catalyst (depending on the loading) was injected as a solution in toluene after which 50 μL aliquots were removed over time and injected into chilled GC vials containing toluene and ca. 5% v/v ethyl vinyl ether. Reactions conducted on the bench showed identical behavior to those conducted using the Symyx™ robot. The best results were obtained from the following catalyst loadings:

4.15—1000 ppm, **4.14**, **4.16**, **4.17**, **4.18**—250 ppm, **4.20**—500 ppm, **4.18**—5000

ppm, **21**—1000 ppm.

Productive TON Determination: Samples for GC analysis were obtained by adding a 50 μ L reaction aliquot to 1 mL of toluene containing ca. 5% v/v ethyl vinyl ether at either -10 °C (bench) or -30 °C (robot). GC response factors were determined for all starting materials and products. Dodecane was used as an internal standard. To determine conversion factors, stock solutions of each compound were prepared and used to make various solutions at different [substrate]/[dodecane] ratios. The ratio of the area percent data was plotted against the molar ratio of each solution and the corresponding factor was determined by fitting the data to a linear trendline. Instrument conditions: Inlet temperature: 85 °C; Detector temperature: 250 °C; hydrogen flow: 30 mL/min; air flow: 400 mL/min; constant col + makeup flow: 25 mL/min. GC Method: 85 °C for 1.5 min, followed by temperature increase of 15 °C/min to 160 °C, followed by a second temperature increase of 80 °C/min to 210 °C with a subsequent isothermal period at 210 °C for 5 min. Total run time was 13.1 min including a 210 °C post-run for 1 min. GC data for each timepoint were analyzed according to the following model spreadsheet.

Aliquot	dodecane	P	SM	ratio P	ratio SM	P (mmol)	SM (mmol)	conv.
1	A	B	C	B/A	C/A	$0.01[1.37(\mathbf{B/A})]$	$0.01[1.14(\mathbf{C/A})]$	$P \text{ (mmol)} / [P \text{ (mmol)} + SM \text{ (mmol)}]$

Table S1. Example for calculation of **4.5-d₂** conversions.

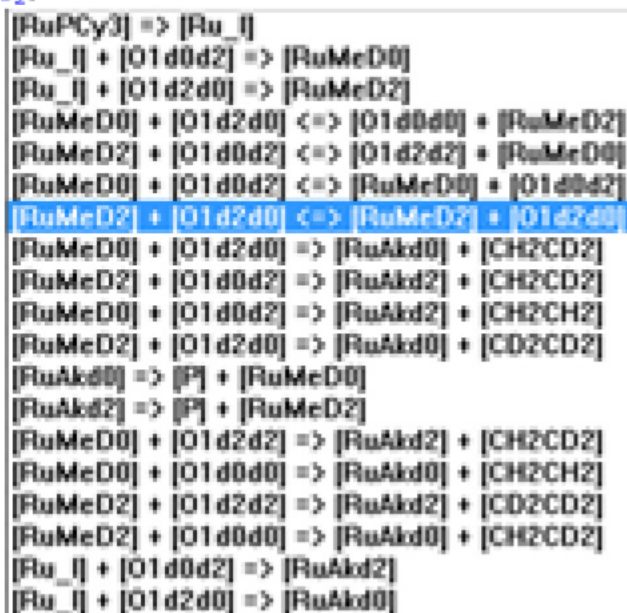
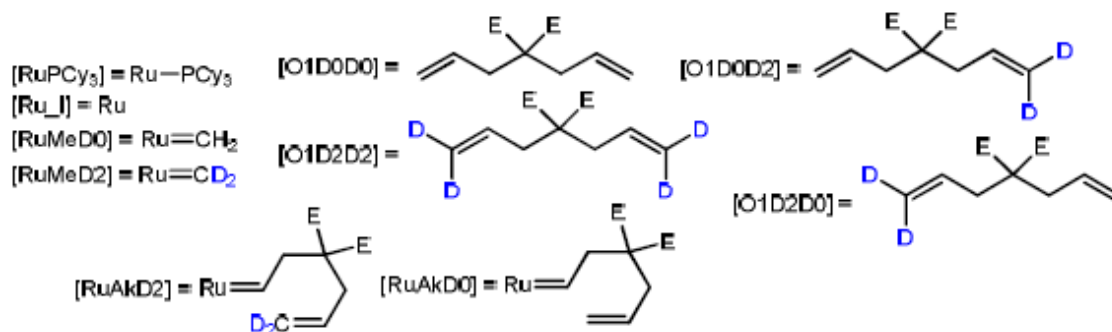
Degenerate TON Determination: Aliquots taken as above were injected (0.75 μ L) into an Agilent 6200 Series TOF LC/MS instrument using a direct-inject 100% MeCN

method. Relative isotopologue counts were obtained from the positive ion spectra and showed good reproducibility when the same sample was injected multiple times.

Using the LCMS-TOF, the counts of **4.5-d₀** and **4.5-d₄** were determined and used to compute a conversion after subtracting the corresponding values for the stock solution (to account for any isotopologues already present). Conversions that resulted in negative values were thrown out. The conversions to **4.5-d₀** and **4.5-d₄** were then each multiplied by 2 and summed together to obtain the total degenerate conversion. This factor of 2 helps account for the degenerate processes that generate the same isotopologue (e.g., **4.5-d₀** reacting with Ru=CH₂ to form **4.5-d₀**). Finally, the degenerate TONs were calculated based on the catalyst loading and compared to the productive TONs which were calculated as above.

Kinetic Modeling: The following model was used in IBM's Chemical Kinetics Simulator. Rate of initial methylidene formation = 1; Rate of initial alkylidene formation = 1; Methylidene equilibrium (forward and reverse rates) = varied; Rate of methylidene to alkylidene = 1; Rate of alkylidene to product = 10.

Procedure for Ethenolysis of Methyl Oleate (4.25): Ethenolysis reactions were carried out using research-grade methyl oleate (> 99%) that was purified by storage over activated alumina followed by filtration. The experiments were set up in a glove box under an atmosphere of argon. Methyl oleate was charged in a Fisher-Porter bottle equipped with a stir bar. A solution of ruthenium catalyst of an appropriate concentration was prepared in dry dichloromethane, and the desired volume of this solution was added to the methyl oleate. The head of the Fisher-Porter bottle was equipped with a pressure gauge and a dip-tube was



adapted on the bottle. The system was sealed and taken out of the glove box to the ethylene line. The vessel was then purged with ethylene (polymer purity 99.9% from Matheson Tri Gas) for 5 minutes, pressurized to 150 psi, and placed in an oil bath at 40°C. The reaction was monitored by collecting samples via the dip-tube at different reaction times. Prior to GC analysis, the reaction aliquots were quenched by adding a 1.0 M isopropanol solution of tris-hydroxymethylphosphine (THMP) to each vial over the course of 2–3 hours. The samples were then heated for over an 1 hour at 60°C, diluted with distilled water, extracted with hexanes and analyzed by gas chromatography (GC). The GC analyses were run using a flame ionization detector. Column: Rtx-5 from Restek (30 m x 0.25 mm (i.d.) x 0.25 μm

film thickness. GC and column conditions: injection temperature, 250 °C; detector temperature, 280 °C; oven temperature, starting temperature, 100 °C; hold time, 1 min. The ramp rate was 10 °C/min to 250 °C, and the temperature was then held at 250 °C for 12 min. Carrier gas: Helium

References

- (1) (a) Casey, C. P.; Tuinstra, H. E. *J. Am. Chem. Soc.* **1978**, *100*, 2270. (b) Casey, C. P.; Tuinstra, H. E.; Saeman, M. C. *J. Am. Chem. Soc.* **1976**, *98*, 608. (c) Handzlik, J. *J. Mol. Cat. A* **2004**, *218*, 91. (d) McGinnis, J.; Katz, T. J.; Hurwitz, S. *J. Am. Chem. Soc.* **1976**, *98*, 605. (e) Tanaka, K.; Takeo, H.; Matsumura, C. *J. Am. Chem. Soc.* **1987**, *109*, 2422.
- (2) Janse van Rensburg, W.; Steynberg, P. J.; Meyer, W. H.; Kirk, M. M.; Forman, G. S. *J. Am. Chem. Soc.* **2004**, *126*, 14332.
- (3) Meek, S.M.; Malcolmson, S.J.; Li, B.; Schrock, R. R.; Hoveyda, A.H. *J. Am. Chem. Soc.* **2009**, *131*, 16407.
- (4) (a) Ritter, T.; Hejl, A.; Wenzel, A. G.; Funk, T. W.; Grubbs, R. H. *Organometallics* **2006**, *25*, 5740. (b) Kuhn, K. M.; Bourg, J.-B.; Chung, C. K.; Virgil, S. C.; Grubbs, R. H. *J. Am. Chem. Soc.*, **2009**, *131*, 5313.
- (5) Ritter, T.; Hejl, A.; Wenzel, A. G.; Funk, T. W.; Grubbs, R. H. *Organometallics* **2006**, *25*, 5740.
- (6) <http://accelrys.com/>. Accessed 06-11-2012
- (7) Stewart, I. C.; Keitz, B. K.; Kuhn, K. M.; Thomas, R. M.; Grubbs, R. H. *J. Am. Chem. Soc.* **2010**, *132*, 8534.
- (8) (a) Sanford, M. S.; Love, J. A.; Grubbs, R. H. *J. Am. Chem. Soc.* **2001**, *123*,

6543. (b) Sanford, M. S. Thesis, California Institute of Technology, 2001.
- (9) (a) Samojłowicz, C.; Bieniek, M.; Grela, K. *Chem. Rev.* **2009**, *109*, 3708. (b) Vougioukalakis, G. C.; Grubbs, R. H. *Chem. Rev.* **2010**, *110*, 1746.
- (10) (a) Romero, P. E.; Piers, W. E.; McDonald, R. *Angew. Chem. Int. Ed.* **2004**, *43*, 6161. (b) Rowley, C. N.; van der Eide, E. F.; Piers, W. E.; Woo, T. K. *Organometallics* **2008**, *27*, 6043. (c) van der Eide, E. F.; Romero, P. E.; Piers, W. E. *J. Am. Chem. Soc.* **2008**, *130*, 4485. (d) Leitao, E. M.; van der Eide, E. F.; Romero, P. E.; Piers, W. E.; McDonald, R. *J. Am. Chem. Soc.* **2010**, *132*, 2784. van der Eide, E. F.; Piers, W. E. *Nature Chemistry*. **2010**, *2*, 571.
- (11) (a) Anderson, D. R.; Lavallo, V.; O'Leary, D. J.; Bertrand, G.; Grubbs, R. H. *Angew. Chem. Int. Ed.* **2007**, *46*, 7262. (b) Anderson, D. R.; Ung, T. A.; Mkrtumyan, G.; Bertrand, G.; Grubbs, R. H.; Schrodi, Y. *Organometallics* **2008**, *27*, 563.
- (12) *Chemical Kinetics Simulator*, version 1.01; International Business Machines: Almaden Research Center, 1996.
- (13) (a) Burdett, K. A.; Harris, L. D.; Margl, P.; Maughon, B. R.; Mokhtar-Zadeh, T.; Saucier, P. C.; Wasserman, E. P. *Organometallics* **2004**, *23*, 2027. (b) Schrodi, Y.; Ung, T.; Vargas, A.; Mkrtumyan, G.; Lee, C. W.; Champagne, T. M.; Pederson, R. L.; Hong, S. H. *Clean* **2008**, *36*, 669. (c) Chikkali, S.; Mecking, S. *Angew. Chem. Int. Ed.* **2012**, *51*, 5802.
- (14) Mandelli, D.; Jannini, M. J. D. M.; Buffon, R.; Schuchardt, U. *J. Am. Oil Chem. Soc.* **1996**, *73*, 229.
- (15) Love, J.A.; Morgan, J.P.; Trnka, T.M.; Grubbs, R.H., *Angew. Chem. Int. Ed.* **2002**, *41*, 4035.

- (16) Blum, A. P.; Ritter, T.; Grubbs, R. H. *Organometallics* **2007**, 26, 2122.
- (17) Thomas, R. M.; Keitz, B. K.; Champagne, T. M.; Grubbs, R. H. *J. Am. Chem. Soc.* **2011**, 133, 7490.
- (18) Marshall, C.; Ward, M. F.; Skakle, J. M. S. *Synthesis* **2006**, 1040.
- (19) Kolsaker, P.; Kvarsnes, A.; Storesund, H. *Org. Mass. Spec.* **1986**, 21, 535.

Chapter 5

Kinetics of Ruthenacyclobutanes Related to Degenerate Metathesis

The text in this chapter is reproduced in part with permission from:

Keitz, B. K.; Grubbs, R. H. *J. Am. Chem. Soc.* **2011**, 133, 16277.

Copyright 2011 American Chemical Society

Abstract

The preparation of new phosphonium alkylidene ruthenium metathesis catalysts containing N-heterocyclic carbenes (NHCs) that result in a preference for degenerate metathesis is described. The reaction of these catalysts with ethylene or substrates relevant to ring-closing metathesis (RCM) produced ruthenacyclobutanes that could be characterized by cryogenic NMR spectroscopy. The rate of α/β methylene exchange in ethylene-only ruthenacycles was found to vary widely between ruthenacycles, in some cases being as low as 3.97 s^{-1} at $-30\text{ }^{\circ}\text{C}$, confirming that the NHC plays an important role in degenerative metathesis reactions. Attempts to generate RCM-relevant ruthenacycles resulted in the low-yielding formation of a previously unobserved species, which we assign as a β -alkyl substituted ruthenacycle. Kinetic investigations of the RCM-relevant ruthenacycles in the presence of excess ethylene revealed a large increase in the kinetic barrier of the rate-limiting dissociation of the cyclopentene RCM product compared to previously investigated catalysts. Taken together, these results shed light on the degenerate/productive selectivity differences observed between different metathesis catalysts.

Introduction

As discussed in Chapter 4, implicit in many olefin metathesis reactions is the presence of degenerate or nonproductive events. For instance, in the cross-metathesis reaction of propylene, a productive reaction would result in the formation of 2-butene, while a degenerate reaction would reform propylene. As the

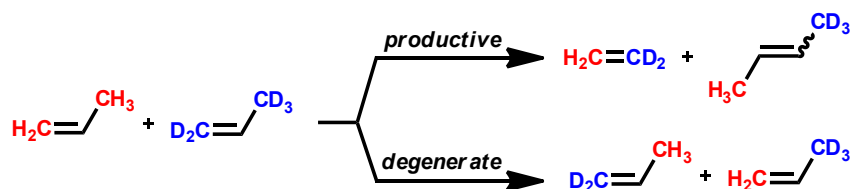


Figure 5.1. Productive and degenerate metathesis of propylene

degenerate reaction reproduces the starting olefin, it can only be reliably studied via isotopic cross-over experiments (Figure 5.1). In Chapter 4, we reported on the study of degenerate events taking place during the ring-closing metathesis (RCM) of an isotopically labeled diethyl diallylmalonate (**5.1**) and discovered the surprising effect of NHC structure on a catalysts propensity to perform either productive or degenerate turnovers (TON).¹ The results of this study validated the importance of degenerate metathesis events and their subsequent effect on catalyst stability and efficiency. We also established that selectivity for degenerate metathesis may actually be beneficial in some applications, such as the ethenolysis of methyl oleate.²

For ruthenium metathesis catalysts, the effect of ligand structure on initiation and stability has been well documented.^{3,4} This information has allowed for the development of increasingly sophisticated catalysts. However, much less is known about the effect of ligand structure on processes that occur within a complex catalytic cycle such as RCM. This lack of understanding has made it difficult to rationalize the behavior of catalysts asked to conduct increasingly challenging transformations. Recently, the situation has been remedied by the development of rapidly initiating catalysts and their ability to efficiently form ruthenacyclobutanes at low temperature, which has facilitated the solution-phase study of previously inaccessible metathesis intermediates by our group⁵ as well as Piers and co-workers

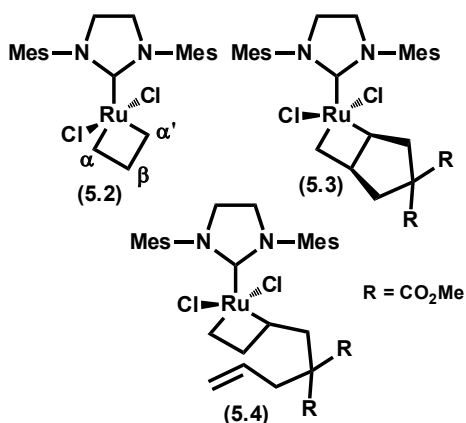


Figure 5.2. Previously observed ruthenacycles relevant to RCM

(Figure 5.2).^{6,7} By analyzing these intermediates and through a combination of kinetics and kinetic modeling, the Piers laboratory has been able to determine the activation energies for the fundamental steps along a productive RCM pathway.⁸

While the above results will undoubtedly facilitate the development of more efficient catalysts, we sought to utilize them as a basis to establish the effect of the NHC on each elementary reaction in the RCM catalytic cycle. Specifically, we wanted to correlate these effects with preference for degenerate selectivity and thereby acquire a more intimate understanding of the role of the NHC in establishing the selectivity for either degenerate or productive olefin metathesis. In this chapter, we report our progress towards this goal.

Results and Discussion

Considering our interest in degenerate metathesis, catalysts incorporating NHCs known to give lower selectivity for productive metathesis in the RCM of **5.1** were selected for study.¹ Thus, we started with previously reported catalyst **5.5** and performed a phosphine exchange in order to expedite the formation of

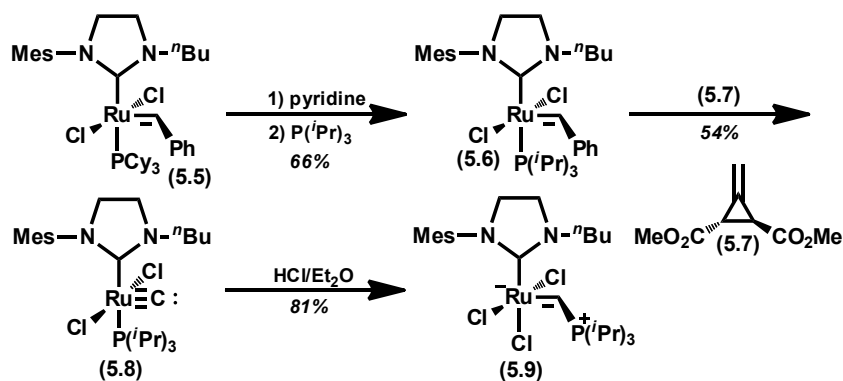


Figure 5.3. Synthesis of phosphonium alkylidene catalyst **5.9**

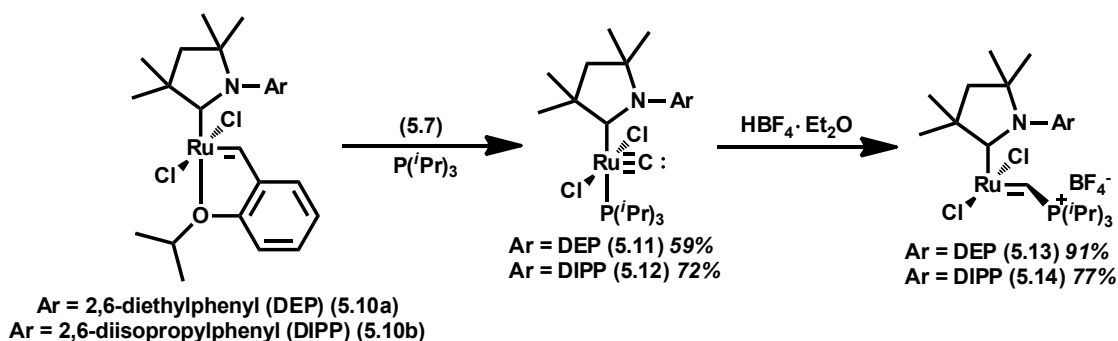


Figure 5.4. Synthesis of catalysts **5.13** and **5.14**

ruthenacycles.^{6,9} Subsequent reaction with Feist's ester (**5.7**) yielded carbide **5.8**, which was then protonated with HCl in Et_2O to afford the desired phosphonium alkylidene complex **5.9** in good yield (Figure 5.3).^{10,11}

Similarly, reaction of the cyclic alkylamino carbene (CAAC) catalysts of type **5.10** with **5.7** in the presence of 1 equivalent of $\text{P}(\text{iPr})_3$ yielded carbides **5.11** and **5.12** which were then protonated in a manner analogous to **5.8** to obtain the desired complexes (**5.13** and **5.14**, Figure 5.4). It should be noted that, this result demonstrates that phosphonium alkylidene complexes may be obtained from Hoveyda-type parent complexes in situations where the corresponding phosphine precursor is synthetically inaccessible.

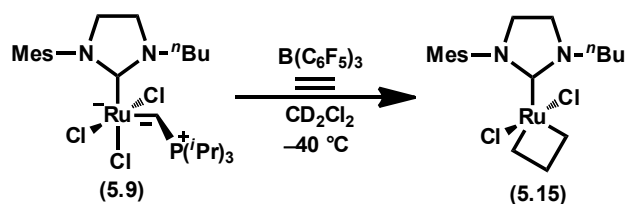


Figure 5.5. Generation of ethylene-only ruthenacycles from **5.9**

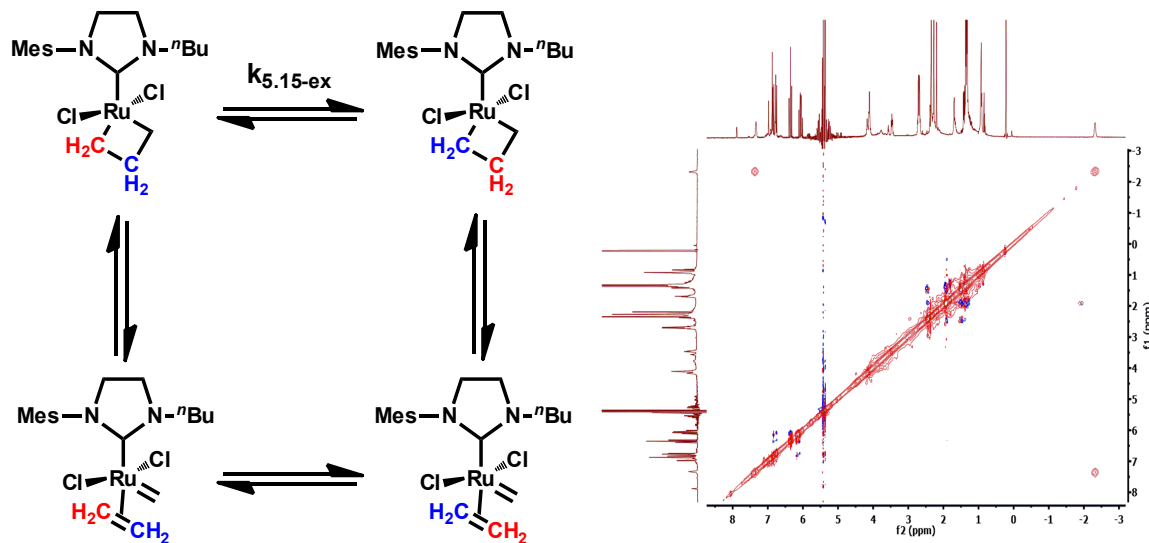


Figure 5.6. Mechanism of ruthenacycle methylene exchange (left) and ROESY spectrum at $-60\text{ }^\circ\text{C}$ with cross-peaks indicative of chemical exchange (right)

With **5.9**, **5.13**, and **5.14** in hand, we next attempted the preparation of ethylene-derived ruthenacycles, as even these simple metallacycles can provide insight into the influence of the NHC ligand. Gratifyingly, complete conversion to metallacycle **5.15** was observed after 3 h at $-40\text{ }^\circ\text{C}$ when **5.9** was exposed to $\text{B(C}_6\text{F}_5)_3$ and 1 atm of ethylene (Figure 5.5). Consistent with analogous complexes, **5.15** displayed an upfield resonance at $\delta = -2.4\text{ ppm}$ characteristic of the hydrogen on the β -carbon of the ruthenacycle. We found compound **5.15** to be stable for several days at $-78\text{ }^\circ\text{C}$ and it could be fully characterized by $^1\text{H-NMR}$ spectroscopy and 2D techniques such as $^1\text{H-}^1\text{H}$ COSY (see Experimental section).¹² A ROESY

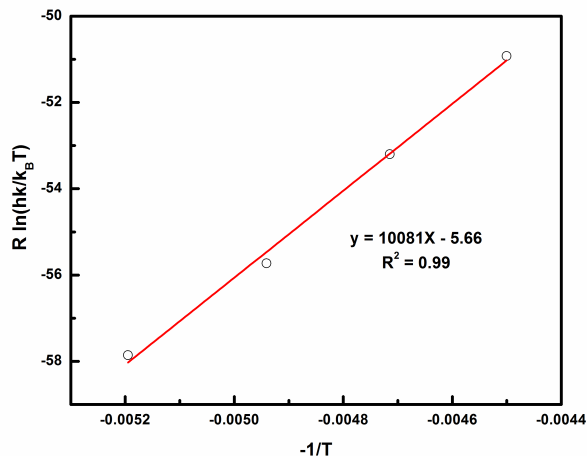


Figure 5.7. Eyring plot for ruthenacycle methylene exchange in **5.15**

spectrum taken at $-60\text{ }^{\circ}\text{C}$ (Figure 5.6) displayed cross-peaks indicative of chemical exchange between the protons on the α and β carbons of the ruthenacycle. Curiously, cross-peaks were only observed between α -H and β -H and not between α' -H and β -H. Although interesting, this situation is not unprecedented, and appears to be a result of asymmetry in the NHC affecting the ruthenacycle.⁵ We next attempted to measure the rate of exchange ($k_{5.15\text{-Ex}}$) between α and β protons using exchange spectroscopy (EXSY). Unfortunately, the presence of a minor peak overlapping with the α -H resonance in **5.15** resulted in irreproducible measurements. However, switching to a magnetization transfer technique allowed us to obtain a $k_{5.15\text{-Ex}}$ of 10.5 s^{-1} at $-60\text{ }^{\circ}\text{C}$ (see Experimental).¹³ This rate is in good agreement with previous reports of ruthenacycles incorporating H_2IMes (H_2IMes = 1,3-dimesitylimidazolidine-2-ylidene) such as **5.2**. An Eyring plot (Figure 5.7) from $-40\text{ }^{\circ}\text{C}$ to $-80\text{ }^{\circ}\text{C}$ yielded values for ΔH^{\ddagger} and ΔS^{\ddagger} of $10.1 \pm 0.5\text{ kcal mol}^{-1}$ and $-5.7 \pm 2.2\text{ cal mol}^{-1}\text{ K}^{-1}$, respectively.

Similar to the case of **5.9** above, the reactions of **5.13** and **5.14** with an

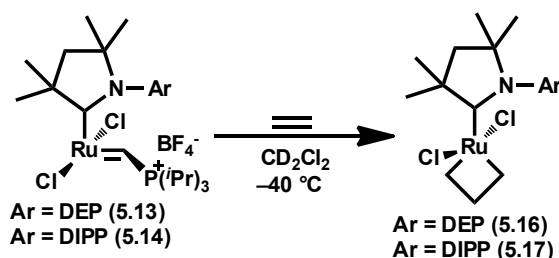


Figure 5.8. Generation of ethylene-only ruthenacycles from **5.13** and **5.14**

Table 5.1. Ruthenacycle methylene exchange rates for all complexes

Complex	Temperature, °C	α/β methylene exchange rate, s ⁻¹
5.15	-60	10.5
5.16	-30	3.97
5.17	-60	1.48

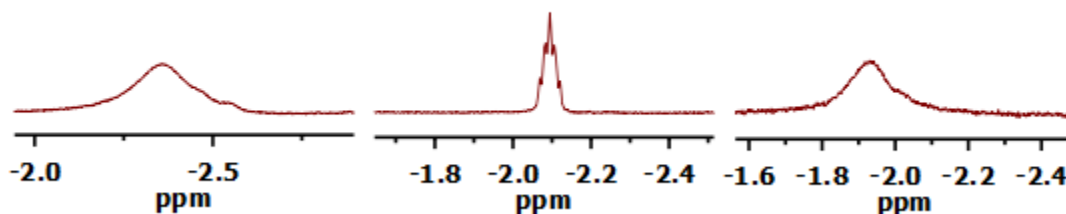


Figure 5.9. ¹H NMR spectrum of β -H ruthenacycles resonance for **5.15** (left), **5.16** (middle), and **5.17** (right) at -30 °C in CD₂Cl₂

excess of ethylene under similar conditions cleanly yielded ruthenacycles **5.16** and **5.17** (Figure 5.8).¹⁴ Characterization of **5.16** was performed according to the same procedure described above, but a ROESY NMR spectrum at -60 °C showed only an NOE between the α -H and β -H; no evidence of chemical exchange was observed. In fact, chemical exchange via ROESY and magnetization transfer was not observed until the temperature was raised to -30 °C! Measurement of the

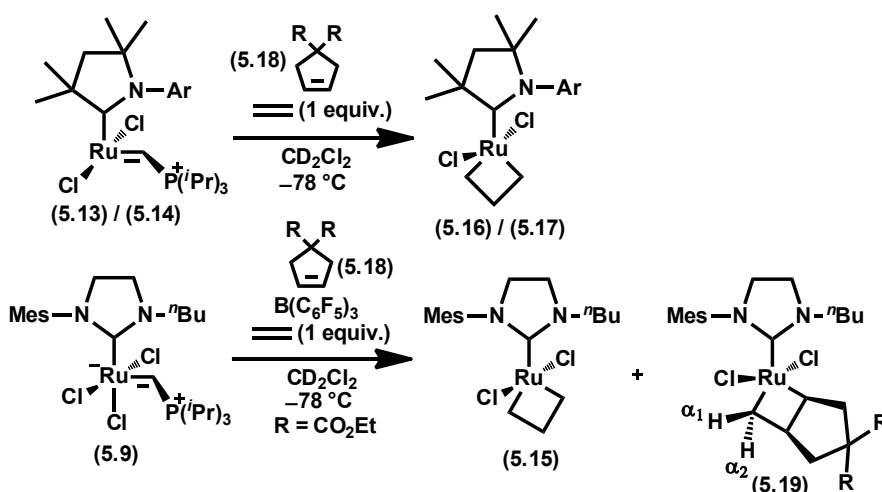


Figure 5.10. Synthesis of substituted ruthenacycles from **5.9** and **5.13**

exchange rate via magnetization transfer yielded an extraordinarily low value of 3.97 s^{-1} at -30°C (Table 5.1). Thus, compared with other catalysts (e.g., **5.2** and **5.15**), $k_{5.16\text{-Ex}}$ is lower, even at higher temperatures. This effect can be qualitatively observed: the ruthenacycle resonances in **5.16** were still sharp at -30°C whereas the same resonances in **5.15** were significantly broadened as a result of chemical exchange (Figure 5.9). In contrast to **5.16**, a ROESY NMR spectrum of ruthenacycle **5.17** taken at -60°C showed evidence of chemical exchange, albeit with a relatively low rate constant (Table 5.1). Although it is difficult to extract definitive conclusions based on such dramatic changes in methylene exchange rates, particularly at the low temperatures under investigation, the extent to which the NHC can affect even the simplest of metathesis reactions is still noteworthy. Furthermore, the low rate of exchange of **5.16**, even at relatively high temperatures, suggests that similar complexes may be viable targets for crystallographic characterization of metathesis-relevant ruthenacycles.

Having established the feasibility of forming simple ruthenacycles with **5.9**,

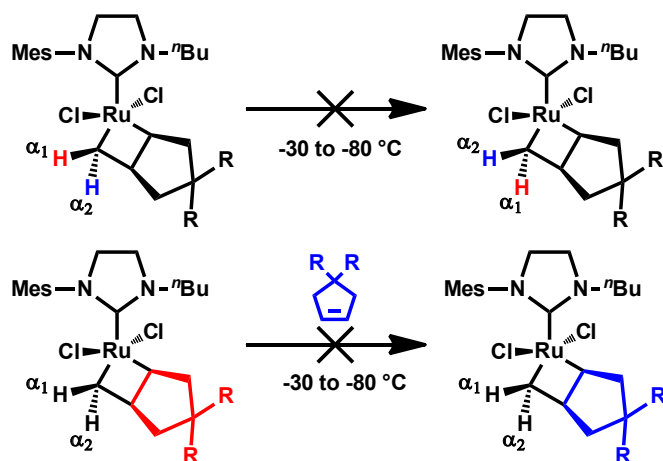


Figure 5.11. Unobserved exchange processes in **5.19**

5.13, and **5.14**, we turned to the preparation and characterization of ruthenacycles relevant to RCM. Adopting a similar approach to the Piers' laboratory, **5.9**, **5.13**, and **5.14** were reacted with the cyclopentene product (**5.18**) resulting from the RCM of diethyl diallylmalonate (**5.1**) in the presence of $\text{B}(\text{C}_6\text{F}_5)_3$ and 1 equiv. of ethylene (Figure 5.10).^{6,8} Unfortunately, under a variety of conditions, both **5.13** and **5.14** reacted to give the ethylene-only ruthenacycles **5.16** and **5.17**, respectively. Such an observation is consistent with the known preference of catalysts containing these NHCs to propagate as methyldiene species in catalytic reactions (e.g., in ethenolysis),¹⁵ but it is nevertheless surprising that no other ruthenacycles were observed.¹⁶ In contrast to **5.13** and **5.14**, when **5.9** was reacted with **5.15** and 1 equiv. of ethylene at -78°C , substituted metallacycle **5.19** was observed, albeit in very low yield (ca. 29%). In all cases, a significant amount of the parent ethylene-only metallacycle **5.15** was also formed (ca. 21% yield). Despite the low yield of **5.19**, we were able to fully characterize the metallacycle resonances by ^1H - ^1H COSY spectroscopy and found them to be consistent with previous literature

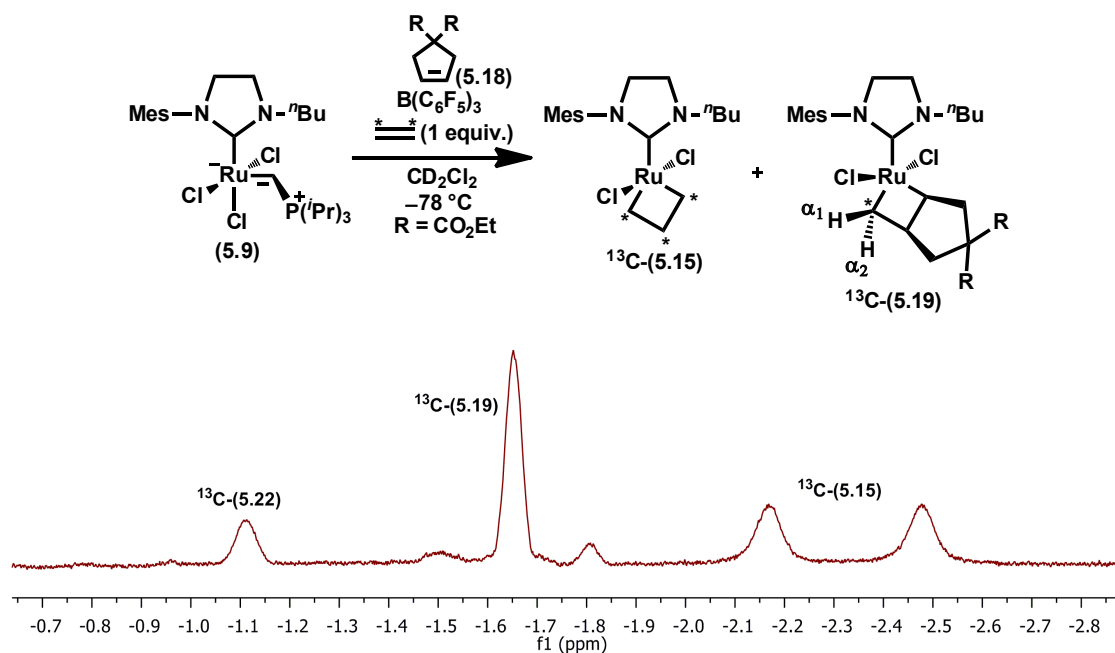


Figure 5.12. Generation of substituted ruthenacycles using ^{13}C -ethylene showing ^{13}C -(5.15) ($\delta = -2.2$ ppm and -2.5 ppm), ^{13}C -(5.19) ($\delta = -1.65$ ppm), and ^{13}C -(5.22) ($\delta = -1.1$ ppm)

reports (*vide infra*).^{6,8} To our surprise, ROESY spectra taken at a variety of different temperatures ($-40^\circ C$ to $-70^\circ C$) and mixing times (up to 600 ms) displayed no evidence of chemical exchange apart from the methylene exchange in **5.15**. This is in contrast to compound **5.3**, which exhibits a number of dynamic processes including exchange between α^1 and α^2 resonances and exchange between **5.3** and free cyclopentene (Figure 5.11).

Upon warming the mixture of **5.15** and **5.19** to $-40^\circ C$ for 2 h, a new peak appeared in the metallacycle region of the NMR spectrum. At first, we believed this peak to be the result of ring opening of **5.19** followed by trapping with ethylene, a process that was observed by Piers (e.g. to form **5.4**).⁸ However, several lines of evidence suggest that, under our conditions, an entirely different intermediate is

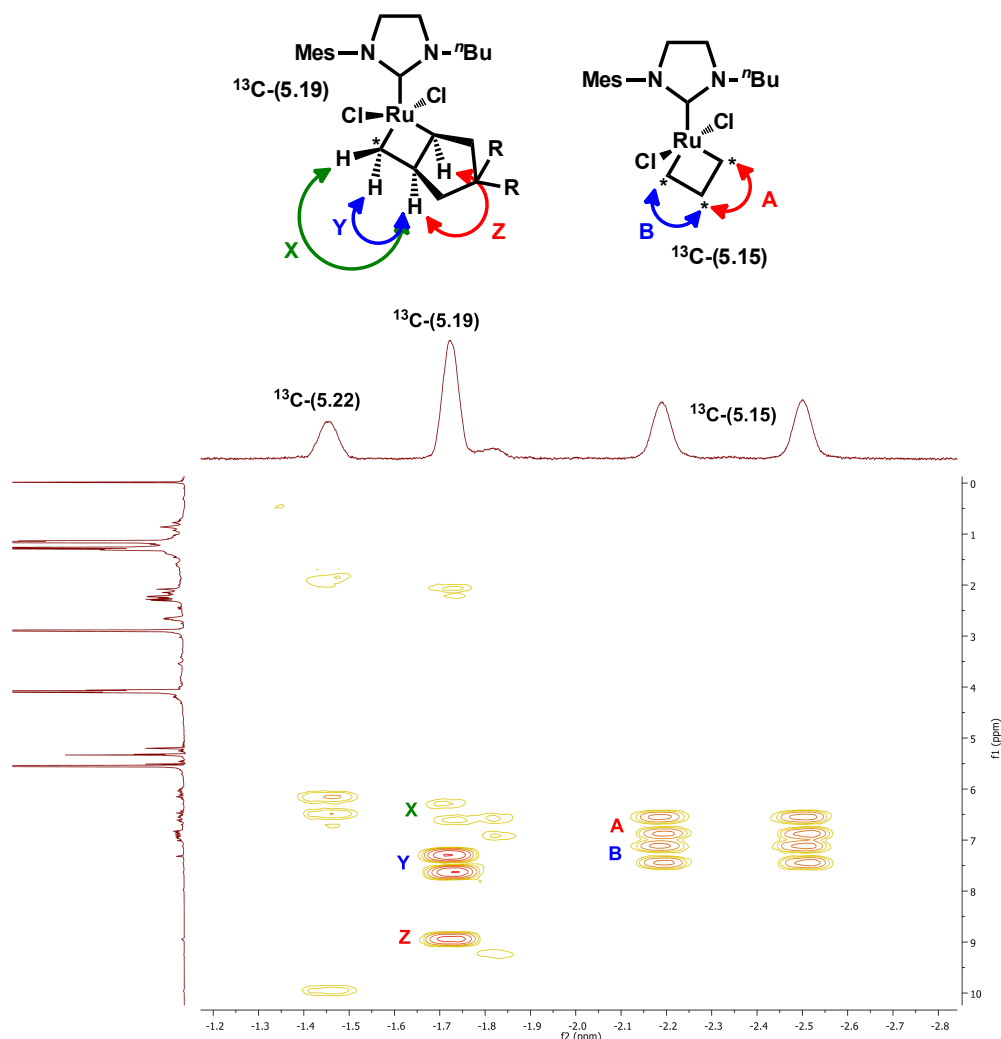


Figure 5.13. ^1H - ^1H COSY of ruthenacycles region for ^{13}C -labelled ruthenacycle mixture at $-90\text{ }^\circ\text{C}$ in CD_2Cl_2 . Note that the assignments of **A** and **B** in ^{13}C -(**5.15**) are arbitrary since there was not enough spectroscopic data to distinguish the two. **X**, **Y**, and **Z** assignments were confirmed by 2D NOESY

formed. First, Piers and coworkers found that ring-opened ruthenacycle **5.4** was only formed at low temperatures (below $-60\text{ }^\circ\text{C}$) whereas the formation of the observed structure only occurred at higher temperatures ($-40\text{ }^\circ\text{C}$). Second and more importantly, substitution at α' should create a set of diastereotopic β -H resonances. Thus, if a structure analogous to **5.4** is correct, there should have been two separate resonances, which were not observed. In order to characterize

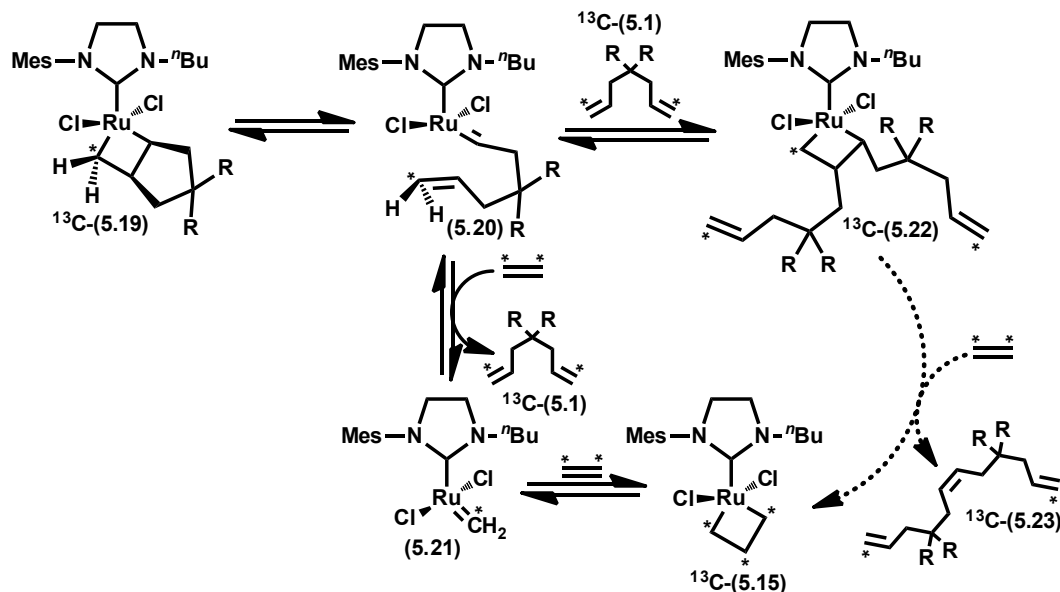


Figure 5.14. Proposed formation of diene **5.1** and ruthenacycles **5.22** from **5.19** and ethylene. Dashed lines represent a possible process that was not observed

this new species and to confirm the identity of **5.19**, compound **5.9** was reacted with **5.18** in the presence of ^{13}C -labelled ethylene (Figure 5.12). The resulting NMR spectrum taken at $-60\text{ }^{\circ}\text{C}$ showed that only one of the three $\beta\text{-H}$ resonances ($\delta = -2.4\text{ ppm}$) was split by virtue of being bound to a ^{13}C -enriched nucleus.¹⁷ This corresponds to the ethylene-only ruthenacycle **5.15**. The other two $\beta\text{-H}$ resonances remained as singlets, which indicated that these protons must have come from substrate **5.18**. These data rules out the presence of a ruthenacycle resulting from the ring opening of **5.19** and trapping of the resulting alkylidene with ethylene. The extremely low concentration of the unknown ruthenacycle and its relatively short T_2 prevented us from establishing its structure by heteronuclear 2D NMR spectroscopy (e.g., HSQC, HMBC).¹⁸ However, we were able to obtain a ^1H - ^1H COSY spectrum at $-90\text{ }^{\circ}\text{C}$ that provided some insight into the structure of the unknown species (Figure 5.13). The COSY confirms our original assignment of **5.15** and **5.19** and

also shows cross-peaks for the unknown species that suggest the following : 1) The β -carbon of the ruthenacycle is substituted with an alkyl group, as shown by a small correlation observed in the alkyl region; 2) The β -H is adjacent to a ^{13}C -enriched nucleus which is shown by a correlation in the α/α' -H ruthenacycle region that is split into a doublet; 3) The α -carbon of the ruthenacycle is also alkyl-substituted as shown by a downfield correlation that is consistent with other α -substituted ruthenacycles. Based on these results, we propose structure **5.22** in Figure 5.14 as the unknown ruthenacycle. If this structure is correct, it would be the first observation of a β -substituted ruthenacycle that is not part of a ring system. However, as a caveat, it must be noted that, it is currently not clear what role (if any) a structure such as **5.22** plays in either productive or nonproductive metathesis. The formation of **5.22** would require ring opening of **5.19** to generate an alkylidene followed by trapping with diene ^{13}C -(**5.1**) instead of ethylene (Figure 5.14). This would obviously require that diene ^{13}C -(**5.1**) be present in solution and an HSQC and ^{13}C NMR spectrum confirmed its presence. Unfortunately, we were unable to reliably establish its concentration due to the overlap of several species in the same region of the 1D ^1H NMR spectrum (see the Experimental).¹⁹ However, reaction of **5.9** with diene **5.1** in place of **5.18** yielded the same three ruthenacycle resonances, although the relative concentration of the various ruthenacycles was largely unchanged compared to previous experiments. Structure **5.22** is consistent with all of our spectroscopic data, but unfortunately, its low concentration has prevented us from establishing its identity with full confidence.²⁰ Furthermore, we were also unable to find conditions where **5.22** did not form, a fact that has

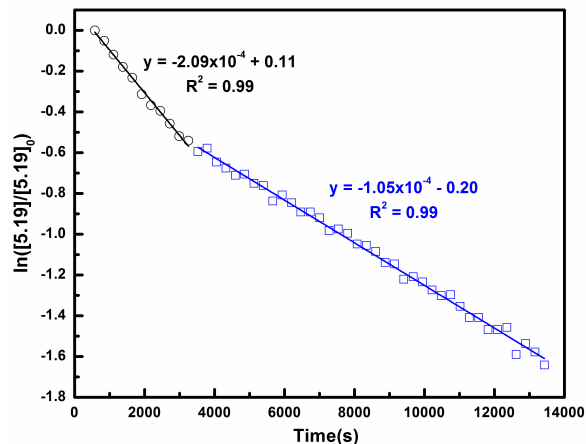


Figure 5.15. Log pot of **[5.19]** showing two apparent first-order decay processes

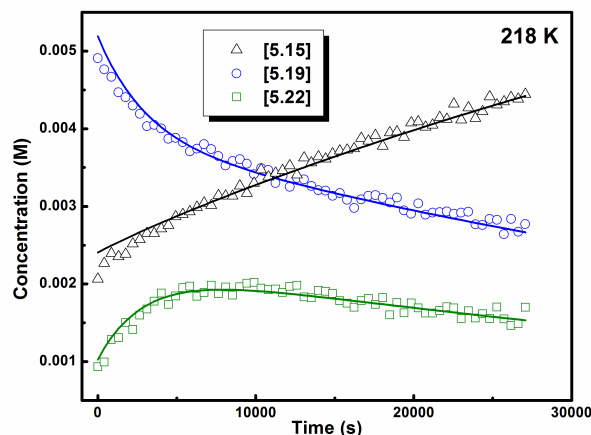


Figure 5.16. Concentration profiles and kinetic fits derived from COPASI for **5.15**, **5.19**, and **5.22** at $-55\text{ }^{\circ}\text{C}$

tremendously complicated our kinetic investigations. Despite these difficulties, we decided to probe the transformation from **5.19** to **5.15**, in the hopes of providing some insight into the effect of the NHC on more advanced ruthenacycle kinetics.

The exposure of an isotopically labeled mixture of ^{13}C -**5.19** and ^{13}C -**5.22** to an excess of ethylene (1 atm) at $-60\text{ }^{\circ}\text{C}$ for 6 hours revealed only a marginal decrease in the intensity of their corresponding resonances. This result is in contrast to what the Piers' laboratory observed with **5.3**, which was consumed

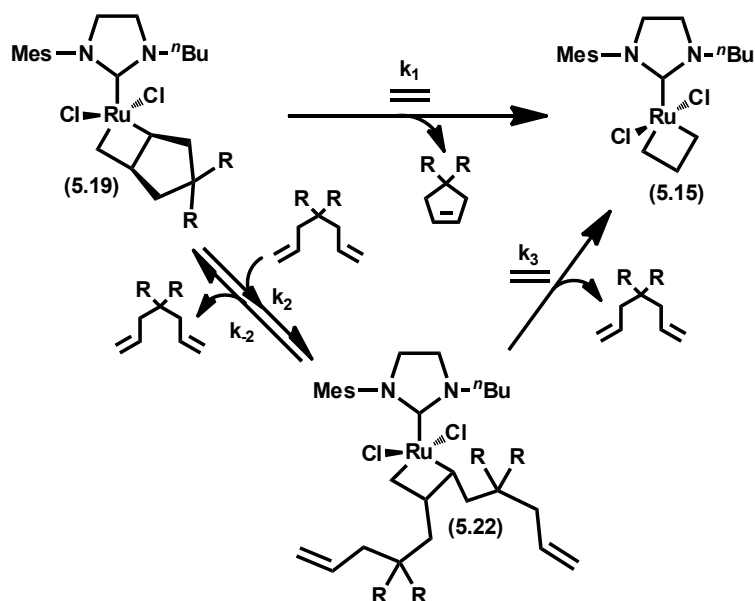


Figure 5.17. Simplified kinetic model for conversion of **5.19** to **5.15** and **5.22** in the presence of excess ethylene

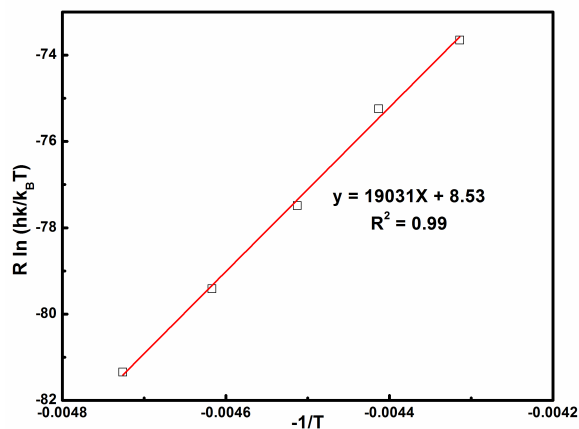


Figure 5.18. Eyring plot for k_1 values (see Figure 5.17) derived from kinetic simulation

within hours under similar conditions. Perhaps more surprising was the slow rate of reaction of ruthenacycle **¹³C-5.15**, which showed almost no significant washing out of the ¹³C label. Again, this is in contrast to catalyst **5.2** formed from ¹³C-labelled ethylene, where the isotopic label was completely washed out within hours, albeit at the higher temperature of $-50\text{ }^{\circ}\text{C}$.⁶ In a separate experiment, increasing the

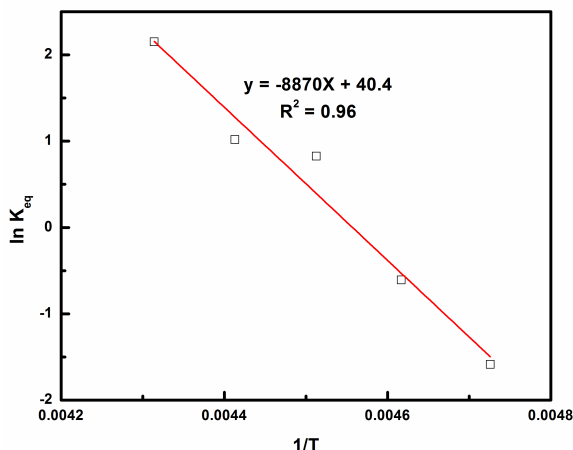


Figure 5.19. Van't Hoff plot using K_{eq} (k_2/k_{-2}) values from COPASI kinetic simulation

temperature of the reaction of **5.19** with excess ethylene to form **5.15** at $-40\text{ }^{\circ}\text{C}$ resulted in clean first-order kinetics that could be monitored on a more manageable timeframe using NMR spectroscopy. However, a closer inspection of the kinetic data revealed a second first-order process that appeared to be occurring at short reaction times (Figure 5.15). We believe this additional process was the result of an equilibrium between **5.19** and **5.22** at early reaction times. Indeed, a time course plot of the concentrations of **5.15**, **5.19**, and **5.22** revealed a slight increase in the concentration of **5.22** followed by a leveling off at later reaction times (Figure 5.16). This result confirms that there are two processes leading to the decrease in the concentration of **5.19**: direct reaction to form **5.15** with release of **5.18**, and an apparent equilibrium reaction to form **5.22**, followed by the subsequent conversion of **5.22** into **5.15** (Figure 5.17).²¹ An analogous sequence of reactions was observed by Piers' under certain conditions, albeit with a different intermediate (**5.4**). Modeling of the simplified series of reactions shown in Figure 5.17 using COPASI²² allowed

for the determination of kinetic parameters k_1 , k_2 , k_{-2} , and k_3 (Figure 5.16).^{23,24} Comparing the k_1 values obtained for **5.19** and **5.3**¹⁶ revealed a stark contrast between the reactivity of the two compounds. For example, at $-60\text{ }^{\circ}\text{C}$, the k_1 value obtained for **5.3** was $7 \times 10^{-4}\text{ s}^{-1}$, whereas the value for **5.19** was two orders of magnitude less at $7.3 \times 10^{-6}\text{ s}^{-1}$. An Eyring plot for k_1 values (Figure 5.18) of **5.19** over a $20\text{ }^{\circ}\text{C}$ temperature range yielded a value for ΔH^{\ddagger} ($19.0 \pm 0.5\text{ kcal/mol}$), which is ca. 3 kcal higher than the corresponding value for **5.3** (16.2 kcal/mol). The ΔS^{\ddagger} values obtained for the two systems were roughly the same ($8.5 \pm 2.3\text{ cal mol}^{-1}\text{ K}^{-1}$ for **19** compared to $3.6\text{ cal mol}^{-1}\text{ K}^{-1}$).

A van't Hoff plot using the values of k_2 and k_{-2} from our kinetic simulations yielded a $\Delta H^{\circ} = 17.6\text{ kcal/mol}$ and a $\Delta S^{\circ} = 80.4\text{ cal mol}^{-1}\text{ K}^{-1}$ (Figure 5.19). Surprisingly, the exothermic ΔH° and large ΔS° differ significantly from the corresponding parameters derived by Piers.⁸ However, the equilibrium reaction presented in Figure 5.17 is fundamentally different from that proposed by Piers, and thus, should be expected to exhibit different thermodynamic parameters. The ΔS° value deserves further discussion as it is unusually large. While we do not currently have an explanation for a ΔS° of such magnitude, it is important to note that the primary purpose of the kinetic modeling was to obtain k_1 values and there is likely a large amount of error in the values of k_2 , k_{-2} , and k_3 (partly evidenced by the relatively poor linear fit in the van't Hoff plot). This being the case, we suspect that a more thorough modeling of the kinetic data would provide a more reasonable estimate of ΔS° .

Although we urge caution in extrapolating these results to behavior under

catalytic conditions and normal operating temperatures, this fundamental transformation in the RCM cycle is clearly much more difficult for **5.19** compared to **5.3**, and may partially explain the lower activities typically associated with complexes of this type. Furthermore, since loss of the cyclopentene product from **5.19** or **5.4** appears to be the rate-determining step in the ring-closing direction, we speculate that the relative increase in the height of this barrier for **5.19** may allow for more degenerate turnovers to occur before a productive turnover can be completed.⁸ This would account for the observation that catalysts containing structurally similar NHCs select for degenerate turnovers during RCM.¹ Finally, the observation of ¹³C-**5.1** in solution suggests that ring opening of the cyclopentene RCM product is facile, and perhaps that the kinetic preference of ring-closing over ring-opening is catalyst dependent.²⁵

Conclusion and Future Outlook

In summary, several new phosphonium alkylidene ruthenium metathesis catalysts incorporating different NHCs have been prepared and used to generate ruthenacycles with the goal of rationalizing degenerate metathesis selectivity. In the case of ethylene-only ruthenacycles, the exchange rate of α and β methylene protons was found to vary considerably across the series of catalysts. With traditional NHCs, the exchange rate was largely consistent with previously reported complexes, while incorporation of a CAAC with DEP as the nitrogen substituent resulted in a severe attenuation of the exchange rate to the point where exchange was not observed until the temperature was increased to $-30\text{ }^{\circ}\text{C}$. Due to this relatively slow exchange rate, one can envision that crystallographic characterization of this complex, or

analogous ones, may be possible. However, subtle changes in ligand architecture can alter the ruthenacycle exchange rate, and by extension, metathesis selectivity and activity. This was demonstrated by the remarkable increase in exchange rate upon substituting DEP with DIPP as the nitrogen substituent on the CAAC ligand. These results demonstrate the significant changes that can occur in even the simplest of metathesis reactions as a result of changes in the NHC structure.

Our attempts to form RCM-relevant ruthenacycles resulted in the formation of a previously unobserved ruthenacycle that we believe to be the first acyclic β -alkyl substituted ruthenacycle. Such a structure is consistent with all of our spectroscopic data, but its low concentration has placed a definitive identification currently out of our technical reach. Nevertheless, this structure plays an important role in ruthenacycle kinetics under an atmosphere of excess ethylene. Our kinetic investigations revealed that the rate-limiting dissociation of the cyclopentene RCM product from the ruthenium center has a much higher energy barrier compared to previously reported complexes. Considering that the majority of the steps along the RCM pathway appear to be reversible, this higher barrier may allow for more degenerate turnovers to occur at the expense of productive ones. At the very least, it provides additional rationale for the generally inferior performance of metathesis catalysts containing *N*-aryl/*N*-alkyl NHC's when compared to those possessing *N*-aryl/*N*-aryl NHCs.

Finally, these studies further illuminate the subtle role that the NHC plays in ruthenium catalyzed olefin metathesis, thus validating efforts to fine tune ruthenium catalysts for specific applications via manipulation of this ligand.

Experimental

General: All reactions were carried out in dry glassware under an argon atmosphere using standard Schlenk line techniques or in a Vacuum Atmospheres Glovebox under a nitrogen atmosphere unless otherwise specified. All solvents were purified by passage through solvent purification columns and further degassed with argon.²⁶ NMR solvents were dried over CaH_2 and vacuum transferred to a dry Schlenk flask and subsequently degassed with argon. Commercially available reagents were used as received unless otherwise noted.

Standard NMR spectroscopy experiments were conducted on a Varian Inova 400 MHz spectrometer, while VT and kinetic experiments were conducted on a Varian 500 MHz spectrometer equipped with an AutoX probe. Accurate temperature measurements of the NMR probe were obtained using a thermocouple connected to a multimeter with the probe immersed in an NMR tube containing a minimal amount of methylene chloride. Experiments and pulse sequences from Varian's Chempack 4 software were used. Chemical shifts are reported in ppm downfield from Me_4Si by using the residual solvent peak as an internal standard. Spectra were analyzed and processed using MestReNova Ver. 7.²⁷ Linear fits and plots were created using OriginPro 8.1.

High-resolution mass spectrometry (HRMS) data was obtained on a JEOL MSRoute mass spectrometer using FAB+ ionization.

Preparation of 5.6: A 100 mL RB flask was charged with catalyst **5**² (0.734 g, 0.93 mmol) and pyridine (3.9 mL) was added under air. The solution changed in color from brown to green over a period of ca. 25 minutes at which point the stirring was

stopped and pentane was carefully layered over the pyridine solution. The flask was placed in a $-10\text{ }^{\circ}\text{C}$ freezer and allowed to stand overnight, at which point a green oil had crashed out. The solvent was decanted away and the green oil was washed with excess pentane, dried in vacuo, and used without further purification (0.611 g).

In a glovebox, the green oil from above (0.611 g) was dissolved in C_6H_6 (10 mL) and $\text{P}(\text{Pr})_3$ (290 μL , 1.38 mmol) was added which caused an immediate color change from green to brown. The solution was stirred for 45 minutes, removed from the glovebox, and conc. in vacuo. The brown/red residue was loaded onto a silica gel column (ca. 70 mL) and flashed with 10% Et_2O /pentane, followed by 40% Et_2O /pentane. The pink/red band was collected and conc. to give **5.6** (0.403 g, 66%). ^1H NMR (400 MHz, C_6D_6) δ 19.45 (s, 1H), 8.04 (br s, 2H), 7.12 (m, 1H), 6.92 (m, 2H), 6.15(m, 2H), 4.16 (m, 2H), 3.11 (m, 4H), 2.59 (m, 3H), 2.27 (br s, 6H), 1.75 (m, 6H), 1.46 (m, 2H), 1.04 (d, $J = 7.3\text{ Hz}$, 9H), 1.01 (d, $J = 7.3\text{ Hz}$, 9H) 0.91 (t, $J = 7.4\text{ Hz}$, 3H). ^{13}C NMR (101 MHz, C_6D_6) δ 295.69, 219.78, 219.02, 151.56, 137.51, 137.38, 136.97, 130.99, 129.13, 50.89, 48.22, 48.19, 30.65, 22.47, 22.31, 21.04, 20.56, 19.64, 18.80, 14.43. ^{31}P NMR (162 MHz, C_6D_6) δ 41.39. HRMS (FAB+): Calculated—666.2219, Found—666.2235.

Preparation of 5.8: In a glovebox, a 100 mL RB flask was charged with **5.7**⁶ (0.108 g, 0.635 mmol) and **5.6** (0.403 g, 0.605 mmol). Methylene chloride (25 mL) was added and the solution was stirred for 14 h, after which it was concentrated inside the glovebox and carefully transferred to a sublimation apparatus. The sublimator was heated to $60\text{ }^{\circ}\text{C}$ under dynamic vacuum (10–100 mTorr) for 2 h. After cooling

to RT, the sublimator was placed back inside the glovebox, and the remaining yellow-brown residue was dissolved in a minimal amount of CH_2Cl_2 and transferred to a 20 mL scintillation vial where the solution was conc. to dryness. Pentane was added and the resulting suspension was stirred vigorously for 5 min after which the pentane was decanted away to yield **5.8** (0.193 g, 54%) as a yellow solid after drying. ^1H NMR (300 MHz, CD_2Cl_2) δ 6.94 (s, 2H), 3.91 (m, 4H), 3.49 (m, 2H), 2.67 (m, 3H), 2.31 (s, 6H), 2.28 (s, 3H), 1.75 (m, 2H), 1.36 (d, J = 7.2 Hz, 9H), 1.31 (d, J = 7.2 Hz, 9H), 1.24 (m, 2H), 0.96 (t, J = 7.4 Hz, 3H). ^{13}C NMR (101 MHz, C_6D_6) δ 471.37, 211.77, 210.93, 138.54, 138.15, 129.47, 51.78, 51.18, 51.15, 49.25, 49.21, 30.65, 22.91, 22.72, 21.40, 20.70, 19.78, 18.53, 14.36. ^{31}P NMR (121 MHz, CD_2Cl_2) δ 42.49. HRMS (FAB+): Calculated—589.1820, Found—589.1815.

Preparation of 5.9: In a glovebox, a Schlenk flask was charged with **5.8** (128 mg, 0.218 mmol) and CH_2Cl_2 (10 mL). The flask was sealed, removed from the glovebox, and HCl (1 M in Et_2O , 3.3 mL, 3.3 mmol) was added in one portion. The flask was sealed under argon and stirred for 16 h at RT, after which the solution was conc. and taken back into the glovebox. The yellow-brown residue was dissolved in a minimal amount of CH_2Cl_2 and transferred to a 20 mL scintillation vial where pentane was carefully layered on top. The vial was chilled to $-35\text{ }^\circ\text{C}$ overnight which resulted in the formation of yellow needle-like crystals that were isolated by decantation of the supernatant followed by washing with pentane. Drying of the washed crystals yielded **5.9** (109 mg, 81%). ^1H NMR (400 MHz, CD_2Cl_2) δ 19.36 (d, J = 51.6 Hz, 1H), 6.97 (s, 2H), 4.51 (m, 2H), 3.82 (m, 4H), 3.31 (dt, J = 15.0, 7.4 Hz, 3H), 2.32 (s, 3H), 2.19 (s, 6H), 1.88 (m, 2H), 1.55 (m, 2H), 1.21 (d, J = 7.4 Hz,

9H), 1.18 (d, $J = 7.3$ Hz, 9H), 1.04 (t, $J = 7.4$ Hz, 3H). ^{13}C NMR (151 MHz, CD_2Cl_2) δ 273.08, 200.80, 138.85, 138.07, 137.81, 130.41, 130.14, 52.84, 52.25, 48.23, 30.91, 25.60, 25.36, 21.31, 20.63, 18.19, 18.01, 17.99, 14.40. ^{31}P NMR (162 MHz, CD_2Cl_2) δ 39.86. HRMS (FAB+): Calculated—626.1479, Found—626.1482.

Preparation of 5.11: In a glovebox, a Schlenk flask was charged with **5.10a**¹⁴ (51 mg, 0.088 mmol), **5.7** (19 mg, 0.114 mmol), $\text{P}(\text{Pr})_3$ (24 μL , 0.114 mmol), and CH_2Cl_2 (2 mL). The flask was sealed, removed from the glovebox, and heated to 35 °C for 2 h. During this period, a color change from green to light yellow occurred. After cooling to RT, the solution was conc., taken back into the glovebox, and transferred to a sublimation apparatus where it was worked up in an analogous manner to compound **5.8**. After removal from the sublimator, the brown-yellow residue was washed with pentane and dried to give **5.11** (12 mg). Chilling the pentane wash to -35 °C for several hours provided an additional crop of **5.11** (19 mg, 31 mg total, 59%). ^1H NMR (400 MHz, CD_2Cl_2) δ 7.31 (m, 3H), 2.83 (m, 2H), 2.72 (d, 3H), 2.53 (m, 2H), 2.09 (s, 2H), 1.72 (s, 6H), 1.36 (s, 6H), 1.34 (d, $J = 7.6$ Hz, 9H), 1.31 (d, $J = 7.6$ Hz, 9H), 1.17 (t, $J = 7.2$ Hz, 6H). ^{13}C NMR (151 MHz, CD_2Cl_2) δ 474.27, 266.11, 265.60, 142.84, 139.82, 139.80, 129.17, 126.69, 80.96, 80.94, 58.68, 58.64, 52.50, 52.48, 31.18, 29.09, 25.43, 22.41, 22.29, 19.76, 14.78. ^{31}P NMR (162 MHz, CD_2Cl_2) δ 40.50. HRMS (FAB+): Calculated—601.1945, Found—601.1967.

Preparation of 5.13: In a glovebox, a Schlenk flask was charged with **5.11** (12 mg, 0.019 mmol) and CH_2Cl_2 (1 mL). The flask was sealed, removed from the box, and $\text{HBF}_4\text{-Et}_2\text{O}$ (5 μL , 0.037 mmol) was added in one portion. After stirring at RT for 1.5 h, the solution was conc. and taken back into the box where the crude product

was vigorously washed with pentane and dried to give **5.13** (12 mg, 91% yield). ^1H NMR (400 MHz, CD_2Cl_2) δ 17.28 (d, J = 34.8 Hz, 1H), 7.66 (t, J = 7.2 Hz, 1H), 7.52 (d, J = 8.0 Hz, 2H), 2.81–2.73 (m, 3H), 2.62–2.55 (m, 2H), 2.37 (s, 2H), 2.32–2.26 (m, 2H), 1.98 (s, 6H), 1.41 (s, 6H), 1.19 (d, J = 7.6 Hz, 6H), 1.16–1.13 (m, 18H). ^{13}C NMR (101 MHz, CD_2Cl_2) δ 265.41, 263.52 (d, J = 21.3 Hz), 247.31, 141.66, 136.88, 130.61, 128.16, 127.41, 82.02, 55.58, 52.02, 51.48, 28.69 (q, J = 27.33), 25.32, 25.06, 24.67, 24.46, 24.02, 21.70, 21.30, 21.12, 20.75, 17.41 (q, J = 33.2 Hz), 13.43 (q, J = 32.5 Hz). ^{31}P NMR (121 MHz, CD_2Cl_2) δ 59.01 (d, J = 19.2 Hz). HRMS (FAB+): Calculated—602.2024, Found—602.2005.

Preparation of 5.12: In a glovebox, a Schlenk flask was charged with **5.10b**¹⁴ (167 mg, 0.276 mmol), **5.7** (61 mg, 0.359 mmol), $\text{P}(\text{iPr})_3$ (68 μL , 0.359 mmol) and C_6H_6 (ca. 4 mL). The flask was sealed, removed from the glovebox, and heated to 80 °C until complete conversion of the starting material (monitored by ^1H NMR spectroscopy, ca. 30 h). After cooling to RT, the reaction was conc. and transferred to a sublimation apparatus inside the glovebox and worked up as above. After removal from the sublimator, the brown-yellow residue was vigorously stirred with pentane for 5 min after which the solvent was removed by decantation and the resulting yellow solid dried to give **5.12** (126 mg, 72%). ^1H NMR (500 MHz, C_6D_6) δ 7.18–7.08 (m, 3H), 3.24 (sept, J = 6.5 Hz, 2H), 2.80–2.53 (m, 3H), 1.90 (s, 6H), 1.64 (s, 2H), 1.56 (d, J = 6.3 Hz, 6H), 1.24 (m, 24H), 1.01 (s, 6H). ^{13}C NMR (126 MHz, C_6D_6) δ 471.88, 268.01, 267.38, 147.52, 136.80, 136.78, 129.67, 125.33, 79.45, 79.42, 58.37, 58.32, 51.99, 51.97, 30.62, 29.83, 28.92, 27.35, 24.62, 22.32, 22.18, 19.63. ^{31}P NMR (162 MHz, CD_2Cl_2) δ 39.66. HRMS (FAB+): Calculated—629.2258,

Found—629.2276.

Preparation of 5.14: In a glovebox, a Schlenk flask was charged with **5.12** (32 mg, 0.051 mmol) and CH_2Cl_2 (4 mL). The flask was sealed, removed from the box, and $\text{HBF}_4\text{-Et}_2\text{O}$ (7 μL , 0.051 mmol) was added which resulted in an immediate color change from orange to brown (Note: When HCl in Et_2O was added to **5.12**, only decomposition was observed). The reaction was stirred for 1 h at RT and conc. before being taken back into the glovebox. Pentane was added and the solution was stirred vigorously until the solution became clear, after which the pentane was removed by decantation, and the resulting solid was washed with additional aliquots of pentane and dried to give **5.14** (28 mg, 77%). ^1H NMR (500 MHz, CD_2Cl_2) δ 17.24 (d, J = 36.6 Hz, 1H), 7.67 (t, J = 7.5 Hz, 1H), 7.53 (d, J = 7.8 Hz, 2H), 2.86 (sept, J = 7.0 Hz, 2H), 2.76 (m, 3H), 2.38 (s, 2H), 1.98 (s, 6H), 1.46 (s, 6H), 1.28 (d, J = 6.7 Hz, 6H), 1.23 (d, J = 7.3 Hz, 9H), 1.19 (d, J = 7.3 Hz, 9H), 0.81 (d, J = 6.6 Hz, 6H). ^{13}C NMR (126 MHz, CD_2Cl_2) δ 246.96, 246.94, 147.28, 134.76, 131.49, 126.91, 82.33, 56.03, 56.00, 50.81, 34.10, 29.90, 28.70, 28.07, 26.65, 24.08, 22.31, 21.71, 21.41, 17.85, 17.82, 13.80. ^{31}P NMR (162 MHz, CD_2Cl_2) δ 59.5 (d, J = 7.8 Hz). HRMS (FAB+): Calculated—631.2415, Found—631.2441.

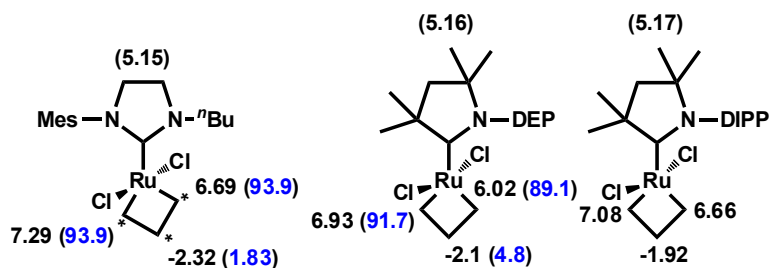


Figure 5.20. Ruthenacycle ^1H NMR and ^{13}C NMR (blue, where available) resonances for **5.15**, **5.16**, and **5.17**

General Procedure for Preparation of Ethylene-only Ruthenacycles (5.15, 5.16, and 5.17): In a glovebox, a 4 mL vial was charged with **9** (12 mg, 0.019 mmol) and $\text{B}(\text{C}_6\text{F}_5)_3$ (12 mg, 0.023 mmol, note that this reagent is not necessary for forming **16** and **17**). The contents of the vial were dissolved in CD_2Cl_2 (0.6 mL) and transferred to a J. Young NMR tube which was sealed, removed from the glovebox and cooled to $-78\text{ }^\circ\text{C}$ in a dry ice/acetone bath. The NMR tube was evacuated and ca. 1 atm of ethylene was added via balloon or through the vacuum manifold. The tube was shaken and then warmed to ca. $-40\text{ }^\circ\text{C}$ in a CO_2/MeCN bath for 2-4 h after which the tube was cooled to $-78\text{ }^\circ\text{C}$ and taken to the NMR spectrometer for analysis. In general, we were only able to accurately assign the ^1H and ^{13}C resonances of the ruthenacycle protons and carbons as the ligand resonances appeared to be complicated by decomposition products. In the case of compound **17**, we were unable to obtain a clean ^{13}C NMR spectrum since the complete

Table 5.2. T_1 Values for catalysts **5.15**, **5.16**, and **5.17**

Complex	Temperature, $^\circ\text{C}$	T_1 , s
5.15	-50	0.271
5.15	-60	0.282
5.15	-70	0.296
5.15	-80	0.267
5.16	-30	0.242
5.17	-60	0.303

conversion of **14** to **17** was never achieved without significant decomposition.

Determination of Methylene Exchange Rates and Eyring Plot: The method used to measure the exchange rate of α and β methylene protons was the spin

saturation transfer method. This method entails the observation of one of the sites of an exchanging system while the other site is saturated with a selective inversion pulse. As a result of the chemical exchange, the intensity of the observed peak decreases until a new steady state is reached. The ratio of the intensity of this new steady-state resonance to the original peak intensity is related to the T_1 of the observed resonance and the rate of chemical exchange by Eq. 1.

$$M_{zA}(\infty) = M_{0A} \frac{T_A}{T_A + T_{1A}} \quad (1)$$

Rearranging Eq. 1 with $k_A = 1/T_A$ and $R_A = 1/T_{1A}$ yields Eq. 2.

$$\frac{M_{zA}(\infty)}{M_{0A}} = \frac{R_A}{R_A + k_A} \quad (2)$$

The T_1 s of the ruthenacycle peaks were measured using the inversion recovery method at the desired temperature.¹²

Ethylene-only ruthenacycles were prepared as described above and equilibrated to the desired temperature. The vNMRj PRESAT pulse sequence was used to selectively invert the downfield exchanging ruthenacycle peak ($\delta \approx 7$ ppm) and an array of delay times (satdly, 0.001 to 1.5 s in 0.1 s intervals) was set up in order to determine the steady state intensity of the peak under observation ($\delta \approx -2$ ppm).²⁸

The exchange rate was then calculated using Eq. 2.

General Procedure for Preparation of Substituted Ruthenacycles (5.15, 5.19, 5.22): In a glovebox, a 1 mL volumetric flask was charged with hexamethyldisiloxane (HMDSO, 28 mg, 0.170 mmol) and filled to the line with CD_2Cl_2 to create a 0.170 M solution of internal standard. A 4 mL vial was charged with 20 μ L of HMDSO stock

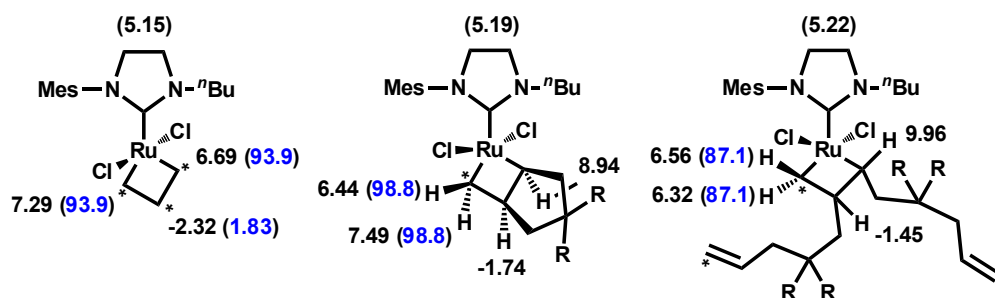


Figure 5.21. Ruthenacycle ^1H NMR and ^{13}C NMR (blue, where available) resonances for **5.15**, **5.19**, and **5.22** in CD_2Cl_2 .

solution and **5.17** (15 μL , 0.067 mmol). A separate 4 mL vial was charged with **5.9** (13 mg, 0.0214 mmol) and $\text{B}(\text{C}_6\text{F}_5)_3$ (13 mg, 0.026 mmol). Both vials were placed in the glovebox cold well which was packed with ChemGlass Lab Armor (CLS-2991-002) and cooled to between $-50\text{ }^\circ\text{C}$ and $-80\text{ }^\circ\text{C}$ using liquid nitrogen (alternatively, the glovebox freezer could be used). A separate vial containing CD_2Cl_2 and an empty J. Young NMR tube were also cooled to the same temperature. Chilled CD_2Cl_2 (0.6 mL) was added to the vial containing **5.9** and after mixing, the vial was placed back in the cold well for 30 min after which the catalyst solution was added to the vial containing **5.17** and the contents quickly transferred to the J. Young tube which was sealed, immediately removed from the glovebox and frozen in liquid nitrogen. After attaching to a high-vacuum manifold, the NMR tube was evacuated and ca. 1 eq. of ethylene was condensed into the tube via a calibrated gas bulb. The tube was carefully warmed to $-78\text{ }^\circ\text{C}$ and shaken several times before warming to $-40\text{ }^\circ\text{C}$ for 2–4 h. For NMR analysis, the tube was transported in a $-78\text{ }^\circ\text{C}$ bath before being placed into the spectrometer which was cooled to the desired temperature.

General Procedure for Kinetics of Conversion of 5.19 to 5.15: A mixture of **5.15**, **5.19**, and **5.22** in CD_2Cl_2 (0.6 mL) was prepared as described above and a spectrum was taken at the desired temperature to determine the initial concentrations of **5.15**, **5.19**, and **5.22**. The NMR tube was then removed from the spectrometer and cooled to $-78\text{ }^\circ\text{C}$ before being attached to a vacuum manifold where it was evacuated and backfilled with ca. 1 atm of ethylene. The tube was shaken and placed back inside the spectrometer and the kinetic run was started at the desired temperature. Spectra were recorded at periodic intervals by arraying the vNMRj 'pad' (pulse acquisition delay) function with a delay of 10 s between pulses. Kinetic runs conducted at $-60\text{ }^\circ\text{C}$ and $-55\text{ }^\circ\text{C}$ were generally too slow to obtain data over several half-lives of **5.19** (e.g., $t_{1/2} > 8\text{ h}$). In these cases, data was collected as long as was practical (ca. 8 h). At all other temperatures, kinetic data was collected for several half-lives of **5.19**.

Spectra were phased and baseline corrected prior to integration of the peaks corresponding to **5.15**, **5.19**, **5.22**, and HMDSO. At higher temperatures ($-40\text{ }^\circ\text{C}$ and $-45\text{ }^\circ\text{C}$), it became difficult to obtain accurate concentrations towards the end of the reaction, hence the large error in the concentration profiles of the reactions conducted at these temperatures.

Discussion of Kinetic Modeling: The experimental concentration profiles of **5.15**, **5.19**, and **5.22** were fitted using the Parameter Estimation function (Levenberg–Marquardt method) in COPASI 4.6 according to reaction sequence presented in Figure 5.17.²¹ Unfortunately, there are more reaction parameters than observable variables (e.g., the concentration of **5.1** could not be determined reliably during the reaction). Therefore, the model is a simplification of what is actually occurring and

any evaluation of the computed rate constants should take this fact into account. Nevertheless, kinetic fits were in generally good agreement with the experimental data (Figure S18).

The following variables were floated in order to allow COPASI to arrive at a solution: initial concentration of **5.15**, initial concentration of **5.19**, initiation concentration of **5.22**, k_1 , k_2 , k_{-2} , and k_3 . The initial concentrations of the ruthenacycle species were varied in order to obtain the best fit possible and were generally in good agreement with the experimentally determined concentrations.

References

- (1) Stewart, I. C.; Keitz, B. K.; Kuhn, K. M.; Thomas, R. M.; Grubbs, R. H. *J. Am. Chem. Soc.* **2010**, *132*, 8534.
- (2) Thomas, R. M.; Keitz, B. K.; Champagne, T. M.; Grubbs, R. H. *J. Am. Chem. Soc.* **2011**, *133*, 7490.
- (3) (a) Sanford, M. S.; Love, J. A.; Grubbs, R. H. *J. Am. Chem. Soc.* **2001**, *123*, 6543. (b) Love, J. A.; Sanford, M. S.; Day, M. W.; Grubbs, R. H. *J. Am. Chem. Soc.* **2003**, *125*, 10103.
- (4) (a) Hong, S. H.; Day, M. W.; Grubbs, R. H. *J. Am. Chem. Soc.* **2004**, *3*, 7414. (b) Courchay, F. C.; Sworen, J. C.; Ghiviriga, I.; Abboud, K. A.; Wagener, K. B. *Organometallics* **2006**, *25*, 6074. (c) Hong, S. H.; Wenzel, A. G.; Salguero, T. T.; Day, M. W.; Grubbs, R. H. *J. Am. Chem. Soc.* **2007**, *129*, 7961.
- (5) (a) Wenzel, A. G.; Grubbs, R. H. *J. Am. Chem. Soc.* **2006**, 16048. (b) Romero, P. E.; Piers, W. E. *J. Am. Chem. Soc.* **2007**, *129*, 1698. (c) Wenzel, A. G.; Blake,

G.; VanderVelde, D. G.; Grubbs, R. H. *J. Am. Chem. Soc.* **2011**, *133*, 6249.

(6) (a) Romero, P. E.; Piers, W. E.; McDonald, R. *Angew. Chem. Int. Ed.* **2004**, *43*, 6161. (b) Rowley, C. N.; Eide, E. F. van der; Piers, W. E.; Woo, T. K. *Organometallics* **2008**, *27*, 6043. (c) Eide, E. F. van der; Romero, P. E.; Piers, W. E. *J. Am. Chem. Soc.* **2008**, *130*, 4485. (d) Leitao, E. M.; Eide, E. F. van der; Romero, P. E.; Piers, W. E.; McDonald, R. *J. Am. Chem. Soc.* **2010**, *132*, 2784.

(7) Ruthenacycles have been studied quite extensively in the gas phase, see : (a) Hinderling, C.; Adlhart, C.; Chen, P. *Angew. Chem. Int. Ed.* **1998**, *37*, 2685. (b) Adlhart, C.; Hinderling, C.; Baumann, H.; Chen, P. *J. Am. Chem. Soc.* **2000**, *122*, 8204.

(8) Eide, E. F. van der; Piers, W. E. *Nature Chemistry*. **2010**, *2*, 571.

(9) Although it would have been advantageous to access ruthenacycles directly from the bis-pyridine adduct of **5.5**, a technique demonstrated in ref. 5c, we found that such a complex could not be isolated as a single clean species. See the Experimental section.

(10) Carlson, R. G.; Gile, M. A.; Heppert, J. A.; Mason, M. H.; Powell, D. R.; VanderVelde, D.; Vilain, J. M. *J. Am. Chem. Soc.* **2002**, *124*, 1580.

(11) Keitz, B. K.; Grubbs, R. H. *J. Am. Chem. Soc.* **2011**, *133*, 16277.

(12) Unfortunately, while the resonances corresponding to the ruthenacycle protons were well resolved, other ligand peaks could not be cleanly identified, most likely due to some decomposition taking place during the reaction as evidenced by the relatively low yield of ruthenacycle.

(13) Sandström, J.; *Dynamic NMR Spectroscopy*, Academic Press Inc.: New York,

1982; pp. 53.

(14) Complete conversion to ruthenacycle **5.17** from **5.14** was never observed, even after extended periods of time at ca. $-40\text{ }^{\circ}\text{C}$. Attempts to raise the temperature resulted in decomposition of **5.17**.

(15) (a) Anderson, D. R. ; Lavallo, V.; O'Leary, D. J.; Bertrand, G.; Grubbs, R. H. *Angew. Chem. Int. Ed.* **2007**, *46*, 7262. (b) Anderson, D. R.; Ung, T. A.; Mkrtumyan, G.; Bertrand, G.; Grubbs, R. H.; Schrodi, Y. *Organometallics*. **2008**, *27*, 563.

(16) The low yielding synthesis of catalysts of type **5.10** hampered our ability to exhaustively examine the behavior of **5.13** and **5.14**.

(17) Several smaller peaks which could correspond to structural analogues of **5.4** are also visible in Figure 5.12. However, due to the extremely low intensity of these resonances, we can only speculate about their identity.

(18) Roberts, J. *ABCs of FT-NMR*, University Science Books : Sausalito, California, 2000; p. 61.

(19) The presence of $^{13}\text{C-1}$ was also confirmed by HRMS (FAB+). Calculated—242.1429, Found—242.1471 after warming the reaction to RT.

(20) Another structure consistent with all of the spectroscopic data is an isomer of **5.19**. However, the large differences in the reactivity of **5.19** and **5.22** with excess ethylene leads us to believe that this is probably not the case.

(21) Direct conversion of **5.22** into **5.15** would require generation of a ruthenium methylidene (**5.21**) and the release of **5.23** (dashed arrows in Figure 5.14). However, neither species was detected by ^1H NMR spectroscopy or HRMS, suggesting that **5.22** prefers to give an alkylidene which subsequently reacts with ethylene to give

5.15.

(22) COPASI (Complex Pathway Simulator) Hoops, S.; Sahle, S.; Gauges, R.; Lee, C.; Pahle, J.; Simus, N.; Singhal, M.; Xu, L.; Mendes, P.; Kummer, U. *Bioinformatics* **2006**, 22, 3067.

(23) Notably, our model does not rely on the positive identification of **5.22**, but only that there is some equilibrium involving **5.19** and another ruthenacycle complex.

(24) At longer reaction times, where the change in concentration of **22** is relatively insignificant and the primary reaction consuming **5.19** is k_1 , the k_{obs} values from a log plot and k_1 values obtained from modeling were generally in good agreement (within a factor of 2 or less).

(25) For a discussion on the kinetic favorability of ring-closing, see ref. 8.

(26) Love, J.A.; Morgan, J.P.; Trnka, T.M.; Grubbs, R.H., *Angew. Chem. Int. Ed.* **2002**, 41, 4035.

(27) www.mestrelab.com

(28) In principle, it is also possible to obtain the same rate by irradiating the downfield resonance and observing the upfield resonance. However, we found it easier to observe the downfield resonance as it is far removed from any overlapping peaks.

Chapter 6

Z-Selective Ruthenium Metathesis Catalysts

The text in this chapter is reproduced in part with permission from:

Keitz, B. K.; Endo, K.; Herbert, M. B.; Grubbs, R. H. *J. Am. Chem. Soc.* **2011**, 133, 9686.

Keitz, B. K.; Endo, K.; Patel, P. R.; Herbert, M. B.; Grubbs, R. H. *J. Am. Chem. Soc.* **2012**, 134, 693.

Keitz, B. K.; Fedorov, A.; Grubbs, R. H. *J. Am. Chem. Soc.* **2012**, 134, 2040.

Copyright 2011 and 2012 American Chemical Society

Abstract

The preparation of C-H-activated ruthenium (Ru) metathesis catalysts for Z-selective olefin metathesis is described. Both the carboxylate ligand and the aryl group of the N-heterocyclic carbene (NHC) ligand have been altered and the resulting catalysts were evaluated using a range of metathesis reactions, including cross metathesis (CM) and ring-opening metathesis polymerization (ROMP). Furthermore, the effect of various ligands on catalyst stability is also discussed along with several unique decomposition structures.

Replacement of the carboxylate ligand on the C-H-activated catalyst with a nitrate group (NO_3^-) resulted in a catalyst with improved activity, selectivity, and tolerance to dioxygen (O_2). This catalyst was found to be capable of ca. 1000 turnovers (TON) with Z-selectivities above 90% in homodimerization reactions.

Introduction

As discussed in Chapter 1, olefin metathesis is a thermodynamically controlled reaction, meaning that there is an equilibrium between the starting materials and the products of a reaction.¹ Moreover, it is well established that in most cases, the *trans* or *E*-olefin is thermodynamically preferred.² Consequently, olefin metathesis gives a higher percentage of *E*-olefins compared to *cis* or *Z*-olefins (Figure 6.1). In order to overcome this limitation and prepare *Z*-olefins via metathesis, chemists have adopted two strategies. One strategy relies on the use of specially designed substrates that yield *Z*-olefins upon metathesis and deprotection.⁴ The other strategy relies on the design of catalysts that are kinetically

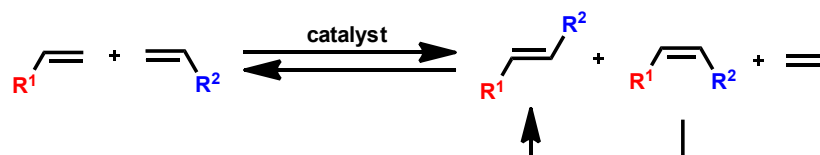


Figure 6.1. Conversion of Z- to E-olefin under thermodynamic control

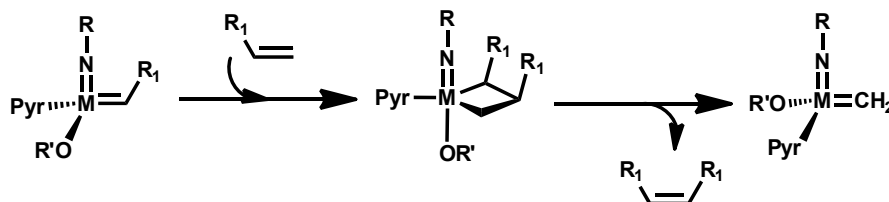


Figure 6.2. Mechanism of Z-selective olefin formation in Mo and W MAP catalysts³

selective for Z-olefins. The preparation of such a catalyst has been extremely challenging since the catalyst must not only be initially selective for Z-olefins but also must not convert Z-olefins into E-olefins via secondary metathesis. Recently, the Schrock and Hoveyda groups reported the first examples of Z-selective olefin metathesis using monoalkoxide pyrrolide (MAP) tungsten (W) and molybdenum (Mo) catalysts.³ These catalysts are effective because they operate through well-defined metallacycle intermediates, the geometry of which is strongly influenced by the pyrrolide and alkoxide ligands (Figure 6.2). In contrast, metathesis-relevant ruthenacycles are much less well defined and have never been characterized by x-ray crystallography.⁵ Moreover, as was shown in Chapter 5, they are also highly fluxional species, even at cryogenic temperatures. For these reasons, and because extremely large ligands shut down Ru activity, a Ru-based analog of the Z-olefin selective Mo and W catalysts has remained out of reach.

However, we recently reported on the synthesis of a C-H-activated Ru metathesis catalyst where the N-heterocyclic carbene (NHC) is chelated to the

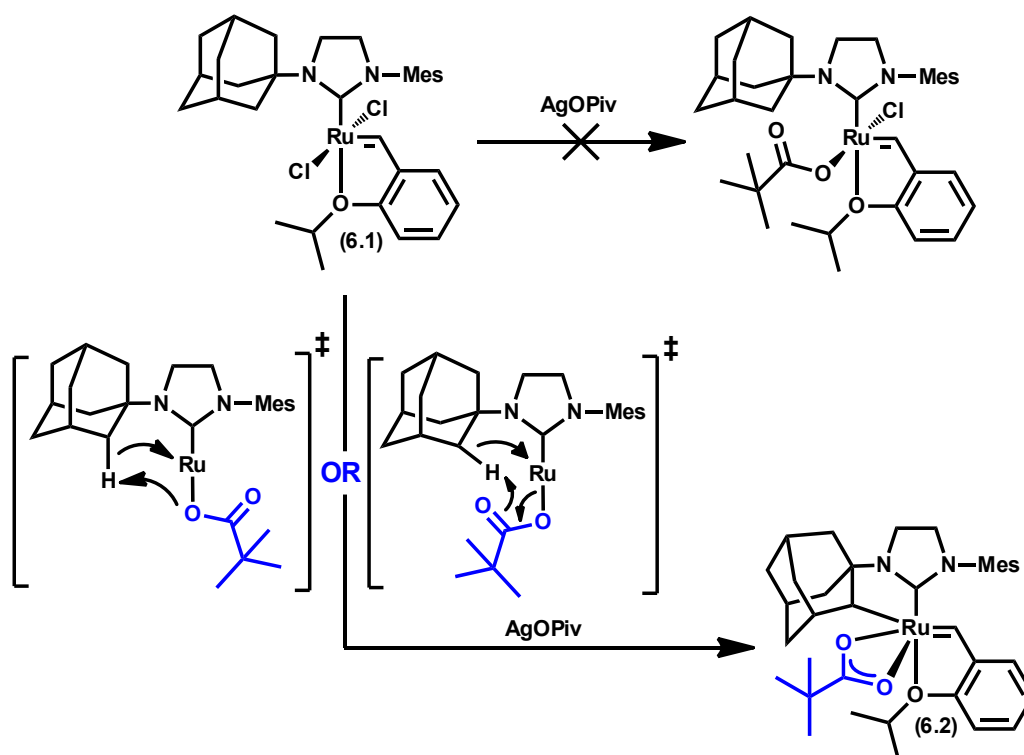


Figure 6.3. Carboxylate-induced C-H activation of **6.1** to form Z-selective catalysts **6.2**

metal center through a Ru-C bond (Figure 6.3).⁶ The unique carboxylate-induced C-H-activation reaction responsible for the generation of the Ru-C bond effectively bypasses the generation of an unstable Ru-H (hydride) species and subsequent decomposition.⁷ Structural analogs of **6.2** have been previously isolated, but were always the result of catalyst decomposition and were never metathesis active themselves. Thus, it was surprising when **6.2** was found to be active at both ring-opening metathesis polymerization (ROMP) and ring-closing metathesis (RCM). More surprising was the fact that **6.2** exhibited remarkable selectivity for Z-olefins during the cross-metathesis of allylbenzene (**6.3**) with *cis*-1,4-diacetoxy-2-butene (**6.4**).⁶

In this chapter, we describe the optimization of **6.2** for the Z-selective

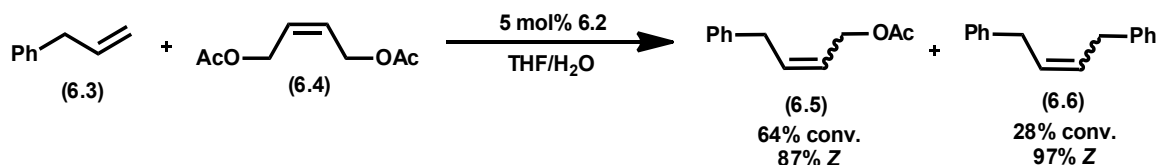


Figure 6.4. Previously reported Z-selectivity of **6.2**

homodimerization of terminal olefins and detail structural changes that have improved the activity and stability of **6.2** by ca. an order of magnitude. The generation of unique decomposition structures and their effect on Z-selectivity is also described. Finally, the application of catalysts like **6.2** towards Z-selective ROMP is discussed.

Results and Discussion

During our early attempts at the cross-metathesis of **6.3** and **6.4**, we observed a significant amount of the homodimer cross-product **6.6** (Figure 6.4). However, this product was only formed in 30% yield, which corresponded to a disappointing TON of 6. Nevertheless, we reasoned that reaction conditions could be optimized to provide good yields of **6.6** and good selectivity for the Z-isomer.

Due to the relatively large adamantyl group on **6.2** and the associative interchange initiation mechanism of complexes of this type, **6.2** required fairly high temperatures in order to initiate efficiently (ca. 70 °C).⁸ Unfortunately, cross-metathesis reactions performed at this temperature and low olefin concentration gave relatively low conversion and showed significant amounts of catalyst decomposition. We suspected that the poor performance of **6.2** under these conditions was the result of ethylene generated as a by-product of the cross-

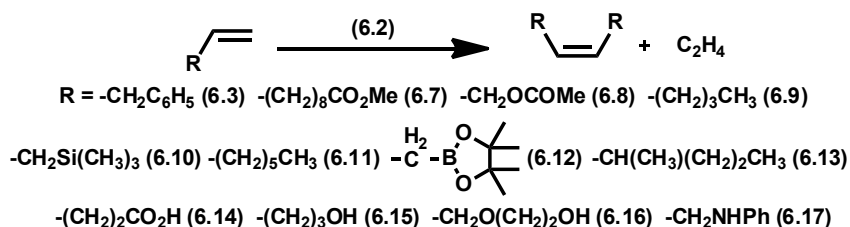


Figure 6.5. Homodimerization of terminal olefins with catalyst **6.2**

Table 6.1. Cross-metathesis of terminal olefins with **6.2** at 70 °C under static vacuum^a

substrate	Solvent	time, h	conv., ^c %	Z, ^c %
Allylbenzene (6.3)	THF	6(10)	>95 (>95)	83 (67)
Methyl undecenoate (6.7)	THF	4(6)	78 (93)	87 (85)
Allyl acetate (6.8)	THF	3(6)	53 (60)	89 (83)
1-hexene (6.9)	THF	6(7.5)	83 (87)	80 (80)
Allyl trimethylsilane (6.10)	THF	6(10)	63 (72)	>95 (>95)
1-octene (6.11)	THF	3(6)	83 (97)	80 (68)
Allyl pinacol borane (6.12)	THF	6	10	>95
3-methyl-1-hexene (6.13)	THF	12	0	0
Allyl benzene (6.6)	MeCN	2.5(21)	12 (15)	>95 (>95)
Methyl undecenoate (6.7)	MeCN	2.5(21)	7 (11)	>95 (70)

^a 2 mol% catalyst in solvent (0.6 M in substrate) at 70 °C under static vacuum. ^b 4 mol % catalyst. ^c Conversion to desired homodimer product measured by ¹H NMR spectroscopy.

metathesis reaction, and indeed, exposure of **6.2** to an atmosphere of ethylene at room temperature resulted in complete decomposition within a few minutes.

While the decomposition of **6.2** in the presence of ethylene was disappointing, it is not uncommon among metathesis catalysts and can be mitigated by the efficient removal of the gas from solution.^{8,9} Therefore, a series of cross-metathesis reactions were run under static vacuum, and under these conditions, **6.2** performed admirably (Table 6.1). For instance, **6.2** was stable in THF and MeCN as long as O₂ was rigorously excluded, and it gave high conversions and Z-selectivity for a

variety of terminal olefin substrates. Some substrates showed a slight decrease in selectivity with increasing conversion, a result which is most likely caused by decomposition products of **6.2**.¹⁰

In contrast to the Group VI metal systems, olefin migration instead of metathesis was observed in some substrates. Attempts to prevent olefin migration via the use of additives such as benzoquinone or mild acid met only with catalyst decomposition (*vide infra*).¹¹ This type of reactivity, although usually undesirable, can be valuable in certain situations.¹² Regardless, olefin migration could be eliminated via careful optimization of reaction conditions (see below). Finally, substrates with even a small amount of substitution (**6.13**) were disappointingly resistant to homodimerization, even at temperatures exceeding 100 °C.

Catalyst **6.2** is clearly functional at high temperature, the presence of deleterious side reactions encouraged us to search for conditions where **6.2** would initiate at lower temperatures. Extensive optimization revealed that **6.2** could affect the homodimerization of terminal olefins at 35 °C with high olefin concentration (ca. 3 M in substrate). This result is not surprising, considering that the initiation of **6.2** should depend on olefin concentration. Nevertheless, we did not anticipate that the activity and selectivity of **6.2** would be superior at 35 °C. Furthermore, reactions performed at lower temperature and higher concentration had the additional advantage of not requiring any special technique to remove ethylene.¹³

For most substrates, reactions with **6.2** at 35 °C showed selectivity similar to that of reactions performed at 70 °C, but improved activity (conversion, Table 6.2). Isolated yields of the homodimerization product were also good. Gratifyingly,

Table 6.2. Cross-metathesis of terminal olefins with **6.2** at 35 °C^a

substrate	time, h	conv., ^b %	Z, ^b %	yield, ^c %
Allylbenzene (6.3)	1	>95	92	81
Methyl undecenoate (6.7)	5.5	>95	73	>95
Allyl acetate (6.8)	4	>95	89	62
1-hexene (6.9) ^d	3	73	69	21
Allyl trimethylsilane (6.10)	3	>95	>95	54
1-octene (6.11)	4	>95	83	79
Allyl pinacol borane (6.12)	4	>95	>95	74
3-methyl-1-hexene (6.13)	24	0	-	-
Pentenoic acid (6.14)	24	0	-	-
4-penten-1-ol (6.15)	1	>95	72	72
2-(allyloxy)ethanol (6.16)	1	87	66	73
<i>N</i> -allylaniline (6.17)	2	70	71	67

^a 2 mol% catalyst in THF (3.33 M in substrate) at 35 °C. ^b Measured by ¹H NMR spectroscopy. ^c Isolated yield. ^d Run in sealed container.

in the case of **6.12**, no detectable amount of olefin migration was observed, and excellent Z-selectivity was maintained up to very high conversion. Emboldened by this success, we attempted to dimerize several more advanced substrates. Unfortunately, in the case of hindered or acidic substrates, no activity was observed. On the other hand, **6.2** was able to dimerize alcoholic substrates with excellent conversion and good selectivity. This latter result is particularly important since it is the first example of Z-selective cross-metathesis with alcohol substrates.

Given that **6.2** is not only stable to water and other protic media, but also shows increased activity, we deemed it appropriate to examine a wide variety of different solvents for the homodimerization of **6.3** at room temperature (RT, Table 6.3)⁶ Several polar and nonpolar solvents were tested, and the majority were conducive to the transformation. Coordinating solvents (e.g., MeCN) resulted in

Table 6.3. Solvent screen for cross-metathesis of **6.7** with **6.2** at RT^a

substrate	Solvent	time, h	conv., ^b %	Z, ^b %
Methyl undecenonate (6.7)	MeCN	3 (28)	19 (76)	94 (91)
	MeOH	3 (28)	49 (87)	88 (75)
	EtOH	3 (28)	50 (86)	89 (76)
	C ₆ H ₆	3 (21)	13 (77)	>95 (84)
	Et ₂ O	3 (7)	50 (85)	93 (73)
	DMF	3 (21)	44 (77)	92 (87)
	CH ₂ Cl ₂	3 (21)	35 (81)	93 (85)
	(CF ₃) ₂ CHOH	3 (28)	0 (0)	-
	Diglyme	3 (28)	31 (81)	95 (80)

^a 2 mol% catalyst in solvent (2.25 M in substrate) at 25 °C. ^b Measured by ¹H NMR spectroscopy.

slower reactions but were able to achieve TON roughly equivalent to those of reactions run in noncoordinating solvents. Protic solvents such as MeOH and EtOH yielded high amounts of Z-olefin product, while hexafluoroisopropanol (CF₃)₂CHOH resulted in immediate catalyst decomposition.¹⁴ The fact that high Z-selectivity is maintained in protic solvents further demonstrates the functional group compatibility of **6.2**. Nevertheless, mildly acidic substrates and solvents appear to result in catalyst decomposition.

Using **6.2**, catalyst loadings as low as 2 mol% were possible for the Z-selective homodimerization of simple terminal olefins. While these results were unprecedented for Ru-based catalysts, the observed degradation in selectivity with increasing conversion and **6.2**'s relative intolerance of dioxygen encouraged us to develop new and improved catalysts.

As previously mentioned, due to the dynamic nature of ruthenacyclobutanes,¹⁵ particularly when compared to molybdocycles and tungstacycles, the origin of the

Z-selectivity in **6.2** has remained unclear. Nonetheless, structure-function relationships derived from systematic changes of **6.2** have demonstrated that the adamantyl group in **6.2** is critical for achieving high levels of Z-selectivity.⁶ Unfortunately, our attempts to make more drastic alterations to this part of the ligand have mostly led to decomposition during the C-H activation step (*vide infra*). As a consequence of attempting to change the adamantyl group in **6.2** with little success, we turned our attention to the carboxylate ligand and to the aryl group on the NHC. Thus, exchanging the pivalate group in **6.2** for other bi- (κ^2) and monodentate (κ^1) ligands, and the mesityl for various aryl groups, has resulted in several new derivatives that yield important insight into the reactivity and selectivity of this class of catalysts. In the subsequent section, we report on the synthesis and selectivity of these new catalysts and demonstrate that several are capable of TON approaching 1000 in cross-metathesis reactions while maintaining excellent Z-selectivity.

We initiated our studies by examining a range of ligands in place of the previously reported carboxylate **6.2** (Figure 6.6). However, bulky carboxylates, such as pivalate, appear to be the only carboxylates capable of inducing the intramolecular C-H activation event necessary to form **6.2**. As such, a new synthetic route was developed in order to access analogues of **6.2** possessing different X-type ligands. We found that reacting **6.2** with NaI in THF cleanly afforded the iodo complex **6.18**, which could then be used to prepare a wide range of catalysts via transmetalation with various silver salts (Figure 6.7). Catalysts with monodentate ligands were obtained in an analogous fashion. Notably, the nitrate complex **6.24**

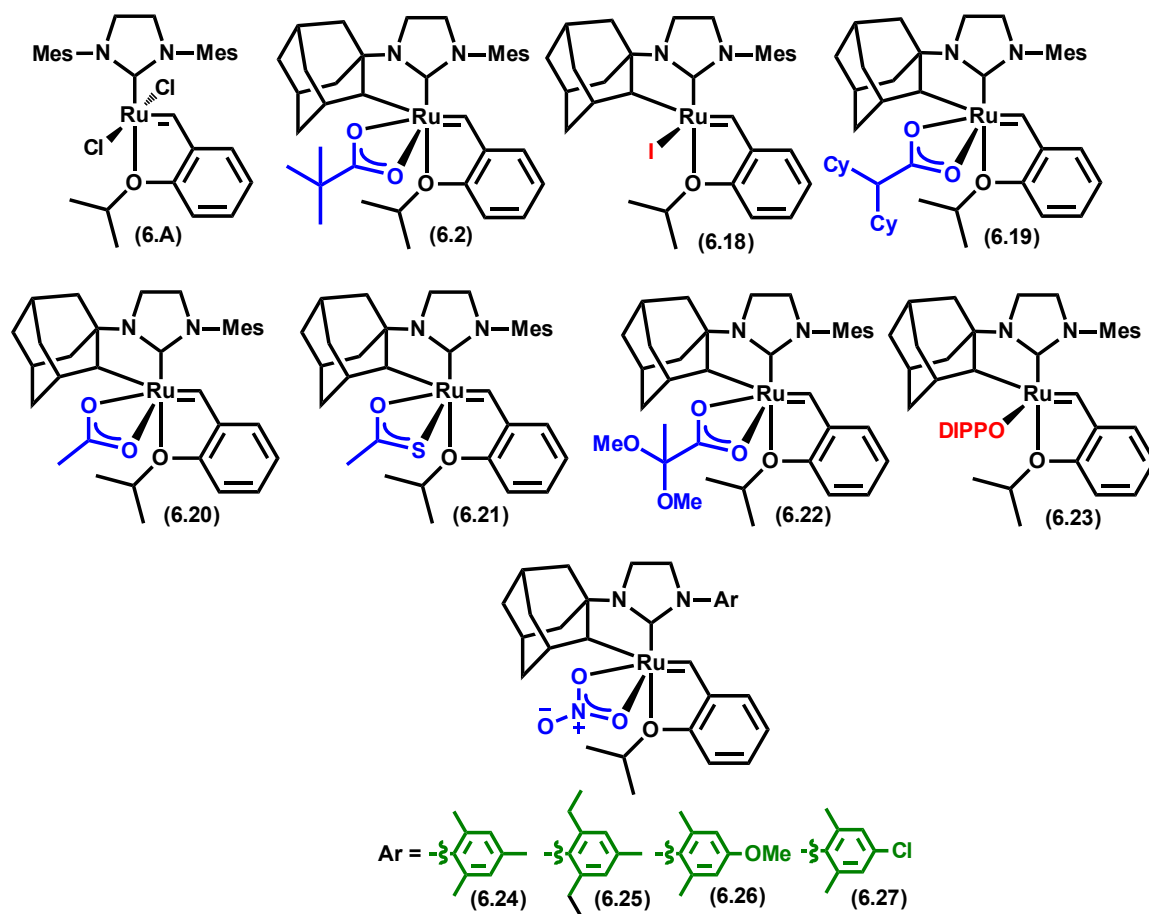


Figure 6.6. Selected variants of C-H activated catalysts. DIPP = 2,6-diisopropyl-phenyl

could be formed either by reaction of **6.18** with AgNO_3 or by direct reaction of **6.2** with NH_4NO_3 , with the latter route being preferred (Figure 6.8). Single-crystal x-ray diffraction revealed that the nitrate ligand in **6.24** is coordinated in a bidentate fashion analogous to **6.2** (Figure 6.9). Structural parameters, including bond lengths and angles were also consistent between **6.2** and **6.24**.

The aryl substituent on the NHC was varied through straightforward ligand synthesis, followed by metalation and C-H activation effected by silver pivalate. In all cases, the pivalate was immediately exchanged for nitrate, since the nitrate

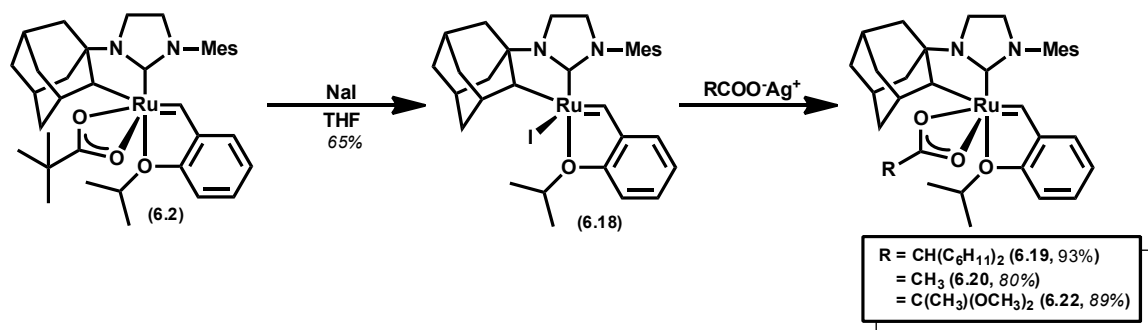


Figure 6.7. Preparation of iodo-precursor **6.18** and catalysts **6.19–6.21**

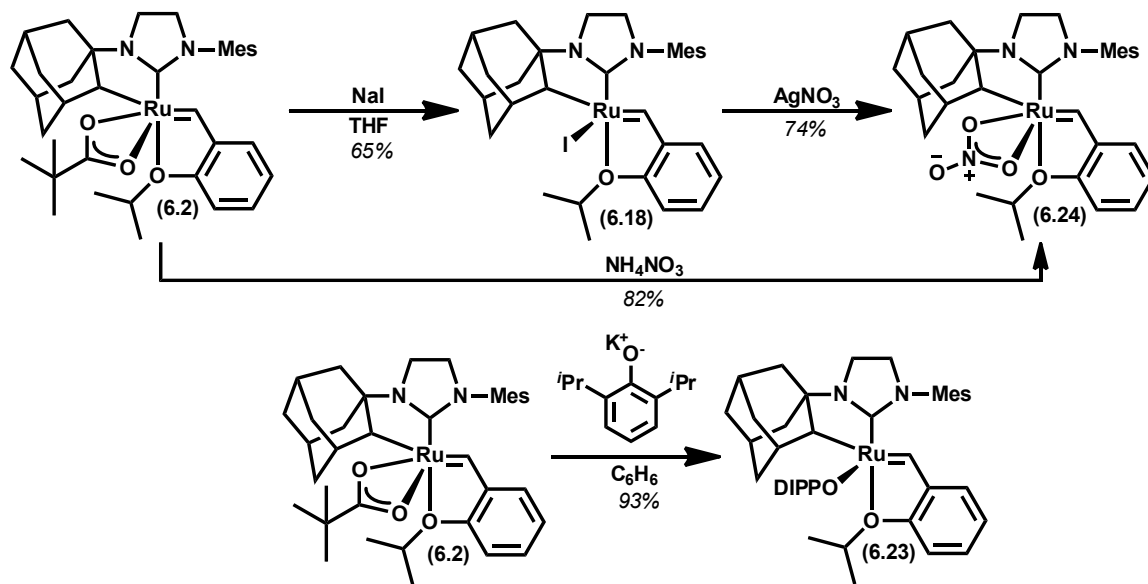


Figure 6.8. Preparation of catalysts **6.24** and **6.23**

complexes were generally more stable and easier to isolate. Only subtle steric and electronic modifications were introduced to the aryl group, as we found that the C-H activation reaction was sensitive to more drastic changes, mainly resulting in decomposition. For example, we have demonstrated that *ortho* substitution on the aryl ring appears to be necessary in order to prevent catalyst decomposition.¹⁶ Decomposition also occurred when large substituents were placed in the *meta* positions of the aryl ring (e.g., Ar = 3,5-di-*tert*-butylphenyl).¹⁷

With a relatively large library of catalysts in hand, we began examining their

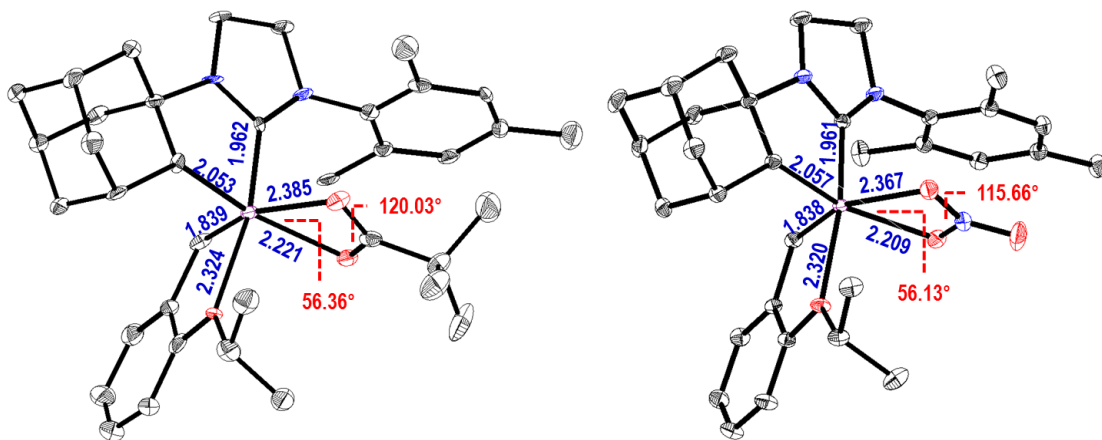


Figure 6.9. Solid state structures of **6.2** (left) and **6.24** (right) with 50% probability ellipsoids. Selected bond lengths are in Å

reactivity in a range of olefin metathesis reactions. Reaction with butyl vinyl ether (BVE) was chosen as the first probe of catalyst activity since this reaction is commonly used to measure the initiation rate of ruthenium catalysts (Figure 6.10).⁸ As shown in Table 6.4, the initiation rate constant, as measured by ¹H NMR spectroscopy, varied by 2 or more orders of magnitude for the examined catalysts! The most striking differences were observed between catalysts containing bidentate (**6.2**, **6.19–6.22**, **6.24–6.27**) and monodentate (**6.18** and **6.23**) ligands. Whereas the bidentate complexes displayed initiation rates comparable to that of **6.A**, complexes **6.2** and **6.24** initiated at significantly slower rates, even at higher temperatures. In particular, **6.23** showed almost no reactivity with BVE, even at temperatures as high as 70 °C. From these data we anticipated that the catalysts with monodentate ligands would be essentially metathesis inactive (*vide infra*).

Besides the differences between κ^1 and κ^2 ligands, several significant changes to initiation rate constant were observed between various bidentate ligands. For instance, exchanging pivalate (**6.2**) for the more inductively electron withdrawing

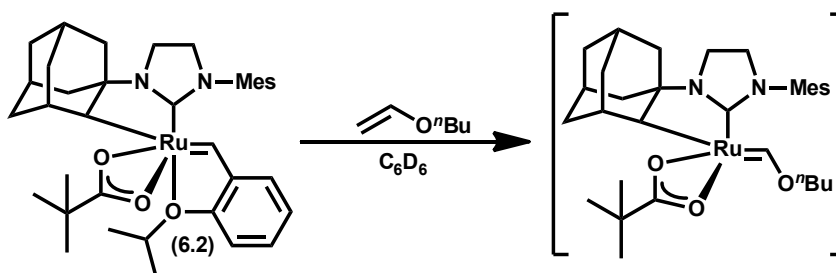


Figure 6.10. Measurement of catalyst initiation rate via reaction with BVE

Table 6.4. Initiation rate constants for C-H-activated catalysts^a

catalyst	temperature, °C	initiation rate constant, 10 ⁻³ s ⁻¹
6.A	30	7.2 ± 0.2
6.2	30	0.87 ± 0.02
6.18	50	0.17 ± 0.01
6.19	30	6.9 ± 0.3
6.20	30	0.17 ± 0.04
6.21	30	0.04 ± 0.02
6.22	30	2.5 ± 0.1
6.23	70	< 0.39 ^b
6.24	30	0.84 ± 0.03
6.25	30	0.77 ± 0.05
6.26	30	0.76 ± 0.02
6.27	30	0.24 ± 0.05

^a Initiation rate constants were determined by measuring the decrease in the benzylidene resonance using ¹H NMR spectroscopy following addition of BVE. Conditions were catalyst (0.003 mmol) and BVE (0.09 mmol) in C₆D₆ (0.6 mL) at given temperature. ^b Value based on single half-life of **6.23**.

2,2-dimethoxypropanoate (**6.22**) led to a small increase in the rate constant. When the steric bulk of the carboxylate was increased (**6.19**) or decreased (**6.20**), initiation rate constants increased and decreased, respectively. This last result was surprising since, in general, complexes with the Hoveyda-type chelates are thought to initiate through an associative or associative interchange mechanism.⁸ Thus, increasing the steric bulk of the carboxylate should have resulted in a decrease in the initiation

rate constant due to the less favorable steric environment around the metal. The exact opposite was observed with the larger 2,2-dicyclohexylacetate (**6.19**) possessing a higher initiation rate than catalysts with smaller carboxylate ligands (**6.20**). Notably, electronic effects play an important role, as evidenced by the differences between **6.2** and **6.22**; thus, complexes of this type likely initiate through a more complicated mechanism compared to catalyst such as **6.A**. Further support for the significance of electronic effects comes from comparing **6.20** and **6.21**, which have ligands of approximately the same size, but exhibit remarkably different initiation behavior. It has been demonstrated that in some situations, thiocarboxylates tend to behave more like monodentate ligands.¹⁸ Such a result would be consistent with our observation that catalysts with monodentate ligands tend to initiate at slower rates. Finally, the nitrate complexes **6.24–6.26** had ca. the same initiation rate as **6.2**, while that of **6.27** was slightly smaller. These latter results demonstrate that minor changes to the aryl group do not have a substantial effect on initiation rate and that **6.24** and **6.2** behave almost identically in this assay.

In order to gain a better understanding of the initiation behavior of the above catalysts and to explain some of our unusual observations, we turned to more detailed kinetic studies. We first focused on steric differences, for example, between **6.20** and **6.2**. Initiation rate constants were measured at several different concentrations of BVE and the expected linear dependence was uncovered. With this same data, a double reciprocal plot was created (Figure 6.11). Assuming a dissociative mechanism (Figure 6.12), the slope and intercept of the linear fits in Figure 6.11 correspond to $k_{-1}/(k_1k_2)$ and $1/k_1$, respectively, (Eqs. 6.1 and 6.2). From

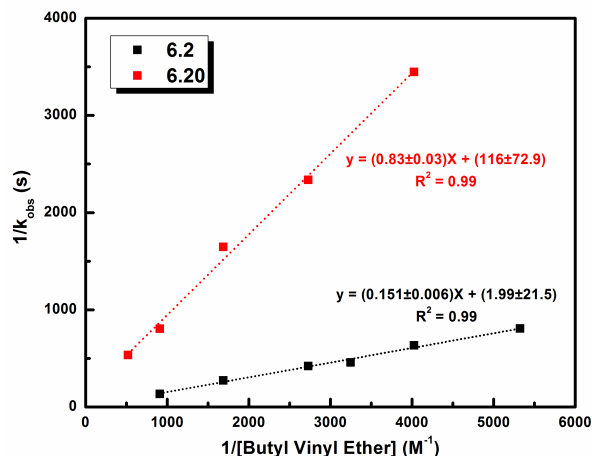


Figure 6.11. Plot of $1/k_{\text{obs}}$ versus $1/[\text{BVE}]$ for reaction of **6.2** and **6.20** with BVE

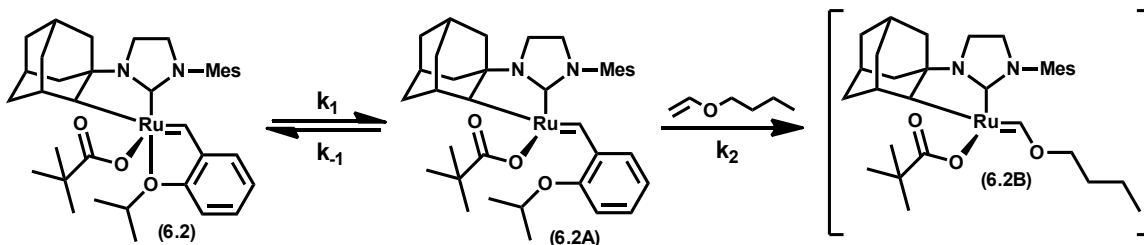


Figure 6.12. Assumed dissociation mechanism for initiation of **6.2**

$$-\frac{d[\mathbf{6.2}]}{dt} = k_2[\mathbf{6.2A}][\text{BVE}] = \frac{k_2 k_1 [\mathbf{6.2}][\text{BVE}]}{k_2 [\text{BVE}] + k_{-1}} \quad (6.1)$$

$$\frac{1}{k_{\text{obs}}} = \frac{k_2 [\text{BVE}]}{k_1 k_2 [\text{BVE}]} + \frac{k_{-1}}{k_1 k_2 [\text{BVE}]} \quad (6.2)$$

these data, k_1 and k_{-1}/k_2 were calculated (Table 6.5) and these values provide some insight into factors governing initiation. For example, k_1 , which corresponds to the dissociation of the chelated oxygen, is much larger for **6.2** than for **6.20**. This suggests that larger carboxylates (e.g., pivalate) facilitate dissociation of the chelated oxygen, which results in faster initiation rates. The values of k_{-1}/k_2 also explain the observed linear dependence on BVE concentration since the value of k_{-1} is larger or at least the same order of magnitude as $k_2[\text{BVE}]$ in the denominator of eq. 6.1, hence the linear dependence on $[\text{BVE}]$. As a disclaimer to the above

Table 6.5. Kinetic parameters for initiation of **6.2** and **6.20** with BVE^a

catalyst	k_1 , s ⁻¹	k_{-1}/k_2 , M
6.2	0.5	0.076
6.20	0.0086	0.0071

^a Derived from linear fits in Figure 6.11.

analysis, we note that we assumed a purely dissociative mechanism. This may or may not be the case depending on the reaction conditions.⁸ Nevertheless, we were able to explain some of the anomalous results from our initiation studies on catalysts with different-sized carboxylate ligands.

Having briefly examined the role of sterics in the initiation of our C-H-activated catalysts, we turned to exploring electronic effects. Several catalysts with substituted benzoate ligands were prepared and their initiation rates were measured. The resulting data was plotted as a function of an induction-based Hammett σ parameter and a positive linear response was obtained (Figure 6.13). This result indicates that inductively electron withdrawing groups (e.g., F, OH) accelerate initiation. Moreover, it also explains the larger initiation rate constant of **6.22** compared to **6.2**. At this time, it is unclear why electron withdrawing groups increase initiation rates, but the explanation may involve the ability of the bidentate ligand to switch between κ^2 and κ^1 coordination modes. Such a process has been theoretically shown to be instrumental in catalytic activity for the C-H-activated catalysts and it would not be surprising if it was affected by the electronics of the bidentate ligand.¹⁹ Unfortunately, our attempts to prepare catalysts with stronger electron withdrawing groups in order to further probe various electronic effects

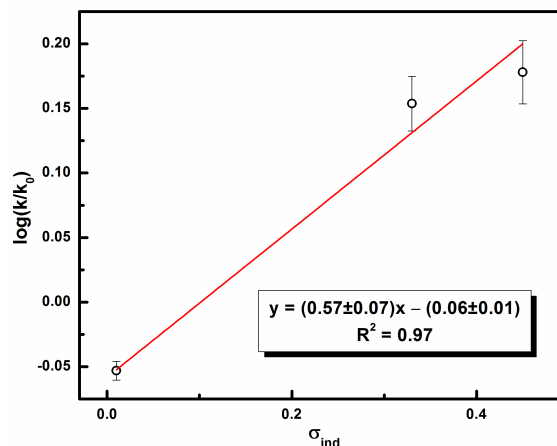
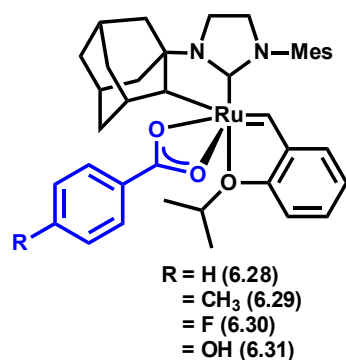


Figure 6.13. Benzoate catalysts and Hammett plot using σ induction values. Conditions were catalyst (0.003 mmol), BVE (0.09 mmol), at 50 °C^{17b}

have met only with decomposition. For example, exposure of **6.18** to AgOOCCF₃ resulted in immediate alkylidene insertion and subsequent decomposition to the Ru-olefin complex **6.32** (Figure 6.14). The identification of complex **6.32** suggests that the electronics of the X-type ligand also effect catalyst stability and not just initiation.

Our initiation studies provided insight into some subtle ligand effects, but were unable to capture the overall activity and more importantly Z-selectivity of our catalyst family. Therefore, we turned to evaluating our complexes in the cross-metathesis homocoupling of allyl benzene (**6.3**). While this reaction is relatively facile for most metathesis catalysts, it provided a useful benchmark to assess the performance of our catalyst library. Reactions were run in THF at 35 °C with a relatively high substrate concentration (ca. 3 M in **6.3**) and 0.1 mol% catalyst loading for a set amount of time, at which point the conversion and percentage of Z-olefin were measured by ¹H NMR spectroscopy (Table 6.6). Low catalyst loadings

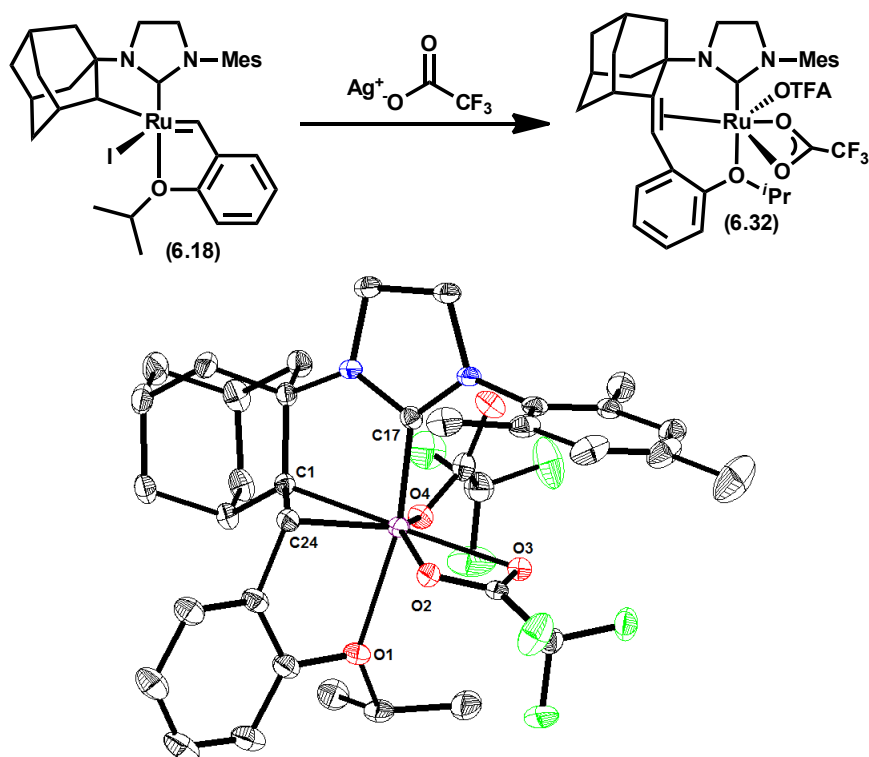
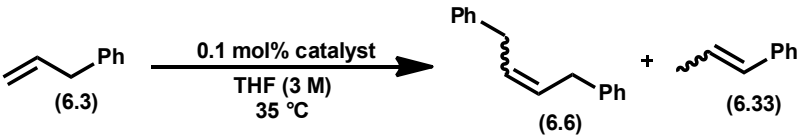


Figure 6.14. Decomposition following transmetalation with silver trifluoroacetate (AgTFA). Solid-state structure of **6.32** drawn with 50% probability ellipsoids. Selected bond lengths (Å): Ru – C1: 2.141, Ru – C17: 1.959, Ru – C24: 2.061, Ru – O1: 2.304, Ru – O2: 2.144, Ru – O3: 2.213, Ru – O4: 2.079

were used to emphasize the differences between catalysts. In most cases, a detectable amount of olefin isomerization product **6.33** was observed, but the amount of this undesired product and the total conversion of **6.3** varied significantly between catalysts. Catalysts **6.18** and **6.23** (both with monodentate ligands) yielded the largest amount of **6.33**; moreover, this was the only detectable product for these catalysts. Among the carboxylate-based catalysts, **6.19** was the least active, giving low conversion of **6.3** and poor selectivity for the desired product **6.6**. Furthermore, no notable improvement was observed with complexes **6.20** and **6.22**.²⁰ Both **6.2** and **6.24–6.27** showed excellent conversion of **6.3** and good

Table 6.6. Homodimerization of allyl benzene (**6.3**)^a



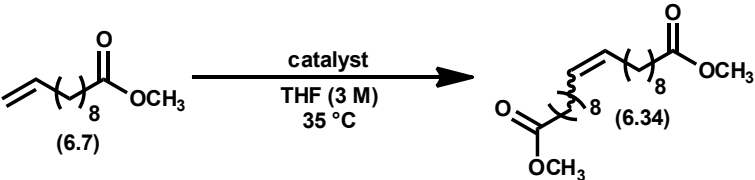
catalyst	time, h	conv., ^b %	Z-6.6, ^b %	13/14 ^b
6.2	3	79	> 95	42
6.18	12	59	-	0 ^c
6.19	12	7	> 95	0.5
6.20	12	65	92	1.4
6.22	12	26	> 95	3.8
6.23	12	> 95	-	0 ^c
6.24	3	90	91	18.4
6.25	3	90	93	18.1
6.26	3	91	93	16.9
6.27	3	90	94	33.6

^a Conditions were catalyst (1 μ mol) and **6.3** (1 mmol) in THF (0.2 mL) at 35 $^{\circ}$ C. ^b Measured by 1 H NMR spectroscopy. ^c No detectable amount of **6.6**

selectivity for **6.6**, with catalysts **6.24–6.27** taking only ca. 3 h to reach ~ 90% conversion. Based on the above results, the nitrate catalysts **6.24–6.27** were clearly the most efficient catalysts examined.

In order to further differentiate the performance of the catalysts, a more challenging homodimerization reaction was chosen, specifically the homodimerization of methyl 10-undecenoate (**6.7**) (Table 6.7). For this reaction, only the catalysts that performed well in the reaction with **6.3** were examined, namely the carboxylate and nitrate catalysts. We were pleased to discover that even at 0.1 mol% loading, most of the catalysts were able to achieve an appreciable degree of conversion. Similar to the reaction with **6.3**, catalysts **6.19**, **6.20**, and **6.22** performed relatively poorly while **6.2** and **6.24–6.27** furnished the best results.

Table 6.7. Homodimerization of methyl 10-undecenoate (**6.7**)^a



catalyst	loading, mol %	time, h	conv., ^b %	Z, ^b %
6.2	0.1	12	16	90
6.19	2	6	67	81
6.20	0.1	12	3	>95
6.22	0.1	12	8.4	>95

^a Conditions were catalyst (0.1–2 mol%) in THF (3 M in **6.7**) at 35 °C. ^b Determined by ¹H NMR spectroscopy

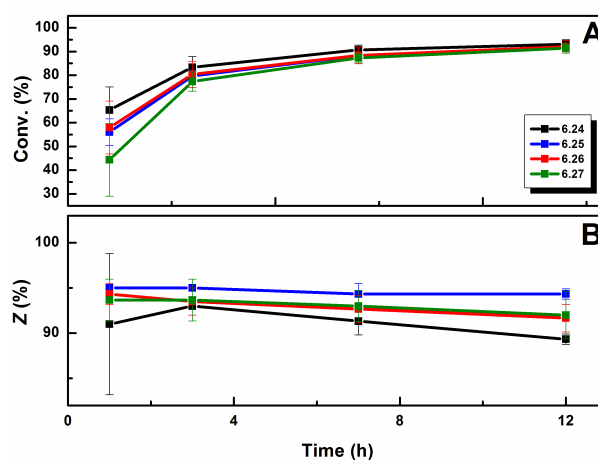


Figure 6.15. Time-course plot for the (A) conversion and (B) selectivity of the homodimerization of **6.7** to **6.34** using catalysts **6.24**–**6.27**. Conditions were **6.7** (1 mmol) and catalyst (1 μmol) in THF (0.1 mL) at 35 °C. Data points and error bars were calculated from the average and standard deviation of three separate runs

In fact, catalysts **6.24**–**6.27** showed excellent conversion (> 90%) at short reaction times with good selectivity for the Z-olefin (90–95%,). This is a clear demonstration of their superior activity and selectivity. A time-course monitoring of the reaction of **6.7** with catalysts **6.24**–**6.27** revealed some subtle differences between the nitrato catalysts (Figure 6.15). Specifically, there were only very slight differences in both

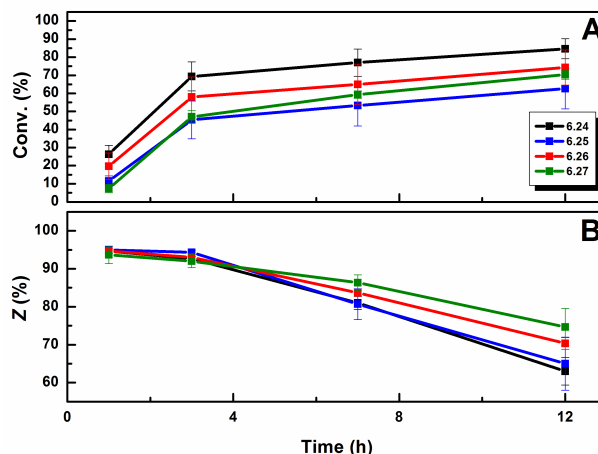


Figure 6.16. Time-course plot for the (A) conversion and (B) selectivity of the homodimerization of **6.15** to **6.34** using catalysts **6.24–6.27**. Conditions were **6.15** (1 mmol) and catalyst (1 μ mol) in THF (0.1 mL) at 35 °C. Data points and error bars were calculated from the average and standard deviation of three separate runs

conv. and Z-selectivity for catalysts **6.24–6.27** which is consistent with the initiation rate constants measured for these catalysts and their reactivity with **6.3**. At shorter reaction times, **6.27** showed slightly reduced reaction conversion compared to its analogues, which is likely a consequence of its slower initiation rate. Nonetheless, given enough time, **6.27** was able to reach similar levels of conversion as **6.24–6.26**. Similar results were achieved for the alcohol substrate **6.15** (Figure 6.16). The time-course study for **6.7** demonstrates that secondary metathesis events are relatively slow for this substrate, as Z-selectivity remains high even after extended periods of time at > 90% conversion. In contrast, secondary metathesis isomerization from Z to E-olefin appears to be faster with substrate **6.15** as evidenced by the relatively fast decrease in the Z-selectivity of the desired product.

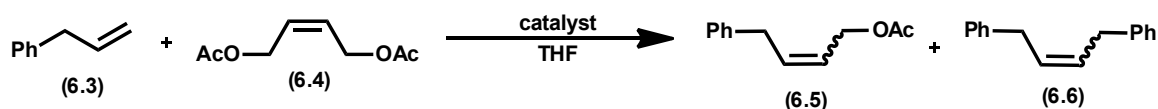
The aforementioned metathesis assays clearly demonstrated the superior

Table 6.8. Homodimerization of terminal olefin substrates^a

substrate	catalyst	time, h	Z, ^b %	yield, ^c %
6.3	6.2	3	86	73
	6.24	3	92	91
	6.25	3	94	91
	6.26	3	95	83
	6.27	3	95	89
6.7	6.2	12	90	13
	6.24	12	91	85
	6.25	12	92	94
	6.26	12	92	92
	6.27	12	94	75
6.11 1-octene	6.2	12	94	30
	6.24	12	92	83
6.15 4-penten-1-ol	6.2	12	43	81
	6.24	12	81	67
	6.25	8	73	78
	6.26	8	78	76
	6.27	8	85	75
6.8 allyl acetate	6.24	12	>95	8 ^d
6.10 allyl TMS	6.24	9	>95	14
6.12 allyl pinacol borane	6.24	3	>95	36
6.16 2-(allyloxy)ethanol	6.24	12	67	30
6.17 <i>N</i> -allylaniline	6.24	12	90	12

^a Conditions were catalyst (5 mmol) and substrate (5 mmol) in THF (ca. 1.7 mL) at 35 °C. ^b Determined by ¹H NMR spectroscopy. ^c Isolated yield after chromatography. ^d Conversion, yield not determined

properties of nitrato catalysts **6.24–6.27** over the carboxylate analogues. However, it was still unclear if this effect was specific to the chosen substrates. To fully evaluate the effectiveness of **6.24–6.27**, several more substrates, including alcohols, were examined (Table 6.8). For the majority of these reactions, catalysts **6.24–6.27** were easily capable of reaching TON greater than 500 and, in some cases, coming close to 1000. Notably, the yields presented in Table 6.8 are

Table 6.9. Cross-metathesis of **6.3** and **6.4**^a

catalyst	loading, mol%	time, h	temp, °C	conv. to 6.5 , ^b %	Z- 25 , ^b %	conv. to 6.6 , ^b %	Z- 6.6 , ^b %
6.2	5	9	70	37	89	26	>95
		6	35	50	86	19	>95
6.19	5	6	70	48	82	33	91
		9	35	45	87	23	>95
6.22	5	3	70	57	75	42	94
		6	35	64	79	22	>95
6.20	5	7	35	54	83	17	>95
6.24	1	9	35	58	91	28	>95

^a Conditions were catalyst, **6.3** (1 equiv) and **6.4** (2 equiv) in THF (0.5 M in **6.3**). ^b Determined by gas chromatography with tridecane as internal standard

calculated based on *isolated yield*, meaning that the actual TON are likely to be higher. Certain substrates, such as **6.8** and **6.17** were problematic and resulted in reduced yields (TON). At this time, we believe this attenuation is not a result of the functional group itself, but of its proximity to the reacting olefin. Nevertheless, the TON for these substrates are still respectable. The nitrato-complexes **6.24–6.27** showed almost no significant differences in either conversion or Z-selectivity for the substrates where they were compared head-to-head. Finally, the selectivity for the Z-olefin was excellent in almost every case.

Having established the effectiveness of **6.24** in several homodimerizations reactions, we turned our attention to more complex reactions including the “standard” cross-metathesis reaction between **6.3** and *cis*-1,4-diacetoxypentene

(**6.4**).²¹ Similar to the case of olefin homodimerization, lowering the temperature and increasing the substrate concentration resulted in higher conversion to the desired product (**6.5**) with comparable selectivity for the Z-olefin (Table 6.9). For this assay, all of the carboxylate catalysts performed roughly the same, reaching around 15 TON. Significant amounts of **6.6** were also formed in each reaction. In contrast, **6.24** was able to achieve similar levels of conversion at catalyst loadings as low as 1 mol%. Furthermore, since **6.4** possibly interferes with **6.24**, as evidenced by the low yields achieved in the homodimerization of **6.8**, we suspect that a judicious choice of substrates will allow for the catalyst loading to be lowered even further.

As mentioned above, we have previously established that the adamantyl group in catalysts such as **6.2** is critical for achieving high levels of Z-selectivity.⁶ The results presented above clearly demonstrate that the other X-type ligand plays an important role in reactivity, stability, and selectivity as well. The best demonstration of the significance of this ligand is the observed difference in initiation rates, where catalysts containing monodentate ligands (**6.18** and **6.23**) were essentially unreactive. This result implies that bidentate ligands are unique in their ability to induce catalyst initiation. Although ruthenium catalysts containing carboxylate²² or nitrato²³ ligands are well known, to the best of our knowledge, there has been no report on their initiation behavior, at least for catalysts with chelated oxygen ligands. However, analogues of **6.A** containing carboxylate or other bidentate ligands are generally metathesis active,²⁴ which is a certain indication that special ligands are not required for standard catalysts to initiate. It is also worth noting that the

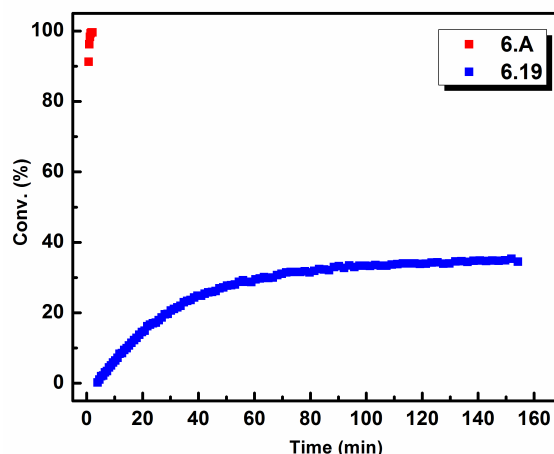


Figure 6.17. ROMP comparison of COD (**6.35**) with catalysts **6.A** and **6.19** (0.1 mol%) and **6.35** (53 μ L, 0.4 mmol), C_6D_6 (0.8 mL)

replacement of chlorides or carboxylates with nitrate in other ruthenium complexes generally resulted in less active and less selective metathesis catalysts.^{22,23} Thus, the C-H-activated catalysts appear to be unique in this regard.

A more general understanding of catalyst initiation can be gained by considering the differences in rates between complexes within the same family (e.g., carboxylates). For instance, electron-withdrawing and bulky groups resulted in an increase in initiation rate while smaller groups lead to a decrease in rate. Considering these results, it would have been interesting to probe the effect of electron-withdrawing carboxylates (e.g., trifluoroacetate). However, we discovered that such complexes were unstable and immediately decomposed upon anion exchange (Figure 6.14). Overall, the differences in initiation rates between catalysts with different carboxylates imply that a simple associative or associative-interchange mechanism is not occurring and that catalysts such as **6.2** likely undergo multiple pre-equilibrium steps (e.g., an equilibrium between κ^2 and κ^1 coordination, and an

equilibrium between association and dissociation of the chelated oxygen) prior to reaction with olefin.

Unfortunately, while our initiation rate studies allowed us to identify poor or unreactive catalysts (e.g., with monodentate ligands), they did not correlate with actual metathesis reactivity. Consider, for instance, the negligible difference in initiation rate between **6.A** and **6.19**. From this result, we predicted that these two complexes might have similar reactivity. A time-course plot for the conversion of cyclooctadiene (COD, **6.35**) during ring-opening metathesis polymerization (ROMP) revealed that this is clearly not the case (Figure 6.17). Catalyst **6.A** is able to complete this reaction within minutes, while **6.19** only reacts over a period of hours and never reaches full conversion. Furthermore, when compared with **6.2** and **6.24**, **6.19** is clearly inferior in terms of both activity and selectivity.

Therefore, simply increasing the initiation rate of the C-H-activated catalysts will not necessarily result in increased activity. On the other hand, decreasing the initiation rate does not result in an improved catalyst either. In the extreme case, this was shown by the inactivity of monodentate ligands, but it was also demonstrated by the lower activity of **6.20**. These observations parallel the behavior of previous generations of ruthenium metathesis catalysts.⁸ Although a complete mechanistic understanding of initiation for C-H-activated catalysts currently remains out of reach, the observed discrepancies between initiation rates and actual metathesis activity can most likely be explained by the fact that the method used to measure initiation does not take into account catalyst stability, the reversibility of metathesis reactions, or degenerate metathesis events (see Chapter 4). All of these factors

likely have a significant effect on the measured activity of the C-H-activated catalysts, particularly in cross-metathesis reactions.

In contrast to the various carboxylate ligands, changes to the aryl group on the NHC had little to no effect on catalyst initiation and activity. One exception was the replacement of mesityl (**6.24**) with 2,6-dimethyl-4-chlorobenzene (**6.27**), which resulted in a slight attenuation of initiation rate. Nonetheless, this only slightly affected catalytic activity as evidenced by the small differences in turnover frequency (TOF) between **6.24** and **6.27**. As mentioned earlier, we have been unable to access aryl groups significantly different from mesityl due to decomposition upon attempted C-H activation. For instance, we have demonstrated that ortho substitution of the aryl ring is required to prevent undesired C-H activation and subsequent decomposition.¹⁶ The remote nature of this part of the NHC ligand makes the predictability of structural effects on catalyst activity and selectivity difficult,²⁵ while the unpredictability associated with the synthesis of C-H-activated catalysts with different N-Aryl groups renders these modifications less convenient for catalyst optimization.

In actual cross-metathesis reactions, the nitrato catalysts **6.24–6.27** were the best catalysts in terms of both activity and selectivity. At this time, we believe this is a result of the nitrato ligand imparting greater stability to the complex compared with carboxylates. Qualitatively, **6.24–6.27** were far more tolerant to O₂ than the carboxylate analogues and also easier to purify. For instance, when a solution of **6.24** in C₆D₆ was exposed to air, the benzylidene resonance of **6.24** was still observed by ¹H NMR spectroscopy after 12 h. In contrast, the benzylidene

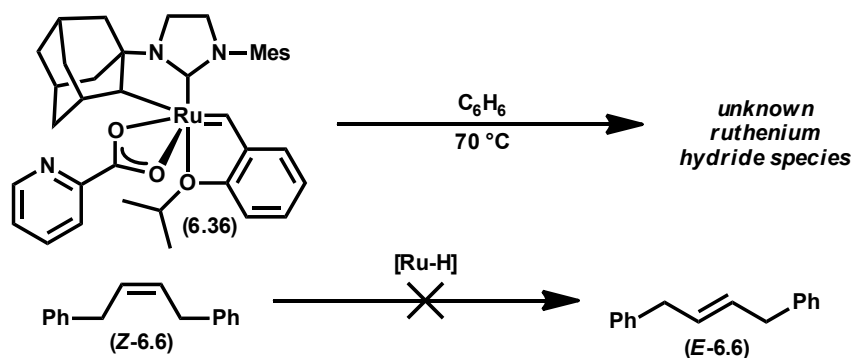


Figure 6.18. Generation of stable Ru hydrides $[Ru-H]$ and attempted isomerization reaction

resonance of **6.2** disappeared after only 2 h following exposure to air. The reasons for this enhanced stability are unclear at this time, but there are clearly substantial steric and electronic effects at play. Thus, the effect of various bidentate and monodentate ligands on C-H-activated ruthenium catalysts will continue to be a focus of our research.

As with Mo- and W-based catalysts, the relationship between conversion and Z-selectivity is critical and warrants further discussion.³ At low reaction conversions, **6.24** is almost perfectly selective for the Z-olefin. Unfortunately, as conversion increases, Z-selectivity decreases at a rate dependent on the nature of the substrate, although it typically stays above 70%. This decrease in selectivity may be due to secondary metathesis events or to hydride-induced olefin isomerization.²⁶ A secondary metathesis mechanism would require the generation of a nonselective metathesis active decomposition product, since the initial catalyst is very selective. Several possible structures can be envisioned, the most likely of which would be a catalyst resulting from cleavage of the Ru-C (adamantyl) bond. Thus far, we have been unable to detect or isolate any species which may be

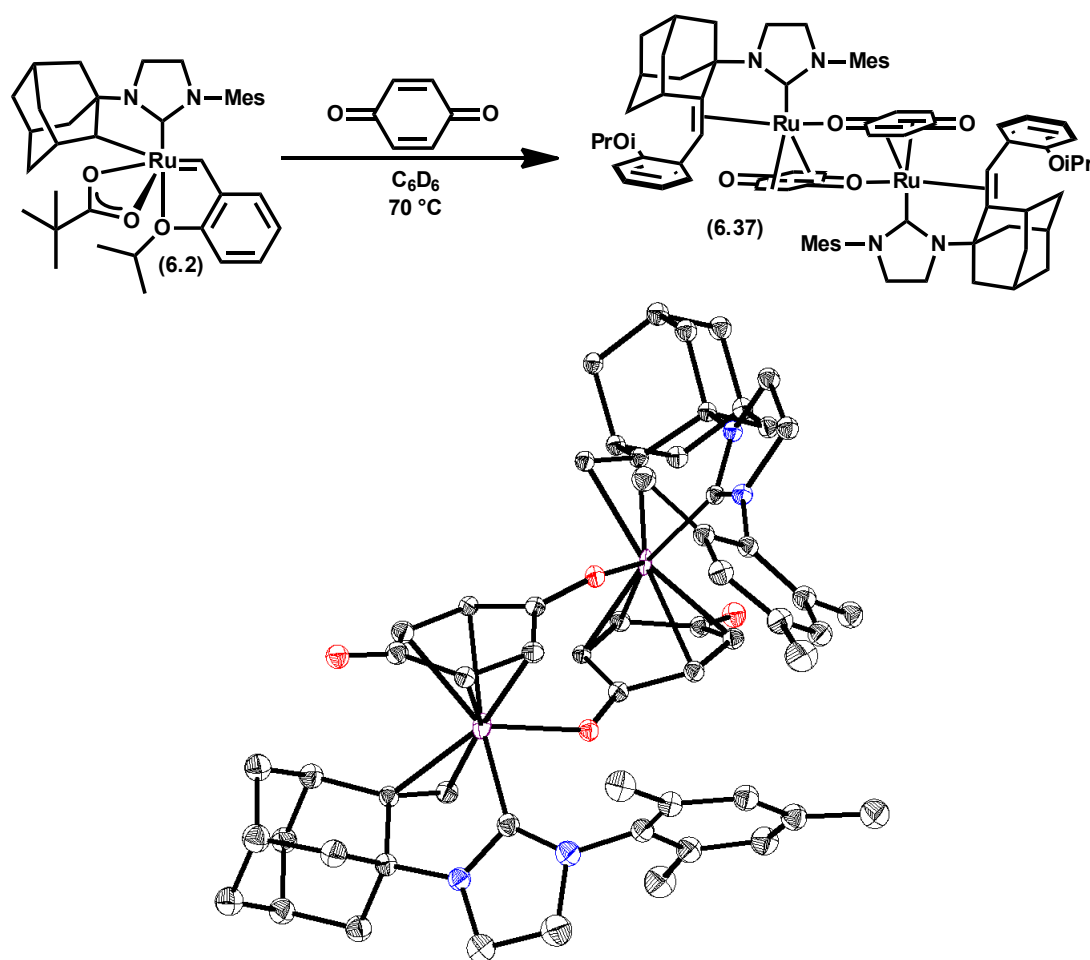


Figure 6.19. Benzoquinone-induced decomposition of **6.2** and solid-state structure of **6.37** drawn with 50% ellipsoids. Phenyl isopropoxy groups admitted for clarity

responsible for secondary metathesis. On the other hand, the existence of ruthenium hydrides can be inferred by the observation of olefin migration in the reaction of **6.3**. Moreover, these species can also be detected by ^1H NMR spectroscopy under special conditions. For example, when **6.18** was reacted with silver picolinate, the desired complex **6.36** was formed. However, **6.32** proved to be thermally unstable and spontaneously decomposed into a mixture of stable Ru hydride species that were detectable by ^1H NMR spectroscopy (Figure 6.18). When this mixture was exposed to a sample of Z-**6.6**, very little Z to E isomerization was

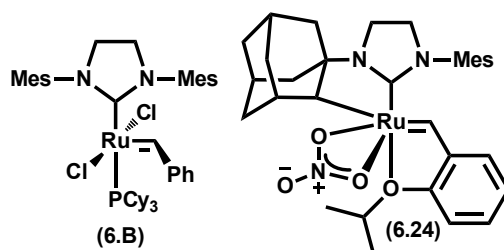


Figure 6.20. Catalysts examined for stereoselective ROMP

observed, suggesting that Ru-H species are not responsible for the degradation in Z-selectivity with certain substrates. Nevertheless, the identification of the species responsible for olefin isomerization (from *Z* to *E*) will be critical in establishing design parameters for future generations of Z-selective catalysts.

We have attempted to suppress the generation of hydride species and other deleterious decomposition products with various chemical quenchers, but have had little luck so far.²⁷ For example, benzoquinone has been shown to reduce olefin isomerization in cross-metathesis reactions. Unfortunately, **6.2** immediately decomposed in the presence of benzoquinone to give the crystallographically characterized dimer **6.37** (Figure 6.19). Other additives such as α,α -dichlorotoluene and chloroform yielded similar results. As a consequence of these results, the design of new catalysts that are less susceptible to either secondary metathesis or hydride formation is of paramount importance. For now, individual researchers must prioritize either conversion or Z-selectivity with substrates that are more susceptible to isomerization (i.e., alcohols).

Having prepared a robust Z-selective catalyst (**6.24**) that excelled at Z-selective cross-metathesis, we turned our attention to other potential metathesis applications, namely Z-selective ROMP. ROMP has long been used as a method

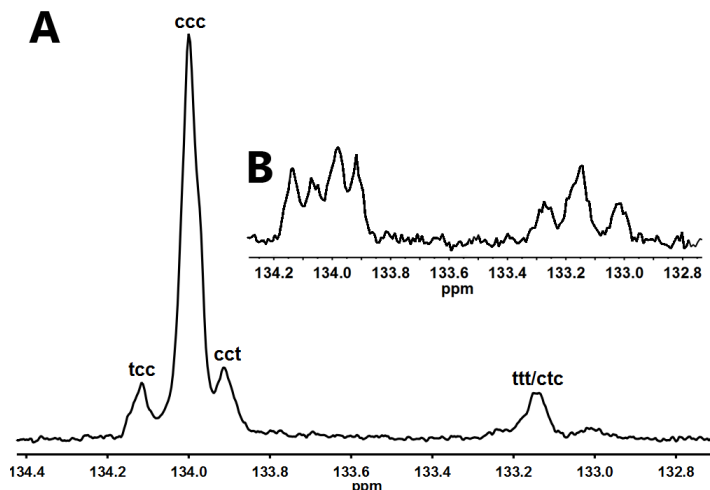


Figure 6.21. (A) ^{13}C NMR spectrum (CDCl_3) of **poly-6.38** prepared from **6.24** (0.5 mmol) and **6.24** (0.005 mmol) in THF (2 mL) at RT. “ccc” and “cct” represent cis-cis-cis cis-cis-trans triads consistent with literature reports.² (B) ^{13}C NMR spectrum of **poly-6.38** prepared from **6.24**

for preparing polymers with specific microstructures comprising various tacticities (e.g., atactic, isotactic, syndiotactic), double-bond geometries (cis/trans), and relative monomer configurations (e.g., head-to-tail, head-to-head, etc.).² Control of these microstructures is essential for preparing polymers with well-defined properties. Several metathesis catalysts based on Re, Os, Mo, and W have demonstrated impressive control over polymer microstructure, including high cis content (% cis) and well-defined tacticities.^{28,29} In contrast, Ru-based initiators such as $(\text{PCy}_3)_2\text{Cl}_2\text{Ru}=\text{CHPh}$ give almost exclusively trans polymer and yield tactic polymers only under very special circumstances.^{30,31,32} Indeed, this has been a serious limitation for previous generations of Ru-based metathesis catalysts, as recently highlighted by Schrock and co-workers.²⁸ The best literature examples of stereoselective ROMP with Ru catalysts including alternating copolymerization of norbornene and cyclo-alkenes to give polymers with 50–60% cis double bonds

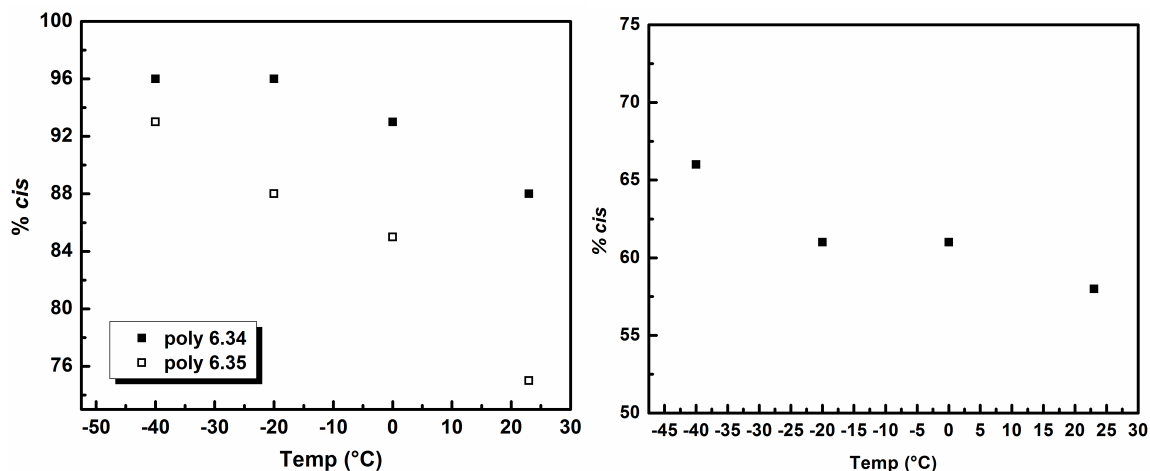
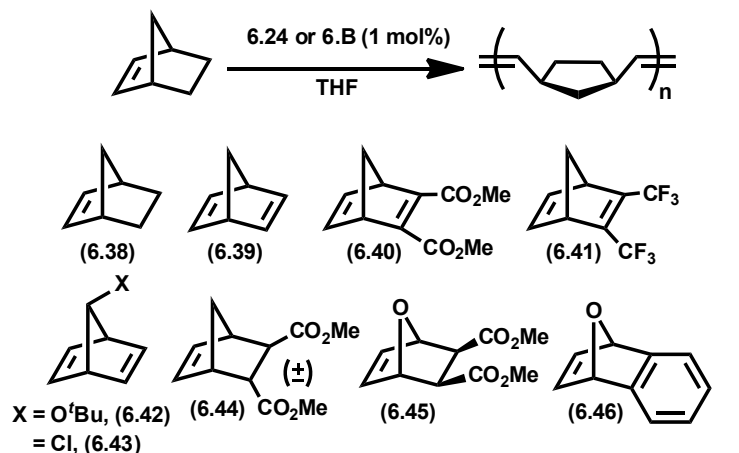


Figure 6.22. (left) change in % *cis* with temperature for **poly-6.38** and **poly-6.39** polymerized with **6.24**. Conditions were monomer (0.5 mmol) and **6.24** (0.005 mmol) in THF (2 mL). *Cis* content was determined by ^1H NMR spectroscopy. (right) Temperature dependence of % *cis* of **poly-6.38** prepared from **6.B**. Conditions were monomer (0.5 mmol) and **6.B** (0.005 mmol) in THF (2 mL). *Cis* content was determined by ^1H NMR spectroscopy. For temperatures 0 °C, –20 °C, and –40 °C, $(\text{H}_2\text{IMes})\text{Cl}_2\text{Ru}(\text{=CH-}o\text{-iPr-Ph})$ (**6.A**) was used as the catalyst.

and more recently up to 75%.^{33,34} Our group has described similar % *cis* values for sulfonate and phosphate substituted NHC-based catalysts as well.³⁵ In light of these results, we decided to examine the performance and selectivity of our *Z*-selective catalyst **6.24** in the context of ROMP.

When **6.24** was added to a solution of norbornene (**6.38**) in THF at room temperature (RT), an immediate increase in the viscosity of the solution occurred. Isolation of the resulting polymer (**poly-6.38**) and subsequent characterization by ^1H and ^{13}C NMR spectroscopy revealed that it contained ca. 88% *cis* double bonds (Figure 6.21). In contrast, **poly-6.38** prepared using **6.B** showed % *cis* values of 58% (Table 6.10).³⁶ These later values are typical of NHC-supported Ru-based metathesis catalysts. Importantly, an even higher selectivity of ca. 96% *cis* could be obtained with **6.24** by lowering the temperature of the monomer solution prior

Table 6.10. Polymerization of **6.38–6.46** with catalysts **6.B** and **6.24**^a



Monomer	Catalyst	Cis, ^b %	Yield, ^c %	M _n , ^d kDa	PDI ^d
6.38	6.B	58	88	112	1.65
	6.24	88	94	347	1.87
6.39	6.B	< 5	93	— ^e	— ^e
	6.24	75	88	—	—
6.40	6.B	93	78	95.5	1.21
	6.24	86	91	—	—
6.41	6.B	78	95	179	1.24
	6.24	61	40	137	1.21
6.42	6.B	58	78	—	—
	6.24	84	73	—	—
6.43	6.B	50	64	144	1.08
	6.24	69	81	328	1.09
	6.24	80 ^f	79	—	—
6.44	6.B	81	95	484	1.49
	6.24	91	78	629	1.33
6.45	6.B	66	> 95	463	1.5
	6.24	74	93	183	1.2
	6.24	80 ^f	79	—	—
6.46	6.B	67	> 95	—	—
	6.24	76	47	—	—
	6.24	91 ^{f,g}	80	—	—

^a Conditions were monomer (1 mmol) and catalyst (0.01 mmol) in THF (4 mL, 0.025 M) at RT. ^b Determined by ¹H NMR and ¹³C NMR spectroscopy. ^c Isolated yield. ^d Determined by multiangle light scattering (MALS) gel permeation chromatography (GPC). ^e Here and below: not determined due to insolubility of the isolated polymer in THF or DMF. ^f Reaction performed at –20 °C. ^g 0.3 mol% catalyst was used.

to the addition of the catalyst. This trend was also observed when norbornadiene (**6.39**) was reacted with **6.24** at different temperatures (Figure 6.22). The almost

exclusive formation of *cis* **poly-6.39** with **6.24** is particularly noteworthy since **6.B** gave no detectable amount of the *cis* isomer. Lowering the temperature of polymerizations using **6.B** resulted in only a slight increase in % *cis* that was never more than 5%. In addition to temperature changes, solvent effects have been shown to increase *cis* content in certain situations.³⁰ However, in the case of **6.24**, no change in *cis* content (for **poly-6.38**) was observed when the reaction solvent was changed from THF to benzene, dioxane, or DME. Moreover, both **poly-6.38** and **poly-6.39** prepared with **6.24** were atactic, as evidenced by the lack of peaks in the ¹³C NMR spectrum corresponding to either isotactic or syndiotactic polymer.

Having established that **6.24** could furnish polymers with high *cis* content for both **6.38** and **6.39**, we turned our attention to more complex monomers. Many of these monomers have been polymerized with very high *cis* selectivity and tacticity control using Mo- and W-derived catalysts, but formed predominantly *trans* polymers when (PCy₃)₂Cl₂Ru=CHPh was used.³⁰ Gratifyingly, we found that in almost every case, **6.24** yielded a polymer with high *cis* content approaching 90%. In the cases where *cis*-selectivity with **2** at RT was below that value, conducting ROMP at –20 °C increased % *cis* by 6–15% (Table 6.10). In general a lower fraction of *cis* double bonds was observed for polymers prepared using **6.B**. However, in the case of monomers **6.40**, **6.41**, and **6.42**, high *cis* content was achieved without the use of a specially designed catalyst! This is particularly surprising since the closely related (PCy₃)₂Cl₂Ru=CHPh is known to give **poly-6.40** with only 11% *cis* double bonds.³⁰ In contrast to **poly-6.40** and **poly-6.44** prepared by Mo-based

Table 6.11. Polymerization of **6.35**, **6.47**, and **6.49** with catalysts **6.B** and **6.24**^a

Monomer	Catalyst	Time(h)	Cis, ^b %	Yield, ^c %	M _n , ^d kDa	PDI ^d
cyclooctadiene (6.35)	6.B	1	10	88	22.9	1.64
	6.24	36	96	19	99.1	1.60
cyclopentene (6.47)	6.B	5	15	68	11.1	1.47
	6.24	3	48	24	102	1.40
<i>trans</i> -cyclooctene (6.49)	6.B	1	18	49	— ^e	—
	6.24	1	70	44	—	—

^a See experimental section for reaction conditions. ^b cis content of polymer determined by ¹H NMR and ¹³C NMR spectroscopy. ^c Isolated yield. ^d Determined by MALS GPC. ^e Not determined due to insolubility of the isolated polymer in THF or DMF

catalysts,²⁹ no long-range order was observed using either of the Ru-based initiators. With **6.24**, the formation of atactic polymers can be explained by fast carbene epimerization relative to the rate of propagation or an inherent lack of facial selectivity. As mentioned above, this result is typical of Ru-based catalysts.

Experimental molecular weights (M_n) for polymers prepared with **6.24** were generally higher than the predicted values, which is indicative of incomplete catalyst initiation or a high rate of propagation (k_p) relative to the rate of initiation (k_i). This could be qualitatively observed as a solution of **6.24** and **6.34** remained purple (the color of **6.24**), even after complete conversion of the monomer. Based on the relatively low initiation rate constant of **6.24**, this result was expected.³⁷

In contrast to norbornene and norbornadiene-type monomers, cyclooctadiene (COD, **6.35**), cyclopentene (**6.47**), and *cis*-cyclooctene (**6.48**) are significantly more difficult to polymerize via ROMP due to their lower ring-strain.³⁸ Furthermore, the Z-selective ROMP of these monomers is particularly challenging due to the prevalence of intra- and intermolecular chain-transfer reactions and secondary metathesis events.³⁹ In fact, the Z-selective ROMP of **6.31** has only

recently been reported using a Mo metathesis catalyst.^{29,40} Given the strong preference of **6.24** for *cis*-selective polymerization of bicyclic monomers, the next logical step was to attempt the ROMP of more difficult substrates, such as **6.35**, **6.47**, and **6.48**.

When **6.35** was exposed to **6.24** (1 mol%) in C₆D₆ (0.6 mL), only minimal conversion (< 20%) was observed after 24 h at RT. Surprisingly, increasing the temperature did not result in higher conversions, despite the fact that no catalyst decomposition was observed by ¹H NMR spectroscopy. Increasing the substrate concentration and switching the solvent to THF also did not increase the conversion of **6.35**, nor did repeating the reaction in neat **6.35**. However, polymerizing **6.35** with **6.24** in THF at RT over a period of 3 days provided a modest amount of **poly-6.35** (19% yield). Isolation and subsequent analysis of **poly-6.35** via ¹³C NMR spectroscopy revealed that it contained 96% *cis* double bonds, a value comparable to that obtained with the Mo-based system (Table 6.11). Similar to the ROMP of **6.38** (norbornene) and **6.39** (norbornadiene), increasing the temperature of the polymerization of **6.35** resulted in polymers with lower *cis* content, although it never went below 80%. The extraordinariness of the above result is highlighted by the fact that **6.B** yielded **poly-6.35** with 90% *trans* selectivity (Table 6.11).³⁷

Subsequent to our experiments with **6.35**, we found that **6.24** was also effective at polymerizing **6.47**, although the isolated yield of **poly-6.47** was still low (Table 6.11). Characterization of **poly-6.47** by ¹³C NMR spectroscopy revealed 48% *cis* content, which is significantly lower than the *cis* content of **poly-6.35** prepared by **6.24**. Similar levels of *cis* selectivity have been reported in

copolymerizations with **6.47**, although these generally resulted from incomplete incorporation of **6.47**.^{33d} Switching to catalyst **6.B** produced **poly-6.47** with only 15% *cis* double bonds. Thus, the use of **6.24** resulted in a significant improvement in the *cis* content of **poly-6.47**, albeit to a lesser extent than was anticipated.

Unfortunately, no conversion of **6.48** was observed when it was exposed to **6.24** under a variety of conditions.⁴¹ This was surprising since the strain energy of **6.48** (7.4 kcal/mol) is greater than that of **6.47** (6.8 kcal/mol).³⁸ At this time, we believe that the steric size of **6.48** prevented its polymerization. Nevertheless, we reasoned that a more significant increase in strain energy, resulting from the use of *trans*-cyclooctene (**6.49**), would provide access to the desired polymer.⁴² Indeed, reaction of **6.24** with **6.49** at RT in THF resulted in the immediate and high yielding production of **poly-6.49**. Characterization of this polymer revealed a *cis* content of 70%, a value that is among the highest reported for ruthenium-based catalysts.⁴³ Notably, **poly-6.49** prepared from **6.B** contained ca. 82% *trans* double bonds.

As mentioned above, secondary metathesis events are common in non-rigid polymers, because the active chain end is capable of intra – (“back-biting”) and intermolecular chain transfer reactions. Taking this into account, the *cis* selective polymerizations of **6.35**, **6.47**, and **6.49** with **6.24** are remarkable. Indeed, given the very high % *cis* of **poly-6.35** and no erosion of *cis* content over the course of polymerization, one should conclude that **6.24** is less prone to isomerizing or reacting with internal double bonds in polymers while displaying high kinetic selectivity for the formation of *cis* double bonds. Our molecular weight data also supports this argument, as **poly-6.35/6.47** prepared from **6.24** had much higher

molecular weights compared to **poly-6.35/6.47** prepared from **6.B**. Such a result is consistent with a reduction in the number of chain transfer events, which tend to lower molecular weight.⁴⁴ The importance of controlling secondary metathesis is reinforced by examination of the polymers prepared from **6.B**. In the case of **poly-6.40/6.41/6.44**, where secondary metathesis is suppressed due to steric effects, catalyst **6.B** yielded polymers with relatively high *cis* content. In contrast, **poly-6.35/6.47** have no protection against secondary metathesis and thus the thermodynamically favored *trans* olefin is eventually formed when these polymers are prepared from **6.B**. Although we have not specifically investigated the mechanistic origin of Z-selectivity in ROMP, calculations performed on an analogue of **6.24** indicate that steric pressure exerted by the NHC on side-bound ruthenacycles is responsible for the observed Z-selectivity during cross-metathesis.^{33c,19} It is likely that a similar mechanism is also responsible for the selectivities observed above.

Conclusions and Future Outlook

In summary, we have prepared a variety of new C-H-activated ruthenium catalysts for Z-selective olefin metathesis. Adjusting the ligand environment around the metal center has yielded significant insight into the initiation behavior, activity, and selectivity of this class of catalysts and has facilitated the development of improved catalysts (**6.24–6.27**) that are capable of ca. 1000 TONs in several cross-metathesis reactions. We note that these catalysts can be used with very low loadings, and do not require reduced pressures, high temperatures, or rigorous exclusion of protic solvents in order to operate

effectively. Secondary metathesis events are also relatively slow for the majority of substrates, meaning that significant reaction optimization should not be required.

Furthermore, we also demonstrated the *cis* selective ROMP of several monomers using Ru-based catalysts. The resulting polymers were recovered in moderate to high yield and *cis* content ranged from 48–96%. While the *cis* content varied significantly based on monomer structure, our C-H activated catalyst (**6.24**) gave polymers with significantly higher % *cis* values compared to those prepared by a more traditional Ru metathesis catalyst (**6.B**), while also showing qualitatively reverse stereoselectivity compared to $(\text{PCy}_3)_2\text{Cl}_2\text{Ru}=\text{CHPh}$. These results culminated in the highly *cis* selective polymerization of **6.35**, thereby proving that *cis* selective ROMP is possible with Ru catalysts, even with monomers that are prone to secondary metathesis. Future work in our laboratory will focus on improvements to both the activity and *cis* selectivity of **6.24**, with an emphasis on the application of this exciting new class of catalysts towards the development of novel polymer architectures.

Based on these results, we anticipate that catalysts such as **6.24** will be swiftly adopted by both industrial and academic researchers interested in the construction of Z-olefins using metathesis methodology. Nevertheless, there is still room for improvement in both catalyst activity and selectivity.

Experimental

General: All reactions were carried out in dry glassware under an argon atmosphere using standard Schlenk line techniques or in a Vacuum Atmospheres Glovebox under a nitrogen atmosphere unless otherwise specified. All solvents

were purified by passage through solvent purification columns and further degassed with argon.⁴⁵ NMR solvents for air-sensitive compounds were dried over CaH_2 and vacuum transferred or distilled into a dry Schlenk flask and subsequently degassed with argon. Commercially available reagents were used as received unless otherwise noted. Substrates for olefin cross-metathesis (**6.3**, **6.7**, **6.8–6.17**) were degassed with argon and passed through a plug of neutral alumina (Brockmann I) prior to use.

Standard NMR spectroscopy experiments were conducted on a Varian Inova 400 MHz spectrometer, while kinetic experiments were conducted on a Varian 500 MHz spectrometer equipped with an AutoX probe. Experiments and pulse sequences from Varian's Chempack 4 software were used. Chemical shifts are reported in ppm downfield from Me_4Si by using the residual solvent peak as an internal standard. Spectra were analyzed and processed using MestReNova Ver. 7.

Gas chromatography data was obtained using an Agilent 6850 FID gas chromatograph equipped with a DB-Wax Polyethylene Glycol capillary column (J&W Scientific). High-resolution mass spectrometry (HRMS) data was obtained on a JEOL MSRoute mass spectrometer using FAB+ ionization, except where specified.

Polymer molecular weights were determined by multi-angle light scattering (MALS) gel permeation chromatography (GPC) using a miniDAWN TREOS light scattering detector, a Viscostar viscometer, and an OptilabRex refractive index detector, all from Wyatt Technology. An Agilent 1200 UV-Vis detector was also present in the detector stack. Absolute molecular weights were determined using dn/dc values calculated by assuming 100% mass recovery of the polymer sample injected into the GPC. No internal standards were used

Improved Synthesis of 6.2: In a glovebox, a 500 mL Schlenk flask was charged with **6.1** (0.98 g, 1.52 mmol), sodium pivalate (1.89 g, 15.2 mmol), THF (12 mL), and MeOH (12 mL). The flask was sealed, removed from the glove box and heated to 40 °C overnight (16 h) at which point the solution had changed color from green to brown to deep purple. The solvent was removed under high vacuum and the Schlenk flask was transferred back into the glove box where the residue was dissolved in CH₂Cl₂ (~ 150 mL), filtered through celite, and concentrated to a deep purple residue consisting of a mixture of the C-H-activated product and pivalic acid. Cold Et₂O was added to this residue and the resulting bright purple solid was collected by filtration. An additional crop of **6.2** was recovered by cooling the Et₂O washes from above to –35 °C and collecting the purple crystals that formed. Total yield was 0.62 mg of **6.2** (61% yield). NMR parameters were consistent with previous reports.⁶

Preparation of 6.18: In a glovebox, a 250 mL RB flask was charged with **6.2** (491 mg, 0.731 mmol), NaI (548 mg, 3.65 mmol), and THF (25 mL). The resulting suspension was stirred for 1 h, at which point a color change from purple to brown had occurred. The solution was concentrated and the residue was dissolved in CH₂Cl₂ (ca. 100 mL), filtered through celite, and concentrated to a brown residue which was triturated with Et₂O until the washes were colorless to give **3** (332 mg, 65%) as a brown solid. ¹H NMR (400 MHz, C₆D₆) δ 13.42 (s, 1H), 7.38 (dd, *J* = 8, 4 Hz, 1H), 7.15 (m, 1H), 6.97 (br s, 1H), 6.80 (dt, *J* = 8, 1 Hz, 1H), 6.76 (br s, 1H), 6.64 (d, *J* = 8 Hz, 1H), 4.81 (sept, *J* = 4 Hz, 1H), 3.46 (q, *J* = 8 Hz, 1H), 3.37–3.30 (m, 1H), 3.11–3.06 (m, 2H), 2.61 (br s, 1H), 2.56 (s, 3H), 2.41 (s, 3H), 2.40 (br s,

1H), 2.13 (s, 3H), 2.03 (br s, 1H), 1.91 (d, $J = 4$ Hz, 3H), 1.86–1.79 (m, 2H), 1.65 (br s, 2H), 1.62 (d, $J = 4$ Hz, 3H), 1.59–1.57 (m, 1H), 1.43–1.37 (m, 3H), 2.30 (br d, $J = 8$ Hz, 2H), 0.54 (br d, $J = 16$ Hz, 1H). ^{13}C NMR (126 MHz, C_6D_6) δ 236.56, 215.48, 154.59, 141.54, 139.13, 138.09, 137.45, 135.36, 125.96, 123.47, 122.63, 112.99, 81.52, 75.78, 63.40, 52.52, 42.24, 41.09, 39.39, 38.12, 37.54, 37.25, 33.81, 30.63, 29.64, 22.72, 21.76, 21.16, 20.99, 19.28. HRMS (FAB+): Calculated—698.1316, Found—698.1343.

Preparation of silver(I) 2,2-dicyclohexylacetate (6.19-Ag): To 2,2-dicyclohexylcarboxylic acid (1.24 g, 5.54 mmol) and NaOH (193 mg, 4.82 mmol) was added H_2O (2.7 mL) and the solution was stirred for 15 min. AgNO_3 (676 mg, 3.99 mmol) dissolved in H_2O (2.6 mL) was added drop-wise, which caused immediate precipitation of a white solid. The suspension was stirred for 15 min after which the white precipitate was collected on a medium porosity frit and washed with H_2O , MeOH, and hexanes. After drying, **4-Ag** was recovered as a white solid (937 mg, 71%). Insolubility precluded analysis using NMR spectroscopy. MS (laser desorption ionization): Calculated—223.1704, Found—223.1788.

Preparation of 6.19: In a glovebox, a 20 mL scintillation vial was charged with **6.18** (24 mg, 0.035 mmol) and **6.19-Ag** (13 mg, 0.038 mmol). THF (ca. 1 mL) was added and the color of the solution immediately changed from brown to deep purple. The reaction was stirred for 1 h and concentrated. The resulting purple residue was dissolved in C_6H_6 , filtered through celite, and concentrated to give **6.19** (25 mg, 93%).

Note: Catalyst **6.19** would change colors from purple to brown upon the addition of solvents which were not rigorously purified of oxygen. Recrystallization from Et₂O at –35°C was used to purify **6.19** when this occurred. ¹H NMR (400 MHz, C₆D₆) δ 14.94 (s, 1H), 7.41 (dd, *J* = 8, 4 Hz, 1H), 7.25 (dt, *J* = 8, 4 Hz, 1H), 6.87–6.83 (m, 2H), 6.80 (br s, 1H), 6.72 (br d, *J* = 8 Hz, 1H), 4.78 (sept, *J* = 8 Hz, 1H), 4.08 (s, 1H), 3.45–3.13 (m, 4H), 2.47 (br s, 1H), 2.44 (s, 3H), 2.33 (s, 1H), 2.25 (s, 1H), 2.10–1.30 (m, 10H), 2.07 (br s, 1H), 1.98 (br d, *J* = 8 Hz, 3H), 1.88 (br d, *J* = 8 Hz, 4H), 1.79 (br s, 3H), 1.76 (br s, 2H), 1.64 (br s, 4H), 1.60 (d, *J* = 4 Hz, 4H), 3.34 (br d, *J* = 16 Hz, 3H), 1.39 (br s, 1H), 1.36 (d, *J* = 4 Hz, 5H), 1.17 (br d, *J* = 8 Hz, 2H), 1.07 (br d, *J* = 8 Hz, 2H), 0.63 (br d, *J* = 12 Hz, 1H). ¹³C NMR (101 MHz, C₆D₆) δ 258.83, 214.74, 183.61, 153.90, 143.52, 137.70, 136.58, 136.43, 136.03, 129.47, 129.20, 124.98, 122.86, 122.83, 113.34, 73.83, 67.67, 62.30, 57.15, 51.31, 42.77, 40.96, 40.04, 37.88, 37.58, 36.76, 33.30, 30.71, 29.60, 21.68, 21.35, 20.86, 18.65, 18.49. HRMS (FAB+, (M+H)–H₂): Calculated—793.3883, Found—793.3894.

Preparation of 6.20: Catalyst **6.20** (23 mg, 80%) was prepared in a manner analogous to catalyst **6.19**. **6.18** (32 mg, 0.046 mmol), AgOAc (11 mg, 0.069 mmol), THF (ca. 1 mL). ¹H NMR (400 MHz, C₆D₆) δ 14.95 (s, 1H), 7.47 (dd, *J* = 7.6, 1.6 Hz, 1H), 7.25 (t, *J* = 7.2 Hz, 1H), 6.88 (dt, *J* = 7.6, 1.2 Hz, 1H), 6.77 (br s, 1H), 6.70 (br s, 1H), 6.65 (br d, *J* = 8.4 Hz, 1H), 4.76 (sept, *J* = 6.0 Hz, 1H), 4.06 (s, 1H), 3.47 (q, *J* = 8.8 Hz, 1H), 3.38–3.21 (m, 4H), 2.43 (s, 3H), 2.40 (br s, 1H), 2.33 (s, 3H), 2.15 (br s, 4H), 2.15–1.04 (m, 2H), 1.98–1.95 (m, 1H), 1.87–1.83 (m, 1H), 1.78 (s, 3H), 1.69 (br s, 1H), 1.57 (d, *J* = 6.4 Hz, 3H), 1.56–1.53 (m, 2H), 1.22–1.15 (m, 2H), 1.05 (d, *J* = 6.4 Hz, 3H), 0.73 (br d, *J* = 12 Hz, 1H). ¹³C NMR (101 MHz,

C₆D₆) δ 259.69, 215.65, 180.15, 154.57, 143.79, 137.76, 137.41, 136.81, 136.42, 129.55, 129.24, 125.51, 123.20, 123.19, 112.90, 74.01, 68.79, 67.84, 62.82, 51.44, 43.38, 41.62, 40.64, 38.27, 37.97, 37.72, 33.59, 31.21, 30.03, 25.84, 24.43, 21.35, 21.04, 20.73, 18.75, 18.48. HRMS (FAB+, (M+H)–H₂): Calculated—629.2318, Found—629.2345.

Preparation of 6.21: Thioacetic acid (2.1 g, 28.2 mmol) was added to a solution of NaOH (1.2 g, 29.4 mmol) in 30 mL H₂O and stirred for 15 min at RT. A solution of AgNO₃ (3.9 g, 23.5 mmol) in 30 mL H₂O was added which resulted in an immediate color change and formation of a brown precipitate. The suspension was stirred for 15 min, after which the precipitate was collected by filtration and washed with H₂O, MeOH, and Et₂O to give **6.21-Ag** as a grey powder (2.49 g, 58% yield) which was used without further purification or characterization.

Catalyst **6.21** (16 mg, 77%) was prepared in a manner analogous to **6.19**. **6.18** (22 mg, 0.0312 mmol), **6.21-Ag** (18 mg, 0.101 mmol), and THF (1 mL). ¹H NMR (400 MHz, C₆D₆) δ 14.89 (s, 1H), 7.38 (dd, *J* = 7.2, 1.6 Hz, 1H), 7.19 (m, 1H), 6.81 (m, 2H), 6.77 (br s, 1H), 6.69 (d, *J* = 8.4 Hz, 1H), 4.81 (sept, *J* = 5.6 Hz, 1H), 4.03 (br s, 1H), 3.45 (m, 1H), 3.36 (m, 1H), 2.59 (s, 1H), 2.43 (s, 3H), 2.35 (m, 1H), 2.29 (s, 3H), 2.22 (s, 3H), 2.18 (br s, 1H), 2.08 (s, 3H), 1.93 (m, 2H), 1.93 (m, 1H), 1.73 (br s, 1H), 1.59 (br m, 3H), 1.49 (d, *J* = 6.4 Hz, 3H), 1.32 (d, *J* = 6 Hz, 4H), 1.25 (m, 3H), 0.76 (m, 1H). HRMS (FAB+, (M+H)–H₂): Calculated—645.2089, Found—645.2068.

Preparation of silver(I) 2,2-dimethoxypropanoate (6.22-Ag): A 100 mL RB flask was charged with 2,2-dimethoxypropanoic acid (488 mg, 3.64 mmol), Ag₂O (507

mg, 2.19 mmol), MeCN (20 mL), and H₂O (6 mL). The solution was shielded from light and stirred at RT under Ar for 5 h. The suspension was filtered through celite, washing with MeCN, and the filtrate was concentrated to a white solid which was washed with hexanes and collected by filtration to give **6.21-Ag** (469 mg, 53%). ¹H NMR (400 MHz, D₂O) δ 3.21 (s, 6H), 1.43 (s, 3H). ¹³C NMR (101 MHz, D₂O) δ 176.37, 101.51, 49.34, 20.26. MS (laser desorption ionization): Calculated—133.0506, Found—133.0539.

Preparation of 6.22: Catalyst **6.22** (31 mg, 89%) was prepared in a manner analogous to catalyst **6.19**. **6.18** (35 mg, 0.050 mmol), **6.22-Ag** (13 mg, 0.055 mmol), THF (ca. 1 mL). ¹H NMR (600 MHz, C₆D₆) δ 14.88 (s, 1H), 7.43 (br d, *J* = 12 Hz, 1H), 7.23 (t, *J* = 6 Hz, 1H), 6.94 (br s, 1H), 6.86 (t, *J* = 6 Hz, 1H), 6.74–6.71 (m, 2H), 4.87 (br s, 1H), 4.16 (s, 1H), 3.50–3.19 (m, 10H), 2.47 (br s, 1H), 2.45 (s, 3H), 2.40 (s, 3H), 2.20 (s, 3H), 2.13–2.08 (m, 2H), 2.01 (br d, *J* = 12 Hz, 1H), 1.96 (br d, *J* = 12 Hz, 1H), 1.82 (br d, *J* = 12 Hz, 1H), 1.66 (br s, 1H), 1.63 (d, *J* = 6 Hz, 3H), 1.57–1.54 (m, 1H), 1.50–1.48 (m, 1H), 1.43 (br d, *J* = 12 Hz, 1H), 1.38 (s, 3H), 1.27 (br d, *J* = 6 Hz, 3H), 1.17 (br d, *J* = 12 Hz, 1H), 1.10–1.09 (m, 2H), 0.68 (br d, *J* = 6 Hz, 1H). ¹³C NMR (151 MHz, C₆C₆) δ 259.06, 216.37, 177.95, 154.78, 144.04, 138.48, 137.86, 136.61, 136.38, 130.46, 129.48, 125.96, 123.52, 123.39, 113.89, 99.58, 75.37, 69.60, 63.10, 51.94, 43.58, 41.83, 40.83, 38.50, 38.32, 37.63, 33.94, 31.45, 30.30, 21.70, 21.41, 21.17, 20.99, 19.11, 18.88. HRMS (FAB+, (M+H)–H₂): Calculated—703.2685, Found—703.2682.

Preparation of 6.23: In a glove box, **6.2** (52.1 mg, 77.5 μmol), potassium 2,6-diisopropylphenoxide (83.9 mg, 388 μmol) and C₆H₆ (5.0 ml) were added into

a 20 ml vial equipped with a stir bar. The reaction mixture was stirred at room temperature for 30 min and filtered. The filtrate was evaporated and the resulting solid was dissolved in small amount of Et₂O and recrystallized at □35 °C. **11** was obtained as dark brown crystals (54 mg, 93%). ¹H NMR (500 MHz, C₆D₆): δ 14.02 (s, 1H), 7.39 (dd, *J* = 7.3, 1.5 Hz, 1H), 7.15 (br s, 1H), 7.06 (dt, *J* = 6.5, 2 Hz, 1H), 6.95 (br s, 1H), 6.83 (q, *J* = 7.5 Hz, 2H), 6.77 (s, 1H), 6.58–6.57 (m, 2H), 4.32 (sept, *J* = 6.4 Hz, 1H), 4.0 (br s, 1H), 3.89 (s, 1H), 3.40 (q, *J* = 11 Hz, 1H), 3.27 (dt, *J* = 10.5, 5 Hz, 1H), 3.10 (m, 2H), 2.57 (s, 3H), 2.33 (s, 3H), 2.30 (br s, 1H), 2.20 (br s, 1H), 2.11 (br s, 1H), 2.03 (s, 3H), 2.01 (br s, 1H), 1.94–1.93 (m, 1H), 1.82 (br t, *J* = 9 Hz, 2H), 1.62 (br s, 1H), 1.55–1.38 (m, 9H), 1.25 (d, *J* = 6.4 Hz, 3H), 1.11 (br d, *J* = 10.5 Hz, 2H), 0.85 (d, *J* = 6.4 Hz, 3H), 0.59–0.41 (br m, 7H). ¹³C NMR (126 MHz, C₆D₆) δ 234.91, 214.14, 150.56, 140.03, 136.31, 134.41, 134.07, 132.39, 127.15, 126.11, 121.95, 119.99, 119.76, 112.66, 110.58, 72.80, 66.00, 60.25, 49.43, 40.14, 38.44, 37.35, 34.95, 34.83, 34.23, 30.62, 27.99, 26.83, 18.48, 18.15, 17.71, 15.97, 15.73. HRMS (FAB+): Calculated—748.3542, Found—748.3576.

Preparation of 6.24: Method A: In a glovebox, a 20 mL scintillation vial was charged with **6.18** (112 mg, 0.161 mmol), AgNO₃ (409 mg, 2.41 mmol), and THF (6 mL). The reaction was stirred vigorously until a color change from brown to dark purple was observed (ca. 3–5 min). At this point, the reaction was immediately concentrated and the resulting residue was dissolved in C₆H₆, filtered, and concentrated. The crude product was triturated with Et₂O several times, until the washes were colorless, to give **7** (73 mg, 72%) as a purple solid. ¹H NMR (400 MHz, C₆D₆) δ 15.22 (s, 1H), 7.37 (d, *J* = 7.2 Hz, 1H), 7.18 (t, *J* = 7.6 Hz, 1H), 6.98

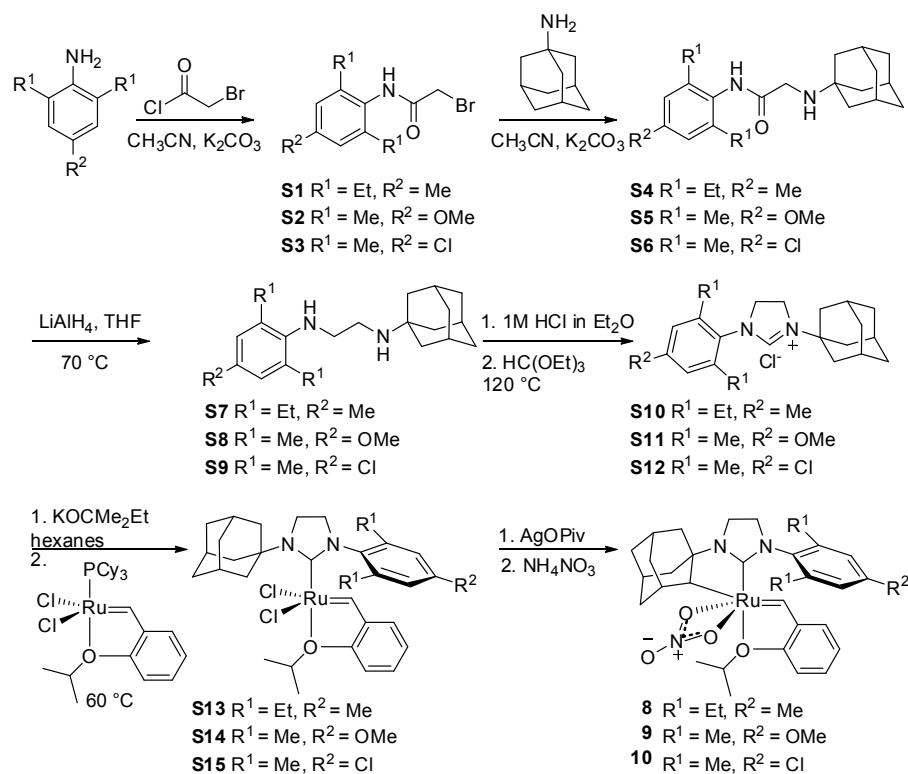


Figure 6.S1. Synthesis of catalysts **6.25**, **6.26**, **6.27**.

(s, 1H), 6.82 (t, $J = 7.6$ Hz, 1H), 6.66 (s, 1H), 6.48 (d, $J = 8.4$ Hz, 1H), 4.57 (sept, $J = 6.0$ Hz, 1H), 4.17 (s, 1H), 3.43 (q, $J = 9.6$ Hz, 1H), 3.28–3.15 (m, 3H), 2.38 (d, $J = 8.4$ Hz, 6H), 2.25 (br s, 1H), 2.15–2.09 (m, 4H), 2.03–1.97 (m, 2H), 1.90–1.87 (m, 1H), 1.77 (br d, $J = 15.2$ Hz, 1H), 1.65 (br s, 1H), 1.55–1.47 (m, 2H), 1.42 (d, $J = 5.2$ Hz, 3H), 1.14–1.10 (m, 3H), 0.96 (d, $J = 6.0$ Hz, 3H), 0.58 (br d, $J = 12$ Hz, 1H). ^{13}C NMR (101 MHz, C_6D_6) δ 265.80, 265.55, 214.16, 154.72, 143.60, 137.69, 137.40, 136.24, 135.45, 130.11, 129.36, 126.83, 123.38, 123.35, 113.00, 74.32, 66.78, 63.05, 51.36, 43.14, 41.84, 40.34, 37.95, 37.81, 37.65, 33.33, 30.98, 29.83, 21.25, 21.09, 20.28, 18.56, 17.44. HRMS (FAB+, $\text{M}-\text{NO}_3$): Calculated—571.2263, Found—571.2273.

Method B: In a glovebox, a 20 mL scintillation vial was charged with **6.2**

(128 mg, 0.190 mmol), NH_4NO_3 (457 mg, 5.71 mmol), and THF (ca. 10 mL). The reaction was stirred until completion as determined by ^1H NMR spectroscopy (ca. 1h) and concentrated. The residue was purified as described in Method A to give **6.24** (98 mg, 82%). Note: crude **6.2** as prepared above could also be used to prepare **6.24**.

Preparation of S1: A solution of 2,6-diethyl-4-methylaniline (1.63 g, 10.0 mmol) and CH_3CN (20 mL) was treated with K_2CO_3 (2.76 g, 20.0 mmol). Bromoacetyl chloride (830 μL , 10.0 mmol) was added drop-wise, and the reaction mixture was stirred at 25 °C over 12-16 h. The mixture was filtered over celite, concentrated under reduced pressure, and recrystallized from CH_2Cl_2 -hexanes providing S1 (1.55 g, 55%) as a white powder: ^1H NMR (CDCl_3 , 500 MHz) δ 7.68 (s, 1H), 6.95 (s, 2H), 4.08 (s, 2H), 2.54 (q, 4H, $J = 7.5$ Hz), 2.32 (s, 3H), 1.19 (t, 6H, $J = 7.5$ Hz); ^{13}C NMR (CDCl_3 , 125 MHz) δ 164.8, 141.2, 138.2, 129.1, 127.4, 29.2, 24.8, 21.3, 14.6; HRMS (FAB+) m/z : Calculated—([M + H]) 284.0650, Found—284.0654 ([M + H]).

Preparation of S2: Prepared from 4-methoxy-2,6-dimethylaniline⁴⁶ (520 mg, 3.44 mmol) and bromoacetyl chloride (286 μL , 3.44 mmol) following the procedure detailed for **S1** providing **S2** (750 mg, 80%) as a white powder: ^1H NMR (CDCl_3 , 500 MHz) δ 7.66 (s, 1H), 6.62 (s, 2H), 4.04 (s, 2H), 3.77 (s, 3H), 2.20 (s, 6H); ^{13}C NMR (CDCl_3 , 125 MHz) δ 164.5, 158.7, 136.9, 125.9, 113.6, 55.4, 29.2, 18.6; HRMS (EI+) m/z : Calculated—271.0208, Found—271.0198.

Preparation of S3: Prepared from 4-chloro-2,6-dimethylaniline (1.55 g, 3.44 mmol) and bromoacetyl chloride (286 μL , 10.0 mmol) following the procedure detailed for **S1** providing **S3** (0.75 g, 28%) as a white powder: ^1H NMR (CDCl_3 , 300 MHz) δ

7.10 (s, 2H), 4.07 (s, 2H), 2.22 (s, 6H); ^{13}C NMR ($(\text{CD}_3)_2\text{SO}$, 125 MHz) δ 164.9, 137.5, 133.3, 130.7, 127.3, 29.1, 17.6; HRMS (FAB+) m/z : Calculated—277.9761, Found—277.9755.

Preparation of S4: A solution of **S1** (950 mg, 3.36 mmol) and 1-adamantylamine (760 mg, 5.0 mmol) in CH_3CN (10 mL) was treated with K_2CO_3 (700 mg, 5.1 mmol) and allowed to stir at 85 °C for 16 h. The reaction mixture was then filtered over celite and concentrated under reduced pressure. Flash chromatography (SiO_2 , 4% MeOH-DCM) provided S4 (1.11 g, 93%) as a white solid: ^1H NMR (CDCl_3 , 500 MHz) δ 9.04 (s, 1H), 6.93 (s, 2H), 3.42 (s, 2H), 2.54 (q, 4H, $J = 7.5$ Hz), 2.31 (s, 3H), 2.11 (br s, 3H), 1.58–1.73 (m, 13H), 1.17 (t, 6H, $J = 7.5$ Hz); ^{13}C NMR (CDCl_3 , 125 MHz) δ 172.2, 140.9, 137.1, 130.2, 127.2, 51.1, 44.1, 42.9, 36.5, 29.5, 25.1, 21.2, 14.7; HRMS (FAB+) m/z : Calculated—([M + H]) 355.2749, Found—355.2758 ([M + H]).

Preparation of S5: Prepared from **S2** (700 mg, 2.58 mmol) and 1-adamantylamine (590 mg, 3.9 mmol) following the procedure detailed for S4 providing S5 (800 mg, 91%) as an off-white solid: ^1H NMR (CDCl_3 , 500 MHz) δ 8.94 (s, 1H), 6.62 (s, 2H), 3.75 (s, 3H), 3.40 (s, 2H), 2.18 (s, 6H), 2.10 (br m, 3H), 1.57–1.71 (m, 13H); ^{13}C NMR (CDCl_3 , 125 MHz) δ 171.9, 158.1, 136.4, 127.0, 113.4, 55.3, 51.1, 44.0, 42.9, 36.5, 29.5, 18.9; HRMS (EI+) m/z : Calculated—342.2307, Found—342.2292.

Preparation of S6: Prepared from **S3** (750 mg, 2.73 mmol) and 1-adamantylamine (620 mg, 4.1 mmol) following the procedure detailed for S4 providing S6 (715 mg, 77%) as a white solid: ^1H NMR (CDCl_3 , 500 MHz) δ 9.06 (s, 1H), 7.05 (s, 2H), 3.41 (s, 2H), 2.18 (s, 6H), 2.10 (br m, 3H), 1.57–1.71 (m, 13H); ^{13}C NMR (CDCl_3 , 125

MHz) δ 171.6, 136.9, 132.8, 132.1, 128.0, 51.2, 44.1, 42.9, 36.5, 29.5, 18.6; HRMS (EI+) m/z : Calculated—347.1890, Found—347.1905.

Preparation of S7: Under an atmosphere of argon, a solution of **S4** (1.0 g, 2.82 mmol) in THF (15 mL) at 0 °C was treated with LiAlH₄ (325 mg, 8.5 mmol). The reaction mixture was allowed to warm to 25 °C and stirred at 65 °C for 36 h. The reaction mixture was allowed to cool to 0 °C and 1 mL H₂O and 1 mL NaOH were added slowly. The mixture was diluted with EtOAc, filtered, and partitioned between EtOAc-H₂O. The organic layer was dried (Na₂SO₄) and concentrated under reduced pressure providing **S7** (0.95 g, 99%) as a yellow oil: ¹H NMR (CDCl₃, 500 MHz) δ 6.88 (s, 2H), 2.98 (m, 2H), 2.85 (m, 2H), 2.70 (q, 4H, J = 7.5 Hz), 2.30 (s, 3H), 2.11 (br s, 3H), 1.62–1.74 (m, 13H), 1.27 (t, 6H, J = 7.5 Hz); ¹³C NMR (CDCl₃, 125 MHz) δ 142.88, 136.3, 131.5, 127.3, 51.1, 50.2, 43.0, 40.6, 36.8, 29.6, 24.4, 20.8, 15.0; HRMS (FAB+) m/z : Calculated—([M + H]) 341.2957, Found—341.2966 ([M + H]).

Preparation of S8: Prepared from **S5** (735 mg, 2.15 mmol) and LiAlH₄ (245 mg, 6.45 mmol) following the procedure detailed for **S7** providing **S8** (685 mg, 98%) as a yellow oil: ¹H NMR (CDCl₃, 500 MHz) δ 6.56 (s, 2H), 3.73 (s, 3H), 2.93 (dd, 2H, J = 6.5, 5.0 Hz), 2.79 (dd, 2H, J = 6.5, 5.0 Hz), 2.29 (s, 6H), 2.07 (br s, 3H), 1.58–1.71 (m, 13H); ¹³C NMR (CDCl₃, 125 MHz) δ 154.5, 139.8, 131.4, 113.8, 55.3, 50.2, 50.0, 43.0, 40.7, 36.8, 29.6, 18.8; HRMS (FAB+) m/z : Calculated—([M + H]) 329.2593, Found—329.2577 ([M + H]).

Preparation of S9: Prepared from **S6** (660 mg, 1.91 mmol) and LiAlH₄ (218 mg, 5.73 mmol) following the procedure detailed for **S7** providing **S9** (634 mg, 99%) as a yellow oil: ¹H NMR (CDCl₃, 500 MHz) δ 6.92 (s, 2H), 2.96 (m, 2H), 2.75 (m, 2H),

2.25 (s, 6H), 2.05 (br s, 3H), 1.58–1.71 (m, 13H); ^{13}C NMR (CDCl_3 , 125 MHz) δ 145.2, 130.4, 128.1, 125.5, 50.1, 49.2, 42.9, 40.3, 36.6, 29.5, 18.6; HRMS (FAB+) m/z : Calculated—([M + H]) 333.2098, Found—333.2094 ([M + H]).

Preparation of S10: A solution of **S7** (950 mg, 2.79 mmol) in Et_2O (5 mL) was treated with 2M HCl in Et_2O (2.80 mL) to provide a white solid that was filtered and dried. A solution of triethylorthoformate (5 mL) was added to this white solid and the mixture was allowed to stir at 120 °C for 30 min. The reaction mixture was concentrated under reduced pressure to provide an off-white powder that was filtered, washed with hexanes and dried to provide S10 (0.55 g, 52%) as a white powder: ^1H NMR (CDCl_3 , 500 MHz) δ 8.65 (s, 1H), 6.97 (s, 2H), 4.48 (t, 2H, J = 10.0 Hz), 4.31 (t, 2H, J = 10.0 Hz), 2.53–2.69 (m, 4H), 2.33 (s, 3H), 2.26 (br m, 3H), 2.10 (d, 6H, J = 2.5 Hz), 1.73 (t, 6H, J = 2.5 Hz), 1.26 (t, 6H, J = 7.5 Hz); ^{13}C NMR (CDCl_3 , 125 MHz) δ 156.2, 140.9, 140.3, 129.6, 127.6, 57.9, 52.1, 45.4, 41.0, 35.3, 29.1, 24.0, 21.3, 14.8; HRMS (FAB+) m/z : Calculated—([M+]) 351.2800, Found—351.2817 ([M+]).

Preparation of S11: Prepared from **S8** (685 mg, 2.10 mmol) and triethylorthoformate (5 mL) following the procedure detailed for S10 providing S11 (565 mg, 72%) as a white powder: ^1H NMR (CDCl_3 , 500 MHz) δ 9.04 (s, 1H), 6.49 (s, 2H), 4.27 (dd, 2H, J = 9.2, 12.3 Hz), 4.12 (dd, 2H, J = 9.2, 12.3 Hz), 3.66 (s, 3H), 2.21 (s, 6H), 2.13 (br m, 3H), 2.01 (d, 6H, J = 3.0 Hz), 1.62 (t, 6H, J = 2.8 Hz); ^{13}C NMR (CDCl_3 , 125 MHz) δ 159.7, 156.8, 137.0, 126.5, 114.0, 57.8, 55.3, 50.9, 45.1, 40.8, 35.3, 29.1, 18.4; HRMS (FAB+) m/z : Calculated—([M+]) 339.2436, Found—339.2448 ([M+]).

Preparation of S12: Prepared from S9 (630 mg, 1.91 mmol) and triethylorthoformate

(5 mL) following the procedure detailed for S10 providing S12 (600 mg, 83%) as a white powder: ^1H NMR (CDCl_3 , 500 MHz) δ 9.47 (s, 1H), 6.98 (s, 2H), 4.26 (m, 2H), 4.14 (m, 2H), 2.24 (s, 6H), 2.14 (br s, 3H), 2.01 (d, 6H, J = 3.0 Hz), 1.63 (t, 6H, J = 3.2 Hz); ^{13}C NMR (CDCl_3 , 125 MHz) δ 157.3, 137.7, 135.1, 132.3, 128.8, 58.1, 50.6, 45.1, 40.9, 35.3, 29.1, 18.2; HRMS (FAB+) m/z : Calculated—([M+]) 343.1941, Found—343.1932 ([M+]).

Preparation of S13: In a glove box, a solution of S10 (200 mg, 0.52 mmol) in hexanes (6 mL) was treated with KCOMe_2Et (75 mg, 0.57 mmol), and the mixture was allowed to stir at 35 °C for 1 h. The reaction mixture was then treated with $\text{RuCl}_2(\text{PCy}_3)(=\text{CH}-o\text{-O}^i\text{PrC}_6\text{H}_4)$ (312 mg, 0.52 mmol), removed from the glove box, and allowed to stir at 65 °C for 3 h. The precipitated solids were filtered and washed well with hexanes to provide S13 (335 mg, 96%) as a green powder: ^1H NMR (CDCl_3 , 500 MHz) δ 16.87 (s, 1H), 7.55 (ddd, 1H, J = 1.7, 7.4, 8.8 Hz), 7.15 (s, 2H), 6.91 (m, 2H), 6.83 (dd, 1H, J = 1.5, 7.5 Hz), 5.06 (hept, 1H, J = 6.1 Hz), 4.02 (dd, 2H, J = 8.4, 11.4 Hz), 3.85 (dd, 2H, J = 8.4, 11.4 Hz), 2.95 (br s, 6H), 2.70 (dq, 2H, J = 7.6, 15.3 Hz), 2.55 (dq, 2H, J = 7.6, 15.3 Hz), 2.53 (s, 3H), 2.41 (br s, 3H), 1.94 (d, 3H, J = 12.0 Hz), 1.83 (d, 3H, J = 12.0 Hz), 1.63 (d, 6H, J = 6.1 Hz), 1.13 (t, 6H, J = 7.5 Hz); ^{13}C NMR (CDCl_3 , 125 MHz) δ 311.7, 208.6, 152.4, 145.6, 143.1, 138.63, 138.59, 130.7, 127.1, 123.6, 122.6, 113.3, 74.2, 57.7, 52.8, 44.5, 42.2, 36.2, 30.0, 23.3, 22.5, 21.7, 14.1; HRMS (FAB+) m/z : Calculated—670.2031, Found—670.2019.

Preparation of S14: Prepared from S11 (100 mg, 0.27 mmol) and $\text{RuCl}_2(\text{PCy}_3)(=\text{CH}-o\text{-O}^i\text{PrC}_6\text{H}_4)$ (160 mg, 0.27 mmol) following the procedure detailed for S13 providing S14 (138 mg, 78%) as a green powder: ^1H NMR (CDCl_3 , 500 MHz) δ

16.98 (s, 1H), 7.56 (ddd, 1H, $J = 1.9, 7.2, 8.9$ Hz), 6.93 (m, 3H), 6.78 (s, 2H), 5.09 (hept, 1H, $J = 6.1$ Hz), 4.04 (dd, 2H, $J = 8.5, 11.9$ Hz), 1.89 (s, 3H), 3.85 (dd, 2H, $J = 8.5, 11.9$ Hz), 2.95 (br s, 6H), 2.41 (s, 3H), 2.26 (s, 6H), 1.93 (d, 3H, $J = 12.0$ Hz), 1.83 (d, 3H, $J = 12.0$ Hz), 1.63 (d, 6H, $J = 6.0$ Hz); ^{13}C NMR (CDCl_3 , 125 MHz) δ 312.4, 208.3, 159.4, 152.4, 145.92, 145.90, 139.6, 135.3, 130.8, 124.0, 122.8, 114.0, 113.3, 74.2, 57.2, 55.7, 51.3, 44.6, 42.2, 36.2, 30.0, 22.5, 18.8; HRMS (FAB+) m/z : Calculated—658.1667, Found—658.1645.

Preparation of S15: Prepared from **S12** (100 mg, 0.27 mmol) and $\text{RuCl}_2(\text{PCy}_3)$ ($=\text{CH}-o\text{-O'}\text{PrC}_6\text{H}_4$) (160 mg, 0.27 mmol) following the procedure detailed for S13 providing S15 (136 mg, 78%) as a green powder: ^1H NMR (CDCl_3 , 500 MHz) δ 16.89 (s, 1H), 7.59 (m, 1H), 7.26 (m, 2H), 6.96 (m, 3H), 5.10 (hept, 1H, $J = 6.2$ Hz), 4.05 (dd, 2H, $J = 8.4, 11.6$ Hz),), 3.83 (dd, 2H, $J = 8.5, 11.6$ Hz), 2.93 (br s, 6H), 2.41 (s, 3H), 2.28 (s, 6H), 1.93 (d, 3H, $J = 12.0$ Hz), 1.84 (d, 3H, $J = 12.5$ Hz), 1.63 (d, 6H, $J = 6.0$ Hz); ^{13}C NMR (CDCl_3 , 125 MHz) δ 310.8, 208.2, 152.4, 145.8, 140.7, 140.4, 133.9, 131.0, 128.8, 124.0, 122.9, 113.3, 74.3, 57.4, 50.9, 44.7, 42.1, 36.1, 30.0, 22.4, 18.4; HRMS (FAB+) m/z : Calculated—664.1143, Found—664.1151.

Preparation of 6.25: In a glovebox, a solution of **S13** (98 mg, 0.14 mmol) and THF (5 mL) was treated with AgOPiv (92 mg, 0.44 mmol). The reaction mixture was allowed to stir at 25 °C for 30 min and a color change from brown to purple was observed. The mixture was immediately filtered over celite and concentrated. The residue was triturated with Et_2O and dried to provide a purple solid. The purple solid was then taken up in THF (3 mL), treated with NH_4NO_3 (350 mg, 4.4 mmol)

and allowed to stir for 1 h. The reaction mixture was concentrated, taken up in benzene, and filtered over celite. The filtrate was dried and triturated with Et₂O until the washes were colorless providing **6.25** (30 mg, 31%) as a purple powder: ¹H NMR (C₆D₆, 500 MHz) δ 15.19 (s, 1H), 7.42 (dd, 1H, *J* = 1.5, 7.5 Hz) 7.18 (ddd, 1H, *J* = 1.5, 7.5, 8.5 Hz), 7.06 (d, 1H, *J* = 1.0 Hz), 6.83 (dt, 1H, *J* = 1.0, 7.5 Hz), 6.79 (d, 1H, *J* = 1.5 Hz), 6.47 (d, 1H, *J* = 8.5 Hz), 4.55 (hept, 1H, *J* = 6.3 Hz), 4.18 (s, 1H), 3.55 (q, 1H, *J* = 10.7 Hz), 3.39 (m, 1H), 3.17–3.29 (m, 2H), 3.06 (dq, 1H, *J* = 7.7, 15.3 Hz), 2.86–3.00 (m, 2H), 2.63 (dq, 1H, *J* = 7.5, 15.0 Hz), 2.24 (m, 1H), 2.15 (s, 3H), 2.10 (m, 1H), 1.96–2.02 (m, 2H), 1.89 (d, 1H, *J* = 11.0 Hz), 1.77 (dd, 1H, *J* = 1.5, 12.0 Hz), 1.66 (m, 1H), 1.44–1.55 (m, 3H), 1.42 (d, 3H, *J* = 6.5 Hz), 1.28 (t, 3H, *J* = 7.5 Hz), 1.20 (t, 3H, *J* = 7.5 Hz), 1.10 (m, 2H), 0.94 (d, 3H, *J* = 6.0 Hz), 0.59 (d, 1H, *J* = 12.0 Hz); ¹³C NMR (C₆D₆, 100 MHz) δ 214.3, 154.7, 143.54, 143.50, 141.1, 137.8, 134.9, 128.5, 127.0, 126.8, 123.37, 123.33, 113.0, 74.3, 66.7, 63.0, 52.9, 43.0, 41.8, 40.3, 37.9, 37.77, 37.73, 33.3, 30.9, 29.8, 24.1, 23.4, 21.4, 21.2, 20.2, 15.7, 15.3; HRMS (FAB+) *m/z*: Calculated—661.2454, Found—661.2422.

Preparation of 9: Prepared from **S14** (118 mg, 0.179 mmol) and AgOPiv (112 mg, 0.54 mmol) following the procedure detailed for **6.25** providing **6.26** (16.5 mg, 14%) as a purple powder: ¹H NMR (C₆D₆, 400 MHz) δ 15.21 (s, 1H), 7.37 (dd, 1H, *J* = 1.6, 7.6 Hz), 7.19 (m, 1H), 6.82 (m, 2H), 6.44 (d, 1H, *J* = 2.8 Hz), 6.49 (d, 1H, *J* = 8.4 Hz), 4.58 (hept, 1H, *J* = 6.3 Hz), 4.16 (s, 1H), 3.40 (m, 1H), 3.33 (s, 3H), 3.10–3.30 (m, 3H), 2.37 (d, 6H, *J* = 2.8 Hz), 2.24 (m, 1H), 2.11 (m, 1H), 1.96–2.01 (m, 2H), 1.85–1.92 (m, 1H), 1.73–1.81 (m, 1H), 1.65 (m, 1H), 1.48 (m, 3H), 1.44 (d, 3H, *J* = 6.4 Hz), 1.06 (m, 2H), 0.97 (d, 3H, *J* = 6.0 Hz), 0.58 (d, 1H, *J* = 12.4

Hz); ^{13}C NMR (C_6D_6 , 100 MHz) δ 214.4, 159.2, 154.7, 143.6, 139.3, 137.0, 131.8, 128.5, 126.8, 123.38, 123.35, 114.2, 113.0, 74.3, 66.7, 63.0, 54.8, 51.5, 43.1, 41.8, 40.3, 37.9, 37.8, 37.6, 33.3, 30.9, 29.8, 21.2, 20.2, 18.8, 17.8; HRMS (FAB+) m/z : Calculated—648.2012, Found—648.2036.

Preparation of 6.25: Prepared from **S15** (195 mg, 0.294 mmol) and AgOPiv (185 mg, 0.865 mmol) following the procedure detailed for **6.25** providing **6.27** (55 mg, 28%) as a purple powder: ^1H NMR (C_6D_6 , 400 MHz) δ 15.08 (s, 1H), 7.36 (dd, 1H, J = 1.6, 7.6 Hz), 7.16–7.24 (m, 2H), 6.81–6.87 (m, 2H), 6.51 (d, 1H, J = 8.4 Hz), 4.58 (hept, 1H, J = 6.2 Hz), 4.09 (s, 1H), 3.10–3.33 (m, 4H), 2.21 (m, 1H), 2.19 (d, 6H, J = 6.0 Hz), 2.10 (m, 1H), 1.96 (m, 1H), 1.85 (m, 2H), 1.75 (m, 1H), 1.63 (m, 1H), 1.46 (m, 3H), 1.41 (d, 3H, J = 6.4 Hz), 1.07 (m, 2H), 0.96 (d, 3H, J = 6.0 Hz), 0.54 (d, 1H, J = 12.4 Hz); ^{13}C NMR (C_6D_6 , 100 MHz) δ 265.9, 214.2, 154.7, 143.5, 140.0, 138.0, 137.4, 133.4, 129.2, 128.6, 127.1, 123.4, 123.3, 113.0, 74.4, 66.7, 63.2, 51.0, 43.0, 41.8, 40.2, 37.8, 37.7, 37.6, 33.2, 30.9, 29.7, 21.2, 20.2, 18.3, 17.3; HRMS (FAB+) m/z : Calculated—652.1517, Found—652.1529.

General Procedure for Homodimerization Reactions: In a glovebox, a 1 mL volumetric flask was charged with catalyst (0.0981 mmol) and filled to the line with THF to create a stock solution (0.0981 M). A portion of the catalyst stock solution (50 μL , ca. 5 μmol) was added to a 4 mL vial containing substrate (5 mmol) and THF (1.1 mL, ca. 3 M). The vial was placed into an aluminum block (IKA #3904400) preheated to 35 $^\circ\text{C}$ using a temperature controlled hotplate and the reaction was stirred while open to the glovebox atmosphere. After completion of the reaction (determined by ^1H NMR spectroscopy), the vial was removed from the glovebox,

quenched with oxygen, and the product was isolated via flash chromatography on silica gel according to literature procedures.⁴⁷ The percentage of Z-olefin product was determined by ¹H and ¹³C NMR spectroscopy, and all spectra were consistent with previous literature reports.³

General Procedure for Determination of Initiation Rates: In a glovebox, a 1 mL volumetric flask was charged with **6.2** (8.1 mg, 0.012 mmol) and filled to the line with C₆D₆ to create a stock solution (ca. 0.012 M). A portion of the stock solution (0.25 mL, 0.003 mmol **6.2**) was added to a NMR tube and diluted with C₆D₆ (0.35 mL). The NMR tube was sealed with a septa cap and placed in the NMR spectrometer at 30 °C. Butyl vinyl ether (12 μL, 0.09 mmol) was added and the disappearance of the benzyldiene proton resonance was monitored by arraying the 'pad' function in VNMRj.

All reactions, with the exception of **6.23**, showed clean first-order kinetics over a period of at least three half-lives. Spectra were baseline corrected and integrated with MestReNova. Estimation of error was determined from the average of three different kinetic runs.

General Procedure for Cross-Metathesis of 6.3 and 6.4: In a glovebox, a 4 mL vial was charged with **6.3** (1.33 mL, 10 mmol) and tridecane (internal standard, 1.22 mL, 5 mmol). A portion (89 μL, 0.35 mmol **6.3**) of this stock solution was added to a second 4 mL vial followed by **6.4** (111 μL, 0.69 mmol) and THF (0.45 mL). This mixture was stirred for several minutes before taking a t₀ timepoint. An aliquot (50 μL, 0.0035 mmol) of a catalyst solution prepared from **6.24** (44 mg, 0.069 mmol)

in THF (1 mL) was added to the substrate solution and the vial was sealed and heated to the desired temperature. Periodically, the reaction was cooled to RT, and an aliquot (20 μ L) was removed from the glovebox, diluted with a solution of ethyl vinyl ether in CH_2Cl_2 , and analyzed via GC.

GC response factors for all starting materials and products (ethylene excluded) were obtained in order to determine accurate conversions and the GC data was worked up according to the literature.²¹

GC instrument conditions: Inlet temperature—250 °C; Detector temperature—250 °C; hydrogen flow—32 mL/min; air flow—400 mL/min; constant col + makeup flow—30 mL/min.

GC Method: 50 °C for 5 min, followed by a temperature increase of 10 °C/min to 240 °C and a subsequent isothermal period at 240 °C for 5 min (total run time = 29 min).

Preparation of 6.28: To benzoic acid (0.305 g, 2.50 mmol) and NaOH (0.104 g, 2.60 mmol) was added H_2O (3 mL) and the solution was stirred at RT for 15 min. A solution of AgNO_3 (0.35 g, 2.08 mmol) in H_2O (3 mL) was added drop-wise which resulted in immediate precipitation of a white solid. The suspension was stirred for 15 min, after which the white precipitate was collected on a medium porosity frit and washed with H_2O , MeOH, and Et_2O . **6.28-Ag** was recovered as a light gray solid (0.51 g, 90%). ^1H NMR (400 MHz, $\text{dms}\text{-d}_6$) δ 8.06–7.83 (m, 2H), 7.54–7.14 (m, 3H).

Catalyst **6.28** (26 mg, 87%) was prepared in a manner analogous to **6.19**.

6.18 (30 mg, 0.043 mmol), **6.28-Ag** (15 mg, 0.065 mmol) and THF (3 mL). ^1H NMR (300 MHz, C_6D_6) δ 15.07 (s, 1H), 8.10 (s, 2H), 7.98–7.91 (m, 1H), 7.50 (s, 1H) 7.44–7.41 (m, 1H), 6.93–6.73 (m, 3H), 6.59 (d, J = 8.6 Hz, 1H), 6.25 – 6.20 (m, 1H), 6.16 (s, 1H), 4.73–4.65 (m, 1H), 4.25 (s, 1H), 3.44 (s, 1H), 3.29 (s, 2H), 2.51 (s, 2H), 2.46 (s, 1H), 2.29 (s, 1H), 2.11 (d, J = 8.5 Hz, 4H), 1.73 (s, 2H), 1.57 (d, J = 6.3 Hz, 3H), 1.42 (s, 1H), 1.38–1.31 (m, 4H), 0.92 (d, J = 6.3 Hz, 3H), 0.83 (d, J = 6.1 Hz, 1H).

Preparation of 6.29: **6.29-Ag** (0.34 g, 56%) was prepared in an analogous manner to **6.28-Ag**. P-toluic acid (0.340 g, 2.50 mmol), NaOH (104 mg, 2.6 mmol), AgNO_3 (350 mg, 2.08 mmol). ^1H NMR (400 MHz, $\text{dms}\text{-}d_6$) δ 7.84 (d, J = 7.8 Hz, 2H), 7.17 (d, J = 7.8 Hz, 2H), 2.33 (s, 3H).

Catalyst **6.29** (15.7 mg, 52%) was prepared in a manner analogous to **6.19**. **6.18** (30 mg, 0.043 mmol), **6.29-Ag** (16 mg, 0.065 mmol), and THF (3 mL). ^1H NMR (300 MHz, C_6D_6) δ 15.06 (s, 1H), 8.07 (d, J = 7.9 Hz, 2H), 7.50 (d, J = 5.8 Hz, 1H), 7.27–7.20 (m, 1H), 6.98 (d, J = 7.9 Hz, 2H), 6.89 (t, J = 7.2 Hz, 1H), 6.79 (s, 1H), 6.60 (d, J = 8.2 Hz, 1H), 6.23 (s, 1H), 4.78–4.63 (m, 1H), 4.29 (s, 1H), 3.45 (t, J = 9.9 Hz, 1H), 3.31 (ddd, J = 20.3, 13.2, 7.8 Hz, 3H), 2.50 (d, J = 9.2 Hz, 3H), 2.16–2.04 (m, 9H), 1.59 (d, J = 6.3 Hz, 4H), 1.41–1.15 (m, 3H), 0.94 (d, J = 6.1 Hz, 2H), 0.88 (d, J = 6.1 Hz, 1H).

Preparation of 6.30: **6.30-Ag** (0.34 g, 56%) was prepared in an analogous manner to **6.28-Ag**. 4-fluorobenzoic acid (325 mg, 2.25 mmol), NaOH (94 mg, 2.34 mmol), AgNO_3 (318 mg, 1.88 mmol).

Catalyst **6.30** (13.5 mg, 44%) was prepared in a manner analogous to **6.19**.

6.18 (30 mg, 0.043 mmol), **6.30-Ag** (15 mg, 0.065 mmol), THF (3 mL). ^1H NMR (300 MHz, C_6D_6) δ 15.06 (s, 1H), 7.95 (s, 1H), 7.81–7.72 (m, 1H), 7.48 (d, J = 5.7 Hz, 1H), 7.44–7.40 (m, 1H), 7.24 (s, 1H), 6.91–6.56 (m, 4H), 6.19–6.13 (m, 1H), 6.09 (s, 1H), 4.72–4.65 (m, 1H), 4.22 (s, 1H), 3.42 (s, 1H), 2.49 (s, 1H), 2.43 (s, 1H), 2.24 (s, 1H), 2.05 (d, J = 13.7 Hz, 3H), 1.72 (s, 1H), 1.57 (d, J = 6.4 Hz, 2H), 1.42 (s, 1H), 1.40–1.29 (m, 3H), 0.92 (d, J = 6.2 Hz, 2H), 0.84 (d, J = 6.1 Hz, 1H).

Preparation of 6.31: **6.31-Ag** (1.14 g, 96%) was prepared in an analogous manner to **6.28-Ag**. 4-hydroxybenzoic acid (354 mg, 2.50 mmol), NaOH (104 mg, 2.60 mmol), AgNO_3 (352 mg, 2.08 mmol).

Catalyst **6.31** (12 mg, 58%) was prepared in a manner analogous to **6.19**. **6.18** (20 mg, 0.029 mmol), **6.31-Ag** (10.5 mg, 0.043 mmol), and THF (3 mL). ^1H NMR (300 MHz, C_6D_6) δ 15.20–14.86 (m, 1H), 8.00–7.92 (m, 2H), 7.52–7.38 (m, 2H), 6.93–6.86 (m, 2H), 6.80–6.73 (m, 1H), 6.58–6.45 (m, 2H), 6.26–6.21 (m, 1H), 4.26 (s, 2H), 2.51 (s, 3H), 2.13 (d, J = 6.5 Hz, 8H), 1.59 (d, J = 6.4 Hz, 5H), 1.12 (s, 1H), 0.95 (d, J = 6.0 Hz, 3H), 0.30 (s, 1H).

Preparation of 6.36: A 100 mL RB was charged with picolinic acid (0.56 g, 4.57 mmol) and silver (I) oxide (0.64 g, 2.74 mmol). MeCN (20 mL) and H_2O (6 mL) were added and the solution was stirred for 3 h under argon while shielded from light. After this time, the solution was filtered and the filtrate washed with copious amounts of MeCN. The supernatant was concentrated, washed with hexanes, and the collected by filtration as a white powder (**6.36-Ag**, 140 mg, 13% yield) that was used without further purification.

In a glovebox, a 20 mL vial was charged with **6.18** (26 mg, 0.037 mmol)

and **6.36-Ag** (9 mg, 0.041 mmol). THF was added and the solution was stirred for 1 h at RT. Workup was analogous to **6.19** to give **6.36** (20 mg, 78% yield) as a thermally unstable green powder. ^1H NMR (400 MHz, C_6D_6) δ 15.28 (s, 1H), 8.13 (d, $J = 7.6$ Hz, 1H), 7.53 (d, $J = 9.2$ Hz, 1H), 7.20 (m, 1H), 6.90 (d, $J = 8$ Hz, 1H), 6.84 (t, $J = 7.6$ Hz, 1H), 6.74 (t, $J = 9.2$ Hz, 1H), 6.44 (d, $J = 8.4$ Hz, 1H), 6.26 (s, 1H), 5.94 (s, 1H), 5.65 (m, 1H), 5.07 (s, 1H), 4.56 (sept, $J = 6.4$ Hz, 1H), 3.33 (m, 3H), 3.19 (m, 1H), 2.35 (s, 4H), 2.28 (br s, 3H), 2.18 (m, 1H), 2.06 (s, 3H), 1.97 (m, 1H), 1.83 (br s, 1H), 1.72 (s, 3H), 1.65 (br s, 3H), 1.39 (m, 1H), 1.24 (m, 4H), 0.83 (m, 1H), 0.39 (d, $J = 6.4$ Hz, 3H). Upon dissolving in C_6D_6 and heating to 70 °C, **6.36** would cleanly decompose into a mixture of yellow-colored hydride species identified by equal intensity resonances at δ –6.64 and –9.98 ppm. These species did not exchange on the NMR timescale, and were indefinitely stable under an inert atmosphere. **6.36** also decomposed in the solid state over a period of several days.

Preparation of 6.37: In a glovebox, a Schlenk flask was charged with **6.2** (24 mg, 0.036 mmol) and *p*-benzoquinone (16 mg, 0.15 mmol). THF (2 mL) was added which resulted in an immediate color change from purple to red/orange. The flask was sealed, removed from the glovebox, and heated to 70 °C for 12 h. After cooling to RT, the reaction was concentrated and the flask was taken back into the glovebox, where the red/brown residue was triturated with Et_2O to give **6.37** (6 mg, 13%) as a red crystalline solid. ^1H NMR (500 MHz, CD_2Cl_2) δ 7.16 (t, $J = 8.0$ Hz, 2H), 7.08 (t, $J = 7.5$ Hz, 2H), 6.92 (br s, 4H), 6.82 (t, $J = 9.0$ Hz, 4H), 6.77 (br s, 2H), 6.65 (s, 4H), 5.14 (s, 2H), 4.77 (dd, $J = 7.5, 2.5$ Hz, 2H), 4.58 (sept, $J = 6.0$ Hz, 2H), 4.19

(dd, $J = 7.5, 2.5$ Hz, 2H), 3.67 (quin, $J = 9.5$ Hz, 2H), 3.61–3.57 (m, 4H), 3.42 (t, $J = 10.0$ Hz, 2H), 3.19 (dd, $J = 7.5, 3.0$ Hz, 2H), 3.01 (br s, 2H), 2.83 (br d, $J = 12.5$ Hz, 2H), 2.43 (s, 6H), 2.16 (br d, $J = 9.0$ Hz, 2H), 2.1–2.08 (m, 2H), 2.06 (s, 6H), 1.93 (br s, 2H), 1.89 (s, 6H), 1.76 (br d, $J = 11.5$ Hz, 2H), 1.69–1.66 (m, 2H), 1.62–1.59 (m, 2H), 1.49 (br d, $J = 11.5$ Hz, 2H), 1.40–1.38 (m, 2H), 1.35–1.32 (m, 2H), 1.22 (d, $J = 6.0$ Hz, 6H), 1.19 (d, $J = 5.5$ Hz, 6H). ^{13}C NMR (126 MHz, CD_2Cl_2) δ 211.45, 163.30, 156.08, 150.53, 138.87, 137.96, 136.29, 135.59, 134.37, 129.98, 129.62, 129.45, 125.98, 119.24, 116.50, 113.50, 90.42, 88.63, 80.35, 77.04, 69.27, 65.11, 58.66, 46.11, 42.07, 41.30, 40.00, 38.66, 37.44, 31.97, 30.63, 29.30, 22.36, 22.27, 21.98, 19.42, 17.64. HRMS (FAB⁺): A mass corresponding to the monomeric species was detected. Calculated—679.2474, Found—679.2458.

General Polymerization Procedure: In a glovebox, a stock solution of catalyst was prepared from **6.24** (78 mg, 0.123 mmol) and THF (1 mL). An aliquot (50 μL , 0.0062 mmol **6.24**) of stock solution was added to a Schlenk flask and diluted with THF (0.5 mL). On a vacuum manifold, a separate Schlenk flask was flame-dried and charged with monomer (0.62 mmol) and THF (2 mL). The monomer solution was degassed via freeze-pump-thaw (3X) and the catalyst solution was injected via gas-tight syringe under argon at a given temperature. After stirring for 1 h, the polymerization was quenched with ethyl vinyl ether (0.1 mL) and, unless otherwise specified, precipitated into vigorously stirred MeOH. The precipitate was collected by vacuum filtration using either a medium or fine porosity frit and dried under vacuum.

References

- (1) (a) Fürstner, A. *Angew. Chem. Int. Ed.* **2000**, 39, 3012. (b) Trnka, T. M.; Grubbs, R. H. *Acc. Chem. Res.* **2001**, 34, 18. (c) Astruc, D. *New J. Chem.* **2005**, 29, 42.
- (2) Grubbs, R.H. *Handbook of Metathesis*, Wiley-VCH, Weinheim, **2003**.
- (3) (a) Jiang, A. J.; Zhao, Y.; Schrock, R. R.; Hoveyda, A. H. *J. Am. Chem. Soc.* **2009**, 131, 16630. (b) Marinescu, S. C.; Schrock, R. R.; Müller, P.; Takase, M. K.; Hoveyda, A. H. *Organometallics* **2011**, 30, 1780. (c) Meek, S. J.; O'Brien, R. V.; Llaveria, J.; Schrock, R. R.; Hoveyda, A. H. *Nature* **2011**, 471, 461. (d) Marinescu, S. C.; Levine, D. S.; Zhao, Y.; Schrock, R. R.; Hoveyda, A. H. *J. Am. Chem. Soc.* **2011**, 133, 11512.
- (4) (a) Wang, Y.; Jimenez, M.; Hansen, A. S.; Raiber, E.-A.; Schreiber, S. L.; Young, D. W. *J. Am. Chem. Soc.* **2011**, 133, 9196. (b) Gallenkamp, D.; Fürstner, A. *J. Am. Chem. Soc.* **2011**, 133, 9232.
- (5) (a) McNeill, K.; Anderson, R. A.; Bergman, R. G. *J. Am. Chem. Soc.* **1995**, 117, 3625. (b) McNeill, K.; Anderson, R. A.; Bergman, R. G. *J. Am. Chem. Soc.* **1997**, 119, 11244. (c) Trnka, T. M.; Day, M. W.; Grubbs, R. H. *Organometallics* **2001**, 20, 3845.
- (6) Endo, K.; Grubbs, R. H. *J. Am. Chem. Soc.* **2011**, 133, 8525.
- (7) (a) Hong, S. H.; Chlenov, A.; Day, M. W.; Grubbs, R. H. *Angew. Chem. Int. Ed.* **2007**, 46, 5148. (b) Hong, S. H.; Day, M. W.; Grubbs, R. H. *J. Am. Chem. Soc.* **2004**, 126, 7414. (c) Hong, S. H.; Wenzel, A. G.; Salguero, T. T.; Day, M. W.; Grubbs, R. H. *J. Am. Chem. Soc.* **2007**, 129, 7961. (d) Vehlow, K.; Gessler, S.; Blechert, S.

Angew. Chem. Int. Ed. **2007**, *46*, 8082. (e) Leita, E. M.; Dubberley, S. R.; Piers, W. E.; Wu, Q.; McDonald, R. *Chem. Eur. J.* **2008**, *14*, 11565. (f) Poater, A.; Cavallo, L.; *J. Mol. Catal. A: Chem.* **2010**, *324*, 75. (g) Poater, A.; Ragone, F.; Correa, A.; Cavallo, L. *J. Am. Chem. Soc.* **2009**, *131*, 9000. (h) Mathew, J.; Koga, N.; Suresh, C. H. *Organometallics* **2008**, *27*, 4666. (i) Rensburg, W. J.; Steynberg, P. J.; Meyer, W. H.; Kirk, M. M.; Forman, G. S. *J. Am. Chem. Soc.* **2004**, *126*, 14332.

(8) (a) Sanford, M. S.; Love, J. A.; Grubbs, R. H. *J. Am. Chem. Soc.* **2001**, *123*, 6543. (b) Hejl, A. PhD. Dissertation, California Institute of Technology, **2007**. (c) Vorfalt, T.; Wannowius, K.-J.; Plenio, H. *Angew. Chem. Int. Ed.* **2010**, *1*, 5533. (d) Ashworth, I. W.; Hillier, I. H.; Nelson, D. J.; Percy, J. M.; Vincent, M. A. *Chem. Comm.* **2011**, *47*, 5428. (e) Thiel, V.; Hendann, M.; Wannowius, K.-J.; Plenio, H. *J. Am. Chem. Soc.* **2012**, *134*, 1104.

(9) Schrock, R. R.; Jiang, A. J.; Marinescu, S. C.; Simpson, J. H.; Müller, P. *Organometallics* **2010**, *29*, 6816.

(10) A small amount (ca. 15%) of migration was also observed for **6.10** although in this case, it did not appear to inhibit the cross-metathesis reaction.

(11) Hong, S. H.; Sanders, D. P.; Lee, C. W.; Grubbs, R. H. *J. Am. Chem. Soc.* **2005**, *127*, 17160.

(12) (a) Schmidt, B. *Eur. J. Org. Chem.* **2003**, *34*, 816. (b) Alcaide, B.; Almendros, P.; Luna, A. *Chem. Rev.* **2009**, *109*, 3817. (c) Donohoe, T. J.; O'Riordan, T. J. C.; Rosa, C. P. *Angew. Chem. Int. Ed.* **2009**, *48*, 1014. (d) Gauthier, D.; Lindhardt, A. T.; Olsen, E. P. K.; Overgaard, J.; Skrydstrup, T. *J. Am. Chem. Soc.* **2010**, *132*, 7998.

- (13) A vent to an inert atmosphere was sufficient.
- (14) Catalyst **6.2** was only sparingly soluble in MeOH.
- (15) (a) Romero, P. E.; Piers, W. E.; McDonald, R. *Angew. Chem. Int. Ed.* **2004**, 43, 6161. (b) Wenzel, A. G.; Grubbs, R. H. *J. Am. Chem. Soc.* **2006**, 128, 16048. (c) Romero, P. E.; Piers, W. E. *J. Am. Chem. Soc.* **2007**, 129, 1698. (d) Rowley, C. N.; Eide, E. F. van der; Piers, W. E.; Woo, T. K. *Organometallics* **2008**, 27, 6043. (e) Eide, E. F. van der; Romero, P. E.; Piers, W. E. *J. Am. Chem. Soc.* **2008**, 130, 4485. (f) Leita, E. M.; Eide, E. F. van der; Romero, P. E.; Piers, W. E.; McDonald, R. *J. Am. Chem. Soc.* **2010**, 132, 2784. (g) Eide, E. F. van der; Piers, W. E. *Nature Chemistry*. **2010**, 2, 571. (h) Keitz, B. K.; Grubbs, R. H. *J. Am. Chem. Soc.* **2011**, 133, 16277.
- (16) Herbert, M. B.; Lan, Y.; Keitz, B. K.; Liu, P.; Endo, K.; Day, M. W.; Houk, K. N.; Grubbs, R. H. *J. Am. Chem. Soc.* **2012**, 134, 7861.
- (17) (a) Keitz, B. K.; Grubbs, R. H. *unpublished results*. (b) Theriot, J. C. Undergraduate Senior thesis, California Institute of Technology, 2012.
- (18) Nyman, M. D.; Hampden-Smith, M. J.; Duesler, E. N. *Inorg. Chem.* **1997**, 36, 2218.
- (19) Liu, P.; Xu, X.; Dong, X.; Keitz, B. K.; Herbert, M. B.; Grubbs, R. H.; Houk, K. N. *J. Am. Chem. Soc.* **2012**, 134, 1464.
- (20) Catalyst **6.21** was not examined.
- (21) Ritter, T.; Hejl, A.; Wenzel, A. G.; Funk, T. W.; Grubbs, R. H. *Organometallics* **2006**, 25, 5740.
- (22) Krause, J. O.; Nuyken, O.; Wurst, K.; Buchmeiser, M. R. *Chem. Eur. J.* **2004**,

10, 777.

(23) (a) Jović, M.; Torker, S.; Chen, P. *Organometallics* **2011**, *30*, 3971. (b) Buchmeiser, M. R.; Ahmad, I.; Gurram, V.; Kumar, P. S. *Macromolecules* **2011**, *44*, 4098.

(24) (a) Buchowicz, W.; Mol, J. C.; Lutz, M.; Spek, A. L. *J. Organomet. Chem.* **1999**, *588*, 205. (b) Buchowicz, W.; Ingold, F.; Mol, J. C.; Lutz, M.; Spek, A. L. *Chem. Eur. J.* **2001**, *7*, 2842. (c) Krause, J. O.; Nuyken, O.; Wurst, K.; Buchmeiser, M. R. *Chem. Eur. J.* **2004**, *10*, 777. (d) Kumar, P. S. Wurst, K.; Buchmeiser, M. R. *J. Am. Chem. Soc.* **2009**, *131*, 387.

(25) For a discussion of the effect of the NHC aryl group on ruthenium metathesis catalysts see: Süßner, M.; Plenio, H. *Chem. Comm.* **2005**, 5417.

(26) For selected examples of olefin migration/isomerization catalyzed by ruthenium hydrides see: (a) Bourgeois, D.; Pancrazi, A.; Nolan, S. P.; Prunet, J. *J. Organomet. Chem.* **2002**, *643/644*, 247. (b) Sworen, J. C.; Pawlow, J. H.; Case, W.; Lever, J.; Wagener, K. B. *J. Mol. Catal. A: Chem.* **2003**, *194*, 69. (c) Krompiec, S.; Kuźnik, N.; Penczek, R.; Rzepa, J.; Mrowiec-Białon, J. *J. Mol. Catal. A: Chem.* **2004**, *219*, 29. (d) Krompiec, S.; Kuźnik, N.; Krompiec, M.; Penczek, R.; Mrzigod, J.; Tórz, A. *J. Mol. Catal. A: Chem.* **2006**, *253*, 132. (e) Faller, J. W.; Fontaine, P. *Organometallics* **2007**, *26*, 1738. (f) Alcaide, B.; Almendros, P.; Luna, A. *Chem. Rev.* **2009**, *109*, 3817.

(27) Some additives, like 1,4-benzoquinone, led to immediate catalyst decomposition, while milder compounds, such as α,α -dichlorotoluene, resulted in decreased reaction conversions.

- (28) (a) Hamilton, J. G.; Ivin, K. J.; Rooney, J. J. *J. Mol. Catal.* **1985**, *28*, 255.
 (b) Cobo, N.; Esteruelas, M. A.; Gonzalez, F.; Herrero, J.; Lopez, A.M.; Lucio, P.; Olivan, M. *J. Catal.* **2004**, *223*, 319.
- (29) (a) Flook, M. M.; Jiang, A. J.; Schrock, R. R.; Hoveyda, A. H. *J. Am. Chem. Soc.* **2009**, *131*, 7962. (b) Flook, M. M.; Ng, V. W. L.; Schrock, R. R. *J. Am. Chem. Soc.* **2011**, *133*, 1784. (c) Schrock, R. R. *J. Chem. Soc., Dalton Trans.* **2011**, *40*, 7484.
- (30) (a) Delaude, L.; Demonceau, A.; Noels, A. F. *Macromolecules* **1999**, *32*, 2091.
 (b) Amir-Ebrahimi, V.; Corry, D. A.; Hamilton, J. G.; Thompson, J. M.; Rooney, J. *J. Macromolecules* **2000**, *33*, 717. (c) Delaude, L.; Demonceau, A.; Noels, A. F. *Macromolecules* **2003**, *36*, 1446. (d) Peeck, L. H.; Leuthäusser, S.; Plenio, H. *Organometallics* **2010**, *29*, 4339.
- (31) (a) Lin, W.-Y.; Murugesu, M. G.; Sudhakar, S.; Yang, H.-C.; Tai, H.-C.; Chang, C.-S.; Liu, Y.-H.; Wang, Y.; Chen, I.-W. P.; Chen, C.-H.; Luh, T.-Y. *Chem. Eur. J.* **2005**, *12*, 324. (b) Lee, J. C.; Parker, K. A.; Sampson, N. S. *J. Am. Chem. Soc.* **2006**, *128*, 4578. (c) Chou, C.-M.; Lee, S.-L.; Chen, C.-H.; Biju, A. T.; Wang, H.-W.; Wu, Y.-L.; Zhang, G.-F.; Yang, K.-W.; Lim, T.-S.; Huang, M.-J.; Tsai, P.-Y.; Lin, K.-C.; Huang, S.-L.; Chen, C.-H.; Luh, T.-Y. *J. Am. Chem. Soc.* **2009**, *131*, 12579. (d) Leitgeb, A.; Wappel, J.; Slugovc, C. *Polymer* **2010**, *51*, 2927.
- (32) (a) Weskamp, T.; Kohl, F.J.; Herrmann, W.A. *J. Organomet. Chem.* **1999**, *582*, 362. (b) Hamilton, J.G.; Frenzel, U.; Kohl, F.J.; Weskamp, T.; Rooney, J.J.; Herrmann, W.A.; Nuyken, O. *J. Organomet. Chem.* **2000**, *606*, 8. (c) Lin, W.-Y.; Wang, H.-W.; Liu, Z.-C.; Xu, J.; Chen, C.-W.; Yang, Y.-C.; Huang, S.-L.; Yang, H.-

C.; Luh, T.-Y. *Chem. Asian J.* **2007**, *2*, 764.

(33) (a) Vehlow, K.; Wang, D.; Buchmeiser, M. R.; Blechert, S. *Angew. Chem. Int. Ed.* **2008**, *47*, 2615. (b) Lichtenheldt, M.; Wang, D.; Vehlow, K.; Reinhardt, I.; Kühnel, C.; Decker, U.; Blechert, S.; Buchmeiser, M. R. *Chem. Eur. J.* **2009**, *15*, 9451. (c) Torker, S.; Müller, A.; Chen, P. *Angew. Chem. Int. Ed.* **2010**, *49*, 3762. (d) Buchmeiser, M. R.; Ahmad, I.; Gurram, V.; Kumar, P. S. *Macromolecules* **2011**, *44*, 4098.

(34) **Poly-6.38** with *cis* content as high as 81% has been previously reported, albeit in very low conversion. See : Ledoux, N.; Allaert, B.; Verpoort, F. *Eur. J. Inorg. Chem.* **2007**, 5578.

(35) Teo, P.; Grubbs, R. H. *Organometallics* **2010**, *29*, 6045.

(36) The *cis* content of **poly-6.38** did not change when the structurally related (H2IMes)Cl2Ru(=CH-*o*-*i*Pr-Ph) and (H2IMes)Cl2Ru(C5H5N)2 were used as catalysts in place of **6.B**. This should not be surprising since all three catalysts initiate to give the same propagating species.

(37) The initiation rate constants of **6.B** and **6.24** are $4.6 \times 10^{-4} \text{ s}^{-1}$ and $8.4 \times 10^{-4} \text{ s}^{-1}$ respectively. Both these values are significantly smaller than the initiation rate constant of (H2IMes)Cl2Ru(C5H5N)2 ($>0.2 \text{ s}^{-1}$), which is the preferred catalyst for ROMP. Note that the initiation rate constant of **6.24** depends on olefin concentration. See the following for a discussion of initiation in ruthenium metathesis catalysts: (a) Sanford, M. S.; Love, J. A.; Grubbs, R. H. *J. Am. Chem. Soc.* **2001**, *123*, 6543. (b) Love, J. A.; Morgan, J. P.; Trnka, T. M.; Grubbs, R. H. *Angew. Chem. Int. Ed.* **2002**, *41*, 4035.

(38) Schleyer, P. v. R.; Williams, J.E.; Blanchard, K.R. *J. Am. Chem. Soc.* **1970**, *92*, 2377.

(39) Bielawski, C. W.; Grubbs, R. H. *Angew. Chem. Int. Ed.* **2000**, *39*, 2903.

(40) For examples of *cis*-selective ROMP of **6.47** using tungsten catalysts see:

(a) Oreshkin, I.; Redkina, L.; Kershenbaum, I.; Chernenko, G.; Makovetsky, K.; Tinyakova, E.; Dolgoplosk, B. *Eur. Poly. J.* **1977**, *13*, 447. (b) Ceaulescu, E.; Cornilescu, A.; Nicolescu, E.; Popescu, M.; Coca, S.; Cuzmici, M.; Oprescu, C.; Dimonie, M.; Hubca, G.; Teodorescu, M.; Grosescu, R.; Vasilescu, A.; Dragutan, V. *J. Mol. Catal.* **1986**, *36*, 163. (c) Wei, J.; Leonard, J. *Eur. Poly. J.* **1994**, *30*, 999.

(41) Subsequent addition of norbornene to the reaction mixture containing **6.49** and **6.24** gives **poly-6.38** with the same selectivity as obtained in the individual polymerization of **6.38** with **6.24**, thus demonstrating that *cis*-cyclooctene does not decompose or inhibit **6.24**.

(42) Walker, R.; Conrad, R. M.; Grubbs, R. H. *Macromolecules* **2009**, *42*, 599.

(43) (a) Bielawski, C.W.; Scherman, O. A.; Grubbs R. H. *Polymer* **2001**, *42*, 4939. (b) Abdallaoui, I. A.; Semeril, D.; Dixneuf, P. H. *J. Mol. Catal. A : Chem.* **2002**, *182*, 577.

(44) Odian, G. *Principles of Polymerization*, 4th ed.; John Wiley & Sons: Hoboken, NJ, **2004**; pp 238-239.

(45) Pangborn, A. B.; Giardello, M. A.; Grubbs, R. H.; Rosen, R. K.; Timmers, F. J. *Organometallics* **1996**, *15*, 1518

(46) Blum, A. P.; Ritter, T.; Grubbs, R. H. *Organometallics* **2007**, *26*, 2122.

(47) Keitz, B. K.; Endo, K.; Herbert, M. B.; Grubbs, R. H. *J. Am. Chem. Soc.* **2011**,

133, 9686.

Appendix A

Ruthenium Olefin Metathesis Catalysts Bearing Carbohydrate- Based N-Heterocyclic Carbenes

The text in this appendix is reproduced in part with permission from:

Keitz, B. K.; Grubbs, R. H. *Organometallics* **2010**, 29, 403.

Copyright 2009 American Chemical Society

Introduction

As discussed in Chapter 1, the development of powerful, air-stable catalysts has made olefin metathesis an indispensable tool in a variety of fields. Recently, efforts to improve catalyst stability and activity have focused on modifications to the N-heterocyclic carbene (NHC).¹ In general, *N*-aryl bulk was found to increase activity while increased backbone substitution decreased activity but increased catalyst lifetime.² However, these structural studies were limited to catalysts with NHCs containing *N*-aryl substituents. NHC-based metathesis catalysts with *N*-alkyl groups on the other hand have received relatively little attention due to their lower stability in solution and generally lower activity.^{3,4} This lower activity was rationalized in Chapters 4 and 5. However, certain *N*-alkyl NHC-based catalysts have demonstrated remarkable activity, including the traditionally difficult RCM of tetrasubstituted olefins.⁵

One class of *N*-alkyl substituents for NHCs which have not yet been explored for metathesis applications are carbohydrates. Carbohydrates are extremely abundant molecules and comprise some of the most important biological machinery in living organisms including glycolipids, glycoproteins, and nucleic acids. Thus, it is no surprise that their synthesis⁶ and their biological function continue to be studied extensively.⁷ As ligands, carbohydrates are advantageous because of their innate chirality and steric bulk in addition to their long history of synthetic manipulation and solubility in water. Indeed, carbohydrates have already shown promise as ligands for asymmetric catalysis⁸ and as chiral synthons.⁹ Additionally, carbohydrates have also been used as ligand scaffolding for platinum and other metals.¹⁰ Finally,

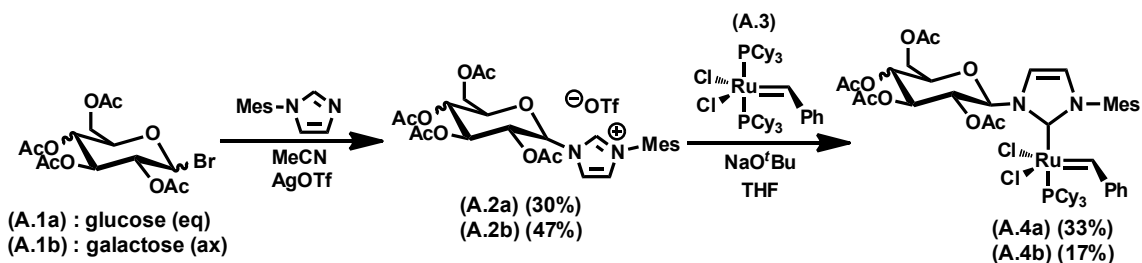


Figure A.1. Preparation of catalysts **A.4a** and **A.4b**

carbohydrates possess multiple, modular stereocenters and a steric environment which can be tuned through the judicious choice of alcohol protecting groups. However, carbohydrate-based NHCs have only recently been synthesized, and, to the best of our knowledge, a rigorous study of their applications in transition metal catalysis or organocatalysis has not been undertaken.¹⁵ Therefore, with the goals of developing a new structural class of highly active, stable, stereoselective olefin metathesis catalysts, and determining the potential of carbohydrate-based NHCs in catalysis, we undertook the synthesis of catalysts containing carbohydrate-based NHCs.

Results and Discussion

Several groups have demonstrated that a carbohydrate containing imidazolium salt may be synthesized from the reaction of an alkyl or aryl imidazole with glucopyranosyl bromide.¹¹ Along these lines, imidazolium salts **A.2a** and **A.2b** were synthesized in acceptable yields from the reaction of mesityl imidazole with 2,3,4,6-tetra-O-acetyl- α -D-glucopyranosyl bromide (**A.1a**) or 2,3,4,6-tetra-O-acetyl- α -D-galactopyranosyl bromide (**A.1b**), respectively, in the presence of silver triflate according to a previous report (Figure A. 1).¹⁵ Subsequent deprotonation with

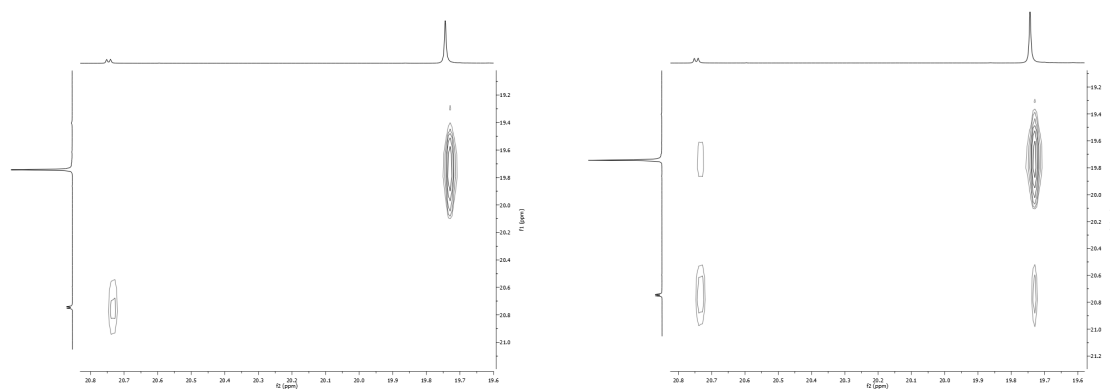


Figure A.2. 600 MHz ^1H NMR NOESY for the benzylidene region of **A.4a** in C_6D_6 at 25 °C. Mixing time = 0 ms (left) and 100 ms (right). Peak intensities are listed clockwise starting at the high field diagonal resonance. Left—589.02, 49.36. Right—1047.03, 71.91, 68.03, 30.99

sodium *tert*-butoxide and reaction with catalyst **A.3** in THF afforded the desired complex (**A.4a**) following column chromatography on silica gel. Complex **A.4a** was isolated as a single anomer (β) while **A.4b** (along with **A.2b**) was isolated as a ca. 1.2:1 mixture of β : α anomers.¹² Other methods of NHC ligation including deprotonation with KHMDS or transmetalation from a silver complex¹³ failed to give significant yields of **A.4a/b**.¹⁴ Both **A.4a** and **A.4b** were bench stable in the solid state and could be stored as a solution in C_6H_6 under a nitrogen or argon atmosphere for a period of at least 3 days as determined by ^1H NMR spectroscopy.

Characterization of complex **A.4a** at 25 °C revealed the unusual presence of two benzylidene resonances at ca. 19.77 (s) and 20.78 (d) ppm in the ^1H NMR spectrum (C_6D_6), both of which were correlated to the main ruthenium complex. Interestingly, the benzylidene resonances were found to exchange with one another using a 2D-NOESY experiment (Figure A.2). Based on the spin multiplicities of these peaks, along with the 2D-NOESY spectrum, the observed exchange was

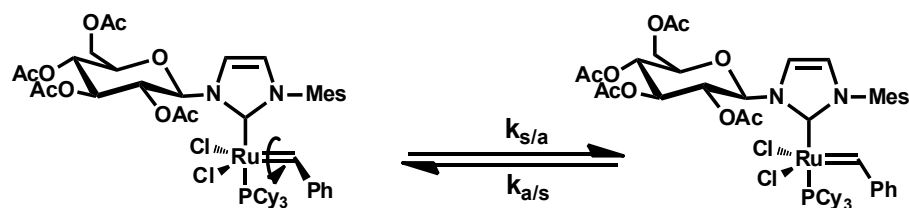


Figure A.3. Equilibrium depicting rotation about Ru – C/benzylidene bond with anti/syn designation denoting relative position of benzylidene phenyl group to the NHC

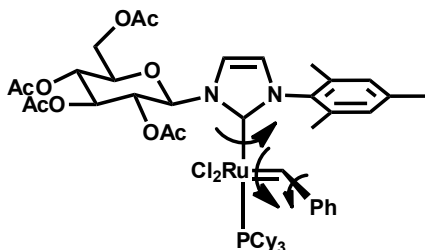


Figure A.4. Summary of rotational processes in complex **A.4a**

attributed to two rotameric species resulting from rotation about the benzylidene C–Ru bond (Figure A.3). At room temperature, such a process is more common among molybdenum and tungsten metathesis catalysts¹⁵ but has also been observed for Ru-based catalysts.¹⁶

Alkylidene rotamers are not just structural curiosities, but also play an important role in the activity and selectivity of metathesis catalysts.¹⁹ Unfortunately, a crystal structure of either rotamer of **A.4a** was unobtainable despite a variety of crystallization conditions. Therefore, in order to fully characterize the unique properties of **A.4a**, a more in-depth structural study of the rotamers of **A.4a** in solution was conducted using NMR spectroscopy.

Cooling a CD₂Cl₂ solution of **A.4a** to –75 °C resulted in the freezing out of the benzylidene C–Ru bond rotation as well as the appearance of a new benzylidene resonance which can be attributed to slow rotation about the Ru–NHC bond (see

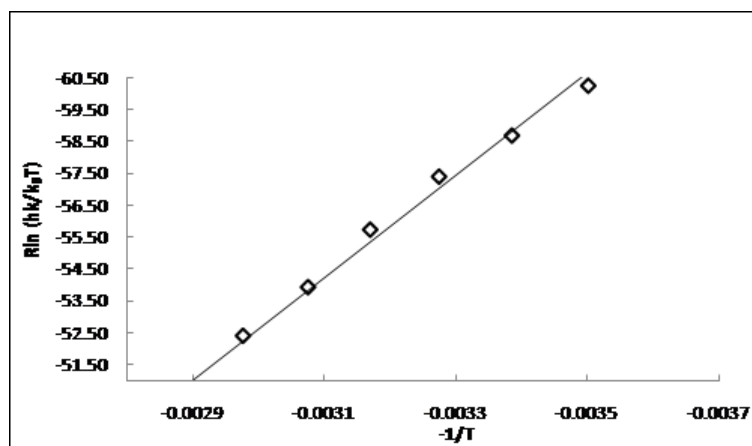


Figure A.5. Eyring plot showing VT-NMR spectroscopy data for complex **A.4a**. $R^2 = 0.989$, $\Delta H^\ddagger = 16.1 \pm 0.8$ kcal/mol, $\Delta S^\ddagger = -4.4 \pm 2.5$ cal/(mol·K)

Experimental).¹⁷ Moreover, at this temperature, the benzyldiene *ortho* protons also became well resolved, indicating that rotation about the C(carbene)–C(phenyl) bond is facile at RT. A graphical summary of observable dynamic processes in **A.4a** at 25 °C is shown in Figure A.4.¹⁸

From a magnetization transfer experiment¹⁹ conducted at 25 °C, $k_{s/a}$ and $k_{a/s}$ for the benzyldiene rotamers were determined to be 1.01 s⁻¹ and 5.28 s⁻¹, respectively.²⁰ These values correspond to a ΔG^\ddagger of 17.42 kcal/mol for the forward reaction (syn to anti) which is consistent with previous reports of Ru–C/benzyldiene rotation and also with the relative site population observed at 25 °C.²⁰ Furthermore, a VT ¹H NMR spectroscopy experiment with subsequent line shape analysis (see Experimental) yielded a value of 17.4 ± 0.2 kcal/mol for ΔG^\ddagger at 25 °C, consistent with the value obtained from the magnetization transfer experiment (Figure A.5). The ¹H NMR spectrum of complex **A.4b** looked qualitatively similar to that of **A.4a** although no attempt was made to determine the kinetic parameters quantitatively. These results demonstrate the structural rigidity of **A.4a** compared to other Ru-

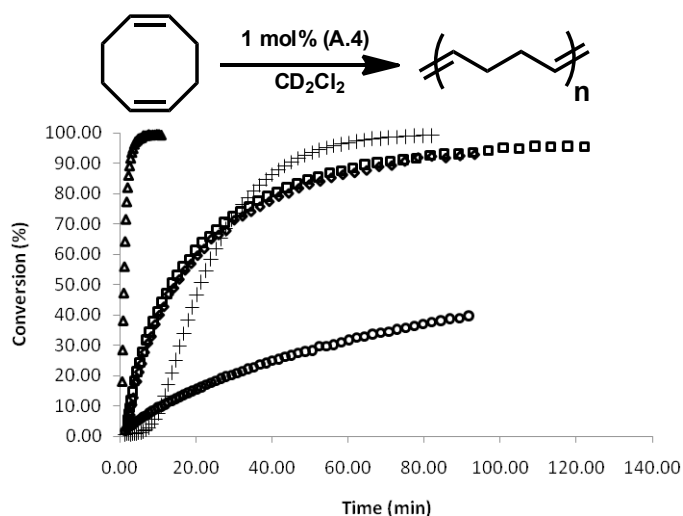


Figure A.6. Conversion of COD with catalyst **A.3** (circles), **A.6** (triangles), **A.5** (crosses), **A.4a** (square, 1 mol%), and **A.4b** (diamond, 1 mol%). Conditions were 1000:1 monomer to catalyst ratio in CD_2Cl_2 (0.1 M in monomer) at 30 °C.

based metathesis catalysts where bond rotation is more facile at 25 °C.^{20b}

Following characterization, both **A.4a** and **A.4b** were subjected to a series of standard reactions for ROMP, RCM, and CM in order to evaluate their activity and selectivity compared with previously reported catalysts.²⁹ Additionally, the effectiveness of **A.4a/b** at asymmetric reactions was also of particular interest considering the chiral nature of the carbohydrate ligand. Therefore, asymmetric ring-opening cross metathesis (AROCM) was chosen as a means of evaluating the performance of **A.4a/b** in asymmetric reactions.

The ROMP of strained olefinic ring systems is one of the earliest industrial applications of olefin metathesis and remains a popular tool for modern polymer synthesis.¹ The effectiveness of catalysts **A.4a/b** at ROMP was examined by measuring the rate of polymerization of cyclooctadiene (COD) (Figure A.6). Despite a relatively slow initiation, both catalysts were able to reach >95% conversion

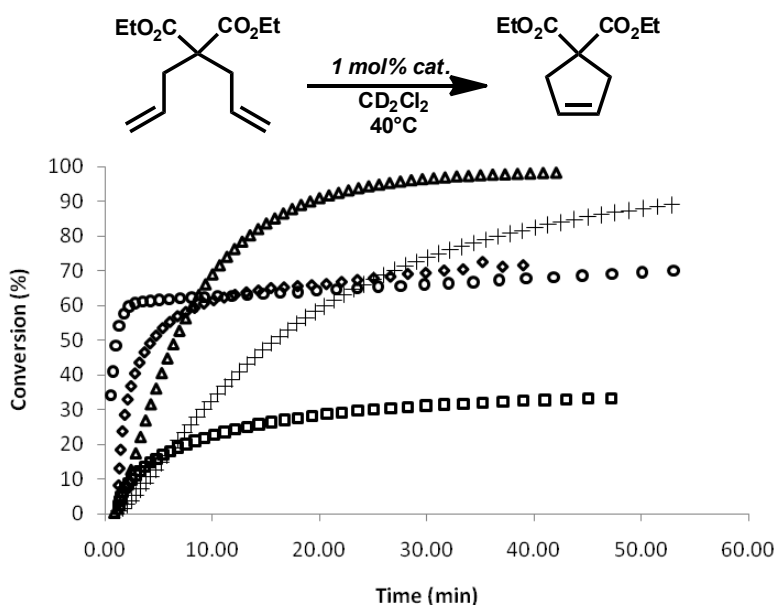


Figure A.7. RCM conversion of DEDAM with catalysts **A.3** (circles), **A.6** (triangles), **A.5** (crosses), **A.4a** (squares), and **A.4b** (diamonds). Conditions were 1 mol% catalyst, 0.1 M in substrate CD_2Cl_2 at 40°C for **A.4a** and **A.4b** and at 30°C for **A.3**, **A.6**, and **A.5**.

within 2 h at 30°C with an initial monomer to catalyst ratio of 100:1. As expected, both **A.4a** and **A.4b** showed similar kinetic behavior. Additionally, both **A.4a/b** performed well compared with other metathesis catalysts, showing a much higher activity than phosphine-based catalyst **A.3** and similar activity to $(\text{Imes})\text{Cl}_2\text{Ru}=\text{CHPh}$ (**A.5**). On the other hand, **8a/b** were less active than catalyst $(\text{H}_2\text{Imes})\text{Cl}_2\text{Ru}=\text{CHPh}$ (**A.6**) which contains a completely saturated NHC ligand.²¹

Norbornene-based substrates and cyclooctene (COE) could also be polymerized effectively using **A.4a/b** with norbornene monomers showing an increase in rate due to the increase in ring strain. Characterization of the isolated polymers by GPC revealed high PDIs and molecular weights much larger than predicted which suggests a relatively slow catalyst initiation step compared to what

is observed for fast initiating catalysts such as **A.6** or its bis-pyridine derivative.²²

Given the good activity of the catalysts in ROMP, we next focused on testing their activity in RCM, which is generally a more demanding reaction for catalysts than ROMP.¹ A standard reaction for testing the RCM activity of a particular catalyst is the ring closing of diethyl diallyl malonate (DEDAM) to the cyclopentene product (Figure A.7).²⁹ Interestingly, **A.4a** and **A.4b** showed reproducibly different kinetic behavior when exposed to DEDAM even though they only differ at one stereocenter (C4).²³ It is possible that the distinct behavior is due to one catalyst being more susceptible to a particular decomposition pathway. Another possibility is that the α anomer, which is observed in **A.4b** but not **A.4a**, is much more reactive than the β anomer under these specific reaction conditions.

At a catalyst loading of 1 mol%, both **A.4a** and **A.4b** showed good performance during the RCM of DEDAM compared with catalysts **A.6** and **A.5**, while **A.4b** displayed similar activity to catalyst **A.3**. Further reaction times or heating did not improve conversion significantly, but better results were achieved by increasing the catalyst loading to 5 mol% (not shown). Although we have not isolated any catalyst decomposition products, the early catalyst death of **A.4a/b** during RCM indicates that the catalysts are particularly susceptible to decomposition pathways involving methyldiene intermediates, similar to catalyst **A.3**.²⁴

Cross metathesis, in contrast to ROMP and RCM, does not possess as strong a driving force that pushes the metathesis reaction to completion. Additionally, secondary metathesis events often change the stereochemistry of the desired product, eventually resulting in an excess of the thermodynamically more stable *E*

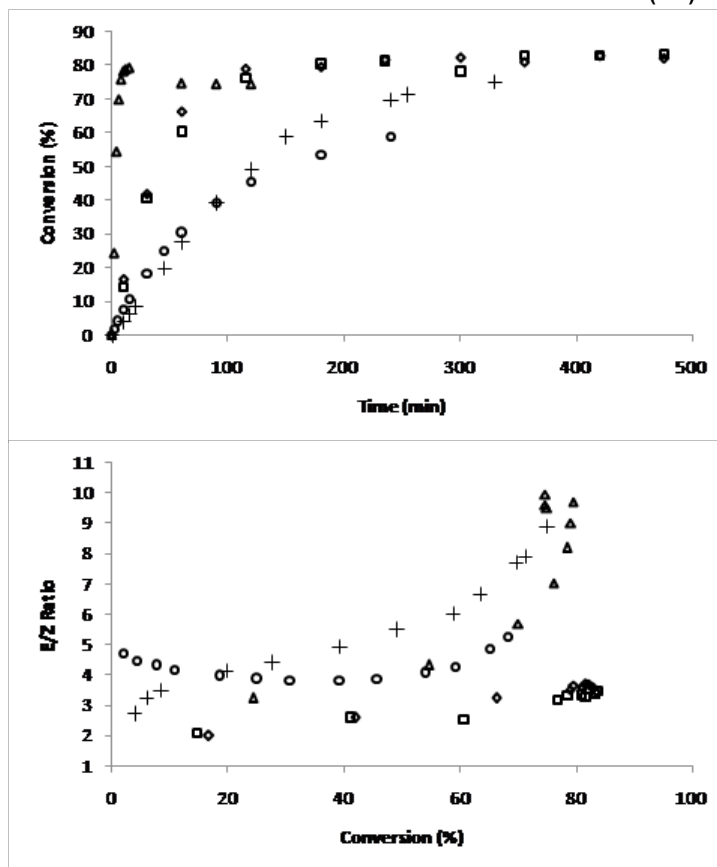
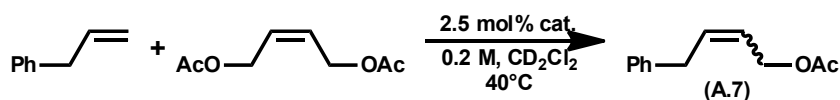
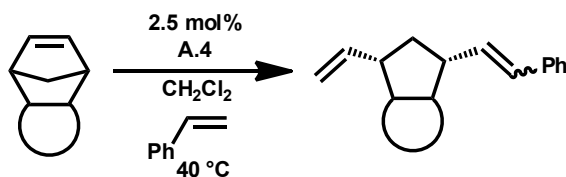


Figure A.8. Conversion to desired cross product **A.7** and E/Z ratio using **A.3** (circles), **A.6** (triangles), **A.5** (crosses), **A.4a** (squares), and **A.4b** (diamonds). Data for **A.3**, **A.6**, and **A.5** obtained at 30 °C. E/Z ratio and conversion determined by GC relative to tridecane standard.

product. Combined, these challenges often result in reactions with low yield and low selectivity. Controlling the stereochemistry of the olefin product in particular has been extraordinarily challenging although progress in this area is being made.²⁵

In order to evaluate the activity and selectivity of catalysts **A.4a/b**, the CM of allylbenzene and *cis*-diacetoxybutene was studied.²⁶ The formation of all reaction products including the desired cross product (**A.7**), *trans*-diacetoxybutene, and the *E* and *Z* isomers of the homocoupled allylbenzene were monitored over time via

Table A.1. AROCM with catalysts **A.4a/b**^a

Entry	Substrate	Catalyst	Solvent	Time (h)	ee % E(Z) ^a	Yield % (E:Z) ^b
1		A.4a	CH_2Cl_2	8	11 (7)	43 (1.3:1)
		A.4a	Toluene	15	20 (7)	88 (2.7:1)
		A.4b	Toluene	15	11(3)	86 (1.4:1)
2		A.4a	CH_2Cl_2	15	22 (n.d.)	36 (n.d.)
		A.4a	Toluene	15	26 (n.d.)	80 (n.d.)
		A.4b	Toluene	15	19 (n.d.)	73 (n.d.)
3		A.4a	Toluene	10	75 (4)	8 (2.7:1)
4		A.4a	Toluene	5	20 (4)	64 (0.7:1)

^a ee% determined by chiral HPLC. ^b isolated yield after column chromatography.

GC (Figure A.8). Catalysts **A.4a/b** reached similar levels of conversion compared with **A.3**, **A.6**, and **A.5** but maintained an exceptional *E/Z* ratio of around 3. Such a low *E/Z* ratio is unusual at high conversions where secondary metathesis events begin to favor the thermodynamic product. Furthermore, this result is also significant because the only difference between **A.5** and **A.4a/b** is the replacement of a mesityl group with a carbohydrate, indicating that carbohydrates can have a substantial effect on catalyst selectivity. However, the low *E/Z* ratio appears to be more a result of catalyst decomposition as opposed to an inherent preference for one isomer over the other since adding a fresh batch of catalyst caused the *E/Z* ratio to increase to ca. 8 over a period of 5 h. No differences in either conversion

or *E/Z* ratio were observed for catalysts **A.4a** and **A.4b**.

A relatively recent application of ruthenium-based olefin metathesis is the AROCM of substituted norbornenes with terminal olefins.³¹ Given the relative selectivity observed during CM and the chiral nature of the sugar moiety attached to the NHC ligand, AROCM was attempted with the hope of observing enantiomeric selectivity. Exposing a variety of norbornene-based substrates to catalysts **A.4a/b** in the presence of styrene for several hours at 40 °C resulted in complete conversion to the desired *cis* and *trans* products. As shown in Table A.1, reactions performed in toluene generally outperformed those conducted in methylene chloride in terms of yield due to the greater long-term stability of the catalysts in nonchlorinated solvents.²⁷ Isolated yields were generally excellent while ee's were poor compared to previously reported ruthenium-based catalysts.²⁸ The extremely low yield and relatively high ee of entry 3 in Table 1 appears to be an anomaly that is specific to that substrate.^{31c} Substrates from entries 3 and 4 were not tested with **A.4b** due to their relatively low isolated yield. Despite the modest levels of enantioselectivity observed, these results demonstrate the potential of carbohydrate-based ligands as tools for asymmetric catalysis. Furthermore, the variety of commercially available carbohydrates and the ability to create a unique steric environment using different protecting groups should allow for the creation of carbohydrate-based catalysts which are more stereoselective.

Conclusions

Olefin metathesis catalysts incorporating carbohydrate-based NHCs have been synthesized and their structural characteristics and reactivity evaluated.

These complexes are characterized by a relatively rigid structure due to the steric bulk of the carbohydrate, and in contrast to many *N*-alkyl NHCs, show excellent stability and good reactivity in a variety of olefin metathesis reactions including ROMP, RCM, CM, and AROCM. Furthermore, they also show surprising selectivity in CM compared to other catalysts, confirming that steric bulk plays a large role in influencing olefin geometry. Similarly, observable levels of enantioselectivity due to the chiral nature of the carbohydrate were also demonstrated. These results demonstrate the viability of using carbohydrate NHCs in olefin metathesis and establish them as a unique structural class of ligand. Finally, with the potential of carbohydrate-based NHCs in olefin metathesis proven, further improvements in catalyst activity and selectivity via modification of the sugar (steric) and NHC backbone (electronic) should be possible.

Experimental

All reactions were carried out in dry glassware under an argon atmosphere using standard Schlenk techniques or in a Vacuum Atmospheres Glovebox under a nitrogen atmosphere unless otherwise specified. All solvents were purified by passage through solvent purification columns and further degassed with argon. NMR solvents were dried over CaH_2 and vacuum transferred to a dry Schlenk flask and subsequently degassed with argon. Commercially available reagents were used as received unless otherwise noted. Silica gel used for the purification of organometallic compounds was obtained from TSI Scientific, Cambridge, MA (60 Å, pH 6.5–7.0).

2D-NMR experiments were conducted on a Varian 600 MHz spectrometer equipped with a Triax (^1H , ^{13}C , ^{15}N) probe while VT and kinetic experiments were

conducted on a Varian 500 MHz spectrometer equipped with an AutoX probe. Accurate temperature measurements of the NMR probe were obtained using a thermocouple connected to a multimeter with the probe immersed in an NMR tube containing toluene. Experiments and pulse sequences from Varian's Chempack 4 software were used without modification except for changes in the number of FIDs and scans per FID. Reaction conversions were obtained by comparing the integral values of starting material and product, no internal standard was used. Chemical shifts are reported in ppm downfield from Me₄Si by using the residual solvent peak as an internal standard. Spectra were analyzed and processed using MestReNova Ver. 5.2.5–4119.

Preparation of A.2b: Mesityl imidazole²⁹ (1.06 g, 5.67 mmol), **A.1b** (2.57 g, 6.24 mmol), and AgOTf (1.60 g, 6.24 mmol) were placed in a dry 100 ml RB flask under argon and dissolved in 30 ml of dry MeCN. The RB was shielded from light and heated to 50 °C for 16 h. The reaction was cooled to 25 °C and the solution filtered through a pad of celite washing with MeCN then concentrated *in vacuo*. The resulting residue was dissolved in CH₂Cl₂ and MTBE was added until the solution became slightly cloudy. After cooling to –5 °C, an oily residue crashed out. The supernatant was removed and the oil was triturated with cold hexanes and concentrated to a light brown powder (1.8 g, 47%). **A.2b** was recovered as a 1.3:1 mixture of β:α anomers and used without further purification. ¹H NMR (CDCl₃, 300 MHz): δ 9.39 (s, 1H), 8.69 (s, 1H), 7.91 (s, 1H), 7.77 (s, 1H), 7.31 (s, 1H), 7.18 (s, 1H), 7.02 (s, 4H), 6.37 (m, 1H), 5.57 (m, 1H), 5.36 (m, 3H), 4.48 (t, J = 6.18 Hz, 1H), 4.19–4.03 (m, 4H), 2.18–1.97 (m, 42H).

Preparation of A.4a: In a glovebox, a 100 ml RB was charged with **A.3** (0.497 g, 0.604 mmol), **A.2a** (0.604 g, 0.906 mmol), and NaO^tBu (0.087 g, 0.906 mmol). 50 ml of dry THF was added and the reaction was stirred for 1 h at 25 °C after which it was removed from the glovebox and conc. in vacuo. The residue was dissolved in a minimal amount of CH₂Cl₂, loaded onto a column of TSI silica gel, and eluted with 10% diethyl ether/pentane to first collect excess **A.3** as a dark purple band, followed by 30% ether/pentane, and finally 60% ether/pentane until a dark pink/red band was collected. After concentration of the relevant fractions, a dark pink residue was obtained which could be lyophilized from benzene to yield **A.4a** (208 mg, 33%) as a dark pink powder. ¹H NMR (C₆D₆, 600 MHz, major isomer): δ 19.74 (s, 1H), 8.4–7.8 (br s, 2H), 7.10 (d, J = 1.8 Hz, 1H), 6.95 (m, 3H), 6.31 (br s, 1H), 6.03 (d, J = 1.8 Hz, 1H), 5.98 (br s, 1H), 5.94 (t, J = 9 Hz, 1H), 5.88 (t, J = 9.6 Hz, 1H), 5.57 (t, J = 9.6 Hz, 1H), 4.39 (m, 2H), 4.26 (ad, J = 10.8 Hz, 1H), 2.53 (m, 3H), 2.23 (s, 6H), 1.98 (br s, 3H), 1.88 (br s, 6H), 1.80 (br s, 12H), 1.73 (m, 9H), 1.59 (m, 6H), 1.23 (m, 9H). ¹³C NMR (151 MHz, C₆D₆) δ 298.0, 192.6, 170.39, 170.22, 169.94, 152.44, 138.70, 137.03, 136.86, 136.51, 129.46, 129.14, 128.90, 124.55, 124.54, 120.36, 120.34, 87.17, 75.50, 74.74, 71.13, 69.30, 62.00, 33.17, 33.06, 30.49, 28.52, 28.49, 28.46, 28.43, 27.24, 21.42, 21.31, 20.94, 20.55, 20.53, 18.97, 18.69. ³¹P NMR (202 MHz, C₆D₆) δ 30.86 (major), 28.17 (minor). HRMS (FAB+) Calculated—1058.332, Experimental—1058.329.

Preparation of A.4b: An analogous procedure to that of **A.4a** was followed yielding **A.4b** (17%) as a 1.2:1 mixture of anomers. ¹H NMR (C₆D₆, 600 MHz, major isomer): δ 19.78 (s, 1H), 8.4–7.9 (br s, 4H), 7.46 (d, J = 1.56 Hz, 1H), 7.06

(d, $J = 5.1$ Hz, 1H), 6.95 (br t, $J = 7.38$ Hz, 2H), 6.76 (d, $J = 3.54$ Hz, 1H), 6.32 (br s, 1H), 6.27 (t, $J = 9.48$ Hz, 1H), 6.03 (d, $J = 2.04$ Hz, 1H), 6.00 (br s, 1H), 5.91 (d, $J = 2.88$ Hz, 1H), 5.82 (m, 1H), 5.71 (m, 1H), 5.67 (m, 1H), 5.63 (m, 1H), 4.64 (br t, $J = 6.78$ Hz, 1H), 4.38 (m, 1H), 4.22 (m, 1H), 4.17 (m, 1H), 4.10 (m, 2H), 2.54 (m, 6H), 2.26 (s, 6H), 1.98–1.55 (m, 77H), 1.24 (m, 15H). ^{13}C NMR (151 MHz, C_6D_6) δ 193.04, 170.52, 170.37, 170.35, 170.20, 170.13, 169.94, 169.92, 169.81, 168.82, 152.49, 138.71, 137.09, 136.88, 136.52, 129.46, 129.17, 128.66, 128.61, 128.53, 128.45, 128.37, 128.29, 128.21, 128.10, 124.60, 124.59, 120.54, 120.52, 92.94, 90.54, 87.65, 74.31, 72.66, 72.22, 71.67, 69.65, 68.86, 68.55, 68.25, 68.17, 68.03, 67.57, 67.51, 61.69, 61.47, 61.21, 33.08, 33.04, 32.97, 30.51, 30.49, 30.37, 30.15, 28.54, 28.51, 28.49, 28.44, 28.43, 27.60, 27.28, 27.16, 27.01, 21.58, 21.32, 20.73, 20.63, 20.53, 20.52, 20.49, 20.47, 20.43, 20.41, 20.39, 20.24, 20.18, 19.01, 18.67. ^{31}P NMR (121 MHz, C_6D_6) δ 31.19 (major), 28.53 (minor). HRMS (FAB+) Calculated—1057.324, Experimental—1057.321.

Representative procedure for ROMP/RCM kinetics: In a glovebox, catalyst **A.4a** (2.5 mg, 0.0024 mmol) was dissolved in CD_2Cl_2 (0.8 ml) and placed in a NMR tube equipped with a rubber septum. The NMR tube was removed from the glovebox and COD (distilled prior to use) (30 μL , 0.24 mmol) was injected after which the tube was immediately placed in the spectrometer and a spectral array started by arraying the “pad” variable for Varian spectrometers.

Representative procedure for CM Kinetics: Allyl benzene and cis-diacetoxybutene were distilled prior to use. In a glovebox, a scintillation vial was charged with allyl benzene (20 μL , 0.153 mmol), cis-diacetoxybutene (49 μL , 0.305 mmol), and

tridecane standard (50 μ L, 0.205 mmol). CH_2Cl_2 (0.75 ml) was added followed by **A.4a** (4 mg, 0.004 mmol) as a solution in CH_2Cl_2 . The vial was equipped with a septa top, removed from the glovebox and stirred under argon. Aliquots were removed via syringe at the specified time points and added to a GC vial containing a solution of ethyl vinyl ether in CH_2Cl_2 in order to quench the catalyst. GC retention times were as follows (min): allyl benzene (10.87), tridecane (11.55), cis-diacetoxybutene (18.13), trans-diacetoxybutene (18.70), cis-12 (21.27), trans-12 (21.48), trans-homocoupled allyl benzene (24.09), cis-homocoupled allyl benzene (24.34).

Figure A.9. ^1H (^{13}C) assignments for major isomer of catalyst **A.4a** based on spectroscopic data

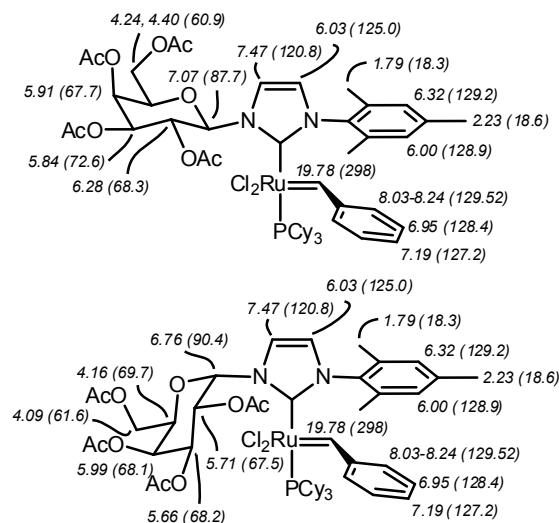


Figure A.10. ^1H (^{13}C) assignments β (top) and α (bottom) anomers of **A.4b**

Measurement of benzylidene rotation rate using line shape analysis: A lineshape analysis of the benzylidene rotation in **A.4a** was performed in order to obtain a more accurate estimate of ΔG^\ddagger . The coalescence temperature could not be reached due to catalyst decomposition, however, a suitable temperature range from 12.5–73.1 °C was found in which there was no observable catalyst decomposition. To measure the rate of benzylidene rotation, **A.4a** was dissolved in ca. 0.6 mL of dry C_6D_6 and placed into a J. Young tube inside of a glove box. The tube was sealed and removed from the box and placed inside the spectrometer where it was allowed to equilibrate at the appropriate temperature for ca. 10 min before acquisition. The probe was calibrated at each temperature according to the method described in the General Information. Each experiment was run with ^{31}P decoupling in order to simplify the line shape analysis of the resulting spectrum. Experimental spectra were simulated using the MEXICO set of programs developed by Professor Alex Bain.³¹ The noniterative version of MEXICO was used through

the SpinWorks (Ver. 3) NMR program which overlays the MEXICO simulation with the experimental spectrum and calculates an RMS value immediately.³²

References

- (1) (a) Van Veldhuizen, J. J.; Garber, S. B.; Kingsbury, J. S.; Hoveyda, A. H. *J. Am. Chem. Soc.* **2002**, *124*, 4954. (b) Despagnet-Ayoub, E.; Grubbs, R. H. *Organometallics* **2005**, *24*, 338. (c) Weigl, K.; Kohler, K.; Dechert, S.; Meyer, F. *Organometallics* **2005**, *24*, 4049. (d) Funk, T. W.; Berlin, J. M.; Grubbs, R. H. *J. Am. Chem. Soc.* **2006**, *128*, 1840. (e) Vehlow, K.; Maechling, S.; Blechert, S. *Organometallics* **2006**, *25*, 25. (f) Anderson, D. R.; Lavallo, V.; O'Leary, D. J.; Bertrand, G.; Grubbs, R. H. *Angew. Chem. Int. Ed.* **2007**, *46*, 7262. (g) Berlin, J. M.; Campbell, K.; Ritter, T.; Funk, T. W.; Chlenov, A.; Grubbs, R. H. *Org. Lett* **2007**, *9*, 1339. (h) Stewart, I. C.; Ung, T.; Pletnev, A. A.; Berlin, J. M.; Grubbs, R. H.; Schrodi, Y. *Org. Lett* **2007**, *9*, 1589. (i) Chung, C. K.; Grubbs, R. H. *Org. Lett* **2008**, *10*, 2693. (j) Vougioukalakis, G. C.; Grubbs, R. H. *J. Am. Chem. Soc.* **2008**, *130*, 2234.
- (2) Kuhn, K. M.; Bourg, J. B.; Chung, C. K.; Virgil, S. C.; Grubbs, R. H. *J. Am. Chem. Soc.* **2009**, *131*, 5313.
- (3) Schuster, O.; Yang, L.; Raubenheimer, H. G.; Albrecht, M. *Chem. Rev.* **2009**, *109*, 3445.
- (4) (a) Weskamp, T.; Kohl, F. J.; Hieringer, W.; Gleich, D.; Herrmann, W. A. *Angew. Chem. Int. Ed.* **1999**, *38*, 2416. (b) Ledoux, N.; Allaert, B.; Linden, A.; Van Der Voort, P.; Verpoort, F. *Organometallics* **2007**, *26*, 1052. (c) Boydston, A. J.; Xia, Y.; Kornfield, J. A.; Gorodetskaya, I. A.; Grubbs, R. H. *J. Am. Chem. Soc.* **2008**, *130*,

12775.

(5) Savoie, J.; Stenne, B.; Collins, Shawn K. *Adv. Syn. Catal.* **2009**, 351, 1826.

(6) Hudlicky, T.; Entwistle, D. A.; Pitzer, K. K.; Thorpe, A. J. *Chem. Rev.* **1996**, 96, 1195.

(7) (a) Gamblin, D. P.; Scanlan, E. M.; Davis, B. G. *Chem. Rev.* **2008**, 109, 131. (b) Murrey, H. E.; Hsieh-Wilson, L. C. *Chem. Rev.* **2008**, 108, 1708.

(8) Dieguez, M.; Pamies, O.; Claver, C. *Chem. Rev.* **2004**, 104, 3189.

(9) Hollingsworth, R. I.; Wang, G. *Chem. Rev.* **2000**, 100, 4267.

(10) (a) Gyurcsik, B.; Nagy, L. *Coord. Chem. Rev.* **2000**, 203, 81. (b) Steinborn, D.; Junicke, H. *Chem. Rev.* **2000**, 100, 4283.

(11) (a) Nishioka, T.; Shibata, T.; Kinoshita, I. *Organometallics* **2007**, 26, 1126. (b) Tewes, F.; Schlecker, A.; Harms, K.; Glorius, F. *J. Organomet. Chem.* **2007**, 692, 4593. (c) Shi, J. C.; Lei, N.; Tong, Q. S.; Peng, Y. R.; Wei, J. F.; Jia, L. *Eur. J. Inorg. Chem.* **2007**, 2221.

(12) Determined by ^1H NMR spectrum analysis of J_{HH} coupling in **A.4b**.

(13) The silver complex was formed via deprotonation by silver (I) oxide. See ref. 11b for details.

(14) Unfortunately, in our hands, this methodology could not be extended to gluco- or galactopyransoyl bromides protected with benzyl (Bn), benzoyl (Bz), pivalate (Piv), or methyl (Me) groups. Attempts to form a phosphine-free catalyst via incorporation of a Hoveyda-type chelating benzyldiene either by direct phosphine substitution or via cross metathesis of **A.4a/b** with β -methyl isopropoxy styrene were also unsuccessful.

(15)(a) Oskam, J. H.; Fox, H. H.; Yap, K. B.; McConville, D. H.; Odell, R.; Lichtenstein, B. J.; Schrock, R. R. *J. Organomet. Chem.* **1993**, 459, 185. (b) Oskam, J. H.; Schrock, R. R. *J. Am. Chem. Soc.* **1993**, 115, 11831.

(16) (a) Grisi, F.; Costabile, C.; Gallo, E.; Mariconda, A.; Tedesco, C.; Longo, P. *Organometallics* **2008**, 27, 4649. (b) Sanford, M. Ph.D. Thesis, California Institute of Technology, Pasadena, 2001

(17) A 2D-NOESY experiment conducted at $-75\text{ }^{\circ}\text{C}$ with a mixing time of 500 ms showed no exchange between the benzyldiene rotamers (doublet and singlet) but small cross peaks between the two singlet resonances indicated that rotation about the Ru-NHC bond is not completely frozen out at this temperature. A low temperature VT-NMR experiment and subsequent line shape analysis yielded a ΔG^{\ddagger} consistent with previous reports of NHC rotation (see ref. 16b), although we cannot completely rule out another process such as oxygen coordination/decoordination at this time. See Supporting Information for relevant spectra and plots.

(18) Although it is tempting to theorize that an oxygen from either an acetate or the sugar is coordinating to the metal center, we found no obvious indications of this during our NMR studies.

(19) Sandström, J.; *Dynamic NMR Spectroscopy*, Academic Press Inc.: New York, New York, 1982; pp. 53-54.

(20) See the experimental section details.

(21) At this time, we have been unable to synthesize a saturated variant of **A.4a** or **A.4b**.

(22) Love, J. A.; Sanford, M. S.; Day, M. W.; Grubbs, R. H. *J. Am. Chem. Soc.* **2003**, *125*, 10103.

(23) The kinetic plots shown were reproducible for different kinetic runs and also for different batches of catalyst.

(24) (a) Hong, S. H.; Wenzel, A. G.; Salguero, T. T.; Day, M. W.; Grubbs, R. H. *J. Am. Chem. Soc.* **2007**, *129*, 7961. (b) Hong, S. H.; Chlenov, A.; Day, M. W.; Grubbs, R. H. *Angew. Chem. Int. Ed.* **2007**, *46*, 5148.

(25) Flook, M. M.; Jiang, A. J.; Schrock, R. R.; Mueller, P.; Hoveyda, A. H. *J. Am. Chem. Soc.* **2009**, *131*, 7962.

(26) Ritter, T.; Hejl, A.; Wenzel, A. G.; Funk, T. W.; Grubbs, R. H. *Organometallics* **2006**, *25*, 5740.

(27) Kuhn, K. M.; Bourg, J. B.; Chung, C. K.; Virgil, S. C.; Grubbs, R. H. *J. Am. Chem. Soc.* **2009**, *131*, 5313.

(28) (a) Van Veldhuizen, J. J.; Garber, S. B.; Kingsbury, J. S.; Hoveyda, A. H. *J. Am. Chem. Soc.* **2002**, *124*, 4954. (b) Van Veldhuizen, J. J.; Gillingham, D. G.; Garber, S. B.; Kataoka, O.; Hoveyda, A. H. *J. Am. Chem. Soc.* **2003**, *125*, 12502. (c) Berlin, J. M.; Goldberg, S. D.; Grubbs, R. H. *Angew. Chem. Int. Ed.* **2006**, *45*, 7591.

(29) Ketz, B. E.; Cole, A. P.; Waymouth, R. M. *Organometallics* **2004**, *23*, 2835.

(30) Berlin, J. M.; Goldberg, S. D.; Grubbs, R. H. *Angew. Chem. Int. Ed.* **2006**, *45*, 7591.

(31) <http://chemistry.mcmaster.ca/faculty/bain/>

(32) Marat, Kirk. SpinWorks. <http://www.umanitoba.ca/chemistry/nmr/spinworks/>

index.html

Appendix B

Miscellaneous C-H-Activated Catalysts

Introduction

This chapter contains several miscellaneous C-H-activated complexes that were partially prepared and characterized. Many of these complexes have not been fully characterized (e.g., ^{13}C NMR spectra and HRMS are lacking), but there is good reason to believe that the target complex was formed based on ^1H NMR spectroscopy and qualitative evidence such as color changes. Selected unsuccessful attempts at other complexes will also be presented. The primary product in these unsuccessful attempts was either an unidentified decomposition product, or a ruthenium hydride species. I will try to briefly discuss the rationale behind the preparation of each complex in a manner that is useful for future researchers.

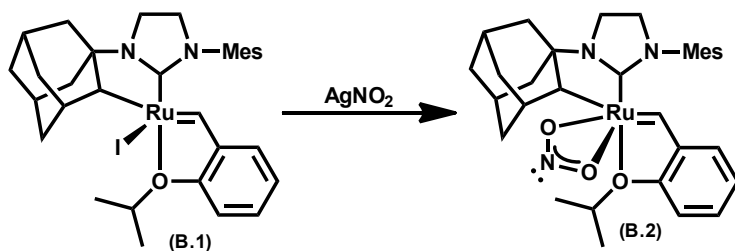


Figure B.1. Preparation of **B.2**

Nitrite Catalyst

Before focusing on the nitrate catalysts presented in Chapter 6, we also prepared a catalyst with a nitrite X-type ligand (Figure B.1). This catalyst was successfully prepared and preliminary results indicate its reactivity is on par with its nitrate-based cousins. Interesting redox chemistry may be possible at the nitrite ligand.

A 20 mL scintillation vial in the glove box was charged with **B.1** (13 mg,

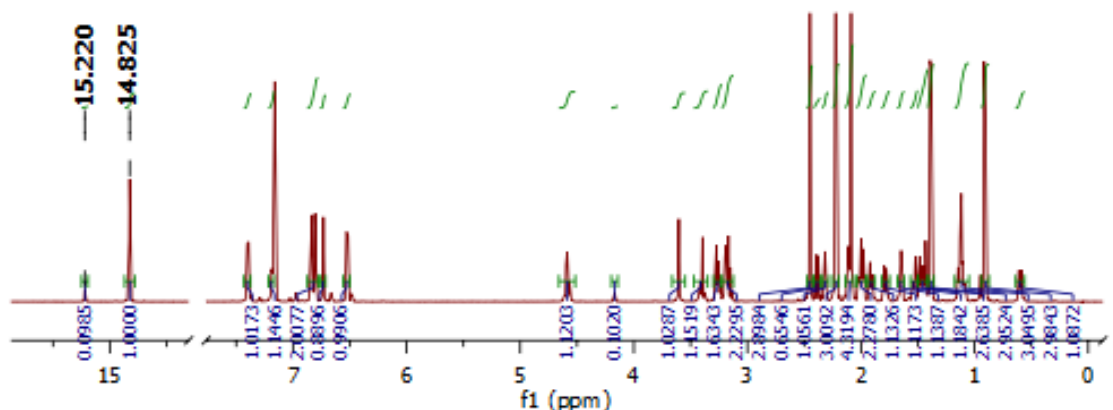


Figure B.2. ^1H NMR (600 MHz, C_6D_6) spectrum of **B.2** at RT. Peak at $\delta = 15.22$ ppm is unknown impurity

0.019 mmol) and AgNO_2 (14 mg, 0.096 mmol) and THF (1 mL) was added. The suspension was stirred vigorously until a color change from brown to red/purple was observed (ca. 3–5 min). The solution was immediately filtered, washing with THF, and concentrated. The resulting residue was triturated with Et_2O to give **B.2** (10 mg, 87%). Note that similar to the formation of the nitrate catalysts in Chapter 6, prolonged exposure of **B.1** (or **B.2**) to AgNO_2 resulted in complete decomposition.

Catalysts with Chiral Carboxylates

Theoretical calculations have established that the C-H activated catalysts most likely proceed through a side-bound ruthenacycle intermediate.¹ Therefore, the ligands in these catalysts may be better able to influence ruthenacyclobutanes. In order to examine this, we prepared C-H catalysts with chiral carboxylates for enantioselective olefin metathesis (i.e., asymmetric ring-opening cross-metathesis).²

A multitude of commercially available chiral carboxylic acids are available

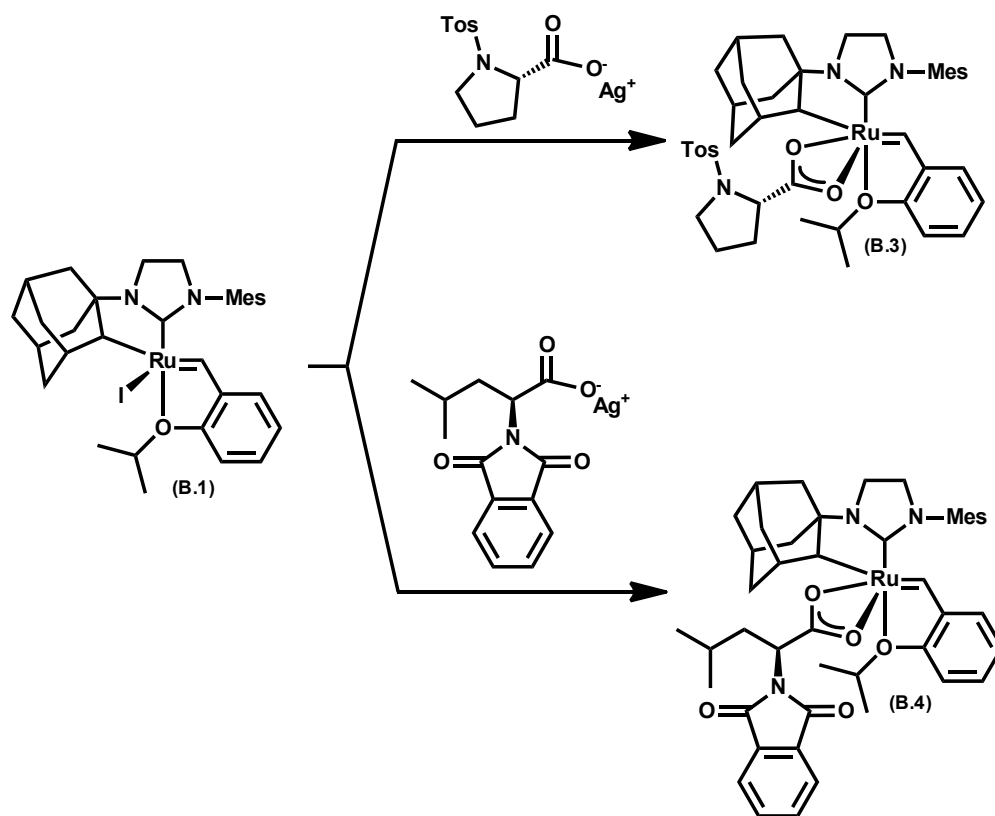


Figure B.3. Preparation of **B.3** and **B.4**

because of their prevalence in enantioselective rhodium-catalyzed cyclopropanation reactions.³ Following the conversion of two selected acids to their corresponding silver salts, transmetalation onto **B.1** was affected using the procedures discussed in Chapter 6 (Figure B.3). The ¹H NMR spectra of both **B.3** and **B.4** contained three resonances each in the benzylidene region (Figure B.4). In the case of **B.3**, these resonances were found to interconvert on the NMR timescale as evidenced by a 2D ROESY spectrum (Figure B.5). In contrast, the benzylidene resonances of **B.4** did not interconvert by ROESY. At this point, it is unclear what structures these benzylidene resonances represent.

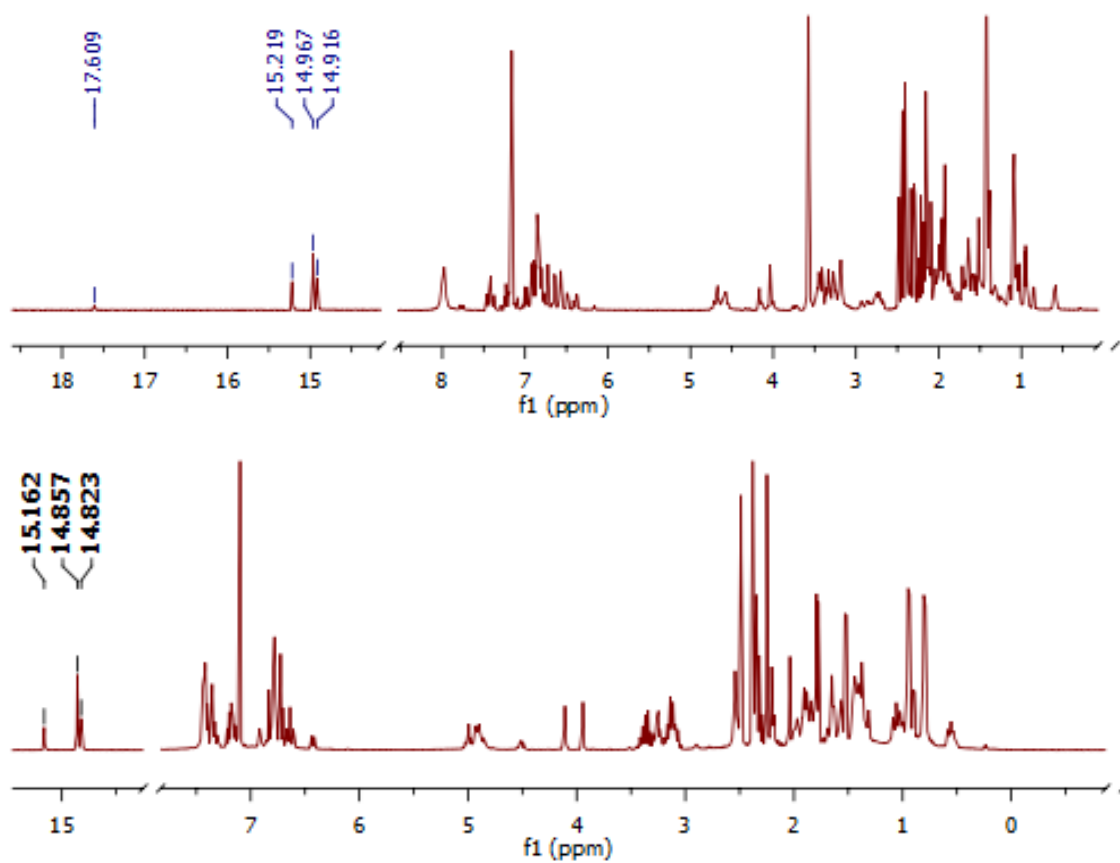


Figure B.4. ^1H NMR (400 MHz, C_6D_6) spectrum of **B.3** (top) and **B.4** (bottom) at RT

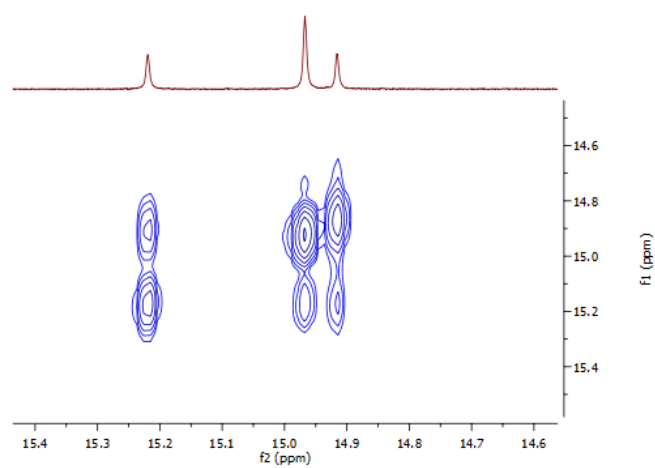


Figure B.5. 2D ROESY of **B.3** showing chemical exchange

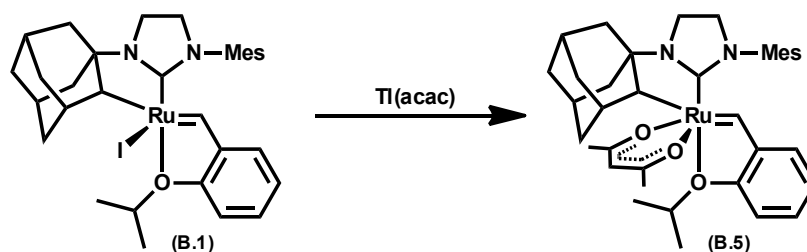


Figure B.6. Preparation of **B.5**

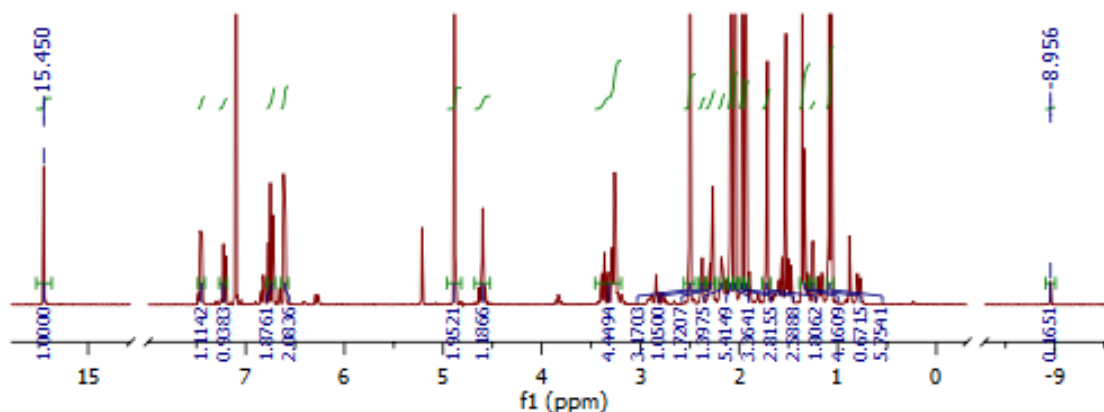


Figure B.7. ^1H NMR (400 MHz, C_6D_6) spectrum of **B.5**

Acetylacetonate (acac) Complexes

In addition to carboxylates, the iodide ligand in **B.1** can also be replaced with acac ligands (Figure B.6). When **6.1** was exposed to Ti(acac) according to the general procedure in Chapter 6, complex **6.5** and an unidentified Ru-H complex were recovered (Figure B.6 and B.7). Complex **6.5** was found to be inactive under standard homodimerization conditions. It's possible that this inactivity may be rem

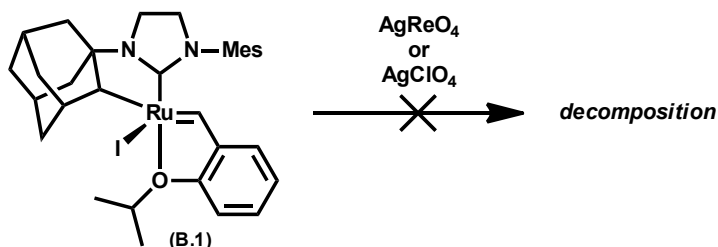


Figure B.7. Attempted preparation of ReO_4^- and ClO_4^- complexes

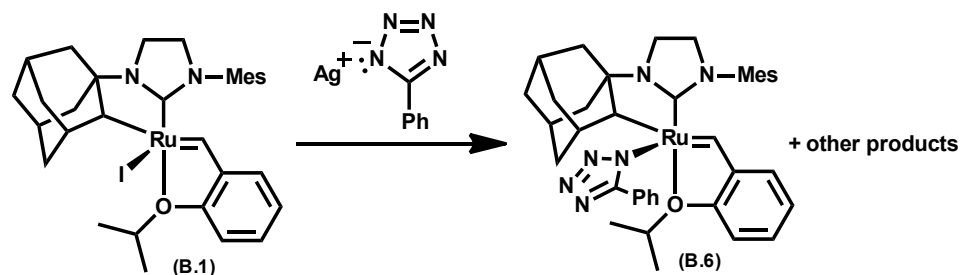


Figure B.8. Tetrazolate complex **B.6**

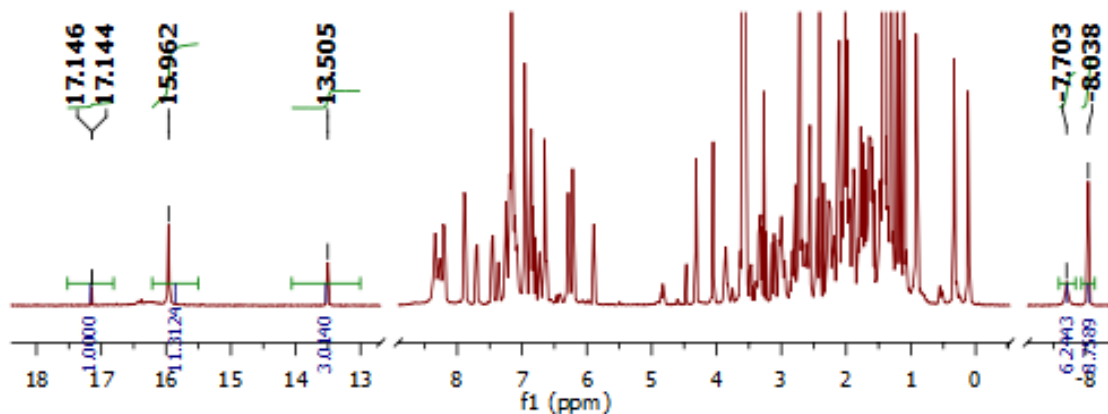


Figure B.9. ^1H NMR (400 MHz, C_6D_6) spectrum of crude reaction mixture from Figure B.8

edied through the addition of exogenous acid (see Chapter 2).

Perchlorate and Perrhenate Ligands

In the hopes finding similar ligands to nitrate, we also attempted to replace the iodide ligand in **B.1** with the heavily oxygenated ligands perchlorate (ClO_4^-) and perrhenate (ReO_4^-), but these reactions resulted in complete decomposition. Extreme care should be taken when handling these heavily oxygenated compounds as they are explosive.

Tetrazolate Complexes

Tetrazolate-type ligands, as close analogues of carboxylates, were also briefly examined (Figure B.8). When **B.1** was exposed to silver (I) phenyl tetrazolate, a mixture of products, starting material, and hydrides was observed (Figure B.9). This may indicate that C-H-activated species with tetrazolate ligands are thermally unstable and decompose under the reaction conditions. However, no attempts were made to isolate or purify the complex mixture.

Sulfonate Complexes

Sulfonate ligands have previously been used in olefin metathesis catalysts, and displayed improved selectivity for Z-olefins compared to halide-ligated catalysts.⁴ Therefore we attempted to prepare C-H-activated catalysts containing sulfonate ligands. Exposure of **B.1** to silver (I) tosylate resulted in the formation of the desired sulfonate complex, but this product quickly decomposed in solution at RT into a mixture of unidentified hydride species. Despite this result, different substituted sulfonates may yield more stable complexes.

References

- (1) Liu, P.; Xu, X.; Dong, X.; Keitz, B. K.; Herbert, M. B.; Grubbs, R. H.; Houk, K. N. *J. Am. Chem. Soc.* **2012**, *134*, 1464.
- (2) (a) La, D. S.; Sattely, E. S.; Ford, J. G.; Schrock, R. R.; Hoveyda, A. H. *J. Am. Chem. Soc.* **2001**, *123*, 7767. (b) (1) Berlin, J. M.; Goldberg, S.; Grubbs, R. H. *Angew. Chem. Int. Ed.* **2006**, *45*, 7591.

- (3) Trindade, A. F.; Coelho, J. A. S.; Afonso, C. A. M.; Veiros, L. F.; Gois, P. M. P. *ACS Catalysis* **2012**, 2, 370.
- (4) Teo, P.; Grubbs, R. H. *Organometallics* **2010**, 29, 6045.